On the molecular pathways supporting the development of structurally coloured cuticle in *Hibiscus trionum*

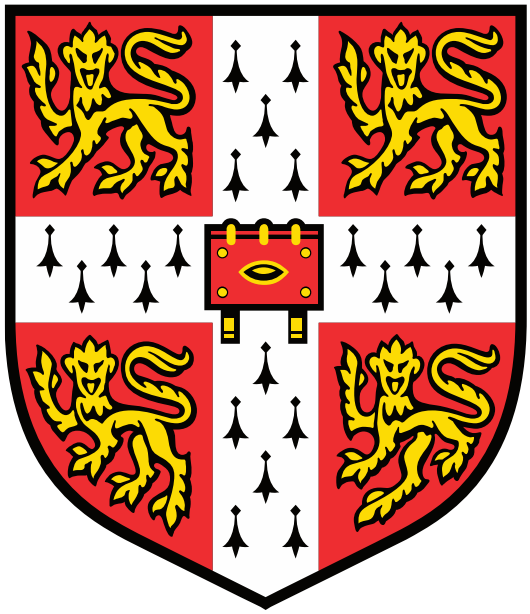

Jordan Ferria

Department of Plant Science

University of Cambridge- St Edmund's College

This dissertation is submitted for the degree of Doctor of Philosophy

June-2021

On the molecular pathways supporting the development of structurally coloured cuticle in *Hibiscus trionum*

Evolving from a single ancestor that appeared between 250 and 125 million years ago, flowering plants are the most diverse group of plants with about 78% of plant species. The staggering diversity of flowering plants is often correlated with their capacity of adaptation to the diversity of niche space offered by numerous different animal pollinators displaying many different sensory and behavioural traits. In response to selective pressure to attract pollinators, flowers have developed many strategies such as the production of volatile compounds, thermal patterns, visual cues, and rewards amongst others. In 2009, observations of the proximal adaxial part of *Hibiscus trionum* petals revealed the presence of structural colours. They are mainly characterised by the specific reflection of blue and UV-light in an angle dependant manner (also known as iridescence). Further observations of the cuticle showed the presence of nano-scaled striations acting as a grating like surface responsible for the diffraction of light. Computational modelling, and existing knowledge in material physics, suggests that the development of such a structure is induced by the buckling of the petal cuticle.

In this PhD, the molecular pathways and mechanisms underpinning the production of nano-scaled petal ridges were investigated in *Hibiscus trionum*. Liquid extraction surface analyses coupled with mass spectrometry were conducted on striated and non-striated tissues, allowing us to highlight the importance of the cuticle chemistry in the development of nano-scaled ridges. The abundance of a specific cutin monomer and the reticulation of the cutin network appeared to be crucial for the buckling of the cuticle. Further investigation using transcriptomic analyses of distal and proximal petal tissues before and after the development of striations revealed the importance of SHN3 and DEWAX transcription factors in the modulation of the cuticle chemistry of the petals. The upregulation of *SHN3* and *DEWAX* expression in the proximal petal region suggested that cuticle buckling could be enabled by a relative abundance of cutin and a decrease in the wax content of the cuticle. Further transcriptomic

analyses revealed the up regulation of numerous genes involved in pectin catabolism in the proximal petal region, consistently with the production of a compliant, softer cell wall for the development of striations. Mutant screen experiments identified 2 mutant lines characterised by the presence of smooth patches of cells and the presence of conical cells in one of them. Further characterisation of the mutant phenotypes suggested the importance of the cell shape and the thickness of the cuticle to achieve proper bucking. Finally, the adhesion properties of structurally coloured cuticle were briefly studied by testing the gripping capacity of *Leptinotarsa decemlineata* on replicas of the structurally coloured cuticle of *Paeonia mascula* petals. Wettability was also investigated by measuring the contact angle of water droplets on similar replicas. Together, these results demonstrate that structurally coloured cuticle resulting from nano-scaled striation decreases the grip ability of *L. decemlineata*, potentially by a decrease in the contact surface between the setose pads and the cuticle.

Declaration

This Thesis is the result of my own work and includes nothing which is the outcome of the work of collaborators unless specifically mentioned.

This Thesis is the result of new work that has never been submitted for the awarding of a degree, diploma or any other certification at the University of Cambridge, or any other University or Academic institution, unless specifically mentioned.

This Thesis does not exceed the limit of 60,000 words prescribed by the Degree Committee of the Faculty of Biology.

Copyrights were inquired to the Copyrights Clearance Center for the use of previously published figures (see copyright licence numbers in figure legends when applicable).

Jordan Ferria, Cambridge, 2021

Acknowledgements

This thesis was an opportunity of immense growth both personally and scientifically. It taught me how to produce scientific data of high quality and gave me all the necessary keys to pursue my life as a researcher. A huge thank you goes to Prof. Beverley Glover who gave me the opportunity to join her team in 2017 and provided guidance all along this adventure. Her patience and her confidence in me and my work allowed me to make of my thesis a very personal project. Her keen eye and insightful comments on my presentations and written work helped me greatly to improve my communication skills.

I am very grateful to Dr. Chiara Airoldi, who provided me with daily supervision, strong scientific training and with stimulating scientific conversations, thus helping me produce high quality data.

I would also like to thank Dr. Edwige Moyroud with whom I had great pleasure collaborating and who helped me understand the scientific background crucial to this project and helped me largely at the beginning of this adventure. Her contribution as well as the one of May Yeo to the collection of the RNA material necessary for the transcriptomic analyses and the mutant screen was very appreciated.

I am also grateful to Dr. Qi Wang who has been essential to the bio informatic work performed on the transcriptomic data. Her help was always provided with patience and kindness and contributed to the acquisition of relevant bioinformatic skills.

I am extending my thanks to Amarnad Venkata Surapaneni who helped me with the acquisition of the adhesion data and with the technicalities of the production of epoxy replicas and Benjamin Droguet who helped me in measuring the wettability of these replicas.

I am also addressing special thanks to Matthew Dorling, who has shown a great deal of patience with me and always provided support when needed.

I am also thanking the members of the Glover group past and present who succeeded in making the lab a very pleasant place to work.

I extend a special thank you to my friends Alfonso Timoneda-Monfort, May Yeo, Philip Carella, Róisín Fattorini, Gabriela Doria-Ramirez, Chiara Airoldi who provided me with the necessary support along this adventure, and without whom my life in Cambridge would not have been as pleasant.

I am also very thankful for the Marie Skłodowska-Curie ITN generous funding which made that project possible and gave me very favourable conditions for the completion of this degree.

Finally, I thank my family from which I remained more apart than I had wished, yet supported me unconditionally along these four years apart, and so much more. This thesis is the result of their care and love for me for which I am extremely grateful.

Commonly used abbreviations

10,16-DHP: 10,16-Dihydroxypalmitic acid/10,16-Dihydroxyhexadecanoic acid

AP2: APETALA 2

bZip: Basic Leucin Zipper Domaine

cDNA: Complementary DNA

Cryo-SEM: Cryogenic scanning electron microscopy

DNA: Desoxyribonucleic acid

dNTPs: Deoxynucleoside triphosphate

EREBP: Ethylene response element binding protein

ERF: Ethylene response factor

FAE: Fatty acid elongase

FAR: Fatty acyl-coenzyme A reductase

gDNA: Genomic DNA

HB: Homeobox

HCT: Hydroxycinnamoyl transferase

IL: Independent line (applied to transgenic lines)

LB: Liquid Broth medium

LTP: Lipid transport protein

MADS: Transcripton factors of the MCM1 AGAMOUS DEFICIENS SRF family

MS: Murashige and Skoog medium

MYB: Myeloblastosis related transcription factor

PCA: Principal component analyses

PCI: Phenol chloroform isoamylalcohol

PCR: Polymerase chain reaction

PM: Plasma membrane

RI: Refractive index

RT-PCR: Reverse transcriptase PCR

SC: Super Cluster

semiQ RT-PCR: Semi quantitative RT-PCR

TEM: Transmission Electronic microscopy

VLCFA: Very long chain fatty acid

X-gal: 5-bromo-4-chloro-3-indolyl—D-galactopyranoside

Figure and table summary

Chapter 1: Introduction

Chapter 2: Material and methods

Chapter 3: Chemical analyses reveal the potential role of the cuticle chemistry in the buckling of the cuticle

Chapter 4: Transcriptomic analyses show two potential regulation pathways for the modulation of the stiffness of the cuticle in the proximal petal region

Chapter 5: Over expression of *HtnsLTP-like* and *HtSHN-like* genes is sufficient to alter the striation pattern

Chapter 6: Discovery of the *blue* and *madeleine* mutants reveals the importance of a proper cuticle layering for the buckling

Chapter 7: Structurally coloured cuticle shows a decrease in the gripping capacity of *Leptinotarsa decemlineata*

Table of content

Chapter 1 : Introduction

1.1 Overview

Evolving from a single ancestor that appeared between 250 and 125 million years ago, flowering plants are the most diverse group of plants with about 78% of plant species (approximately 300,000 out of 374,000 species) (Christenhusz & Byng, 2016; Sun et al., 2002; Taylor et al., 2006). Flowers are the reproduction structure and constitute a synapomorphy of the group. Flowers are usually characterized as an ordered series of 4 whorls consisting of sepals, petals, stamens and carpels. Stamens and carpels constitute the reproductive parts of the flower. Different variations of this model exist, but the minimal floral element distinguishing early angiosperms from gymnosperms is the production of a carpel (Specht & Bartlett, 2009). The staggering diversity of flowers is often correlated with their capacity of adaptation to the diversity of niche space offered by numerous different animal pollinators displaying many different sensory and behavioural traits. In response to selective pressure to attract pollinators, flowers have developed many strategies such as the production of volatile compounds, thermal patterns and visual cues amongst others.

Pigments usually provide a specific colour to the petal resulting from the reemission of light at a specific wavelength in every direction. The different pigments produced by plants are usually limited to flavonoids (such as anthocyanins) or betalains as well as carotenoids and chlorophylls (Młodzińska, 2009). A wide variety of these molecules can be produced in different combinations rendering a large array of colours along the visible light spectrum. However, deep blue and UV colours, both visible to pollinators are not efficiently reemitted by pigments making of structural colour a privileged strategy to produce short wavelength colours. Furthermore, pigment-based colours are static on the petal surface and may blend out in the background whereas structural colours relying on grating-like surfaces are usually angle dependant and may provide dynamic signals consisting of brief ‘flashes’ of colours or arrays of static colours to the passing pollinator (Stuart-Fox, et al., 2021). Interestingly, most structurally coloured flowers are also pigmented suggesting that petal structural colours may consist of an extra cue to pollinators without fully subsidising for pigments. Other types of blue-UV emitting

structures relying on multiple layering are abundant in tropical shade dwelling plants suggesting a potential role in shade adaptation (Jacobs et al., 2016).

Despite an appearing prevalence of structural colours in birds, insects and some fish and cephalopods, structural colours are also widely spread in plants, and more specifically in flowers. However, they often constitute more subtle visual signals tailored to insects' visions and may thus appear as seemingly less frequent in plants. Structural colours present on the surface of *Grielum humifusum*, *Paeonia mascula* and *Adonis aestivalis* are not easily visible to the naked eye, yet scanning electron microscopy has revealed the presence of nano-scaled striations on their petals producing iridescence (Moyroud et al., 2017). Often, the presence of an intense underlying pigmentation is sufficient to perturb our perception of iridescence, hiding it from the human eyes. Structural colours in plant are also not limited to flowers and have been reported in the Lycophyte *Selaginella willdenowii* and the shade dwelling plant *Begonia pavonina* (Jacobs et al., 2016; Thomas et al 2010) where once more, a strong background pigmentation interferes with our perception of structural colours. Structurally coloured plants may also evolve in remote locations like dense tropical forest and thus cannot be accessed easily, contributing to the seeming scarcity of structurally coloured plants.

In 2009 the iridescent properties of *Hibiscus trionum* petals were reported for the first time (Whitney et al., 2009). According to the observation angle of the petals, blue, green and yellow hues can be observed in the purple-pigmented region of the petal (fig. 1.1e). Transparent epoxy replica casts of the iridescent region of the *H. trionum* petal and of similarly iridescent regions of the tepal of the tulip 'Queen of the Night' were able to produce iridescent colours, showing that iridescence in these species is independent of pigments and a result of the surface properties of the flower. Scanning electron microscopy of these cuticle casts and petal sections revealed the presence of long ordered cuticular striations or ridges. A similar pattern was found in both the tulip and *H. trionum* petal cuticle (fig. 1.1d) (Whitney, Kolle, et al., 2009).

Transmission electron microscopy on the iridescent region of *H. trionum* petals showed ridges in the cuticle separated by 1.3 ± 0.3 μm, covering elongated flat cells (15 x 70 μm) (fig. 1.1d), thus forming a surface with many of the properties of a diffraction grating. Direct analysis of the petal with a goniometer-spectrometer later showed that the principal wavelength reflected from the surface

depends on the observation angle (a specific property of iridescence) and that a significant part of the reflected light is in the ultraviolet part of the spectrum (Vignolini et al., 2015).

Petal iridescence has since been demonstrated in many other species across different angiosperm orders, including *Penstemon barrettiae* (Lamiales), *Tulipa* 'Queen of the Night' (Liliales), *Leucocoryne purpurea* (Asparagales) and *Lathyrus aureus* (Fabales) (Moyroud et al., 2017). Iridescence thus appears to be the result of convergent evolution amongst angiosperms suggesting a significant role for iridescence. Previous studies have demonstrated that petal derived iridescence constitutes a visible signal for bumblebees (*Bombus terrestris*) and makes flowers more salient, without compromising search image formation, suggesting a role in signalling to pollinators (Whitney et al., 2016). Recent work suggests that the blue and UV portion of petal iridescence may be particularly significant as its relatively strong signal is conserved across different species and is sufficient to increase pollinator foraging capacity (Moyroud et al., 2017).

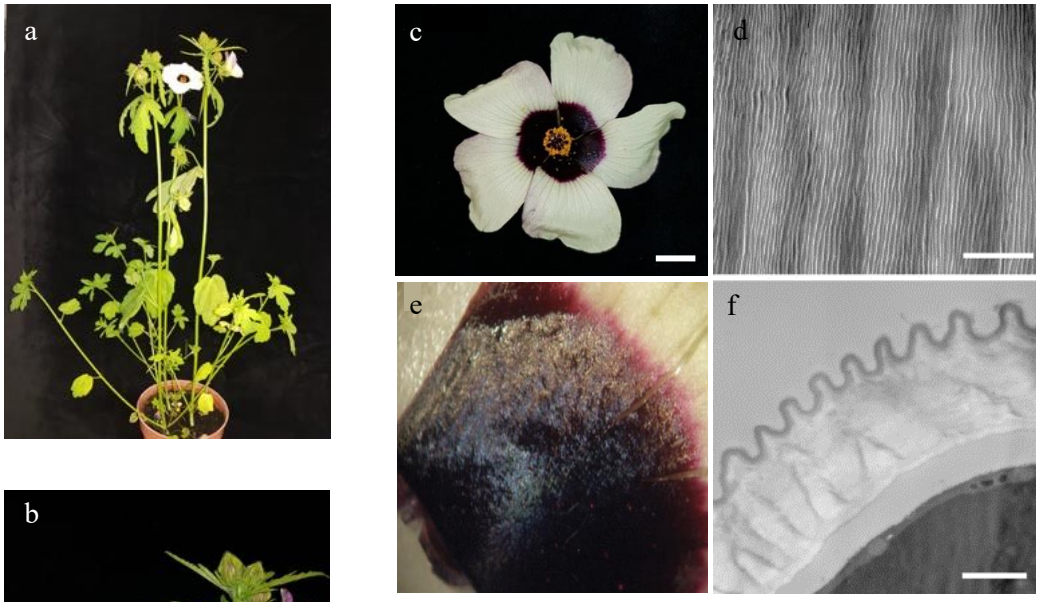

Figure 1.1: *Hibiscus trionum* plant and electron microscopy of the striated petal region. **(a)** *H. trionum* whole plant; **(b)** close up view of the flowers; **(c)** *H. trionum* flower (scale bar = 1 cm); (**d**) Scanning electron microscopy of the ridged region of *H. trionum* petals (scale bar = 20 µm) after Vignolini et al., 2015; **(e)** Zoom in the purple iridescent region of the flower where the iridescence produces blue, green and brown hues (from Whitney et al., 2009 copyright license 5095380539584); **(f)** Transmission electron microscopy of a cross section of the ridged region (scale bar: 2µm) (from Vignolini et al., 2015, license number 5095370937875).

The molecular pathways underlying the development of cuticle gratings remain however unclear. It is suggested that genes involved in the production of cuticle are also involved in its patterning. However, this does not reflect the complexity of the mechanisms at play necessary to generate structurally coloured semi-ordered nano-scaled ridges (C.A. Airoldi, Ferria, & Glover, 2019). Helped by the principles of material science and more specifically the theory of buckling (Bowden et al., 1998; Kourounioti et al., 2013), I have investigated the different molecular mechanisms that potentially contribute to the development of the physical constraints necessary for buckling, in an attempt to bridge the physics of buckling and its genetic regulation in *Hibiscus trionum*. Using chemical analyses, I also investigated whether differential chemical composition of the cuticle could explain potential difference in the cuticle properties of striated epidermises.

1.1.1 Structural colour

Structural colours can be understood as colours resulting from the interference of light with ordered nano-scaled structures. The cuticular striations on *Hibiscus trionum* petals can produce such colours which originate from the differential reflection of light according to its wavelength - usually in an angle dependent manner (iridescent) - independently from the inherent colour or opacity of the material.

Structural colours are widespread in nature and can serve a large variety of functions in plants and animals (Airoldi, Ferria & Glover, 2019). In animals they have been demonstrated to act as a means of targeted communication between individuals, often as part of a mating strategy without signalling to potential rivals or predators (Doucet & Meadows, 2009). It is also a means to produce brief and intense light signals to other individuals and may act as a deterrents to predators (Doucet & Meadows, 2009). In the lycophyte *Selaginella willdenowii*, it has been suggested that they serve a photoprotective role to prevent intense light from damaging young leaves (Thomas et al., 2010). In shade dwelling begonias, however, they seem to fill the opposite purpose as they help to capture light in the chloroplast and enhance photosynthesis (Jacobs et al., 2016). In flowers it is likely that structural colours serve as a visible cue to pollinators.

The capacity of pollinators to discriminate iridescent surfaces from non-iridescent surfaces was first assessed by Whitney et al. in 2009 using compact disk replicas and moulded plastic dyed with 3 different colours. Iridescent disks offered a reward whereas non-iridescent replicas contained a drop of bitter quinine hemisulfate salt solution acting as a 'punishment'. After 80 visits, it was observed that bumble bees visited iridescent disks more often than during the first visits, showing that bumble bees can detect iridescence. All the bees were then exposed to a new setting containing 5 iridescent and 5 non iridescent disks dyed with a previously unseen colour and bumblebees continued to visit iridescent flowers with about 83.4 per cent accuracy (Whitney et al., 2009).

Flower iridescence relies on imperfectly ordered ridges usually producing subtle structural colours when compared to iridescence produced by animals or CDs (Whitney, Kolle, et al., 2009). This could contradict the supposed attraction role of iridescence. Different colours of disks were produced with 2 different types of surfaces: an artificial grating like surface producing 'perfect' iridescence and a more subtle, 'imperfect', iridescence produced by castings of the tepals of the tulip 'Queen of the night'. It was demonstrated that bumblebees can detect red disks with floral -'imperfect'- iridescence faster than red disks with 'perfect' iridescence or the non-iridescent red disks, showing that 'imperfect' floral iridescence is sufficient to attract pollinators (Whitney et al., 2016). Furthermore, it was demonstrated that in the case of pigments that are more similar in hues within bee vision, 'perfect' iridescent disrupts the pigment-based identity of the target which was not found with 'imperfect' iridescence. Flower iridescence is then sufficient to increase visibility without compromising the pigmentation identity of the flower (Whitney et al., 2016).

Moyroud et al showed that in Malvales (*Hibiscus trionum*), Liliales (*Tulipa* 'Queen of the Night'), Ranunculales (*Adonis aestivalis*), Fabales (*Lathyrus aureus*), Myrtales (*Oenothera stricta*), Saxifragales (*Paeonia mascula*), Cornales (*Mentzelia lindleyii*), Lamiales (*Penstemon barrettiae*) and Asterales (*Ursinia speciosa*) the level of disorder in floral striations was correlated to a specific reflection of blue and UV light with the highest intensity between +25° and -25° perpendicular to the striations, regardless of differences in the aspect ratio of the ridges. This phenomenon is referred to as the 'blue halo' and directly results from relatively disordered cuticular ridges (Moyroud et al., 2017). The physical explanation for the selective reflection of blue-UV light in the context of plant nano-scaled

ridges has not been investigated yet, however, it can be suggested that the irregularity of the striations alter the diffraction angle of the different light wavelength, maintaining a preferential diffraction of the blue and UV lights within 25° perpendicular to the striations. Behavioural studies performed on bumblebees using artificial surfaces producing a 'blue halo' (reflecting preferentially blue and UV-light), a 'full' iridescence (reflecting with equal intensity the different wavelengths of light) or no iridescence at all showed that bumblebees are able to spot the 'blue halo' and that they were quicker to identify rewarding artificial flowers when they display a 'blue halo' than when they display 'full iridescence', consistent with the work of Whitney et al., 2016 (Moyroud et al., 2017). Finally, yellow, blue and black artificial flowers topped with disordered ridges (producing a blue halo) or not were produced. Foraging experiments using bumblebees showed that the blue halo improved their foraging time only when topping a black or a yellow substrate, suggesting that the 'blue halo' can increase contrast by providing the flower with a supplementary 'blue/UV' signal when the flower does not already have blue pigments (Moyroud et al., 2017).

Further studies investigated how the perturbation of the iridescent signal by the flower pigmentation influences the perception of bumblebees. Bumblebees trained with lightly pigmented iridescent disks displayed improved cognitive behaviour compared to those trained with intensely pigmented iridescent disks: They needed fewer visits to learn the visual discrimination between iridescent and non-iridescent targets, generalized faster their response to a novel object with a different colour but displaying the same iridescence and pigmentation level as previously learned, and exhibited better retention in early long-term memory tests performed 24 h after training (de Premorel et al., 2017).

Thus, floral iridescence has an important influence on pollinator behaviour and a may induce a change in plant/pollinator relationships, thus promoting reproductive isolation from other related flowers, inducing speciation.

Interestingly, the frequent and diverse occurrence of structural colours amongst plants and animals indicates that they have evolved repeatedly. As evoked above, grating like iridescence has evolved multiple times in flowering plants (noticeably amongst Malvales, Liliales, Ranunculales, Fabales, Myrtales, Saxifragales, Cornales, Lamiales and Asterales (Moyroudet al., 2017)). This

repeated evolution in evolutionarily distant orders argues that many different molecular pathways might be involved in the production of structurally coloured grating-like surfaces.

Thus, 2 types of structures are responsible for the production of iridescence in plants: multi-layered structures (thin film interference) and grating like surfaces (diffraction gratings).

The successive deposition of layers of different refractive index (RI) - usually alternating high and low RI layers - is a recurrent phenomenon in epidermal organs. If the layers' thicknesses are of the same order of magnitude as the wavelengths of light, they can induce interference leading to the specific reflection of a range of wavelengths or colours. The cuticle of leaf epidermal cells of *Selaginella willdenowii* has been shown to include four different layers of high and low RI, inducing thin film interference and resulting in a blue iridescent aspect to the leaves (Hebant & Lee, 1984). Similarly in the epidermis of *Chondrus crispus* (Rhodophyta) the succession of approximately 24 cuticular layers of different RI creates light interference resulting in the reflection of a vivid blue light (Chandler et al., 2015). Finally, it is worth mentioning the presence of iridoplasts (specialised chloroplasts) in shade dwelling begonias which can create light interference by a specific arrangement of their grana (Jacobs et al., 2016).

Bouligand structures in cell walls consist of multiple layers of oriented cellulose microfibrils arranged in such a way that the layers are stacked with a constant rotation angle forming a helicoidal structure. This type of structure has also been recorded in the scales of the ray-finned fish *Arapaima gigas* (pirarucu) (Zimmermann et al., 2013) and in beetle cuticle (Sharma et al., 2014). The fruit of *Margaritaria nobilis* displays a bright metallic blue colour that changes with its degree of hydration. This structural colour has been attributed to the presence of a Bouligand structure in the fruit cell walls. It has also been shown that this structure specifically reflects left-handed polarized light. The fruit of *Pollia condensata* also displays structural colours relying on Bouligand structures, however, the variation of the multilayer thickness from cell to cell induces the reflectance of red, yellow, green and blue light giving an over-all pointillist impression. The light reflection is also increased by the multi-layered cell wall structure which makes of each cell a curved micro-Bragg reflector, increasing its brightness. Finally, because the cell wall helicoid layering changes orientation from one cell to another, the over-all fruit can reflect both left and right polarised light (Vignolini et al., 2012).

The molecular pathways regulating the production of such structures and their ecological relevance in fruit remain unclear, however, it has been hypothesised, that the vivid colours of *Viburnum*

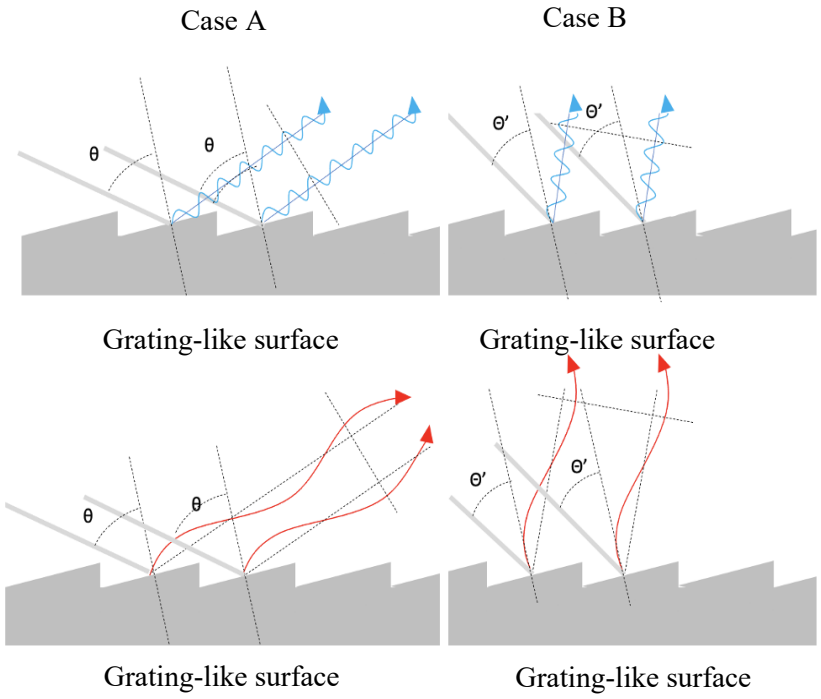

Figure 1.2: Cartoon explaining the iridescence produced by a diffraction grating. In case A, the 2 blue light waves reflected are separated by exactly 3 times the wavelength (3λ). Hence, they interact constructively and are visible to the observer. Conversely, the 2 reflected red light waves are separated by about 0.5λ, thus interact destructively and are not visible to the observer. In case B, the opposite happens. By changing the observation angle the blue light waves are now separated by 0.5λ and interact destructively: the blue light is not visible anymore. The red waves are shifted by 1λ. The interaction is thus constructive and red light is visible.

tinus fruit could act as an honest signal of nutritional reward to birds (Middleton et al., 2020) and that such coloration could also attract varieties of birds looking for brightly coloured objects to use in mating displays, thus helping with fruit dispersion (Vignolini et al., 2012).

Grating like surfaces as a source of structural colours are abundant in flowers as mentioned previously (Moyroud et al., 2017). They consist of a succession of crests and valleys, or grooves formed on the cuticle thus creating a 'grating-like' surface. When a light wave hits a small structure such as a hair or a hole of similar dimensions, light is scattered in every direction, this is called diffraction. Surfaces composed of a regular ordering of these micro elements will give as many events of diffraction as there are holes or hairs. On a grating like surface such as the cuticle of *Hibiscus trionum* petals, grooves and crests create a large amplitude of reflection angle at a single point resulting in the dispersal of light in every direction or diffraction. Depending on their wavelength and observation angle, some

waves will interact constructively or destructively (fig. 1.2), resulting in an angle dependent change of hue on the surface also known as iridescence.

The number of grooves per space unit and their amplitude defines the aspect ratio of a grating (amplitude divided by wavelength), and different aspect ratios harbour different optical properties at different angles of observation (Y. Yang et al., 2017). Analyses of the scattering spectrum of *A. aestivalis*, *O. stricta* and *H. trionum* grating-like structures revealed partial iridescence with a prevalent scattering of the blue-UV parts of the spectrum. Plant generated gratings are usually considered imperfect as they lack ordering (striations may not be perfectly parallel with one another) and regularity (variations in the aspect ratio of the striations can be observed). The light scattering properties of three replicas of *H trionum* cuticle produced with 0, 25 and 50 percent of the disorder observed in real flowers were studied. Results showed that proportionally more light was scattered in the blue-UV wavelengths and with increasing intensity as disorder increases (Moyroud, Wenzel, et al., 2017). This might explain the dominance of blue-UV scattered light in petal surfaces with grating-like structures. As mentioned earlier, this can play a major role in plant-pollinator interactions since it was demonstrated in the same study that the blue-UV light reflected by disordered ridges was not only visible to bumble bees (*Bombus terrestris*) but also allowed more efficient foraging than did either smooth or orderly ridged (ie perfectly iridescent) surfaces (Moyroud et al., 2017).

These striated surfaces are found on top of pigmented epidermal cells which absorb most light and only reflect a narrow range of wavelengths. The combination of the optical properties of the grating-like cuticle and the pigmented layer underneath result in the specific optical properties of the petal.

1.2 Development of nano-scaled ridges

1.2.1 **The theory of Nano-scale ridge formation**

The mechanism underlying the formation of cuticular ridges has not yet been confirmed. The ridges could result from ridges of the underlying cell wall, from the production of subcuticular mineral crystals, from folds in the cuticle or from epicuticular wax production (Koch et al., 2008). However, in *Hibiscus trionum*, the ridges appear to consist of simple folds of the cuticle (fig. 1.1f), and no ridging of the cell wall or subcuticular crystals have been observed (Vignolini et al., 2015). From a mechanical

perspective, the relative over-production of cuticle and sudden anisotropic growth in the longitudinal axis of a flat cell could cause a buckling phenomenon that could in theory produce such striations on the cuticle (Bowden et al., 1998; X. Huang et al., 2017; Kourounioti et al., 2013).

This theory proposes that the buckling mechanism can explain the formation of nanoscale wrinkles in response to two-dimensional compressive stresses on a thin stiff layer. Some *in vitro* experiments have shown that compressive stress applied to a thin and stiff layer of metal on top of a homogenous compliant polymer layer (PDMS) causes buckling (Bowden et al., 1998), thus suggesting the hypothesis of a vertically organized cuticle with a thin stiff cuticle layer topping a more compliant one. The contrast in mechanical properties of the two layers dictates the strain that is necessary to produce wrinkles (Chen et al., 2014). Furthermore, unpublished results from the Glover team have demonstrated the buckling capacity of stage 3 *Hibiscus trionum* petals under artificial longitudinal stretching applied with an extensometer, supporting the buckling theory (Airoldi et al., 2021). Layering of the cuticle, as well as differential growth, therefore appear as the two parameters important in the induction of buckling. Another important element is the stiffness of the substrate and the upper layer, described by the Young's modulus. Previous studies in engineered systems have suggested that the aspect ratio of the ridges arising from buckling is directly proportional to the Young's modulus of the substrate (Stafford et al., 2004). It appears that the buckling of *Hibiscus trionum* cuticle, and hence the production of nanoridges, is a consequence of the layered structure of the petal cuticle, its stiffness and the 2-dimensional forces exerted by the growth of the petal epidermal cells.

Kourounioti et al. proposed in 2013 a model predicting the formation of nano-scale ridges on conical cells considering the cuticle production rate, or cuticle thickness (β), and the orientation and the strengths of the 2-dimensional stresses (λ_1 and λ_2) (fig. 1.3). In figure 1.3, only four graphs representing four different cuticle production rates (or values of β) are displayed, but the β function is of course continuous, just like the λ terms. This model allows the prediction of wrinkling patterns if the cuticle thickness and stretch terms are known. Four different patterns were predicted according to the stretches applied (λ_1 and λ_2): domain I is smooth and consists of a failure of the buckling, domains II and III describe parallel striations that coincide with the development of patterns holding optical properties on *Hibiscus trionum* flat epidermal cells, and domain IV displays an isotropic buckling (without any

privileged orientation axis of the striations). The prevalence of these four domains highly correlates with the amount of cuticle produced (β), which suggests that cuticle production is a critical parameter for the buckling. As shown in fig. 1.3, cuticle production rates (β) inferior to 1 correlate with a reduction of domains II and III. Therefore, the λ_1 and λ_2 parameters must reach higher values separately to force the buckling. Cuticle synthesis thus appears as necessary for the proper buckling and appears as prevailing over the 2-dimensional constraints. A β cuticle production rate superior or equal to 1 appears as the most favourable condition of the buckling, and for β = 1, conditions appear optimal to produce ordered striations. Furthermore, when the constraints are equal or similar ($\lambda_1 = \lambda_2$), oriented buckling cannot be achieved suggesting that anisotropic growth is necessary to achieve striations displaying optical properties.

Analyses were carried out on tulip, *H. trionum*, *Antirrhinum majus* as well as *Arabidopsis thaliana* transgenic lines in which the cuticle regulator *SHINE1* was either silenced or overexpressed, and *A. thaliana* lines in which either *SHINE2* or *SHINE3* were downregulated (fig. 1.3). This model was able to predict the behaviour of the cuticle in each of these examples.

This mechanical model represents our current best hypothesis to explain cuticle folding in iridescent petals. However, even if these physical properties do explain entirely or partially the presence of striations on the cuticle, they do not explain fully the patterns observed or reveal the underlying molecular mechanisms.

To date, cuticle biosynthesis regulatory genes have been implicated in the formation of surface nanoridges in *Solanum lycopersicum* and *Arabidopsis thaliana*, through studies exploring the function of genes involved in cuticle deposition. Genes encoding MIXTA-like transcription factors MYB106 and MYB16 were shown to be expressed with the *WAX INDUCER 1/SHN1* (*WIN1/SIN1*) genes responsible for waxy substance biosynthesis regulation in *Arabidopsis thaliana,* and their expression was correlated with nanoridge production on the cuticle. Over expression of *MYB106* was even associated with ectopic nanoridge formation (Oshima et al., 2013). MIXTA-like proteins were also shown to regulate cuticle biosynthesis in *Solanum lycopersicum.* The activity of CUTIN SYNTHASE 2 (CUS2) protein was demonstrated to be implicated in striation maintenance on the sepal cuticle in *A. thaliana* (Hong et al., 2017).

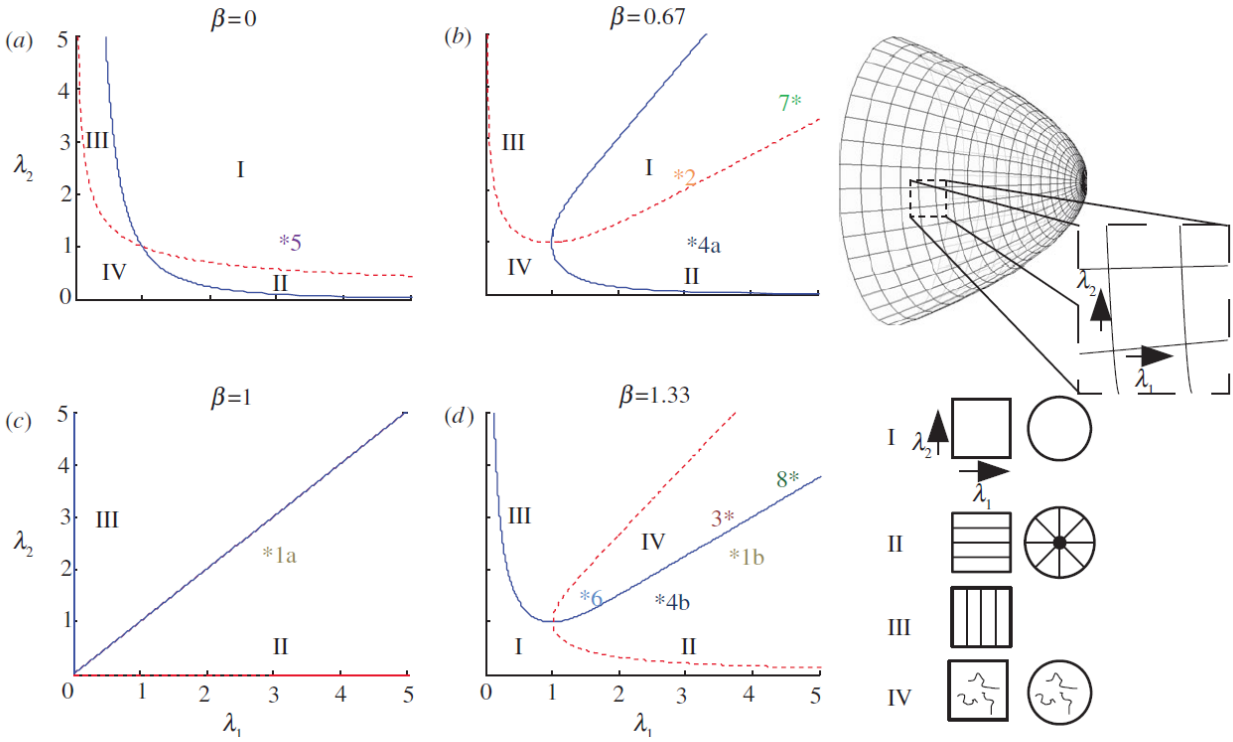

Figure 1.3: Model predictions of cuticle ridge patterns. **(a–d)** The dependence of the predicted patterns on λ_1 and λ_2, which are the stretches parallel and perpendicular to the long axis for rectangular cells, and in the radial and azimuthal directions for conical or domed cells, respectively, for a number of different values of the cuticle production rate β (β < 1 corresponds to under-production; β > 1 to over-production; the case β = 0 is representative of cases in which the growth-induced stress is weak relative to elastic stress in the cuticle layer). Regions I–IV correspond to patterns of the type illustrated in the right-hand diagram (for rectangular and domed cells). Asterisks in (a–d) mark representative parameter values for each of the following cases: 1a, *H. trionum* (ridged region); 1b, tulip abaxial petal surface; 2, *H. trionum* (junction between the purple and the white smooth region); 3, tulip adaxial petal surface (discontinuous ridges); 4a, (Arabidopsis ridged conical cell regions); 4b, *Antirrhinum* (ridged conical cell regions); 5, Arabidopsis 35S:miR-SHN1/2/3 (smooth conical cells); 6, *Antirrhinum mixta* mutants (flattened conical cells); 7, WT Arabidopsis leaf (smooth flat cells); 8, Arabidopsis leaf 35S::SHN1 (patchwork of ridged flat cells). From Kourounioti et al., 2013, license number 1128332-1

1.2.2 The Hibiscus trionum model

Our main model in this work is *Hibiscus trionum,* which is part of the Malvaceae family (along with the commercially important *Theobroma cacao* (cocoa) and *Gossypium* sp. (cotton)). *H. trionum* encompasses several varieties from different parts of the world that present slightly different floral forms, including details of their petal shape, pigmentation and iridescence (Murray et al., 2008). Several of them are studied in this Thesis: *Hibiscus trionum* var. New Zealand, Netherlands and CUBG (Cambridge University Botanic Garden) are all structurally coloured varieties while *Hibiscus trionum* var. Botswana is not structurally coloured (see fig. 3.1). *Hibiscus trionum* is an annual herb widely spread in temperate, tropical and subtropical regions, native to the Old World and cultivated as an

ornamental plant worldly. It usually stands 30-150 cm tall with flowers of 2.5-4.0 cm in diameter (fig. 1.1).

Flower development in *H. trionum* can be divided into five different stages for gene expression and functional analyses, according to the orientation of the epicalyx and the growth of the corolla (fig. 1.4a, Moyroud et al, in preparation). Previous developmental analyses have shown that the striations only appear at stage 4 in the purple region of the petal and increase in number and aspect ratio until stage 5. Meanwhile in the white part of the petal, cells differentiate into conical cells topped with an evenly smooth cuticle (fig. 1.4b). Further detailed analyses with optical microscopy have revealed a gradual appearance of striations during stage 3, leading to its subdivision into substages a, b and c reflecting a gradient of striation starting from smooth cells at stage 3a, to the emergence of partially striated cells at stage 3c (fig. 1.4c).

H. trionum can be easily grown in a glass house at a large range of temperatures and takes about 6 to 8 weeks to grow from seed to flowers.

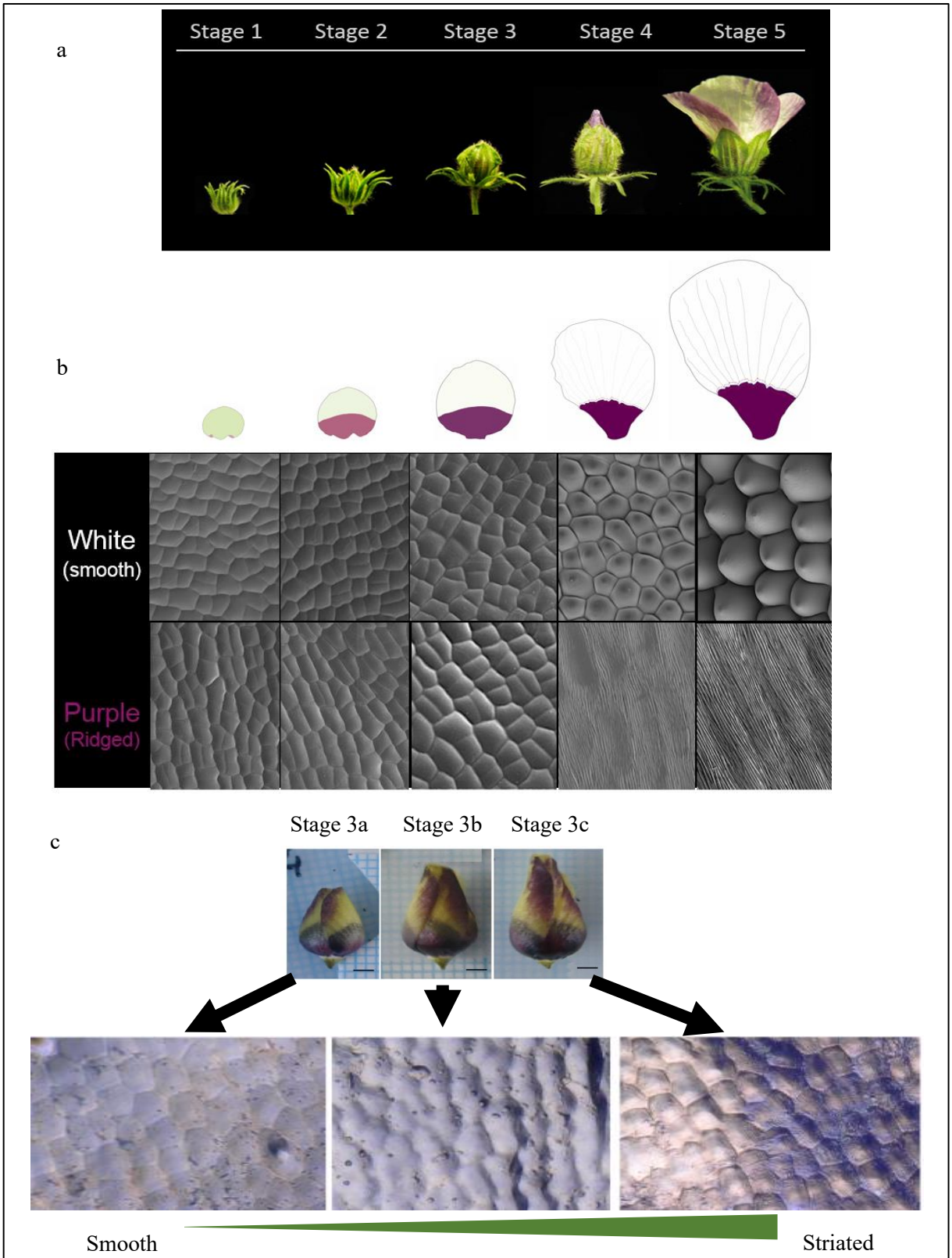

Figure 1.4: *Hibiscus trionum* flower development and formation of striations. **(a)** Pictures of the 5 developmental stages of *H. trionum*. **(b)** Cartoon of the petal development along with SEM images of the smooth and ridged regions on *Hibiscus trionum* petal for each of these developmental stages (Edwige Moyroud's unpublished work**)**; **(c)** Division of the stage 3 developmental stages into substages 3a, 3b and 3c, here presented without calyx and epicalyx, along with optical microscopy of the purple region at these 3 different stages illustrating the gradual development of striations resulting in the appearance of blue hues**.**

The *H. trionum* genome is composed of 14 pairs of chromosomes, and the CUBG line used for molecular work is diploid (2 n= 28). The genome is approximately 12 times bigger than the *Arabidopsis thaliana* genome (2C = 3.85 pg ≈ 1.9 Gbp/C for *H. trionum versus* 135 Mbp for *A. thaliana*), which means it is rather small compared to many other plants. The *Hibiscus trionum* genome had not been sequenced and assembled at the time of this project, but the phylogenetic proximity of *Theobroma cacao* and the *Gossypium* genus, both with fully sequenced genomes, provides some support in terms of gene and transcript identification. Furthermore, previous work in the lab has established solid molecular techniques for *Hibiscus trionum* transformation with *Agrobacterium tumefaciens* as well as for DNA and RNA extraction.

Despite an incomplete knowledge of the molecular mechanisms underpinning the production of a grating like surface on the cuticle of *H. trionum* petals, previous unpublished molecular work by the Glover group has implicated a few genes in the development of such structures. cDNA sequences of *H. trionum* and *A. thaliana* genes were thus placed under the control of a double CaMV35S promotor and occasionally fused to the transcriptional activator VP16 (from the *Herpes simplex* virus transactivator) or the transcription repressor SRDX (also known as EAR-repression domain: ERF-associated amphiphilic repression) (table 1.6 and see fig. 3.2) (SRDX and VP16 sequences are available in annex IV).

Three *SHINE* (SHN) genes of the type-A and type-B subgroups were found to play a central role in the regulation of the cuticle production in *A. thaliana* (Aharoni et al., 2004; Shi et al., 2011) (fig. 1.5). In *H. trionum* 3 *SHINE* genes were also found. Two of them were identified as type-C *SHN* genes (*HtSHN3* and *HtSHN2*) and one as a type-B *SHN* gene (*HtSHN1*). The *Hibiscus trionum SHN3* gene was found as the most highly expressed of them in the proximal petal region (unpublished results from Edwige Moyroud), suggesting a role in the development of striated cuticle. The cDNA of *HtSHN3* (sequence available in annex III) was therefore isolated and used to produce *35S:HtSHN3-VP16* and *35S:HtSHN3-SRDX* transgenic lines to alter the cuticle thickness and chemistry of the petal cuticle in an attempt to modulate the buckling conditions, and test our model predicting cuticle striations (table 1.6, see also fig/ 3.2).

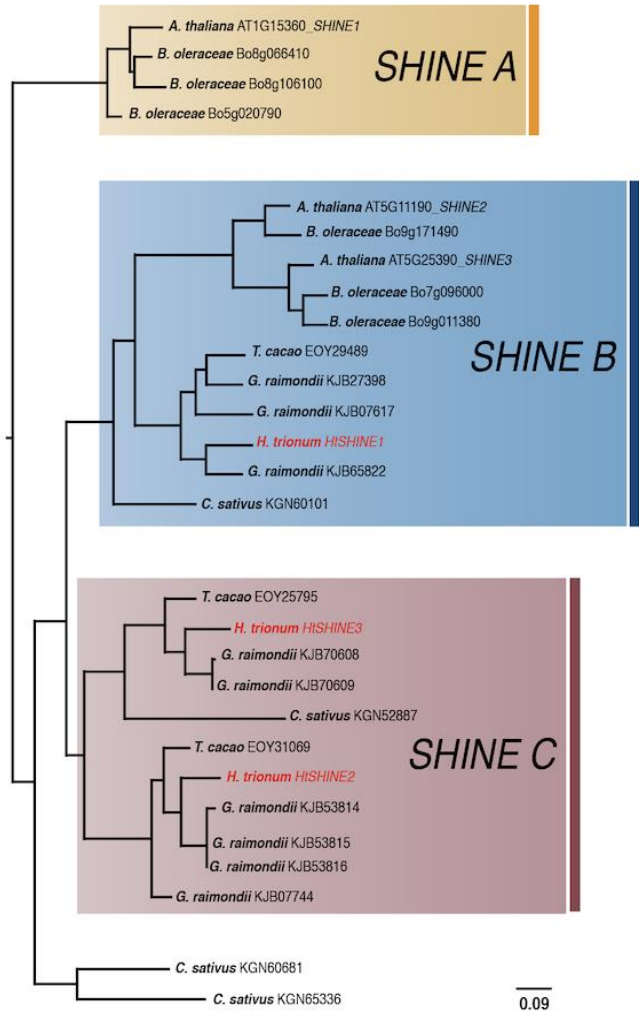

Figure 1.5: Phylogeny of the *SHINE* clade of the AP2/ERF transcription factor family in Brassicales-Malvales. Malvaceae: *G. raimondii*, *T. cacao* and *H. trionum*. Brassicaceae: *A. thaliana*, *B. oleraceae*. Three major subgroups were identified. Another rosid, *C. sativus* (Cucurbitales) is used as outgroup. From Moyroud et al. in preparation.

Quantitative PCR analyses revealed a silencing of the potential downstream targets of *HtSHN3* (*cyp77a6-like1* and *GDSL-like*) in a *35S:HtSHN3-VP16* line suggesting that the *35S:HtSHN3-VP16* construct resulted in an unexpected dominant negative (data from Chiara Airoldi, not shown). Both *35S:HtSHN3-VP16* and *35S:HtSHN3-SRDX* transgenic lines resulted in a complete loss of striation (table 1.6 and fig. 3.2)

In order to alter the chemistry of the cuticle, 4 other over-expressing transgenic lines have been produced: *35S:AtDEWAX, 35S:HtCD1.1, 35S:AtCDEF1* and *35S:HtMIXTA-like1*.

The *DEWAX* gene codes for an AP2/ERF-type transcription factor that has been shown to negatively regulate wax biosynthesis in *A. thaliana*. (Go et al., 2014). In *H. trionum*, its over expression induced a loss of striations between the proximal adaxial epidermal petal cells.

The cutin synthase CD1.1 is a GDSL esterase lipase protein that was shown to catalyse the esterification of 2 cutin monomers in the cuticle of tomato fruit (Yeats et al., 2012). Hence, modulation of its expression induces changes in the reticulation of the cutin network by producing more or less ester-bonds between the cutin monomers. The mechanical properties of the cuticle can thus be altered by modulation of *HtCD1.1* expression. Over expression of *HtCD1.1* the over expression of *CD1.1* in *H. trionum* resulted in an almost-complete loss of striation (table 1.6 and see fig. 3.2).

The *CUTICLE DESTRUCTION FACTOR* or *CDEF1* encodes for an esterase that also belongs to the GDSL esterase/lipase family that was shown to degrade the cutin network in *A. thaliana* and its over expression induces defects in cuticle function (Takahashi et al., 2010). In this way, the catalytic activity of CDEF1 can be understood as opposite to the one of CD1.1. Its over expression in *H. trionum* led to the presence of patches of smooth cells in the proximal adaxial petal region (see fig1.6 and 3.2).

The MIXTA transcription factor was initially chosen for its capacity to induce the production of conical cells on the epidermis of *Antirrhinum majus* (Glover et al., 1998). The primary objective behind the construction of a *35S:MIXTA-like* transgenic line was to change the cell shape in the proximal part of the petal cuticle of *H. trionum* in order to assess whether the tabular cell shape of the epidermal cells was determinant in the development of striations. Meanwhile other studies have shown the role of MIXTA-like genes in the production of cuticle (Oshima & Mitsuda, 2013; Oshima et al., 2013). The over-expression of *HtMIXTA-like1* in *H. trionum* did not result in any alteration of the petal cell shape. However, its over expression did not affect cell shape and only resulted in a loss of striations in the overall proximal adaxial petal epidermis with faint striations occasionally present in-between epidermal cells.

Transgenic line	cDNA	Nature	Organism	Reported function in other organisms	Phenotype in H. trionum
35S:HtSHN3-VP16	*SHN3/WIN1*	AP2/EREBP transcription factor	*H. trionum*	Transcription factor regulating the production of cuticle and more specifically the *LACS*, *DCR, GPAT6* and *GDSL* genes in *Solanum lycopersicum* (shi et al., 2013).	Absence of striations
35S:HtSHN3-SRDX	*SHN3/WIN1*	AP2/EREBP transcription factor	*H. trionum*	Transcription factor regulating the production of cuticle and more specifically the *LACS*, *DCR, GPAT6* and *GDSL* genes in *Solanum lycopersicum* (shi et al., 2013).	Absence of striations
35S:AtDEWAX,	*DEWAX*	AP2/ERF-like transcription factor	*A. thaliana*	Regulates cuticle production and regulates *CER1* and *LACS2* genes (Go et al., 2014).	Absence of striation at cell junctions
35S:HtCD1.1	*CD1.1*	GDSL esterase lipase	*H. trionum*	Cutin polymerization/ cutin monomer esterification (Yeats et al., 2012).	Scarce striations limited to cell junctions
35S:HtMIXTA-like1	*MIXTA-like1*	*MIXTA-like* transcription factor	*H. trionum*	Cell shape and cuticle synthesis (Glover et al., 1998; Oshima et al., 2013; Oshima and Mitsuda 2013)	Scarce striations limited to cell junctions
35S:AtCDEF1	*CDEF1*	GDSL esterase lipase	*A. thaliana*	Acts as a cutinase and hydrolyses of the ester bonds between cutin monomers (Takahashi et al. 2010).	Striations in patches

Table 1.6 Summary table of the different transgenic lines produced by Edwige Moyroud and their resulting phenotypes

None of these observations are entirely surprising; it is apparent that any perturbation in cuticle production may also disturb the formation of ridges. However, from this recent work, it seems that the amount of cuticle produced is correlated with the capacity to produce nanoridges. Qualitative aspects of the cuticle also seem important in the production of ridges. A perturbation of the cutin network is likely to alter its elastic properties and its ability to buckle, as seen for the *AtCDEF1* over expressing lines and similarly with the proportion of waxes in the *AtDEWAX* transgenic line. Altogether a tight regulation of cuticle production is necessary to the proper production of ridges.

The longitudinal growth of cells is also likely to play a role in the build-up of 2-dimensional mechanical constraints and might influence buckling. Preliminary work from the Glover lab

successfully modified cell-size in striated regions using hormones and drugs, resulting in a change in the 2-dimensional constraints λ_1 and λ_2. Despite a successful modification of cell size (+81% and -131% along the longitudinal axis and +24% and -28% along the width axis), no alteration to the striation pattern was observed (unpublished results of Halliwell 2016). It is possible that cuticle buckling is rather robust to the modification of the mechanical constraints, suggesting a more significant role for the properties of the cuticle in the induction of buckling.

In *Hibiscus trionum* the nanoridges remain limited to a very precise area of the petal, raising the issue of the spatial regulation of cuticle synthesis and growth regulation along the petal. It is also very likely that some boundary-determining factors are involved in specifying the limit between ridged and smooth regions. Since there is an almost perfect overlap of the pigmented region, the structurally coloured region and the flat cell domain, similar factors are likely to be implicated in the patterning of these regions.

Structural colours in *Hibiscus trionum* likely arise from a complex of transcription factors regulating the oriented growth of epidermal cells, as well as a tight regulation of the cuticle properties. They may also involve morphogens limiting the extension of structurally coloured cuticle to the centre of the flower.

1.2.3 Cuticle nature and formation, a substrate for ridge formation

1.2.3.1 Cuticle composition

All terrestrial plants produce a cuticle on their aerial parts. The acquisition of plant cuticle was a key evolutionary adaptation in the colonization of the aerial environment, as it prevents water loss. This cuticle consists of a non-cellular structure organised into three different layers. The outer layer is formed by epicuticular waxes only, the innermost one comprises both cuticular compounds and cell wall polysaccharides, and the middle one, also referred to as the cuticle proper, mostly contains cutin, cutan and intracuticular waxes (fig. 1.7). On the structural level, the cuticle proper can be divided into a network of cutin and cutan with numerous loose elements.

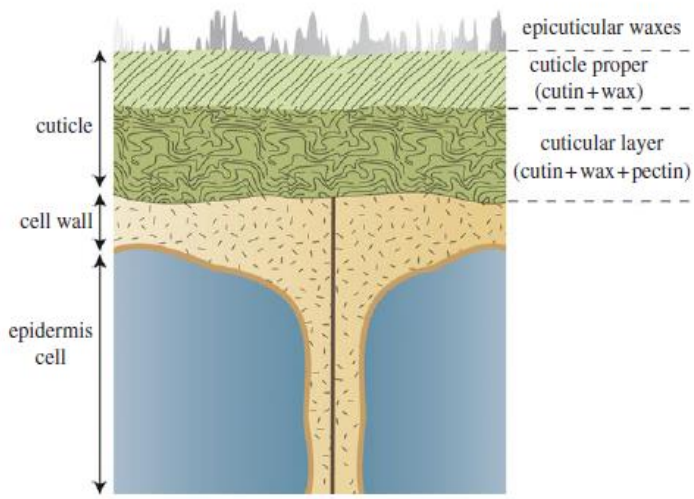

Figure 1.7: Cartoon representing the organisation of the plant cuticle. Epidermal cells produce the cuticle, known to contain cutin, cutan, waxes and polysaccharides (such as cellulose and pectin). From Kourounioti et al., 2013 license number 1128332-1

The methanolysis of 7 different plant cuticles revealed that cutin consists of an insoluble polyester-biopolymer made from the esterification of the hydroxyl and carboxyl groups of C_{16} and C_{18} aliphatic acids. The majority of cutin monomers are made of ω-hydroxy acids with 1, 2 or 3 hydroxyl functions and an occasional epoxy group. Usually, only 5% of the cutin monomers are saturated ω-hydroxy acids, alkanoic acids and alkan-1-ol. Coumaric acid, an aromatic compound, is consistently present in the cuticle but accounts for less than 1% of the cuticle composition. Glycerol has also been revealed as an important constituent of cutin with up to 14% of the monomers released from cutin methanolysis (Graça et al., 2002). In *Arabidopsis thaliana* more recent studies also confirmed the dominant role of glycerol in the formation of the cutin polymer by the formation of ester bonds between glycerol and dicarboxylic fatty acids, another component of the cuticle (Yang et al., 2016).

De-esterification of the cuticle usually leaves behind another type of polymer resistant to ester hydrolysis: cutan. The composition and the type of bonds forming the cutan network remain unclear due to the difficulty in attempting to hydrolyse and solubilise it. Tetramethylammonium hydroxide (TMAH) thermochemolysis of the cutan fraction of *Agave americana* revealed the presence of C_5 to C_{35} straight hydrocarbons chain of aliphatic nature (95% of carbon species recovered), alkenes and fatty acid methylesters. In smaller proportions aromatic elements and long polymethylenic chains were also detected (Deshmukh et al., 2005; Mckinney et al., 1996). Mckinney et al. (1996) also suggested that the absence of polysaccharide in their analyses indicated that the cutan network is located further away

from the cell wall polysaccharides. The non-de-esterifiable character of cutan suggests the presence of other types of bonds, forming with the cutin polymer a network that can withstand constraints and confer mechanical properties to the cuticle.

The term waxes is used to designate the elements of the cuticle that can be extracted with low polar organic solvents. Waxes can make up from 20% to 60% of the total cuticle mass (Samuels et al., 2008). They consist of a large variety of elements of different structures (aromatic or linear) and different natures (primary and secondary alcohols, di-alcohol, ketones, diketones, alkenes and esters) (Riederer & Muller, 2006) that typically range from 20 up to 34 carbon residues (Samuels et al., 2008). Fully saturated aliphatic acids make up most of the waxes, and, in contrast to cutin and cutan, do not form a reticulated network. A variety of non-waxy compounds can also be found embedded in the wax fraction such as pentacyclic triterpenoids, triterpenoid derived ethers (Riederer et al.,2006), phenylpropanoids and flavonoids (Samuels et al., 2008).

Waxes are present through the entire cuticle. Some are integrated into the cutin and cutan network and are referred to as 'intra-cuticular waxes' whilst others are deposited on the outermost part of the cuticle and are referred to as epi-cuticular waxes. Intra- and epi-cuticular waxes can differ in their relative abundance of cyclic and acyclic compounds (Buschhaus & Jetter, 2011), suggesting regulated transportation of wax compounds throughout the cuticle. Epicuticular waxes are often arranged into crystals. These wax crystals can be responsible for the formation of precise structures and patterns, as on the lower leaves of *Heliconia collinsiana* where they form 'chimneys' around stomata (Koch & Ensikat, 2008). However, in *Hibiscus trionum* transmission electron microscopy of a cross-section of the purple region revealed that the nano-scaled ridges are part of the cuticle proper, and not due to organised crystallization of waxes (fig. 1.1f).

Closer to the primary epidermal cell wall, under the cuticle proper, a layer referred as a cuticularized cell wall can be found. It consists usually of a mixture of cuticular elements including cutin, cutan and waxes, and cell wall components such as cellulose, pectin, and phenolic compounds (Heredia-Guerrero et al., 2014; Samuels et al., 2008).

Proteins are also present in the entire cuticle and cell wall where they take part in cutin polymerization or hydrolysis, and cuticle component transportation. Such proteins will be described further in section 1.2.2.2.

The structure of the cuticle is usually conceptualised and represented in terms of regular and almost perfectly delimited layers (fig. 1.7). However in real tissues the structure and thickness of the different layers is variable in the same tissue, especially at the junctions between cells (Fernández et al., 2016; Heredia-Guerrero et al., 2014). In *Hibiscus trionum* the cuticularized cell wall appears to be the largest section of the cuticle, with a reduced cuticle proper (< 500 nm) without any epicuticular wax crystals and a very thin primary cell wall layer at the very base of the cuticle (fig. 1.1f, and fig. 5.1).

The relative abundance of the different constituents of the cuticle and their organization determines the chemical and mechanical properties of the cuticle, and ultimately its ability to buckle and produce nano-scaled ridges.

1.2.3.2 Cuticle biosynthesis

Wax and cutin biosynthesis start with the production of $C_{16/18}$ fatty acids in chloroplasts and leucoplasts. These $C_{16/18}$ fatty acids result from the condensation of an acetyl~CoA with a C_2 moiety and a malonyl-CoA carrier protein (ACP). Fatty acid synthases (FASs) then catalyse reduction and dehydration reactions to release an acyl molecule 2-carbons longer than the original one. $C_{16/18}$ fatty acids then undergo a series of modifications in the endoplasmic reticulum (ER) to form either cutin monomers or waxes (Samuels et al., 2008).

Cutin monomers are produced in the ER by various oxygenations of $C_{16/18}$ fatty acids resulting in the production of diverse cutin monomers associated with different functional groups such as hydroxyl, carboxyl, carbonyl, ketoyl and cyclic ether.

$C_{16/18}$ modification is a multiple-step process requiring activation by acyl~coA (Fich et al., 2016). Deficiency in LACS1 (Long-chain Acyl~CoA Synthase) and LACS2 proteins in *Arabidopsis thaliana* was correlated with a higher permeability of the cuticle, organ fusion and increased sensitivity to drought, suggesting a role in cuticle biosynthesis (Weng et al., 2010). LACS3 has also been suspected

as potentially involved in cuticle synthesis, but there is insufficient evidence to confirm this yet (Fich et al., 2016).

Interestingly, the *Arabidopsis thaliana defective in cuticular ridges* (*dcr*) mutant showed a loss of ridges on the cuticle of the abaxial epidermal cells of the petals as well as a depletion in 9/10,16-dihydroxypalmitic acid (10,16-DHP) (also known as 9/10,16-dihydroxyhexadecanoic acid), a C_{16} cutin monomer which constitutes a large proportion of *A. thaliana* cutin (Panikashvili et al., 2009). *In vitro* catalytic essays suggest that DCR plays an important role in the hydroxylation of mono-hydroxylated hexadecenoic acid, although the actual catalytic mechanisms remain unclear (Molina & Kosma, 2015).

Proteins of the large cytochrome p450 family (known as CYP proteins) are involved in most oxidation events of $C_{16/18}$ fatty acids in the endoplasmic reticulum (Fich et al., 2016; Halkier, 1996; K.-H. J. Ling & Hanzlik, 1989). CYP86A proteins are involved in the ω-hydroxylation and carboxylation of fatty acids, whilst CYP77A proteins are involved in mid-chain hydroxylation. *cyp86a2,-4* and *-8* mutants have been associated with altered cuticle composition and *cyp86a2* and *-8* mutants also showed defects in cuticle structure (Fich et al., 2016).

A T-DNA insertion mutant of *AtGPAT6*, which codes for a glycerol phosphate acyltransferase, resulted in a drop of 58% of the amount of 10,16-dihydroxypalmitate (10,16-DHP) and a loss of striations in *A. thaliana* petal cuticle (Yonghua Li-Beisson et al., 2009). This suggests the importance of glycerol ester bonds with 10,16-DHP for the formation of a functional cuticle and nano-scaled ridges. Similarly to *cyp86a2* and *-8* mutants, it was also shown that the organization of the cuticle was highly altered in *gpat6* mutants of *Arabidopsis thaliana*, which confirms the idea that deficiency in the production of 2-(10,16-dihydroxipalmitate)-glycerol has consequences for the structure and chemistry of the cutin network (Mazurek et al., 2017).

A double mutant of *cyp77a6* and *gpat6* showed phenotypes similar to the *cyp77a6* single mutant, demonstrating that *cyp77a6* is epistatic to *gpat6* in the cuticle biosynthesis. However, the *dcr* and *gpat6* double mutant resulted in stronger developmental abnormalities than either parent, suggesting that they function in different pathways in the production of cutin (Mazurek et al., 2017). It has also been reported that the DCR protein has glycerol acyltransferase activity, suggesting a putative partial redundancy with GPAT6 (Rani et al., 2010).

a

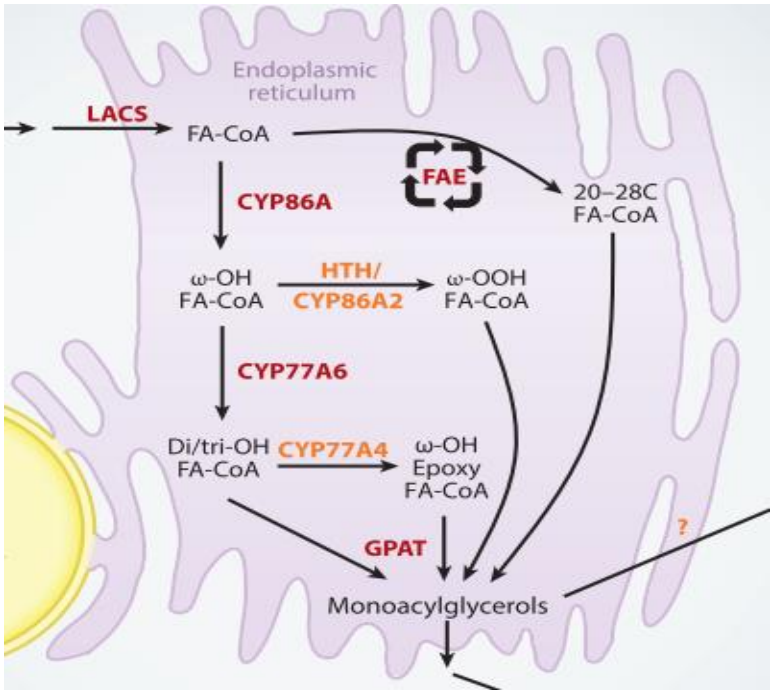

b

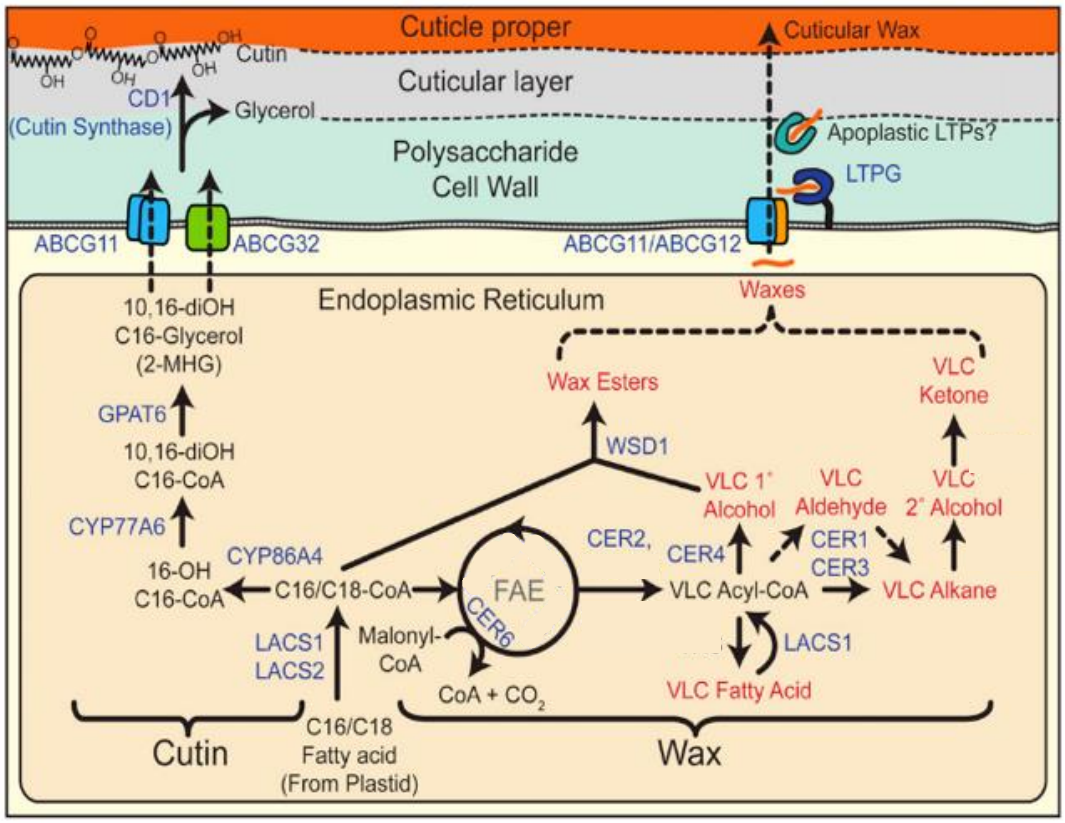

Figure 1.8: Illustration of the possible synthesis and secretion pathways of cuticular compounds. (**a**) Illustration of the sequential activity of LACS, CYPs and GPAT enzymes in the modification of fatty acids into cuticle monomers. From Fich et al., 2016, license number 1128359-1. (**b**) Global illustration of the cuticle biosynthesis mechanism from Yeats and Rose 2013, license number 5095421148698.
Abbreviations: C, carbon; CoA, coenzyme A; FA, fatty acid; FAE, fatty acid elongase complex; FAS, fatty acid synthase complex.

Sequential action of the CYPs and GPAT proteins has thus been proposed to explain the production of mature cuticle monomers (acyglycerols) from acetyl~CoA fatty acids (fig. 1.8a).

Wax synthesis begins with the elongation of $C_{16/18}$ fatty acids into very long chain fatty acids (VLCFAs): $C_{16/18}$ fatty acids are released from the Acyl Carrier Protein (ACP) and activated to coA-thioesters at the ER membrane, then fatty acid elongases (FAEs) act as fatty acid synthases and elongate fatty acids two by two. The resulting C_{28}, C_{30} and C_{32} fatty acids are then processed into alkanes, secondary alcohols or ketones and the $C_{28/26}$ fatty acids can be condensed with a C_{16} fatty acid to form wax esters (Samuels et al., 2008). Several proteins implicated in waxy compound biosynthesis in *Arabidopsis thaliana* have already been identified. Mutation of the β-ketoacyl-coA transferase CER6/CUT1 (in *eceriferum* mutants of Arabidopsis) was linked to an accumulation of C_{24} acyl groups and a defect in C_{28} and above fatty acids, suggesting a crucial role in wax production (Fiebig et al., 2000). CER4 and WSD (Wax Synthase/Diacylglycerol transferase) proteins cooperate to produce wax esters: CER4, an alcohol-forming fatty acyl-coenzyme A reductase (FAR), hydroxylates C_{24} and C_{26} fatty acids while WSD is responsible for the production of esterified fatty acids by condensing 2 hydroxyl groups (Rowland et al., 2006) (fig. 1.8b).

1.2.3.3 Cuticle compound transportation

The method of transportation of wax and cutin monomers from the ER to the extracellular environment remains unclear. On the basis of circumstantial evidence, and by analogy with other cellular lipid transportation processes, two transportation routes to the plasma membrane have been proposed. The first one consists of the secretion of wax through the Golgi-mediated vesicular traffic secretory pathway, and the second supposes a direct transfer at ER and plasma membrane (PM) contact sites (fig. 1.8b) (Domínguez et al., 2015; Kunst & Samuels, 2003).

Regarding the first hypothesis, very little data effectively supports the idea that the secretion of cuticle is mediated by the canonical vesicular secretion pathway (Yeats & Rose, 2013). However, based on the *in vitro* properties of cutin monomers, transmission electron microscopy and antibody mediated detection, it has been shown that fatty acids can travel from the golgi to the plasma membrane in the form of lipid droplets also called cutinsomes characterised by a center of self-esterified di-hydroxyfatty acids and an outer layer of dicarboxylic heads thus forming a versicle-like body. These cutinsomes are also supposed to be transolcated along microtubules (Stępiński et al., 2020). Consistently with the

second hypothesis, electron microscopy revealed the presence of regions where the ER membrane and the plasma membrane are in close proximity (10 nm apart) (Staehelin, 1997). Due to their high hydrophobicity, it is assumed that waxes can pass from the ER membrane onto the PM, but nothing is known regarding the actual mechanism.

Part of the export mechanism of wax from the PM to the apoplast was unravelled by the discovery of CER5/ABG12/WBC12 and ABCG11/WBC11, two ATP binding cassette (ABC) transporters in *Arabidopsis thaliana.* Mutants unable to produce these proteins displayed lipid inclusion in epidermal cells and depletions in alkanes and in cutin load on the plant surface (Bird et al., 2007; Pighin et al., 2004). These transporters belong to the ABCG sub-family (formerly white-brown complex) and are composed of one ATP binding site and one transmembrane domain. It was also proposed that CER5 and WBC11 could form dimers together (Samuels et al., 2008), but no interaction between them has been demonstrated yet. Surprisingly, a similar protein, GhABCG1, was showed to be implicated in cotton fibre synthesis in *Gossypium hirsutum* (a *Hibiscus* relative) (Zhu et al., 2003). An *abcg13* loss of function mutant line of *A. thaliana* displayed post-genital organ fusion, a loss of striation on the abaxial part of the petals and a decrease in the amount of most of the cutin monomers. Interestingly, most of the wax levels remained unchanged, suggesting that ABCG13 is required for cutin monomer transportation but not wax transport. This also suggests that the cutin monomers may be important for the formation of nano ridges (Panikashvili et al., 2011). Although no direct evidence for the ABCG transporter family's capacity to move wax lipids has been found so far, some similarities with human lipid transporters of the ABCG sub-family suggest a capacity to handle wax molecules (fig. 1.8b and 1.9) (Samuels et al., 2008).

Once out of the epidermal cells, the wax compounds must cross the very hydrophilic cell wall. Lipid transfer proteins are thought to be implicated in the shuttling of lipids through the cell wall as they are abundantly expressed in the epidermis, small enough to pass through the cell wall pores, and they possess a hydrophobic pocket (Samuels et al., 2008). The expression of the non-specific LTP (nsLTP) *TsnsLTP4* from *Thelluginella salsuginea* (a member of the *Brassicaceae* family) was correlated with cuticular wax deposition, supporting a possible role in transporting cuticular material through the cell wall (Sun et al. 2015). The nsLTP proteins may also play different roles as suggested

by (Jacq et al., 2017) who proposed that AtLTP2 proteins could be implicated in the integrity of the cuticle/cell-wall interface.

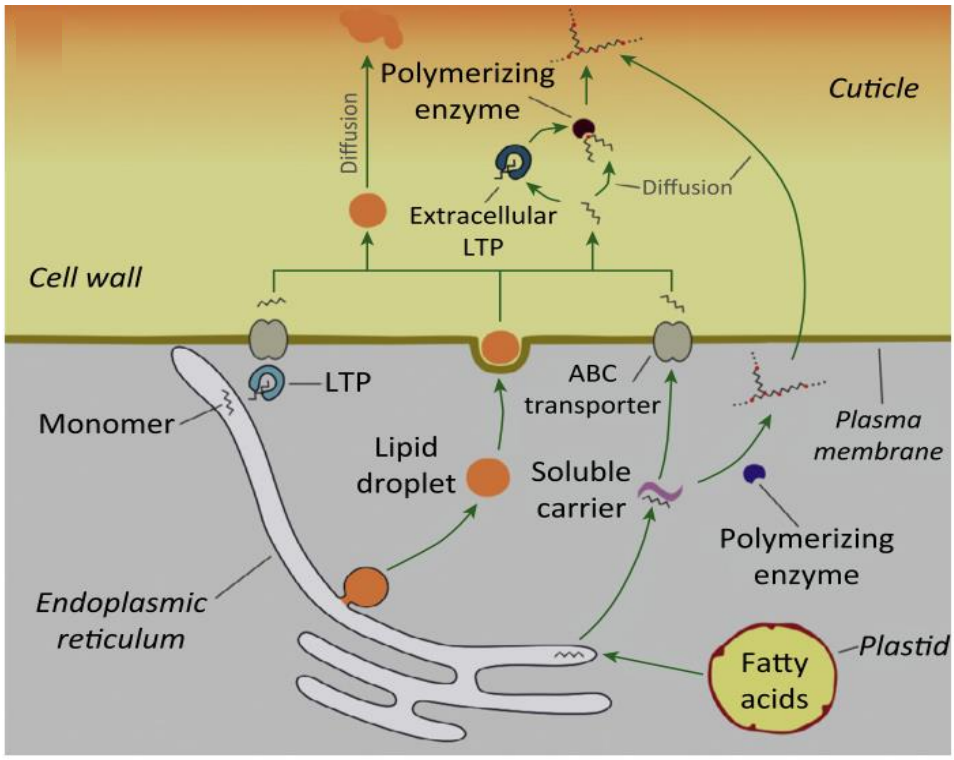

Figure 1.9: Possible translocation pathways of wax compounds and cuticle monomer polymerisation. From Domínguez et al., 2015, license number 5095430159301.

1.2.3.4 Cuticle assembly

Once the cutin monomers have passed through the cell wall polysaccharides, enzymes are required for their efficient assembly. The Cutin Synthase 1 (SlCUS1/CD1, formerly GDSL1 or SlGDSL2) protein, a GDSL lipase of *Solanum lycopersicum*, is implicated in the self-esterification of two cutin monomers (Girard et al., 2012; Yeats et al., 2012). *In vitro* assays of SlCUS1 activity demonstrated its capacity to polymerize two molecules of 2-mono(10,16-dihydroxyhexadecanoyl)glycerol into a 10,16-dihydroxyhexadecanoyl dimer by hydrolysis of the terminal glycerol ester bond and its condensation with the terminal hydroxyl group of the second molecule, liberating one glycerol (San Segundo et al., 2019). Hence, the presence of glycerol in the cuticle could be a marker of cutin polymerisation. Preliminary results from our laboratory have shown that overexpression of *HtCD1* was correlated with a loss of ridges in *Hibiscus trionum* petal cuticle

(unpublished results of Edwige Moyroud). Recently another Cutin Synthase gene was identified in *A. thaliana* (*AtCUS2*) and its expression was correlated with the formation of (non-iridescent) ridges on sepal cuticle (Hong et al., 2017).

Another pair of *A. thaliana* mutants named *bdg-1* and *bdg-2 (bodyguard)* showed an alteration in the production of cuticle associated with toluidine blue permeability, increased chlorophyll leaching in ethanol, leaf fusion, deformed leaves and a general growth deficiency. Immunolocalization of BDG showed its preferential localization to the outermost layer of the plant epidermis and specificity to this tissue. Together with the loss of cuticle structure, it was suggested that BDG could play a role in the cross linking of cutin monomers and/or a cross link between the cuticle network and the epidermal cell wall. However, AtBDG is not of the esterase lipase family like *SlCUS1*, but of the α/β-hydrolase fold-containing protein family, suggesting an indirect role in cuticle assembly (Kurdyukov et al., 2006). Recent work also suggests an important role in the production of unsaturated C_{18} molecules and corroborates the previous results. A role in fatty acid deacetylation has been suggested, however, no mechanism has yet been unravelled for the enzymatic function and role of BDG (Jakobson et al., 2016).

1.2.4 Regulation of cuticle synthesis and production of striated cuticle

The production of cuticle is a complex process requiring the coordination of many different enzymes in order to match growth and external stress. Thus, many genes implicated in cuticle biosynthesis are found to be regulated by factors governing cell differentiation, cell growth, organ development and environmental-stress responses. MYB proteins constitute the largest super family of transcription factors in plants with about 198 family members out of the 1700 predicted transcription factors in *Arabidopsis thaliana* (Riechmann & Ratcliffe, 2000; Yanhui et al., 2006), closely followed by the AP2E/EREBP family (about 150 out of 1700). The bHLH/MYC, NAC and bZIP families represent about 100 transcription factors each and the MADS and HB families account for about 80 to 90 transcription factors each (Riechmann & Ratcliffe, 2000). In this section I provide a general overview of the regulatory processes underpinning cuticle production as well as the formation of cuticular patterns by studying the role of various transcription factors.

1.2.4.1 AP2/ERF transcription factors

The AP2/ERF transcription factor family is a widespread family of transcription factors, unique to plants, characterised by a functional domain originally identified in *A. thaliana* APETALA2 and *Nicotiana tabacum* EREBP1 proteins (Saleh & Pagés, 2003).

Expression of *WAX INDUCER1/SHN1*, encoding an AP2/EREBP-like transcription factor, was correlated with wax and cutin accumulation in leaf and flower cuticle. Furthermore, gene expression analyses indicated that a number of genes, such as *CER1* and *CER2*, which are known to be involved in wax biosynthesis, were induced in *WIN1/SHN1* overexpression lines. Similarly, the relative composition of waxes was also altered in *WIN1/SHN1* overexpressing transgenic lines, suggesting a central role for *WIN1*/*SHN* in cuticle production (Aharoni et al., 2004; Borisjuk et al., 2018; Broun, Poindexter et al., 2004; Kannangara et al., 2007). Studies in *Arabidopsis thaliana* have shown that SHN1 can directly bind promoters of cuticle biosynthesis genes, suggesting that AtSHN1 is a direct regulator of cutin synthesis (Kannangara et al., 2007b). *MIXTA-LIKE* genes *MYB16* and *MYB106* of Arabidopsis were also shown to regulate cuticle production co-ordinately with *SHN1* (Oshima et al., 2013).

A transgenic line of *Oryza sativa* ectopically expressing *AtSHN2* also showed alteration of the molecular pathways responsible for cellulose and lignin production, resulting in a decrease of the global lignin amount and an increase in the cellulose content in the secondary cell wall of the epidermal stem cells, the sclerenchyma cells and the bundle sheath cells (Ambavaram, Krishnan et al., 2011). This suggests that *AtSHN2* may play an important role in the coordination of cell wall deposition and might also regulate its mechanical properties via the regulation of cell wall lignification.

The silencing of *SlSHN3* resulted in significant reduction of the cuticle thickness and further gas chromatography coupled with mass spectrometry experiments revealed a depletion in waxes and in most cutin monomers, and gene expression assays revealed a significant down regulation of two esterase-lipases, *SlGDSL1* and *SLGDSLb/SlGDSL1*, two acyltransferases, *SlDCR* and *SlGPAT6,* and one long chain acyl-CoA synthetase, *SlLACS,* amongst others. Altogether this reveals the substantial role of SlSHN3 in the regulation of cuticle production (Shi et al., 2013).

Overall, the *SHN/WIN* genes are strongly expressed in floral tissue and have been demonstrated to coordinate wax, cutin, cellulose and lignin deposition, making them an important group of transcription factor genes in the study of petal cuticular patterning. Furthermore, a line with silencing of all three of *SHN1, 2* and *3* resulted in alteration of cuticular nanoridges on both petal sides in *A. thaliana*, demonstrating the importance of these genes in cuticular pattern development (Shi et al., 2011).

Recently, a *SHN-like* gene *PeERF1*, was studied in the orchid *Phalenopsis.* Upregulation during flower opening correlated with a thickening of the cuticle and the formation of nanoridges on the lip of the flower. Interestingly, further molecular characterisation revealed that only the AP2 domain of PeERF1 was necessary to produce cuticular ridges. However, both domains were found necessary to induce the normal expression of *DCR* and *PeCYP77A4* (Lai et al., 2020). This suggests that 2 potentially distinct routes are implicated in the production of cuticle and the production of nanoridges.

WAX PRODUCTION1 (WXP1), another AP2/ERF transcription factor has also been shown to be involved in cuticle biosynthesis in *Medicago truncatula.* Its overexpression led to the production of higher level of waxes on the leaves, particularly of C_{30} primary alcohols. Furthermore, gene expression analyses in *WXP1* overexpressing lines revealed an upregulation of the genes coding for the cytochrome P450 monooxygenase, which is implicated in cutin monomer synthesis. *WXP1* could thus play a role in the regulation of cuticle biosynthesis in both the wax and cutin pathways (Zhang et al., 2005). *WXP2*, a homologue of *WXP1*, showed a similar role in the regulation of cuticle production, yet its overexpression led to a decrease in primary alcohols in contrast to *WXP1* overexpression (Zhang et al., 2007). No role of these genes in regulating cuticle striations has yet been demonstrated.

Interestingly, DEWAX, another member of the AP2/ERF-like transcription factor family, acts as a repressor of wax biosynthesis. Its overexpression was correlated with lower cuticle loads and a down regulation of *LACS2* and *CER1* genes in *Arabidopsis thaliana* (Go et al., 2014).

Another AP2/ERF-like transcription factor, *Arabidopsis thaliana* WRINKLE1 (WRI1), has been demonstrated to play a major role in triacylglycerol (TAG) storage in the seeds, suggesting an important role in lipid biosynthesis (Cernac & Benning, 2004). More recently, WRI3 and WRI4 were identified

in *Arabidopsis thaliana*, and the triple T-DNA insertion mutants of *WRI1,3* and *4* led to the production of immature flowers. Strong floral organ fusion and cuticle permeability in the flower were suggested to be the cause of flower abortion (To et al., 2012). Together this suggests that the WRI genes are responsible for the proper production of cuticle in petals, via induction of the lipid metabolic pathway. More specifically, the triple mutant of *WRI1, 3* and *4* resulted in a decrease of the levels of 10,16-DHP acid of about 50%. It has also been suggested that WRI effectors act upstream of the SHN effectors in the cutin monomer biosynthetic pathway (To et al., 2012).

1.2.4.2 MYB transcription factors

R2R3-MYB transcription factors constitute a family of the MYB transcription factor super family along with 3 other families: R1R2R3-MYB, MYB-related and atypical MYB protein. They have been studied extensively and reported to play many roles in plant development (Yanhui et al., 2006). Among other elements, their role in petal conical cell formation, as well as the differentiation of other cell types, has been demonstrated extensively (Glover et al., 1998; Jaffe et al., 2007; Lau et al., 2015; Perez-Rodriguez et al., 2005). In this section I summarise the role of several MYB transcription factors of the R2R3-MYB (Z. Li et al., 2016) and R1R2R3-MYB (Stracke et al., 2001) families in the production of cuticle and nanoridges.

Expression of *AtMYB41* (a member of the *SBG20-R2R3-MYB* subgroup) is induced under abiotic stress in *Arabidopsis thaliana*. Toluidine blue staining experiments in lines overexpressing *AtMYB41* revealed a permeable cuticle on the leaves and siliques. Together with decreased drought tolerance and faster chlorophyll leaching in ethanol, this suggests a potential role of AtMYB41 in cuticle biosynthesis regulation. Interestingly, alteration of epidermal cell shape was also reported (Cominelli et al., 2008). This suggests a coupling of cell shape with cuticle biosynthesis, 2 essential elements to cuticle buckling and nano-ridge formation.

The *AtMYB96* (a SBG1-R2R3-MYB) gene was shown to mediate accumulation of triacylglycerol in vegetative tissues under drought conditions (Lee et al., 2019), as well as the ABA signalling response (H. G. Lee & Seo, 2019). T-DNA insertional knock out of *AtMYB96* resulted in a wax production deficiency. Complementation with *AtMYB94* (another *SBG1-R2R3-MYB*) partially restored the

phenotype, suggesting partially redundant functions in *AtMYB94* and *AtMYB96*. A T-DNA insertion double knock-out of *MYB94* and *MYB96* resulted in increased permeability of the cuticle, indicating a potential role in wax biosynthesis pathways. Further analyses of gene expression revealed that both AtMYB96 and AtMYB94 regulate *CER1, CER2, CER3, KCS1* and *KCS2* under drought conditions (S. B. Lee, Kim, & Suh, 2016). Thus, the *AtMYB94* and *AtMYB96* seem to play a major role in wax biosynthesis.

The RNAi mediated silencing of *MYB16* (also known as *AtMIXTA*) and *AtMYB106* (both belonging to the SBG9-R2R3-MYB/MIXTA-like subgroup of the MYB transcription factor family) resulted in a complex phenotype. In both cases, flattened trichomes, fused flowers with narrow petals, high toluidine blue staining in every flower organ, and altered petal cell shape were observed (Oshima & Mitsuda, 2013; Oshima et al., 2013). Scanning electron microscopy also revealed a loss of cuticular nanoridges in stamen cells in both cases, but a loss of striations on petal cells was only observed in *AtMYB106* transgenics. Similarly, overexpression of *AtMYB106* using a single CaMV 35S promotor and fused to *VP16*, a constitutive transcriptional activator, led to the production of ectopic nanoridges on leaves. Higher epicuticular wax crystals were also observed on all above-ground organs. Transcriptional analyses revealed a change in cuticle biosynthesis related genes in a transgenic line expressing ectopically a recombinant MYB106 protein fused with the constitutive transcription repressor domain SRDX and placed under the control of a 35S promotor (*35S:AtMYB106-SRDX*), demonstrating the role of AtMYB106 in cuticle synthesis regulation. Highly similar regulation patterns were observed in the transcriptomes of *35S:AtSHN1-SRDX* and *35S:AtSHN1* transgenic lines: more than 50% of the genes downregulated in the *AtSHN1* dominant negative construct were also downregulated in AtMYB106 dominant negative lines. Analyses of *AtSHN1* and *AtMYB106* in these 4 transgenic lines showed that AtMYB106 acts as a positive regulator of *AtSHN1* (Oshima et al., 2013). Hence, *AtMYB106* regulates petal cell shape as well as well as cuticle production in both a *SHN* dependent and independent manner.

Although no modification of the cuticle striation pattern was reported in *Solanum lycopersicum MYB12* (R2R3-MYB subgroup) mutants (*yellow*, (*y*)), mechanical tests on the tomato fruit revealed a shorter elastic phase in the mutant cuticle without alteration of its Young's modulus. Further

characterization also showed thinner cuticle. Principal component analyses (PCA) of the chemical composition of *y* mutant and WT peels showed significant differences in secondary metabolite content. More specifically, a reduction in all the flavonoids of the naringenin-chalcone/naringenin subgroup was recorded in the mutant (Adato et al., 2009). These data show the potential relationship that can exist between the cuticular content of flavonoids and its mechanical properties. It is possible that *MYB12* or a related gene plays a role in the modulation of the properties of the *H. trionum* petal cuticle, and hence its capacity to buckle.

MYB transcription factors can regulate a large array of processes in plants and more specifically, cuticle production and cell shape, two components that are believed to be essential for cuticle buckling. Their potential role in the regulation of *SHN* expression make them ideal candidates to understand the general forces driving the development of nano-scaled ridges.

1.2.4.3 HD-Zip Class IV transcription factors

The HomeoDomain leucine Zipper transcription factor family (HD-Zip) is a rather small family of transcription factors with about 30 proteins identified (Elhiti & Stasolla, 2009; Nakamura et al., 2006). They are involved in various biological processes such as abiotic stress response (Class I), phototropism (Class II), morphogenesis (class III) and epidermal fate, trichome formation and anthocyanin production (Class IV) (Elhiti & Stasolla, 2009). On top of this, the HD-ZIP Class IV transcription factors have been shown to play a role in cuticle production.

Initially, only a very discreet phenotype was reported in *ZmOCL1* dominant negative transgenic lines of *Zea mays*: no specific alteration of the cuticle was observed (Khaled et al., 2005). However, transcriptional analyses in *ZmOCL1* overexpressing lines revealed a differential expression of lipid metabolism related genes amongst which were an atypical lipid transfer protein (*LTP*), a non-specific type-2 lipid transporter (*ZmLTP2.12*), a *WBC11/ABCG11-like* ABC transporter, a relative of the *A. thaliana* carboxylesterase *AtCXE18,* an *Indole 3-glycerol phosphate lyase* (*Igl*) and another relative of *A. thaliana CYP78A6* (Javelle et al., 2010)*,* all of which are implicated in cuticle biosynthesis. Despite similar total cuticular wax loads in transgenic and WT plants, chemical analyses displayed variation in

wax composition, and especially in alcohols and esters (Javelle et al., 2010). Strong evidence suggests that *ZmOCL1* plays a role in the biosynthesis of cuticular waxes and their export to the cuticle.

A regulatory pathway controlling cuticle production involving the HD-Zip class IV transcription factor AtHDG1/HomeoDomain GLABROUS1 has also been reported (Borisjuk et ., 2014). Over expression of the gene encoding a WW Domain Protein, CFL1, resulted in severely altered cuticle both in *A. thaliana* and *O. sativa*, with typical organ fusion and toluidine blue staining in *A. thaliana.* Transmission electron microscopy also showed lighter cuticular density and chemical analyses revealed higher cutin monomer contents (Yephremov et al., 1999). Further gene expression analyses demonstrated that *AtCFL1* overexpression induced an overexpression of *AtBDG* and *AtFIDDLEHEAD* (*AtFDH)* which are involved in the fatty acid elongation pathway, and repression of *AtSHN1*. Moreover, it was noted that the phenotype of *35S:AtCFL1* transgenic lines resembled the phenotype of *AtHDG1-SRDX* transgenic lines. The insertion of *AtHDG1-SRDX* into *Atcfl1-1* mutant*s* (an *AtCFL1* over expressing mutant) rescued the phenotype, suggesting that *AtHDG1* complements the *Atcfl-1* mutation. Yeast-2-hybrid analysis showed that AtHDG1 can bind L1-BOX DNA motifs, hence potentially the promotors of *AtBDG* and *AtCFL1* (Yephremov et al., 1999). No interaction between AtHDG1 and the *AtSHN1* promotor has yet been demonstrated.

A *cutin deficient 2* (*cd2*) mutant was characterized by highly reduced cutin content of the tomato fruit cuticle, without alteration in the ratios of cutin monomers, and, conversely, a normal total wax load with altered wax compound ratios. The *SlCD2* gene encodes a transcription factor of the HD-ZIP Class IV (Isaacson et al., 2009). Later, two other mutants affected in the *SlCD2* gene were also characterized. They showed a similar phenotype of altered cuticle in leaves and tomato fruits and the *lg (light green)* mutant revealed an increase in chlorophyll b content in young leaves. Downregulation of *SlCD2* in transgenic plants revealed a similar phenotype (Kimbara et al., 2013). Interestingly, *cd1* and *cd3* mutants display phenotypes that are very similar to that of *cd2* (Isaacson et al., 2009) suggesting that SlCD2 might regulate *SlCD1* and *SlCD3.* Transcriptomic analyses later revealed that *SlCD1* was indeed regulated by SlCD2 (Martin et al., 2016). The *SlCD1* (also known as SlCUS1) gene does not encode for a transcription factor but for an effector containing an hydrolase/lipase GDSL motif and belongs to the CUtin Synthase (CUS) family (Yeats et al., 2014). Overexpression of *HtCD1,* a GDSL-

motif protein has already been correlated with a loss of petal striation in *H. trionum* (unpublished results of Edwige Moyroud) (see fig. 3.2). The nature of *SlCD3* has not been reported yet.

HD-Zip Class IV transcription factors therefore play an important role in the regulation of cuticle production, particularly regarding its loading and its chemical properties. A role has also been identified as a potential regulator of *SHN1*, which may imply a larger role in cutin synthesis regulation and nanoridge development.

1.2.4.4 bHLH transcription factors

The basic helix-loop-helix (bHLH) transcription factors have versatile biological functions in plants. They have been shown to regulate ion uptake (H.-Q. Ling et al., 2002), seed germination (Oh et al., 2004), flower development (Szécsi et al., 2006), root hair development (Lin et al., 2015), fruit pigmentation (Gonzalez et al.,2008; Z. Zhu et al., 2017), and cuticle development (Li et al., 2016).

Once again, the WW domain transcription factor AtCFL1 is at the heart of cuticle regulation pathways tightly connected to transcription factors of the bHLH family. Yeast 2 hybrid assays using a library of *A thaliana* transcription factors revealed an interaction with a bHLH transcription factor AtCFLAP1/FBH3, and the previously discussed HD-Zip class IV AtHDG1. Over expression of *AtCFLAP1* resulted in cuticle defects including modification of wax components. AtCFLAP2, a similar protein, was also shown to interact with AtCLF1. Finally, high throughput transcriptome analyses revealed changes in the regulation of lipid metabolism related genes in these lines (S. Li et al., 2016).

Together with the results described in previous sections, this suggests a significant role for the WW domain transcription factor AtCFL1 in cuticle regulation through interactions with both *AtCFLAP1* and 2, and with the HD-Zip AtHDG1 transcription factor, with the latter being implicated in *AtSHN1* regulation.

Alteration of transcription factor expression often results in an alteration of the balance of cuticle compounds and might therefore induce an alteration of the mechanical properties of the cuticle such as a modification of its structure or its Young's modulus. Together this may hinder or induce cuticle buckling, as with *AtDCR* or *SlCD1*.

It seems that many transcription factors regulate cuticle biosynthesis. These regulatory pathways are often inter-connected making it difficult to identify the specific role of each protein. Expression of *SHN* genes has often been found to result from alteration of the expression of other transcription factors and may constitute the last element of the cuticle synthesis regulation pathway resulting in direct modulation of the cuticle metabolism and transportation. Previous work in the lab has demonstrated a clear role for *HtSHN3* in nanoridge production on *Hibiscus trionum* petals (unpublished results of Edwige Moyroud). Moreover SlTAGL1, a MADS Box transcription factor, was found to regulate *SlSHN1, SlSHN3* and *SlCD2* expression (Giménez et al., 2015), linking flower development and cuticle regulation. CFL1 on the other hand interacts with 3 other transcription factors, HDG1 and CFLAP1/2, suggesting a central role in the coordination of cuticle synthesis. The capacity of MYB factors to modulate cell shape and cuticle may explain how the coordination between cuticular properties and developmental dynamics of the petal can lead to the production of ordered cuticular ridges resulting in optical properties.

Cuticle plays a major role in plant life; thus, its regulation is likely to be driven by many different parameters, and many different transcription factors. Unravelling the specific role of one of them, or the specific implications of some in nanoscale ridge production, remains a complex task. Here I have only presented the main transcription factors shown so far to regulate cuticle production and patterning, but some others might play a significant role. Their mode of action remains unclear and they are often only identified as a result of abiotic stress response, such as EguCBF1a, a member of the C-repeat/dehydration-responsive element binding factor (CRB/DREB) family which was correlated with higher epicuticular wax content in overexpressing lines of *Eucalyptus gunii* (Navarro et al., 2011).

1.2.5 Anisotropic cell growth

Even if striations have been reported on conical cell (Panikashvili et al., 2009), structurally coloured gratings have exclusively been reported in striated tabular cells (X. Huang et al., 2017; Moyroud al., 2017) suggesting that the formation of structurally coloured nanoscaled ridges relies on the development of a flat epidermis (X. Huang et al., 2017; Kourounioti et al., 2013).

Cell expansion depends on the internal turgor pressure mediated by the vacuole and the resistance opposed by the cell wall. The stiffness of cellulose microfibrils usually prevents cell expansion along their axis, hence, their orientation as well as their reticulation induces an anisotropic resistance of the cell wall and the development of preferential growth axes (Geitmann & Ortega, 2009). Typically, a ring-like arrangement of cellulose microfibrils induces growth perpendicularly to the microfibrils whilst the absence of preferential cell wall deposition usually allows for a mild isotropic growth. Thus, the regulation of cell growth in plants is mediated by the oriented deposition of cellulose. In turn, microfibril deposition is organized along the cortical microtubule network (Bashline et al., 2014; Chan, 2012; Cyr, 1994). This demonstrates that cell shape and cell growth rely heavily on the regulation of cortical microtubule organization.

Despite an apparent softness of the primary cell wall, cell growth usually requires controlled loosening of the cell wall. Loosening of the cell wall network involves EXPANSINS, a family of proteins responsible for the disruption of hydrogen bonds between cellulose microfibrils and glucan cross-linking (Brummell et al., 1999; Choi et al., 2003; Zenoni et al., 2004), allowing cell expansion.

Hormones such as auxin were shown to be partially responsible for cellular expansion in *Chrysanthemum morifolium* (Wang et al., 2017). The use of 1-methylcyclopropene, an ethylene antagonist, was sufficient to promote the expansion of petal cells in *Gerbera hybrida*, suggesting an important role of ethylene in the repression of petal cell expansion (G. Huang et al., 2020). *TCP5*, a member of the TEOSINTE BRANCHED 1 CYCLOIDEA PCF transcription factors was identified as playing an important role in cell elongation via the repression of the ethylene pathway (van Es et al., 2018).

The study of the *angustifolia* (*an*) and *rotundifolia* (*rot*) mutants of *A. thaliana* provided understanding of the mechanisms underpinning anisotropic growth of the petal cells. The *an* mutant showed slightly longer and narrower petals, and enhanced cell elongation on leaves despite an apparently similar overall leaf shape to the WT. Four *rot* mutants showing short, rounded leaves were also identified and attributed to two different alleles of two different loci. The *rot3* mutant showed an alteration of petal, sepal, stamen and pistil length, suggesting a general alteration in cell elongation processes. Further characterization of the growth dynamics of the epidermal cells showed a defect in

transversal growth in the *an* mutant and conversely, a defect in longitudinal growth in the *rot3* mutant. It has thus been proposed that the AN and ROT3 proteins act together to induce polar elongation of epidermal cells; ROT3 would promote longitudinal elongation while AN promotes width elongation by the repression of directional growth repressors (Tsuge et L., 1996). Later molecular characterization identified ROT3 as a member of the CYTOCHROME P450 protein family and a GUS reporting system showed expression of the gene in the midsection of the petals of *A. thaliana* (Kim et al., 1999).

Two other mutants, *longifolia1* and *2,* displayed elongated leaves, siliques, petals and sepals in *A. thaliana*. Such a phenotype was attributed to overexpression of *AtLNG1* and *AtLNG2* and slight differences in phenotype suggest only a partial redundancy of these 2 genes. Further study on the *lng1lng2* double mutant revealed an additive phenotype. Furthermore, characterization of the *rot3lng1lng2* triple mutant revealed that LNG1 and LNG2 regulated cell elongation in a *ROT3* independent manner (Y. K. Lee et al., 2006).

Silencing of *AtSPK1,* coding for a small GTPase, resulted in the formation of narrower yet longer petals in *A. thaliana.* Microscopic observations also revealed that both abaxial and adaxial petal epidermal cells showed anisotropic growth in the *AtSPK1* silenced lines, in contrast to the wild-type strain Col-0. In *spk1* mutants, the microtubule network showed highly arranged cortical microtubules oriented transversely relative to the axis of cell elongation (Ren et al., 2016).

Two different *spiral* mutants (*spr1* and *spr2*) of *A. thaliana* were characterized by the formation of spiral cells surrounding the hypocotyl of 7-day old seedlings, instead of perfectly aligned and elongated cells in the growth axis. A double mutant was also produced, and the seedlings displayed round bumpy cells that look like conical cells. Study of the microtubule (MT) network and experiments using MT growth inhibitors suggests that the *AtSPR1/2* gene could control the anisotropic growth of hypocotyl cells through modification of microtubule cytoskeleton (Furutani et al., 2000).

1.3 Project objectives and experimental strategy

The aim of this study is to develop a better understanding of how molecular pathways may modulate the physical parameters required for the development of the semi-ordered nanoscale ridges responsible for the production of structurally coloured cuticle on the petals of *Hibiscus trionum*. More

specifically: What are the molecular pathways involved in the production of a structurally coloured petal cuticle? How does differential gene regulation can influence the physical parameters of the adaxial petal cuticle? In order to do so, three different approaches were followed. Finally, in a fourth part, I briefly investigated whether structurally coloured striations could lead to an alteration in the gripping capacity of insects.

1. Unravelling the molecular pathways and developmental mechanisms necessary for the buckling of the cuticle

    a. Identifying differences in the chemistry of striated and non-straited cuticle

The previously produced mathematical model predicting the production of structurally coloured cuticle focused on the anisotropic growth of the epidermis and the amount of cuticle generated. This model was however not able to predict accurately the presence of epidermal striation in the case of *35S:HtSHN3-EAR* and *35S:HtSHN3-VP16* transgenic lines (unpublished data from Edwige Moyroud) suggesting that other parameters interfere in the production of nano-scaled ridges. In collaboration with Sara Steimer and Chiara Giorio, I conducted chemical analyses in order to assess the potential role of the cuticle chemistry in the buckling of *Hibiscus trionum* petal epidermis. I thus compared the chemistry of non-structurally coloured and structurally coloured cuticle naturally present in the distal and proximal regions respectively of *Hibiscus trionum* varieties*, Hibiscus panduriformis, Hibiscus richardsonii* as well as the non-structurally coloured *Hibiscus cannabinus* and *Hibiscus sabdariffa* and in various transgenic lines displaying more or less altered striations (see chapter 3).

Specific differences in some compounds were also analysed and some molecular targets were identified for the production of transgenic lines.

b. Identifying new genes involved in the production of structural colours through transcriptomic analyses

Another way to identify genes involved in the development of cuticle striation is to compare the transcriptomes of iridescent and non-iridescent parts of the petals both before and after the striations develop (fig 1.2b and 1.2c). This matrix-based approach allowed the identification of genes that are up- and downregulated according to the presence or absence of nanoridges. A selection of these genes was

carried forward for future functional analysis using transgenic approaches. Expression of genes identified in other species and that have been shown to regulate cuticle production and formation of nanoridges was also assessed.

c. Identifying new genes involved in the production of structural colours through random mutagenesis

In collaboration with Edwige Moyroud and May Yeo from SLCU, I conducted a mutant screen to identify alterations in the development of iridescence. Random mutagenesis was conducted by incubating *Hibiscus trionum* seeds in ethylmethane sulfonate (EMS). An M1 generation of plants was grown from these M0 seeds, and selfed. M2 families derived from the M1 plants were then grown up, allowing segregation of homozygous recessive mutantss. The populations were screened using optical microscopy for mutants with altered iridescence. Subsequently, two mutants were discovered: the *blue* mutant and the *madeleine* mutant. Crossings were performed in order to explore the Mendelian inheritance of characters. Mutant lines were also characterized morphologically using SEM and optical microscopy.

2. determining the adhesive properties of structurally coloured cuticle

Finally, I briefly investigated the adhesion properties of structurally coloured cuticle in order to determine whether such cuticle could be responsible for an alteration of the adhesion properties of petals and thus modulate interactions with landing pollinators. Therefore, I analysed the gripping capacity of *Leptinotarsa decemlineata* (Colorado potato beetle) on replicas of the structurally coloured petals of *Paeonia mascula*. The wettability of nano-scaled striations was also investigated in collaboration with Benjamin Droguet from the Department of Chemistry of the University of Cambridge, using the same replicas used for beetle gripping assays.

Chapter 2 : Materials and methods

This section aims to detail the methods used for routine lab techniques such as cloning, PCR, plant growth and plant transformation supporting the work of this thesis. Materials and methods specific to individual experiments will be detailed further within each result chapter.

2.1 Plant material

Wild-type plants used in the chemical analyses were purchased as seeds from Chiltern seeds (UK). Transgenic plants used in the chemical analyses were produced from *Hibiscus trionum* seeds purchased as seeds from Chiltern seeds (UK). Plant material used in random mutagenesis and transcriptomic analyses was grown from seeds of the Cambridge University Botanic Garden (CUBG).

2.2 Plant growth and Imaging

All plants were grown on Levington's M3 (UK) compost, however, they were exposed to different environments according to the experiment's needs and the restriction imposed by our collaboration with other teams.

2.2.1 **Transcriptome**

Hibiscus trionum of the 'CUBG' variety used in the transcriptome study was grown at the experimental glass house of the Cambridge University Botanic Garden with supplemented light from 5 am until 9 pm (16 hours) for a minimal radiance of 88w/m^2 for a day temperature of approximately 25°C and a night temperature of 15°C. Shading was provided for light exposure superior or equal to 500w/m^2 and cooling was implemented for temperatures above or equal to 30°C. Humidity was not regulated.

2.2.2 **Mutant screen**

Plants grown from mutagenised seeds were grown in a tropical glass house at the Cambridge University Botanic Garden Experimental Glasshouses, due to the need for large spaces, under controlled

conditions with a day and night temperature of 28°C and 23°C respectively, a humidity of approximatively 60% and a supplementary light of 390-410w/m² for 12 hours (06:00-18:00)

2.2.3 General growth conditions

Wild type plants as well as the *blue* and *madeleine* mutants and subsequent crosses were grown in the glasshouse of the Plant Science Department of Cambridge University under 16h of artificial light per day (06:00-22:00) with an approximate temperature of 21°C, depending on external temperature, and 60% humidity. Transgenic plants were grown in the Plant Growth Facility of the Plant Science Department of Cambridge University under similar conditions.

2.2.4 Plant imaging

All optical microscopy pictures were obtained using a Keyence VHX optical microscope. All scanning electron microscopy pictures were obtained using the microscopy facilities of the Sainsbury Laboratory of Cambridge University (SLCU) with a Zeiss EVO HD15 Scanning Electron Microscope (SEM). Samples were dissected and then glued onto a brass stub before snap-freezing in solid nitrogen. Cryo-fracture was performed in a vacuum chamber using a pivoting blade on previously snap frozen samples. Tissues were coated with 2 and 3 nm of platinum for classical SEM and cryo-fracture coupled microscopy, respectively. The scanning electron microscope was operated by Dr Raymond Wightman and Gareth Evans.

2.3 Molecular biology

2.3.1 DNA extraction

A small piece of leaf (1-2 mm^2) was ground in a microtube with 400 µL of extraction buffer (250 mM Tris-HCl pH 7.5, 250 mM NaCl, 25 mM EDTA, 1% SDS) using a plastic pestle, then vortexed and centrifuged at 85,024 g for 10 mn. The supernatant was then collected and supplemented with 1 volume of isopropanol (about 400 µL), gently mixed and followed by a 30mn centrifugation at 85,024 g. The supernatant was then discarded, and the DNA pellet washed with 500 µL of ethanol 70%, then centrifuged once again at 85,024 g for 5 mn and then left to dry before being resuspended in 40 µL of

Tris-EDTA (TE) water (10 mM Tris-HCl pH 8.75 and 5 mM EDTA pH 7.5) supplemented with RNAse A at 10 mg/mL. DNA was then diluted at 1/100 for subsequent work.

2.3.2 RNA extraction

RNA was extracted from young leaves or dissected flowers following the same protocol. Tissues were carefully collected with tweezers and gloves into a 1.5 mL microtube and snap frozen in liquid nitrogen. Frozen tissues were then stored at -80°C until further processed. Samples were ground using a pestle and a mortar that were both washed with bleach and ethanol and cooled down with liquid nitrogen. Twenty-five milligrams of ground frozen tissue were then processed using Sigma Aldrich Spectrum™ Plant Total RNA Kit. The RNA content of two RNA-binding columns were eluted one after the other using the same 30 µL of elution buffer, and each column was eluted twice with the same elution solution to optimise RNA yields. RNA was then quantified with a nanodrop and run on 1% agarose gel for quality control (see 2.3.6). RNA was kept at -80°C.

2.3.3 RNA quantification

RNA quantification was performed using a nanodrop ND1000 spectrophotometer from ThermoFischer Scientific. Before sample reading, a 'blank' was made 1 µL of the elution buffer of the Sigma Aldrich Spectrum™ Plant Total RNA Kit.

2.3.4 cDNA preparation

RNA was treated with ThermoScientific® DNaseI to remove potential gDNA contamination. Five micrograms of RNA extracted with Sigma Aldrich Spectrum™ Plant Total RNA Kit were prepared with 10X DNAseI buffer and 1.5 µL of DNAseI in a total volume of 100 µL and then placed at 37°C for 30 mn.

In order to stop DNAse activity and eliminate its buffer a Phenol:Chloroform:isoamylalcohol (PCI) (25:24:1) RNA clean-up was performed. One volume of cold PCI was added to the RNA solution and then vortexed for a few seconds before being centrifuged at 21,460 g at 4°C for 5 mn. The supernatant was carefully placed into another tube and RNA was precipitated with 3 volumes of 100% ethanol and 0.1 volume of 3 M sodium acetate. Tubes were briefly inverted and stored at -80°C for 15

to 30 mn. Samples were then centrifuged cooled down to 4°C at 21,460 g for 20 mn. The supernatant was then removed, and the RNA pellets were washed with 1 mL of 70% ethanol: tubes were briefly inverted and then centrifuged at 21,460 g for 5 mn. Seventy per cent ethanol was then removed with a pipette and the sample left to dry under a laminar flow hood for about 10 mn. Finally, RNA pellets were resuspended in 11 µL of sterile deionised water. RNA concentration was assessed using nanodrop (see section 2.3.3).

RNA reverse transcription was then performed: RNA was denatured at 70°C for 5 mn and then snap cooled on ice for more than 1 mn. Two to three micrograms of RNA were then prepared in 10 µL of water and mixed with 10 µL of reverse transcription (RT) solution in a 1.5 mL microtube (1 µL of oligodT at 10 µM, 1 µL of dNTP at 10 mM, 4 µL of 5X Bioscript reverse transcriptase buffer, and 1 µL of Rhibosafe® and 1 µL of Biolab Bioscript™(200 U/µL) reverse transcriptase and 2 µL of sterile deionised water). Reverse transcription was performed at 42°C for 45 mn in a water bath and stopped at 85°C for 5 mn in a heating block.

2.3.5 **PCRs**

Three different PCR protocols were used according to our needs: Gene cloning was performed using Thermofischer® HF Phusion™ polymerase which holds a proofreading activity. Semi-quantitative PCRs were performed using PCRBIOSYSTEMS® Taq polymerase and finally, colony PCRs were performed with a homemade Taq based polymerase (reaction mix and cycling programmes are presented in table 2.1)

Every pair of primers was assessed for hetero- and homo- dimers using the following website from Thermofischer®: https://www.thermofisher.com/uk/en/home/brands/thermo-scientific/molecular-biology/molecular-biology-learning-center/molecular-biology-resource-

library/thermo-scientific-web-tools/multiple-primer-analyzer.html and designed to have a 60 > GC% ≥ 40.

a

Typical reaction mix	PHUSION® PCR	PCRBIOSYSTEM®	Homemade taq
Matrix	0.5-2 µL	0.5-1.5 µL	0.5-5 µL
Forward Primer	0.5 µM	0.5 µM	0.5 µM
Reverse Primer	0.5 µM	0.5 µM	0.5 µM
dNTP	0.2 µM	1 mM dNTPs (included in buffer)	0.2 µM
$MgCl_2$	1.5 mM	3 mM	2 mM
Enzyme	0.04 U/µL	0.1 U/µL	0.04 U/µL (estimation)
Final volume	20 µL	20 µL	20 µL

b

Typical cycle	PHUSION®		PCRBIOSYSTEMS®		Homemade taq base polymerase	
	Time	Temperature	Time	Temperature	Time	Temperature
First denaturation	30 s	98°C	1mn	95°C	1mn	95°C
Cycle step1: Denaturation	10 s	98°C	15 s	95°C	30 s	95°C
Cycle step2: Hybridation	30 s	45-72°C	15 s	45-72°C	15 s	45-72°C
Cycle step3: Polymnerisation	30 s/kb	72°C	20 s/kb	72°C	15 s/kb	72°C
Final elongation	10 mn	72°C	10 mn	72°C	1 mn	72°C
end	Inf. 4°C					

Table 2.1: PCR reaction mixes and programmes. (**a**) Various DNA polymerases and their associated reaction mix. (**b**) PCR programmes used for DNA amplification. Thirty-five cycles were used for most amplifications. Every concentration displayed is a final concentration.

Primer melting and annealing temperature were calculated using the Thermofischer® scientific TM calculator website: https://www.thermofisher.com/uk/en/home/brands/thermo-scientific/molecular-biology/molecular-biology-learning-center/molecular-biology-resource-library/thermo-scientific-web-tools/tm-calculator.html. Typical PCR programmes are detailed in table 2.1. A Labnet™ MultiGen™ Optimax and a Techne™ Flexigen™ thermocycler were used.

2.3.6 DNA and RNA electrophoresis

DNA and RNA electrophoreses were performed on a 1% (w/v) agarose gel made with Tris Boric acid EDTA (TBE) Buffer (5,4 g/L of Tris base [tris(hydroxymethyl)aminomethane], 2,75 g/L of boric acid and 0,375 g/L of EDTA) and supplemented with 1,6 µL of ethidium bromide at 10 mg/mL (in water) for each 80 mL of gel. Gels were left to solidify and then placed into a tank filled with TBE buffer. DNA and RNA sampled were loaded in the gel after mixing with a 6X homemade loading buffer (Glycerol 60% (v/v), EDTA 60 mM, Tris-HCl pH 8 20mM, blue bromophenol and xylene cyanol 0.03% (w/v)) and run between 100 and 130 Volts. DNA and RNA were revealed under UV light using a G:BOX device from Syngene™ and the GeneSnap software. Electrophoresis material, gel moulds and combs were cleaned with soapy water for the electrophoresis of RNA to avoid degradation.

2.3.7 Sequencing

Sequencing was outsourced to the sequencing facility of the Biochemistry Department of the University of Cambridge.

2.3.8 Production of transgenic lines

2.3.8.1 Blunt-end ligation into pBlueSCRIPT

Complementary DNA (cDNA) was synthesized from proximal and distal flower tissues of *Hibiscus trionum* and used as a template for PCR amplification of *HtSHN1, HtSHN2, HtSHN3* and *HtLTP2-like* genes (see table of primers and cDNA sequences in Annexes II and III respectively). PCR products were then run on a 1% agarose gel and relevant bands were cut out for gel extraction using the QiAquick™ Gel extraction kit. Genes were then ligated into pBlueSCRIPT for further white/blue selection in the DH5α strain of *E. coli* (see section 2.3.8.2) and subsequent amplification and digestion with restriction enzymes for oriented cloning into an expression vector.

pBlueSCRIPT was extracted with QIAprep® Spin Miniprep Kit. Twenty-five micrograms of plasmid were then blunt end digest with EcoRV (from New England Biolabs®) over night at 37°C in a 50 µL digestion mix containing 1.5 µL of EcoRV, 5 µL of bovine serum albumin and 5 µL NEB buffer 3.

A Ligation mix was then prepared using 10X ligation Buffer, 0.5 µL of T4 DNA ligase (from NEB® 400 U/µL) and a Vector:insert ratio of 1:3 in a total volume of 5 or 10 µL depending on the concentration of the purified insert, and placed at 16°C overnight.

2.3.8.2 DH5α *E. coli* transformation

DH5α is a strain of *Escherichia coli* engineered for high-efficiency cloning. It is defined by 3 mutations: the endA1 mutation which reduces endonuclease degradation to enhance plasmid transfer rates, the recA1 mutation which prevents homologous recombination and the lacZ ΔM15 mutation which enables blue-white screening with X-Gal/IPTG.

Competent DH5α *E. coli* were produced as follow: under sterile conditions, a colony of *E. coli* DH5α was used to inoculate 10 ml of LB (see annex I for recipe) and agitated overnight at 180 rpm at 37°C in a Stuart® Orbital Incubator |SI500|. About 120 mL of LB were then inoculated with 4 mL of this culture and incubated for 3 hours at 180 rpm and 37°C, once again in a Sturart® incubator. In a cold room, the 124 mL of bacterial culture were centrifuged at 4000 rpm in a 4°C centrifuge for 5 mn. Supernatant was then discarded, and bacteria were resuspended in 40 mL of fridge cold 100 mM $MgCl_2$ solution. Cells were left for 5 mn, and then centrifuged once again at 4,000 rpm for another 5 mn at 4 °C. The cells were resuspended in 8 mL of sterile *E. coli* 'freezing solution' (15% glycerol, 10 mM PIPES pH 7 and 60 mM $CaCl_2$). Fifty microlitre aliquots of competent cells were then transferred into sterile 0.5 ml microtubes and then snap-frozen in liquid nitrogen and stored at -80 °C.

pBlueSCRIPT ligation product was used to transform homemade competent DH5α *Escherichia coli* bacteria. The DH5α strain contains the lacZ ΔM15 mutation which is complemented by the alpha fraction of the LacZ gene brought by pBlueSCRIPT. The endogenous mutated protein brought by the bacteria and the alpha peptide brought by the plasmid are able to complement each other and restore a functional β-galactosidase.

In turn, this functional protein cleaves the X-gal into a blue compound. However, the EcorV restriction site used for blunt end ligation (see pBlueSCRIPT map in annex V and insert ligation in section 2.3.8.1) is located inside the ORF of the LacZ α peptide, thus preventing α-complementation.

Bacteria transformed with a recombinant plasmid will thus appear white in the presence of X-gal. IPTG (Isopropyl β-D-1-thiogalactopyranoside) acts as a repressor of the Lactose operon inhibitor thus allowing for the transcription of the *LacZ* gene.

Fifty microliters of DH5α competent cells were thawed on ice and incubated with the ligation product described in 2.3.8.1 on ice for 30 mn, then heat shocked at 42°C for 1 mn and then placed on ice again for 1 mn. One millilitre of liquid LB (recipe in annex I) was then added to the mix and then incubated at 37°C for 30 mn. Then, 140 microliters of culture were spread on solid LB (recipe in annex I) supplemented with ampicillin (100 mg/L final concentration) and topped with 100 µL of IPTG (0.1 M) and 40 µL of X-gal (20 mg/mL (in DMSO)). The rest of the transformation was pooled down by centrifuged at 1,250 g and resuspended in another 140 µL of liquid LB before spreading on solid LB as described above. Bacteria were left to grow at 37°C for about 16 hours.

Successful transformation was assessed with colony PCR: a single colony was collected with a toothpick and vigorously agitated into 20 µL of water in a PCR tube. The tubes were then placed in a thermocycler at 95°C for 5 mn to induce cell lysis. Five microliters of this mix were then used as template for PCR using the Homemade Taq based DNA polymerase (reaction mix and PCR programme are available in table 2.1). Positive colonies were then cultivated for plasmid extraction following the alkaline lysis method (see 2.3.8.3.1). Three microlitres of plasmid supplemented with 7 µL of water were then sent for sequencing using M13F and M13R primers (see primer sequence in annex II) at a final concentration 10 µM.

2.3.8.3 Plasmid extraction

Plasmid was extracted using the alkaline extraction method. Transformed bacteria were cultured overnight in 3 mL of liquid LB supplemented with ampicillin (100 mg/mL final concentration). Half of the culture (1.5 mL) was centrifuged at 85,024 g for 1 mn and supernatant was then removed. The pellet was then resuspended in 300 µL of Solution 1 (50 mM glucose, 25 mM Tris-HCl pH 8, 10 mM EDTA) and 5 µL of RNAseA (10 mg/mL). Another 300 µL of Solution 2 (1% SDS and 0.2 N NaOH) and 300 µL of solution 3 (3 M potassium and 5 M acetic acid) were then added to the mix and then centrifuged at 85,024 g for 10 mn. Supernatant was collected into another tube and 640 µL of isopropanol was

added to it and then centrifuged for 20 mn at 85,024 g. The supernatant was removed this time and the pellets were washed with 70% ethanol and finally resuspended in distilled water.

2.3.8.4 Restriction ligation in pEM110

The pEM110 plasmid is an over-expression vector made by Dr. Edwige Moyroud from pGREENII (Hellens et al., 2000) that contains a plant kanamycin-resistance gene placed under the control of the nopaline Synthase (NOS) promotor and terminated with a NOS terminator, a bacterial kanamycin resistance cassette, a double CaMV 35S promotor and a single CaMV 35S terminator framing the multicloning site, and an eYFPmyr reporting gene under the control of the Ubiquitin 10 promotor and terminated by another single CaMV35S terminator (plasmid map is available in annex V).

In most cases a second PCR step with tailed primers (see table of primers in annex II) was needed to add restriction sites in 5' and 3' of a gene of interest to proceed to a restriction-site oriented cloning into pEM110. PCR product was then run on a gel and extracted before ligation into pBlueSCRIPT and *E. coli* transformation (see section 2.3.8.1). The plasmid thus produced was extracted using the alkaline lysis method, and pEM110 was extracted using the QIAprep® Spin Miniprep Kit.

Plasmids were then digested with appropriate restriction enzymes in a 50 µL mix containing 1.5 µL of restriction enzyme (from NEB), 5 µL of the recommended 10X buffer and all the plasmid obtained from alkaline lysis method or about 3 µg of plasmid obtained with the QIaprep® Spin Miniprep Kit. Reaction mixes were then placed at the recommended temperature for 1 to 2 hours.

Digestion products were run on a gel and the insert and the linearised pEM110 vector were extracted from the gel using a QiAquick™ Gel extraction kit. The purified insert and vector were then ligated in 5 to 10 µL depending on their concentration using 50 ng of digested pEM110 and the needed quantity of insert to obtain a 1:3 vector:insert ratio as well as T4 ligase buffer (from NEB®) and 0.5 µL of T4 DNA ligase (from NEB® 400 U/µL final concentration). Ligation mix was then placed at 16°C overnight. Ligation product was then used to transform *E. coli* once again as described in 2.3.8.2. Transformed *E. coli* were then plated on LB (recipe available in annex I) supplemented with kanamycin

(50 mg/L final concentration). Successful transformation was then assessed once more by colony PCR (see 2.3.8.2.2.3).

Plasmid was then extracted using the alkaline lysis method (see 2.3.8.3.1). Successful transformation was assessed by sequencing using 3 µL of plasmid supplemented with 7 µL of water with JF 35S F and JF 35S R primers (see sequence in annex I) prepared at a final concentration of 10 µM. Recombinant plasmids were then used to transform *Agrobacterium tumefaciens*.

2.3.8.5 *A. tumefaciens* transformation

The LBA4404 strain of *Agrobacterium tumefaciens* was used for *Hibiscus trionum* transformation. This strain contains a chromosomic rifampicin resistance cassette, a disarmed pTi plasmid containing a streptomycin resistance cassette as well as the machinery necessary for the transformation of the host plant, and a pSOUP (see annex V) helper plasmid containing a tetracycline resistance gene and elements necessary for the replication of pEM110.

Competent LBA4404 cells were prepared as follow: a single fresh colony growing on LB supplemented with rifampicin (50 mg/L final concentration) and tetracycline (100 mg/L final concentration) was inoculated into 2 mL of LB (recipe in annex 1) supplemented with Rifampicin and tetracycline (with similar final concentrations) and incubated at 28°C for 24h and agitated at 180 rpm. Two milliliters of this culture were then transferred into 200 mL of LB without antibiotics and incubated overnight at 28°C in a 2 L flask and agitated at 180 rpm. Liquid cultures were then pooled down by centrifugation at 13,980 g for 10 mn in a centrifuge chilled to 4°C. Bacteria were then resuspended in 20 mL ice-cold 1 mM HEPES pH 7 (filter sterilised) and pooled down once more by centrifugation at 13,980 g for 10 mn. Bacteria were cleaned twice more with ice-cold 1 mM HEPES pH 7 as indicated above and finally resuspended in 8 mL of sterile ice-cold 10% glycerol. Finally, 40 µL aliquots of bacterial solution were made and snap-frozen in liquid nitrogen and then stored at -80°C.

Transformation of *Agrobacterium tumefaciens* was mediated through electroporation of competent cells. Plasmid extract was added to 40 µL of competent cells and then placed into a Bio-rad® electroporation cuvette of a capacitance of 25 µF and a resistance of 200 Ω and electroshocked at 2400 V using a Bio-rad® GenePulser Xcell™. One mL of liquid LB was then added to the cuvette to

resuspend the cells and then pipetted into a microtube and incubated at 30°C for 3 hours. Transformed bacteria were then plated on solid LB supplemented with kanamycin and streptomycin (respectively 50 and 25 mg/L final concentration).

2.3.8.6 *Hibiscus trionum* transformation

A fresh colony of *Agrobacterium tumefaciens* containing the plasmid of interest was inoculated into 5 mL of LB supplemented with streptomycin and kanamycin at a final concentration of 25 mg/L and 50 mg/L respectively and incubated for 24 hours at 28°C and agitated at 190 rpm. 500 µL of saturated preculture were then used to start 2 sub-cultures of 50 mL of LB supplemented with kanamycin and streptomycin for another 24 hours, at 28°C under agitation at 190 rpm. *A. tumefaciens* cultures were then pooled down and resuspended together into 20 mL MS 3% sucrose solution (recipe is available in annex I) with acetosyringone at a final concentration of 200 µM to induce transformation capacity, and incubated for one hour at 28°C, at 190 rpm.

Hibiscus trionum seeds were sterilised in a 70% ethanol 0.01% SDS solution for 5 mn, and then in a 95% ethanol solution for 1 mn. Seeds were then rinsed with sterile water and germination was induced by incubation in 90°C sterile water, then left to cool down at room temperature for 10 mn. In sterile conditions seeds were then placed onto MS/2 medium (see composition in annex I) in Magenta GA-7 plant culture boxes (20 seeds per box) and incubated at 30°C in the dark for 36 hours.

Hypocotyls were then dissected from germinated seeds and multiple cuts were made transversally along the hypocotyls on both sides and each end was split into 2, creating a total of 4 free ends per hypocotyls. Hypocotyls prepared in this manner were then incubated for 20 mn in the induced *A. tumefaciens* solution, then carefully dried out on filter paper and finally placed on MS Hib medium (recipe available in annex I) supplemented with benzylaminopurine, thidiazuron and acetosyringone (at a final concentration of 50 µg/L, 10

µg/L and 200 µM respectively) for 48 hours. Finally, hypocotyls were placed on fresh medium containing the same hormone concentrations, but without acetosyringone and supplemented with cefotaxime and kanamycin at a final concentration of 25 mg/L and 150 mg/L, respectively, to prevent the growth of *A. tumefaciens* and select transformed hypocotyls. After 7 and 14 days, hypocotyls were placed onto fresh MS Hib medium supplemented with 4 times more benzylaminopurine, reaching a final concentration of 200 µg/L, with the same concentrations of antibiotics and no thidiazurone. From day 21 onwards, the calli resulting from the hormone treatment were weekly placed onto fresh medium supplemented with antibiotics as during the previous steps and without hormones. Callus transformation was regularly assessed using a Leica M205 transmission microscope using a lumencor® Sola light engine light source and a ET YFP filter.

2.3.8.7 Plant regeneration from transformed calli

Shoots forming from transformed calli and fluorescent in the green part of the spectrum under epifluorescence were assumed to be transformed and separated from the callus with a sterile blade and placed onto MS/2 medium (recipe available in annex I) in a cylindrical jar and left there until roots started forming. Young, regenerated plantlets displaying roots were then carefully separated from the medium and placed into soil where they were left to grow.

2.3.9 Semi quantitative RT-PCR

Semi quantitative RT-PCRs were conducted to check that proper over expression had been achieved in transgenic lines using a recombinant pEM110 plasmid containing the cDNA sequence of the gene of interest placed under the control of a double CaMV 35S promotor. Over expression was assessed in young leaves where genes involved in floral cutin production display a weaker expression. Young leaves were collected in 1.5 mL microtubes and snap frozen in liquid nitrogen. Frozen tissues were then stored at -80°C until further processed. RNA extraction, quantification, quality control and DNAse treatment were performed as described in section 2.3.4. Finally for homogeneity between samples, 2.15 µg of clean RNA were retrotranscribed for each genotype as detailed in section 2.3.4.3.

1 µL of cDNA was diluted in 5 µL of sterile deionised water and 3 µL were used for housekeeping gene amplification (in our case the *ActinS4* gene (primers available in Annex II) and 3 µL were used for specific gene amplification to guarantee that similar amount of matrix were used for amplification. PCRBIOSYSTEM® DNA polymerase was used to perform cDNA amplification (see table 2.1 for reaction mix and annex II for primer sequences). Five microliters of PCR reaction were taken from the tube after 25, 30 and 35 cycles typically. One microliter of 6X loading buffer (see section 2.3.6 for recipe) was then added and finally run on a gel as prepared in section 2.3.6.

2.4 Plots

All boxplots and dotplots were produced using the ggplot2 package of R-Studio and the heatmaps using the pheatmap package of R-studio.

Chapter 3 : Chemical analyses reveal the potential role of the cuticle chemistry in the buckling of the cuticle

The transgenic lines presented in this chapter are the result of the work of Edwige Moyroud. Liquid extraction surface analyses were performed by Sara Steimer from the Department of Chemistry from Cambridge University.

3.1 Introduction

3.1.1 Chemical nature of the cuticle

The chemistry of the cuticle was largely described in the Introduction. However, the work presented in this section reminds us that the chemical nature of the cuticle is of high complexity and is composed of a large array of molecules, functional groups and bonds in different proportions corresponding to different structural and chemical units such as the cutin network, the epicuticular waxes and the intra-cuticular waxes. The abundance of 135 compounds found in cuticle was measured in this work, and the structure of many of them remains unidentified. Interpreting them as part of the wax or cutin fraction of the cuticle can therefore be hazardous. It is however common to characterize cutin monomers as more or less saturated aliphatic acids of 16 and 18 carbon residues with various functional groups (hydroxyl and epoxy) (Yeats & Rose, 2013) such as the $C_{16}H_{32}O_4$ compound presented in this study and referred to as 10,16 dihydroxypalmitic acid (10,16-DHP) also known as 10,16-dihydroxyexadecanoic acid, and confirmed as a cutin monomer (Mazurek et al., 2017). Similarly, compounds composed of 20 to 40 carbon residues are usually considered as waxes and mostly refer to aliphatic acids usually consisting of primary alcohols, aldehydes and alkanes (Bernard & Joubès, 2013; Riederer & Muller, 2006). Compounds of higher molecular weight can also be formed via esterification of aliphatic acids.

Adding to the number of carbon residues, another determinant factor in the identification of chemical compounds is the relative proportion of oxygen atoms. Molecules displaying a low degree of oxidation are likely to be aliphatic acids as they are the main components of cutin and cuticular waxes, with a limited number of functional groups such as hydroxy, epoxy or ketoyl. It remains however difficult to infer the position of these functions along the carbon chain. Furthermore similar raw formulas may also account for minor wax constituents such as triterpenoids (Riederer & Muller, 2006). Highly oxidised compounds such as $C_{12}H_{24}O_{12}$, $C_{18}H_{34}O_{17}$, $C_{26}H_{26}O_{17}$, $C_{26}H_{26}O_{18}$, $C_{27}H_{28}O_{18}$ and $C_{27}H_{28}O_{19}$ can be difficult to identify. Some match polysaccharide formulas and may originate from the cell wall or protein glycosylation ($C_{12}H_{24}O_{12}$ and $C_{18}H_{34}O_{17}$), others could correspond to glycosylated flavonoids ($C_{27}H_{28}O_{18}$ and $C_{27}H_{28}O_{19}$) or ellagitannins ($C_{26}H_{26}O_{17}$ and $C_{26}H_{26}O_{18}$). Glycosylated flavonoids have been reported to play an important antifungal role (Sudheeran et al., 2020), while

ellagitannins consist of a glycosylated ellagic acid related to tannins and often play a structural role in the cell wall (Vattem and Shetty, 2005). Naturally occurring hydrolysation of ellagitannins releases ellagic acid which has been largely studied for its antioxidant and anticarcinogenic properties in human health (Quave et al., 2012; Vattem & Shetty, 2005).

Study of the *Arabidopsis thaliana defective in cuticular ridges* (*dcr-1*) mutant revealed a correlation between a strong depletion in 10,16-DHP and a loss of cuticular striations on the adaxial conical cells of the petals (Rani et al., 2010), suggesting that the 10,16-DHP may play an important role in the buckling of the cuticle. Indeed, the abundance of 10,16-dihydroxypalmitate may alter the degree of reticulation of the cutin network thus potentially modulating its elastic properties.

In this chapter I aimed to study the difference in chemistry of ridged and non-ridged cuticle in various Hibiscus species, *Hibiscus trionum* varieties and transgenic lines in an attempt to identify compounds implicated in the production of striated cuticle.

3.1.2 Iridescence in *Hibiscus* sp.

The *Hibiscus* genus is a large genus comprising 197 species (USDA, Agricultural Research Service, 2020) both non-iridescent and iridescent. For example, *H. sabdariffa* and *H. cannabinus* are not structurally coloured, while two other species, *H. panduriformis* and *H. richardsonnii* are iridescent (Giorio et al., 2015). Similarly to *H. trionum*, the proximal adaxial region of their petals also presents nano-scaled ridges. Moreover, it has been observed that iridescence is not consistent amongst the varieties of *Hibiscus trionum*: the 'CUBG', 'New Zealand' and 'Commercial' varieties are iridescent in the proximal adaxial region of their petals while the 'Botswana' variety is not (fig. 3.1).

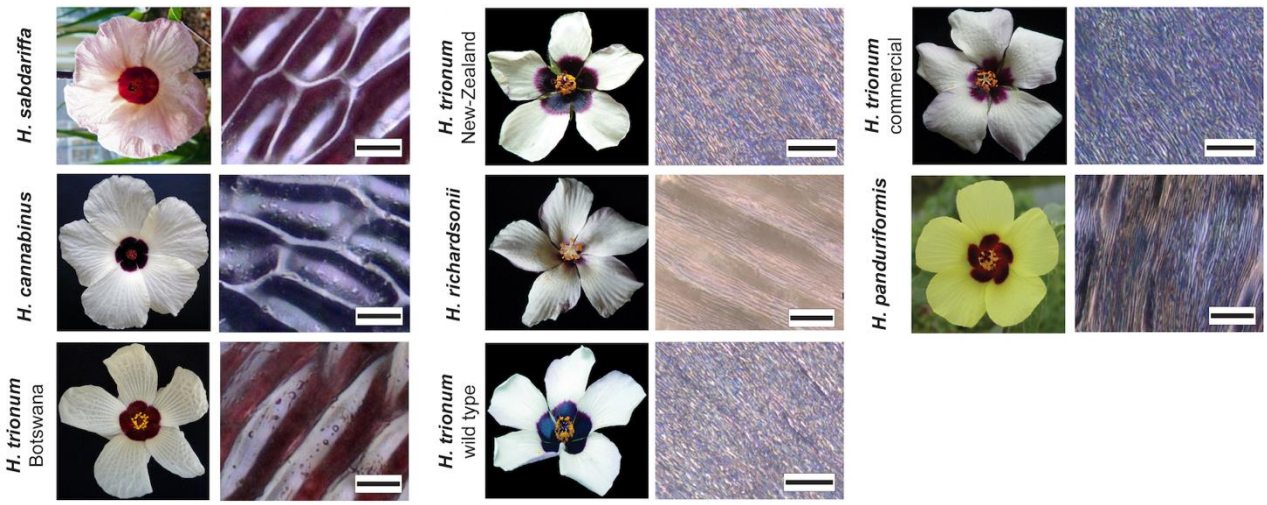

Figure 3.1: Pictures of the different varieties of *Hibiscus trionum* and *Hibiscus* species flowers and optical microscopy of their proximal adaxial petal cuticle. Scale bar = 30 µm (after Edwige Moyroud et al., in preparation).

These variations present within the *Hibiscus* genus and *Hibiscus trionum* subspecies can be used as valuable points of comparison to determine the role of cuticle chemistry in the production of structural colours.

In addition, iridescence in *H. trionum* var. 'CUBG' is limited to the adaxial part of stage 4 and stage 5 flowers, offering the possibility to assess potential developmental modification of the chemical composition leading to the formation of an iridescent cuticle by analysing the chemistry of the cuticle of stage 3 buds (see fig. 1.2). The abaxial part also gives us an interesting point of comparison: since the global developmental mechanics are relatively similar, it has the potential to reveal of the role of the chemistry in the development of structural colours.

3.1.3 Iridescence in *Hibiscus trionum* transgenic lines

Based on their implication in the production of striations in other plant systems or in the regulation of cuticle production, several genes were selected for molecular work.

Several transgenic lines of *Hibiscus trionum* were thus constructed by previous members of the Glover group using a double CaMV 35S promotor (from the cauliflower mosaic virus), and *Hibiscus trionum* or *Arabidopsis thaliana* cDNA sequences and occasionally a constitutive transcriptional activator domain: VP16 (from the *Herpes simplex* virus), or transcriptional repressor domain: SRDX

(also known as EAR-repression domain: ERF-associated amphiphilic repression) (see table 1.6 and annex IV for VP16, SRDX and double 35S promotor sequences).

The *AtSHN* genes play a central role in the regulation of cuticle production (Aharoni et al., 2004; Shi et al., 2013, 2011). The *HtSHN3* gene of *H. trionum*, presents relative similarities with *AtSHN* genes, however, phylogeny work showed no orthology with the *AtSHN* genes (see fig. 1.5). The production of *35S:HtSHN3-VP16* and *35S:HtSHN3-SRDX* transgenic lines aimed to alter the cuticle thickness and chemistry in an attempt to modulate the buckling conditions and test our model predicting cuticle striations (see fig. 1.5 and table 1.6).

However, quantitative RT-PCR analyses on the potential downstream targets of *HtSHN3* revealed that *CYP77A-like1* and *GDSL-like* are silenced in a *35S:HtSHN3-VP16* line suggesting that the *35S:HtSHN3-VP16* construct resulted in an unexpected dominant negative (data from Chiara Airoldi, not shown). Both *35S:HtSHN3-VP16* and *35S:HtSHN3-SRDX* transgenic lines resulted in a complete loss of striation (see table 1.6)

In order to alter the chemistry of the cuticle, four other over-expressing transgenic lines were produced: *35S:AtDEWAX, 35S:HtCD1.1, 35S:AtCDEF1* and *35S:HtMIXTA-like1*.

Like *HtSHN* genes, *AtDEWAX* encodes an AP2/ERF-type transcription factor that has been shown to negatively regulate wax biosynthesis in *A. thaliana.* In *H. trionum*, the over expression of *DEWAX* helps us understand the potential role of waxes in the development of striations (see table 1.6).

The cutin synthase CD1.1 is a GDSL esterase lipase protein that was shown to catalyse the esterification of two cutin monomers in the cuticle of tomato fruit (Yeats et al., 2012). Hence, modulation of its expression induces changes in the reticulation of the cutin network by producing more or less ester-bonds between the cutin monomers. The mechanical properties of the entire cuticle (including the cuticle proper) can thus be altered by modulation of *CD1.1* expression. Over expression of *HtCD1.1* can help us assess the importance of the mechanical properties of the cuticle in the process of its buckling (see table 1.6).

The *CUTICLE DESTRUCTION FACTOR* or *CDEF1* encodes an esterase that also belongs to the GDSL esterase/lipase family, that was shown to degrade the cutin network in *A. thaliana.* Its over

expression induces defects in cuticle formation (Takahashi et al., 2010). In this way, the catalytic activity of CDEF1 can be understood as opposite to that of CD1.1. Hence, its over expression in *H. trionum* is another way to assess how the mechanical properties of the cuticle might influence its buckling (see table 1.6).

Finally, the MIXTA transcription factor was initially chosen for its capacity to induce the production of conical cells on the epidermis of *Antirrhinum majus* (Glover et al., 1998). The primary objective behind the construction of a *35S:HtMIXTA-like1* transgenic line was to change the cell shape in the proximal part of the petal cuticle of *H. trionum* in order to assess whether the tabular cell shape of the epidermal cells was determinant in the development of striations. Meanwhile other studies have shown the role of *MIXTA-like* genes in the production of cuticle (Oshima & Mitsuda, 2013; Oshima et

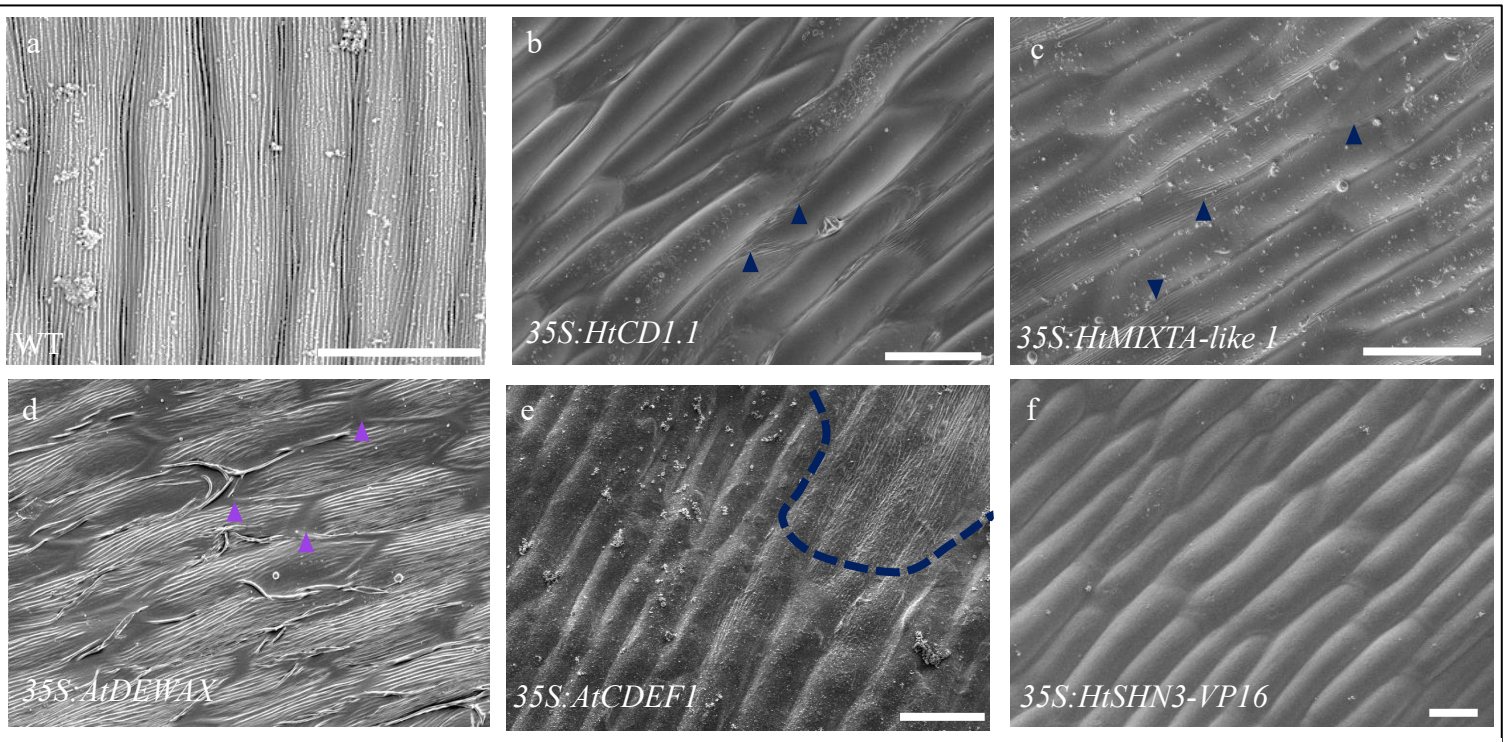

Figure 3.2: Cryo-scanning electron microscopy (Cryo-SEM) of the adaxial proximal petal cuticle of *H. trionum* transgenic lines. **(a-g)** Blue arrows indicate isolated striations; blue dashed lines delimit striated patches and purple arrows indicate isolated smooth cuticle**. (a)** WT corresponds to *Hibiscus trionum* variety 'CUBG'. **(b, c, d and e)** Showing altered striations of the cuticle in *35S:HtCD1.1*, *35S:HtMIXTA-like1*, *35S:HtDEWAX* and *35S:AtCDEF* transgenic lines, respectively. **(f and g)** Showing a complete loss of striations in *35S:HtSHN3-VP16* and *35S:HtSHN3-SRDX* transgenic lines, respectively**.** After Edwige Moyroud and Chiara Airoldi unpublished work (scale bar = 40 μm).

al., 2013). Hence the MIXTA-like sequence isolated by Edwige Moyroud might hold the dual role of cell shaping and cuticle synthesis regulator (see table 1.6).

Overexpression of *AtDEWAX, HtCD1.1, HtMIXTA-like1* and *AtCDEF1* in *Hibiscus trionum* all resulted in an alteration of the striation pattern in an inconsistent manner (fig. 3.2). Over expression of the *HtMIXTA-like1* transcription factor did not induce any cell shape modification, contrary to our hypothesis and induced an almost complete loss of striations with very isolated cuticular patterns between cells (fig. 3.2c). The *35S:AtCDEF1* transgenic lines displayed patches of striated and smooth cuticle (fig. 3.2e). The *AtDEWAX* over expressing transgenic line was characterised by a major perturbation of cuticle integrity, resulting in a loss of inter-cell striations (fig. 3.2d). Interestingly, the over-expression of the cutin polymerase *HtCD1.1* showed a severe loss of striations, which occasionally still appear at the cell border (fig. 3.2b), which might suggest that an 'excessive' polymerization of the cuticle was sufficient to alter its buckling properties.

The production of transgenic lines affected in the production of striated cuticle as well as the presence of closely related species and varieties of *Hibiscus trionum* provided a large diversity of striated and non-striated cuticles, improving the robustness of the chemical analyses presented here.

3.1.4 Aims

The aim of this chapter was to clarify how the cuticle chemistry influences its capacity to buckle by studying the chemical composition of striated and non-striated cuticles.

3.2 Methods

3.2.1 Cuticle chemistry analyses

Cuticle chemistry analyses were performed in collaboration with Sara Steimer from the Department of Chemistry of the University of Cambridge following the protocol elaborated by Giorio et al., 2015. Liquid Extraction Surface Analyses coupled with Mass Spectrometry (LESA-MS) were used to partially solubilise and identify chemical compounds present in the cuticle of various Hibiscus species and varieties as well as transgenic lines in the proximal and distal regions of the petals. Two types of solvents were used to extract cuticle compounds. A 90:10 Acetonitrile-water mixture acted as a relatively polar solvent, and a 49:49:2 chloroform-acetonitrile-water mixture acted as a relatively non-polar solvent. 0.1% of formic acid was added to the water used in these 2 mixtures for spray and ionization stability purposes. These two solvents successfully solubilised lose polar and nonpolar

compounds of the cuticle (sugar, flavonoids, fatty acids, amino acids and low molecular weight organic acids) in previous work (Giorio et al., 2015), and 135 compounds were routinely detected in our study. These two mixtures were not able to break ester bonds, hence, this approach was not sufficient to resolve the degree of reticulation between the cuticle compounds.

A droplet of 3 μL of solvent was deposited at a height of 1.4 mm from the sample plate at the maximum dispensation rate (60 μL/min). The contact between the cuticle and the droplet of solvent was maintained for 30 s for the nonpolar mixture and for 45 s for the polar mixture. Longer contact times led to a breakdown of the contact with the cuticle, because of solvent evaporation. The droplets containing the dissolved compounds were then aspirated at a height of 1.2 mm from the sample plate at the maximum aspiration rate (60 μL/min) and infused in a chip-based nano Electro Spray Ionisation (ESI) source to ionise the chemical compounds solubilised in the droplet (Triversa NanoMate Advion, Ithaca, NY, USA). Blanks were analysed by repeating the same procedure on clean aluminum foil, with a dispensation height of 1.2 mm and an aspiration height of 1.0 mm from the surface. A high-resolution mass spectrometer (LTQVelos Orbitrap, Thermo Scientific, Bremen, Germany) with a resolution of 100,000 at m/z 400 and a typical mass accuracy within ± 2 ppm was used to analyse the organic compounds present in the samples following extraction by LESA. Samples were sprayed at a gas (N2) pressure of 0.30 psi at 1.8 kV in positive ionization mode and 0.80 psi at −1.4 kV in negative ionization mode with a transfer capillary temperature of 210 °C. Data were acquired using an automated acquisition method to measure the full scan in m/z range 80−600 and 150−1000 and auto MS/MS analysis on the five most intense peaks with a collision-induced dissociation (CID) energy of 30 (normalised collision energy). For each droplet, a minimum of 30 scan routines was acquired (ca. 3 min of acquisition). The instrument was calibrated routinely to within an accuracy of ± 2 ppm, using a Pierce LTQ Velos ESI Positive Ion Calibration Solution and a Pierce ESI Negative Ion Calibration Solution (Thermo Scientific).

3.2.2 Computational chemical analyses

Of all the compounds found with mass spectrometry, 135 were regularly found in *Hibiscus trionum*. This list of 135 compounds was used to filter the mass spectrometry results in all the samples analysed with LESA. Our solvents were not able to consistently extract all cuticle compounds, hence I interpreted the results for each sample as a probability to find a given compound, or a relative abundance of a given compound expressed as a percentage. Principal Compound Analyses (PCA) were then plotted using R 'ade4' package to visualise the similarity in the chemical profiles of the different conditions.

The 10 compounds contributing the most to principal component one (PC1) of each PCA were extracted using the R package 'ade4' v1.7.15 (Dray & Dufour, 2007) and compiled into a list of 22 unique compounds. The relative abundance of each compound was assessed amongst different species of *Hibiscus* and different varieties of *H. trionum* using the R 'ggplot2' package v3.3.1 (Wickham, 2016). Differences in abundance were statistically tested with R: A Shapiro test was used to assess normal distribution of the data and an unpaired Bartlett test to assess the homoscedasticity of the two datasets to compare. An unpaired t-test was used in case of normal distribution and equality of variances. A non-parametric unpaired Wilcoxon test was used in any other case.

The nature of the mass spectrometry technology used did not allow the full resolution of the structure and nature of the studied chemical compounds. Their potential structures and names were predicted using 'PubChem'.

3.2.3 Imaging

See section 2.2.4

3.3 Results

3.3.1 Chemical analyses revealed different chemistry between striated and smooth cuticles

A PCA was performed on the chemical profiles of several *Hibiscus* species and varieties. Despite the proximity of three striated and smooth samples in the PCA (samples 11 and 20, 11 and 15, and 13 and 2), striated and smooth cuticles clustered separately from one another (fig. 3.3a). Interestingly, non-striated cuticles have a relatively similar chemical profile despite the variety of tissues that were analysed (abaxial, distal and proximal parts of the petals, and early developmental

stage). Conversely, despite apparent similarities in the striated cuticles (all proximal adaxial petals), they all displayed very different chemical profiles, even within the same species (*Hibiscus trionum* var. 'CUBG', fig. 3.3a, number 9 in legend). Despite differences within striated samples, they do occupy generally a different area of the PCA than the non-straited do.

A strong difference between the stage 3 proximal cuticle and stage 5 proximal cuticle (which is iridescent) can also be observed, revealing an important change of the cuticle chemistry during development (fig. 3.3a number 19 and 9 respectively).

3.3.2 *35S:HtSHN3-VP16* and *35S:HtSHN3-SRDX* transgenic lines display both a loss of striation and a chemical profile typical of smooth cuticles.

The PCA comparing the chemical profiles of the *HtSHN3* transgenic lines (both *35S:HtSHN3-SRDX* and *35D:HtSHN3-VP16*) and the wild type shows a similar clustering of the smooth tissues on one side and the striated tissues on the other side. Interestingly, the proximal cuticle of the petals of the *35S:HtSHN3-VP16* transgenic line occasionally showed similarities with the equivalent striated region in the wild type, which could suggest little difference in their cuticle chemistry (fig. 3.3b number 9 and 21). However, the PCA shows a smaller variability between the proximal cuticle of different flowers in the *35S:HtSHN3-VP16* than in the WT suggesting that the cuticle chemistry is consistently altered in this transgenic line despite some similarities with the WT. Furthermore, this analysis shows that the chemical profile of the *35S:HtSHN3-SRDX* transgenic line is radically different from the one of the WT, but also from the one of the *35S:HtSHN3-VP16* transgenic line despite apparent identical phenotypes, and potential similarities in the molecular effects of the *35S:HtSHN3-VP16* and *35S:HtSHN3-SRDX* constructs.

3.3.3 Modulation of gene expression resulting in altered striations is correlated with alteration of the cuticle chemistry

The distribution of the different chemical profiles of the transgenic lines displaying an altered striation pattern overlaps both the chemical profiles of striated and non-striated regions (fig. 3.3c). Interestingly the *35S:AtCDEF1* transgenic line produces patches of iridescent cuticle and displays a

chemical profile that is intermediate between fully striated proximal cuticle and one of the 'loss of striation' transgenic lines (fig. 3.3c number 25, 9 and 21, respectively). A similar scattering of the *35S:HtMIXTA-like1* can be observed despite a much lower proportion of striated cuticle across the proximal region (fig. 3.3c number 23).

The *35S:AtDEWAX* transgenic line shows a chemical profile further apart from the one of the striated cuticle and the non-striated cuticles, which suggests a limitation to the cuticle chemical domain favourable to the production of ordered striations, correlating with its original striation pattern.

Interestingly, the chemical profile of the *35S:HtCD1.1* transgenic line shows more variation between the different flowers and seems to spread across the 'striated domain' delimited by the altered striation of the *35S:AtDEWAX* transgenic line and the WT (fig. 3.3c number 29, 31 and 9, respectively) despite a phenotype similar to that of the *35S:HtMIXTA-like1* transgenic line.

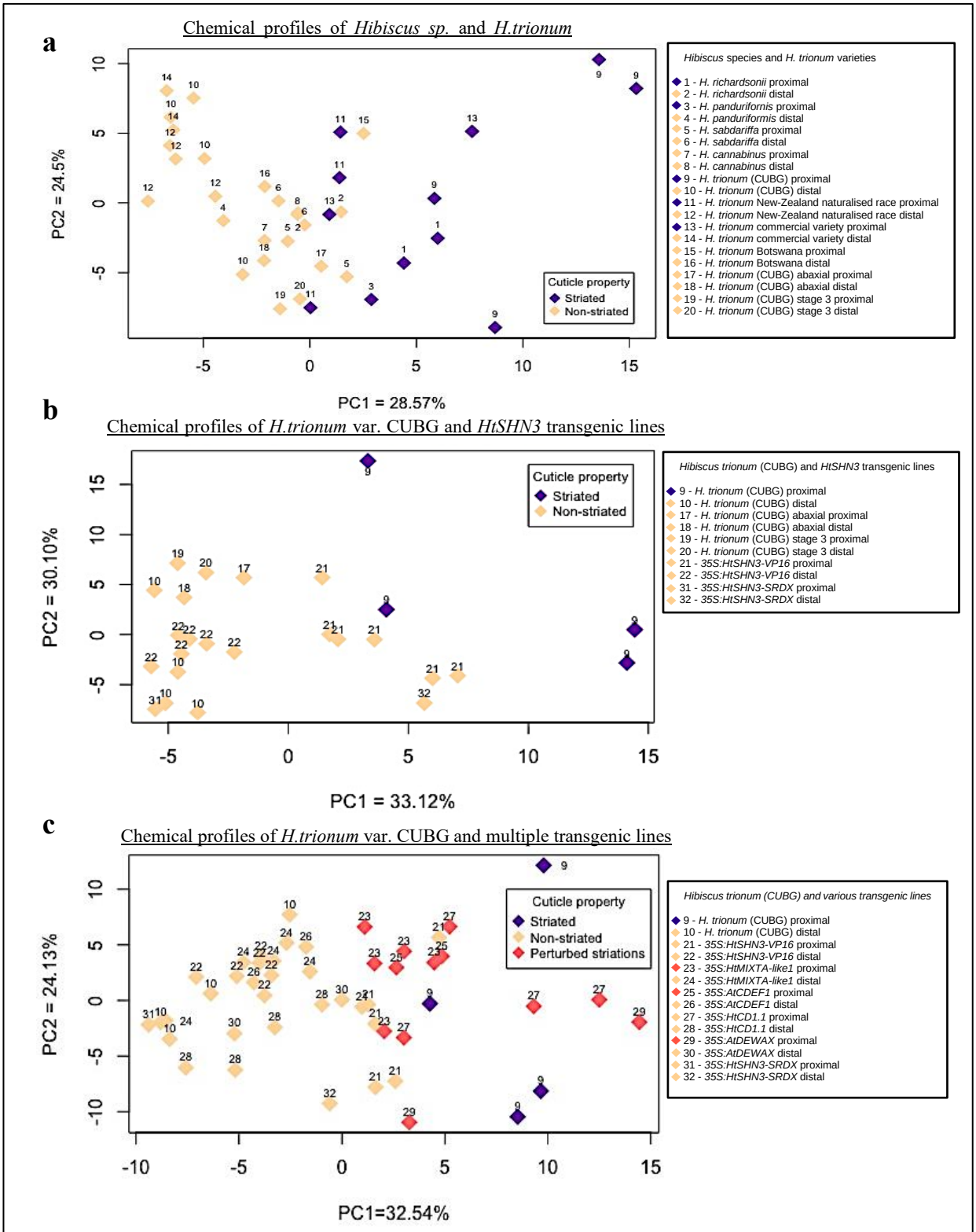

Figure 3.3: Principal component analyses performed on the chemical profiles of striated and non-striated cuticles. **(a, b** and **c)** Each diamond stands for a set of measures performed on one flower analysed systematically on the adaxial surface of the petal unless specified. **(a)** Analysis of several *H. trionum* varieties and stage 3 buds as well as *Hibiscus sp.* of which *H. richardsonii*, *H. panduriformis* and *H. trionum* var. 'CUBG', 'New Zealand' and 'Commercial' are striated (and iridescent) in their proximal regions. **(b)** Analysis of the chemical profile of the *35S*:*HtSHN3-SRDX* and the accidental downregulating *35S*:*HtSHN3-VP16* transgenic line and the WT *H. trionum* var. 'CUBG'. **(c)**. Analysis of the chemical profile of 7 transgenic lines including the over expressing *HtMIXTA-like*, *AtCDEF1*, *HtCD1.1*, *AtDEWAX* and the *35S*:*HtSHN3-SRDX* and *35S*:*HtSHN3-VP16* transgenic lines compared to the WT *H. trionum* var. 'CUBG'.

3.3.4 **The 10,16-Dihydroxypalmitate is typical of striated cuticle**

In order to investigate further the nature of these differences in chemical profiles between striated and non-striated cuticle, a list of 22 unique compounds was extracted from the analyses of the 10 chemical compounds explaining the largest proportion of variance in the principal component one of each PCA (fig. 3.4), and their frequency was assessed in striated and smooth samples. Corroborating the results from the principal component analyses, these 22 chemical compounds display very different frequencies between striated and smooth samples, noticeably with higher frequency of 16 compounds ($C_{16}H_{32}O_4$, $C_{28}H_{50}O_4$, $C_{30}H_{54}O_4$, $C_{32}H_{56}O_4$, $C_{32}H_{58}O_3$, $C_{34}H_{60}O_4$, $C_{36}H_{64}O_4$, $C_{36}H_{66}O_4$, $C_{38}H_{66}O_9$, $C_{38}H_{70}O_4$, $C_{40}H_{72}O_9$, $C_{45}H_{64}O_{11}$, $C_{47}H_{68}O_{11}$, $C_{47}H_{68}O_{12}$, $C_{49}H_{72}O_{12}$, $C_{51}H_{76}O_{12}$) out of 22 in striated cuticles. Amongst these 16 compounds, 8 have a formula matching potentially long chain fatty acids comprised between C_{28}-C_{38} and with low oxidation levels matching the description of waxy aliphatic compounds, 7 are made of 38 and above carbon residues with relatively higher oxidation, potentially matching sterols, poly-aromatic-like and poly-aliphatic-ester-like compounds, and one is a typical cutin monomer compound: $C_{16}H_{32}O_4$, most likely corresponding to 10,16-DHP (10,16-dihydroxypalmitic acid) (fig. 3.4). Six of these 16 compounds appear to be almost specific to striated tissues: $C_{51}H_{76}O_{12}$ and $C_{28}H_{50}O_4$ (most likely triterpenoids), $C_{38}H_{70}O_4$ (most likely a waxy aliphatic acid), $C_{40}H_{72}O_9$ and $C_{45}H_{64}O_{11}$ (exact structure unknown), and $C_{16}H_{32}O_4$ (most likely 10,16-DHP) (fig. 3.4a).

Only six compounds ($C_{12}H_{24}O_{12}$, $C_{18}H_{34}O_{17}$, $C_{26}H_{26}O_{17}$, $C_{26}H_{26}O_{18}$, $C_{27}H_{28}O_{18}$ and $C_{27}H_{28}O_{19}$) out of 22 were identified as more abundant in non-striated regions and comprise carbon chains ranging from 12 to 27 carbon residues and relatively high oxidation levels potentially matching polyols, flavonoids including potential C-glycosyl-flavones and ellagic acid-derived compounds.

3.3.5 **Disruption of the cuticle striations in transgenic lines is consistent with a chemical profile typical of neither smooth nor striated cuticles**

The frequency of proximal petal parts presenting each of the 22 compounds was then calculated within the transgenic lines and the receiving strain *H. trionum* (CUBG) for each tissue type (striated, smooth and 'perturbed striations') (fig. 3.4b). Two transgenic lines presented a completely smooth adaxial proximal petal cuticle: *35S:HtSHN3-SRDX* and *35S:HtSHN3-VP16*, and four presented

'perturbed striations': *35S:HtMIXTA-like*, *35S:HtCD1.1*, *35S:AtCDEF1* and *35S:AtDEWAX* (fig. 3.2). Similarly, to the non-iridescent parts of various *Hibiscus* species and *Hibiscus trionum* varieties, the proximal cuticle of non-striated 35S:*HtSHN3-VP16* and 35S:*HtSHN3-SRDX* transgenic lines is highly depleted in $C_{51}H_{76}O_{12}$, $C_{28}H_{50}O_4$ and $C_{16}H_{32}O_4$ (fig. 3.4b). However, no differences in the abundance of $C_{38}H_{70}O_4$, $C_{40}H_{72}O_9$ and $C_{45}H_{64}O_{11}$ and $C_{46}H_{68}O_{11}$ were observed between WT striated cuticle and the smooth cuticle of these two transgenic lines, suggesting that the chemistry of the cuticle was only partially altered and that a limited number of compounds may be involved in the development of cuticular striations.

For most compounds, a similar frequency was observed in striated cuticle and cuticle presenting perturbed striations, including $C_{51}H_{76}O_{12}$, $C_{28}H_{50}O_4$, $C_{38}H_{70}O_4$, $C_{40}H_{72}O_9$, $C_{45}H_{64}O_{11}$ and $C_{16}H_{32}O_4$ which were previously described as almost exclusive to striated cuticles (fig.3.4a see also section 3.3.4), thus failing to explain the apparent perturbation of the striations. Another compound, the $C_{18}H_{34}O_{17}$ (a potential trisaccharide) was only detected in the transgenic lines of the 'perturbed striation' group, suggesting its differential synthesis in this group. The $C_{12}H_{24}O_{12}$ compound, another potential disaccharide, was also differentially abundant in the WT and the 'perturbed' striation group. None of the genes used for the transgenic lines described above is predicted to be involved in the regulation of protein glycosylation or cell wall metabolism, thus failing to explain the difference of frequency of $C_{18}H_{34}O_{17}$ and $C_{12}H_{24}O_{12}$.

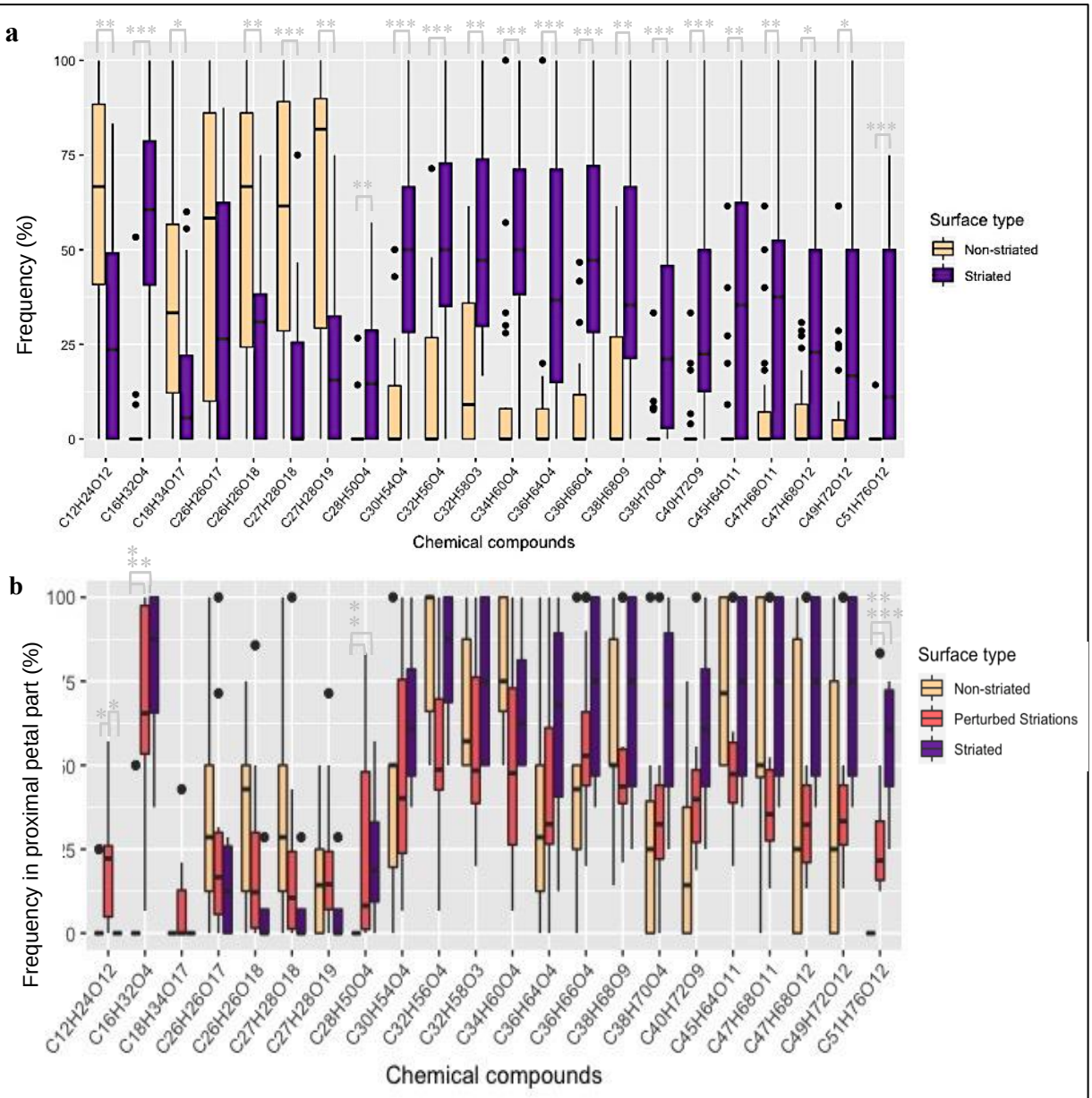

Figure 3.4: Frequencioes of the 22 chemical compounds extracted from the PC1 of the different PCAs described in fig. 3.3. (**a**) Frequencies assessed amongst striated and non-striated cuticles of *Hibiscus sabdariffa, H. panduriformis, H. cannabinus,* and *H richardsonii* and *H. trionum* var. 'CUBG', 'Botswana', 'New Zealand' and 'Commercial'. **(b)** Frequencies assessed amongst cuticles of WT *Hibiscus trionum* var. CUBG and transgenic lines: 'non-striated' (*35S:HtSHN3-VP16* and *35S:HtSHN3-SRDX*), 'perturbed-striation' (*35S:HtMIXTA-like1*, *35S:HtCD1.1*, *35S:AtCDEF1* and *35S:AtDEWAX*), 'striated' (receiving strain *Hibiscus trionum* var. 'CUBG'). * ⇔ 0.01 < p-value < 0.05; ** ⇔ 0.001 < p-value < 0.01; *** ⇔ p-value < 0.001. Dots represent outliers**.**

3.4 Discussion

In this chapter it was shown that naturally striated and non-striated petal cuticles display different chemical profiles. Transgenic lines displaying abnormally smooth cuticles had a chemical profile similar to naturally smooth cuticle, suggesting an important link between the chemistry of the cuticle and its capacity to buckle and produce striations. Closer analyses of the chemical profiles of the cuticle

of *Hibiscus sp., Hibiscus trionum* varieties and transgenic lines revealed differences in the abundance of 6 different compounds in striated cuticle: $C_{51}H_{76}O_{12}$, $C_{28}H_{50}O_4$, $C_{16}H_{32}O_4$, $C_{38}H_{70}O_4$, $C_{45}H_{64}O_{11}$ and $C_{40}H_{72}O_9$. Some of these were identified with relative confidence, such as $C_{16}H_{32}O_4$ which corresponds to the cutin monomer 10,16 dihydroxypalmitate, and $C_{28}H_{50}O_4$ corresponding to a long chain aliphatic acid. The structure and origin of the 4 other compounds remain unclear and might be waxy aliphatic acids ($C_{38}H_{70}O_4$) or combinations of long chain fatty acids and other functional units such as sterol or glycerol ($C_{40}H_{72}O_9$ and $C_{45}H_{64}O_{11}$).

It is likely that variation in the chemistry of the cuticle influences its mechanical properties, hence its ability to buckle. In the tomato fruit, an increase in flavonoid content was also associated with an increase of the elastic modulus of the cuticle (Domínguez et al., 2009), supporting the potential role of glycosyl flavones ($C_{27}H_{28}O_{18}$ and $C_{27}H_{28}O_{19}$) in the production of altered striations in several transgenic lines.

The presence of these compounds in the solvent used for LESA-MS might not only reflect their presence in the cuticle. The 2 different solvents used to solubilise the cuticle do not disrupt the cuticle polymers, hence the abundance of a compound in the extraction liquid is also a reflection of its availability. The 10,16-dihydroxypalmitic acid is one of the most abundant constituents of plant cuticle (Baker & Holloway, 1970), consequently, its absence observed in non-striated cuticles most likely reflects its unavailability resulting from its integration into the cutin polymer. The abundance of the 10,16-DHP could then be interpreted in terms of relative polymerisation of the cutin monomers translating in differences in the cuticle stiffness. This suggests that the regulation of striation production is the consequence of regulation of the cutin network polymerisation. Furthermore, the production of a cutin polymerase overexpressing transgenic line (*35S:HtCD1.1*) altered the buckling capacity of the cuticle (fig. 3.2), corroborating that the degree of polymerisation of the cutin network influences the production of cuticle striations. Nevertheless, the depletion in 10,16-DHP in both the polymerised cutin and the non-polymerized fraction of *A. thaliana* cuticle was correlated with a loss of striations on petal conical cells, which supports the observations made in this chapter and the potential role of the 10,16-DHP in the production of cuticular striations (Panikashvili et al., 2009).

3.5 Conclusion

This study showed a correlation between the chemistry of the cuticle and its ability to buckle. Further analyses also suggested that the 10,16-DHP (a cutin monomer) plays a relevant role in the development of striations. Due to the specificity of LESA-MP and the use of non-depolymerising solvents, it can be supposed that differences in the abundance of 10,16-DHP in striated and non-striated epidermises also reflect differences in the degree of reticulation of the cutin network. In turn, this may lead to modulations of the mechanical properties of the cuticle. Together this suggests that the regulation of the cuticle chemistry may be responsible for the capacity of an epidermis to buckle, most likely via modulation of its mechanical properties.

Chapter 4: Transcriptomic analyses show two potential regulation pathways for the modulation of the stiffening of the cuticle in the proximal petal region

Sample collection was performed in collaboration with Edwige Moyroud and May Yeo from the Sainsbury Laboratory Cambridge University (SLCU), and data analyses were performed with the support of Qi Wang from the Plant Science Department of Cambridge University

4.1 Introduction

During the development of *H. trionum* flowers, striations start to appear between late stage 3 and early stage 4 in the proximal region of the petals (see fig. 1.2). Beforehand, the epidermal cells and cuticle are very similar in both proximal and distal petal regions: small cuboid cells topped with a smooth cuticle. Different transcription factors and effectors are expressed in the distal and proximal regions of the petal, leading to the development of two different epidermal regions, a distal one formed of conical cells topped with smooth cuticle and a proximal one formed of flat elongated cells topped with striated cuticle. According to the theory of buckling (Bowden et al., 1998) (see fig. 1.4), a bilayer system is needed to produce striations and the upper layer must be stiffer (with a higher Young's modulus) than the layer below, which remains relatively more compliant with a lower Young's modulus. In this chapter I aimed to highlight the possible molecular pathways leading to the development of nano-scaled striations under the prism of the theory of buckling.

4.1.1 Regulation of cuticle production

The abundant literature describing the regulation of cuticle biosynthesis and the preliminary papers addressing the production of cuticular ridges *in planta* provide us with a list of candidate genes with the potential to be involved in the production of a layered cuticular system capable of producing structural colours.

As discussed in the introduction (see chapter I) the *AtSHN* genes, encoding AP2/ERF transcription factors, play a central role in the regulation of cuticle production (Shi et al., 2013) through the activation of multiple target genes such as *CYP86A4/7*, *BDG3* and genes encoding proteins of the GDSL family such as *LTL1* and *CUS2* (Hong et al., 2017; Shi et al., 2011). Furthermore, the production of *35S:HtSHN3-VP16* and *35S:HtSHN3-SRDX* transgenic lines of *Hibiscus trionum* led to a loss of cuticular striations, pointing to *HtSHN3* as one of the potential regulators of the production of cuticular nano-ridges. A member of the *cytochrome P450* family, *CYP77A6,* and the glycerol 3-phosphate acyltransferase *GPAT6* were also identified as essential for the production of nano-ridges on the petal abaxial epidermal surface of *Arabidopsis thaliana* (Li-Beisson et al., 2009). CYP77A6 acts as a midchain hydroxylase involved in the synthesis of 10,16 dihydroxypalmitate subsequently to CYP86A4 and GPAT6 which are involved in ω-hydroxylation and palmitic acid synthesis respectively (Li-Beisson et al., 2009) (see also fig. 1.8a). CUS2, a GDSL esterase lipase protein, was identified in *Arabidopsis thaliana* as involved in the maintenance of cuticular ridges on sepal conical cells and more moderately on petal cells. *CUS2* is considered very similar to *SlCUS1*/*CD1*, which encodes the enzyme responsible for the polymerisation of cutin monomers (Hong et al., 2017).

AtSHN1 was also found to play a major role in cuticle regulation and its over expression in *Arabidopsis thaliana* led to the overproduction of multiple cutin monomers and waxes in leaves and was shown to regulate *LACS2* (Kannangara et al., 2007b). LACS2 plays an important role in lipid metabolism and is crucial for the production of very long chain fatty acids and cutin monomers in cooperation with other LACS proteins (Zhao et al., 2019).

Similarly to *AtSHN1* and *AtSHN3, AtDEWAX* also encodes an *AP2/ERF* transcription factor. However, AtDEWAX has been shown to negatively regulate wax biosynthesis via inhibition of acyl~CoA transferases such as *ECERIFERUM2* (*CER2*) (Go et al.,2014) which is involved in the production of fatty acids longer than 28 carbon residues (Haslam et al., 2012; Negruk et al., 1996; Xia et al., 1997), thus participating in the production of cuticular waxes. *CER4 (ECERIFERUM4)* also encodes an acyl~CoA alcohol forming transferase, however its expression is not influenced by DEWAX (Go et al., 2014). The overexpression of *CER4* was linked to excessive loads of C_{26} and C_{24} primary

alcohols in yeast (Rowland et al., 2006) suggesting that CER4 functions upstream of CER2 in the production of cuticular waxes.

The translocation of cuticular lipids to the extra cellular environment remains poorly understood. However, it has been shown that ABCG11, a half transporter of the ATP-Binding Cassette transporter family and capable of homo and hetero-dimerisation, has a strong affinity for C_{29} alkanes suggesting a potential role in their translocation across the plasma membrane (Bird et al., 2007) .

Finally, BODYGUARD, an extracellular protein of yet unknown biochemical function was found to be essential for the integrity of the cell wall and the cuticle. Overexpression of *BDG* led to a strong increase in the cutin load without any alteration of the wax load, suggesting that *BDG* is involved in the cutin synthesis pathway. Strong differences in the abundance of polyunsaturated C_{18} were also observed between *BDG* over-expressing transgenic lines, WT lines and *BDG* defective mutant lines suggesting that BDG is involved in the biosynthesis of polyesters of polyunsaturated C_{18} monomers. This also suggests that *BDG* is a limiting factor in the cutin synthesis. Differential expression of the *BDG* could thus modify the chemical and mechanical properties of the cuticle and subsequently modulate its capacity to buckle (Jakobson et al., 2016; Kurdyukov et al., 2006).

4.1.2 **Regulation of cell wall production**

Intertwined with cuticular compounds, the cell wall consists of a complex polymer of cellulose (polymer of β(1→4)-D-glucose) arranged in microfibrils crosslinked to one another by hemicellulose fibres, pectin (polymer of α(1→ 4) galacturonic acid), xyloglucans and eventually lignin, amongst other polysaccharides. Its mechanical properties depend on the orientation of the successive layers of microfibrils and the degree of reticulation between them. Below the cuticle proper, polysaccharides typical of the cell wall coexist with cuticle compounds such as the cutin network and waxy substances. Modulation of the mechanical properties of the cell wall can thus have an impact on the stiffness of the extracellular matrix.

The *WAT1* (*WALLS ARE THIN 1*) gene, homologue of *Medicago truncatula NODULIN 21*, encodes a protein of the plant drug/metabolite exporter (P-DME) family and was identified in *Arabidopsis thaliana* as responsible for the deposition of secondary cell wall fibres and cell elongation.

It is located at the tonoplast and a defective mutant was also linked to a reduction of cell growth and secondary metabolites associated with the secondary cell wall as well as a perturbation of the auxin and tryptophan pathways (Ranocha et al., 2010).

The *COBRA-like2* gene codes for a glycosylphosphatidylinositol-anchored protein involved in the production of a mucilage coating in *A. thaliana* seeds. It was shown to be involved in crystalline cellulose deposition and influence pectin solubility (Ben-Tov et al., 2015). In *Solanum lycopersicum*, the expression of a *COBRA-like* gene was also altered in the exocarp in a *GPAT-6* mutant context (Petit et al., 2016), which suggests a link between cuticle and cell wall production.

Other proteins may modulate the reticulation of the cellulose network by altering the pectin properties. Pectin acetylesterase can hydrolise acetyl groups on galacturonic acid, thus potentially changing its binding capacities to cellulose. Ecotpic expression of *Populus trichocarpa PECTIN ACETYL ESTERASE 1* (*PtPAE1*) in *Nicotiana tabacum* resulted in an impairment of cellular elongation of floral styles and filaments, pollen grain germination and pollen tube growth (Gou et al., 2012). Furthermore, acetylation may play an important role in its gelling properties and its degradability (Dongowski, 2001; Gou et al., 2012)

Finally, the ectopic expression of *Asperigillus* xyloglucanase in poplar caused marked degradation of the xyloglucan in the walls and accelerated cell elongation in the apical growing region of the stems, consistently with the idea that xyloglucanase increase the plasticity of cell wall by degradation of the xyloglucan cross-links present between cellulose microfibrils and hemi-cellulose (Hayashi & Kaida, 2011)

4.1.3 Transcriptomic analyses

The history of transcriptomic analyses is now about 25 years old and typically consists of a snapshot of all the genes expressed in a cell or a specific group of cells at a given time (McGettigan, 2013). In 2006 the RNA-sequencing technologies (also known as whole transcriptome shotgun sequencing) replaced microarray technologies further developing the accuracy of expression quantification and representation of mRNA, making of transcriptomic analyses a more objective tool for molecular biology (McGettigan, 2013). In 2008, the short read technology developed by Solexa

(now Illumina) holding a processing capacity of 600 GB enabled the dramatic decrease of the costs of the RNA-sequencing technology (McGettigan, 2013). The increase in the number of reads produced by illumina technology also required the development of numerous computational tools for data curation, read mapping, read counting and annotation. The development of specific programmes such as SOAP denovo and Trinity enabled the production of *de novo* assemblies producing a scaffold based on all the sequenced transcripts against which reads can be mapped and counted, thus allowing the use of transcriptomic analyses for non-model species (Lu et al., 2014; Wang et al., 2017). Transcriptomic analyses are often boosted by gene annotation programmes such as transdecoder, translating cDNA sequences into protein sequences, and Trinotate as well as protein databases allowing the prediction of function for each transcript. Gene-Ontology (GO) analyses then help with the grouping of these genes under categories of biological processes.

By comparing transcriptomes of different tissue types, it becomes possible to identify sets of genes involved in specific physiological phenomena.

Transcriptomic analyses were used to assess the molecular pathways and genes enabling petal cell elongation in *Chrysanthemum morifolium* by comparing petal transcriptome at 4 different stages of development. The subsequent transcriptomic comparisons unravelled the role of 21 bHLHs, 2 TCPs and 5 MADS-box transcription factors (Wang et al., 2017). In *Litchi chinensis*, transcriptomic analyses highlighted the genes differentially expressed during oxidative stress and helped understand the mechanisms supporting the resulting abortion of rudimentary leaves observed in nature (Lu et al., 2014). Thus, transcriptomic analyses enable the identification of genes involved in complex biological processes providing an integrative overview of the molecular pathways at play, even in non-model species.

The large amount of data coming from RNA sequencing and the short size of the reads can however lead to ambiguities in the counting of reads and the generation of a *de novo* assembly. The difference in parameters that can be set when using the different programmes was demonstrated to lead to ambiguities of read counting when it comes to certain genes. In maize, a simulated set of reads aligned with different parameters showed that over 25% of the genes deviated by more than 20% from the expected count values (Hirsch et al., 2015). In comparative analyses of transcriptomes based on *de novo*

assemblies, the detection of false positives (FPs) when looking for differentially expressed genes (DEGs) is another challenge of transcriptomic analyses. FPs usually result from computational uncertainty when reads are mapped back to two or more isoforms of a gene resulting in biased estimated abundance frequencies of isoforms (González & Joly, 2013). If the sequencing strategy does not greatly impact the number of false positives, the use of paired-end read alignment significantly reduces the number of false positives when compared to single-end read alignment. Interestingly, the sequence length did not have the same impact on the number of FPs (González & Joly, 2013).

In the case of the transcriptomic analyses of *Hibiscus trionum* paired-end sequencing was performed by Genewiz®. Subsequently, I used trinity to perform *de novo* assembly on the 15 different plants that were used (five per stage of development) to increase the representation of the various alleles of the different plants cultivated before concatenating the assemblies into one scaffold, which was then further curated from redundancy using the Evigene programme. This enabled a representation of the various alleles present in our sampling population whilst reducing the number of FPs. After processing of the raw data (section 4.2.2, table 4.2), 117,961 loci were identified.

To investigate the different molecular mechanisms underpinning the production of nano-scaled striations in *Hibiscus trionum*, I performed a total RNA-sequencing of the proximal and distal part of the petals at stage 2, 3 and 4 of flower development, giving us information on the genes that are expressed before, during and after the development of striations (see fig. 1.2). The transcriptomic data obtained were then used in two different ways: I firstly investigated the expression profile of genes found in the literature that are known to have a role in cuticle production or that have already been correlated with an alteration of striations. Secondly, I selected a subset of genes that displayed expression profiles compatible with a potential role in the development of nano-scaled cuticular striations. Gene Ontology (GO)-term annotation was used to predict the biological process in which the different genes could be involved, and the enrichment in various biological processes was then calculated for each subset and the genes. Several genes involved in the regulation of cellulose production and alkane metabolism were identified for further analyses.

4.2 Materials and methods

4.2.1 **Tissue collection and raw data production**

Five biological replicas per developmental stage (stage 3 and 4) were selected and the proximal and distal parts of the petals were collected from the same individuals. Simultaneously, May Yeo and Dr Edwige Moyroud collected the proximal- and distal petal regions of stage 2 buds from 5 biological replicas (table 4.1). All the samples were collected in microtubes and snap-frozen in liquid nitrogen. Frozen tissues were ground in liquid nitrogen using a pestle and mortar previously washed with soapy bleach and rinsed with 70% ethanol. RNA was extracted using the Sigma-Aldrich™ Spectrum Plant-Total RNA Kit™. The alternative 'A' for 'extremely difficult tissues' was used, and 30 µL of elution solution was passed twice through 2 binding-columns to maximise RNA yield.

RNA purity was assessed using nanodrop and degradation was measured using gel migration (see section 2.3.6). The mean of the OD 260/280 and 260/230 for all the 30 samples was superior to 2.04 and 1.59, respectively, with a mean for OD 260/230 = 1.8. Gel migration showed no sign of RNA degradation. Samples were then sent to Genewiz® for subsequent quality control, library preparation and sequencing.

There, RNA quality was assessed a second time by nano-drop, and then by Qubit and TapeStation: RNA samples were quantified using Qubit 2.0 Fluorometer (Life Technologies, Carlsbad, CA, USA) and RNA integrity was checked with Agilent TapeStation (Agilent Technologies, Palo Alto, CA, USA). RNA library preparation, sequencing reaction, and bioinformatics analysis were conducted at Genewiz, LLC. (South Plainfield, NJ, USA). RNA sequencing library preparations used the NEBNext Ultra RNA Library Prep Kit for Illumina by following the manufacturer's recommendations (NEB, Ipswich, MA, USA). mRNAs were first enriched with OligodT beads and then fragmented for 15 minutes at 94 °C. First strand and second strand cDNA were subsequently synthesized. cDNA fragments were end repaired and adenylated at 3' ends, and universal adapter was ligated to cDNA fragments, followed by index addition and library enrichment with limited cycle PCR. The sequencing libraries were validated on the Agilent TapeStation (Agilent Technologies, Palo Alto, CA, USA), and quantified by using Qubit 2.0 Fluorometer (Invitrogen, Carlsbad, CA) as well as by quantitative PCR (Applied Biosystems, Carlsbad, CA, USA). The sequencing libraries were clustered on one lane of a

flowcell. After clustering, the flowcell was loaded on the Illumina HiSeq instrument according to the manufacturer's instructions. The samples were sequenced using a 2x150 Paired End (PE) configuration. Image analysis and base calling was conducted by the HiSeq Control Software (HCS). Raw sequence data (.bcl files) generated from Illumina HiSeq were converted into fastq files and de-multiplexed using Illumina's bcl2fastq 2.17 software. One mis-match was allowed for index sequence identification.

The average read size was 337 bp. The average adaptor size was 130 bp. The average insert size was 207 bp. Between 24 and 30 million reads were obtained for each replica, with a mean of about 28 million reads per replica (table 4.1).

Tissue collection and RNA extraction of proximal and distal regions of stage 2 was performed by Edwige Moyroud and May Yeo simultaneously, in the same room, on plants grown in the same

Tissue type	Individual	Number of reads	Yield (Mbases)	Average read length without adaptors (bp)
P2	1	27,120,946	8,137	300.0264076
P2	2	30,084,112	9,025	299.9922351
P2	3	29,461,405	8,838	299.9856931
P2	4	26,629,457	7,989	300.0061173
P2	5	24,025,974	7,208	300.008649
D2	1	30,070,050	9,021	299.9995012
D2	2	27,439,983	8,232	300.0001859
D2	3	29,896,395	8,969	300.0027261
D2	4	29,953,936	8,986	299.9939641
D2	5	30,084,493	9,025	299.9884359
P3	6	30,083,385	9,025	299.9994848
P3	7	26,301,010	7,890	299.9884795
P3	8	27,990,866	8,398	300.0264443
P3	9	24863457	7,460	300.0387275
P3	10	29,460,506	8,837	299.9609036
D3	6	26,430,812	7,930	300.0286181
D3	7	29,856,043	8,956	299.9727727
D3	8	30,033,186	9,009	299.9681752
D3	9	31,028,079	9,308	299.9863446
D3	10	26,381,486	7,914	299.9831018

Tissue type	Individual	Number of reads	Yield (Mbases)	Average read length without adaptors (bp)
P4	11	25,357,922	7,608	300.024584
P4	12	27,864,659	8,359	299.9857274
P4	13	26,852,348	8,055	299.9737677
P4	14	30,605,183	9,181	299.9818691
P4	15	29,982,598	8,994	299.9740049
D4	11	30,171,348	9,052	300.0197406
D4	12	29,983,800	8,996	300.0286822
D4	13	30,081,114	9,024	299.98889
D4	14	30,102,241	9,031	300.0108862
D4	15	29,871,803	8,961	299.9818926

Table 4.1: Transcriptomic data general information. Details of the number of reads that were sequenced per condition and biological replicas as well as the total number of bases that were processed (see 'yield' column) and the average read length after adaptor trimming. In the 'tissue type' column 'D' indicates 'distal' petal regions, 'P' 'proximal' petal regions, and the digit corresponds to the developmental stages. Adaptor sequences that were used for this transcriptome are AGA-TCG-GAA-GAG-CAC-ACG-TCT-GAA-CTC-CAG-TCA-C and AGA-TCG-GAA-GAG-CGT-CGT-GTA-GGG-AAA-GAG-TGT-A

glasshouse and sampled at the same time. They followed the exact same process as described for stage 3 and 4 and were processed by Genewiz® together with stage 3 and stage 4 samples.

4.2.2 Raw data transformation

Adaptors and low quality reads were trimmed using the 'trimmomatic' v 0.34 package using default parameters (Bolger et al., 2014). One *de novo* assembly was performed per biological replica using 'Trinity' v 2.8.4 (Haas et al., 2013). The quality of the assembly was assessed using 'bowtie2' v 1.2.2 (Langmead & Salzberg, 2012). More than 95% of the reads could be mapped against their respective assembly. Assemblies of the different biological replicas were merged into one file and redundancy was removed using 'Evigene' (Gilbert & Don, 2016). Mapping, redundancy removal, and clustering were done using 'Salmon' V 0.9.1 and 'corset' V 1.07 packages (Patro et al., 2017; Urbano, 2017). The 'DEseq2' v 1.22.2 R package (Love et al., 2014) was used to interpret and analyse the count files generated with corset. Depth of sequencing was corrected using regularised log transformation from the 'DEseq2' package (fig. 4.2). Heatmaps were plotted using the 'pheatmap' package v 1.0.12 (Kolde, 2019).

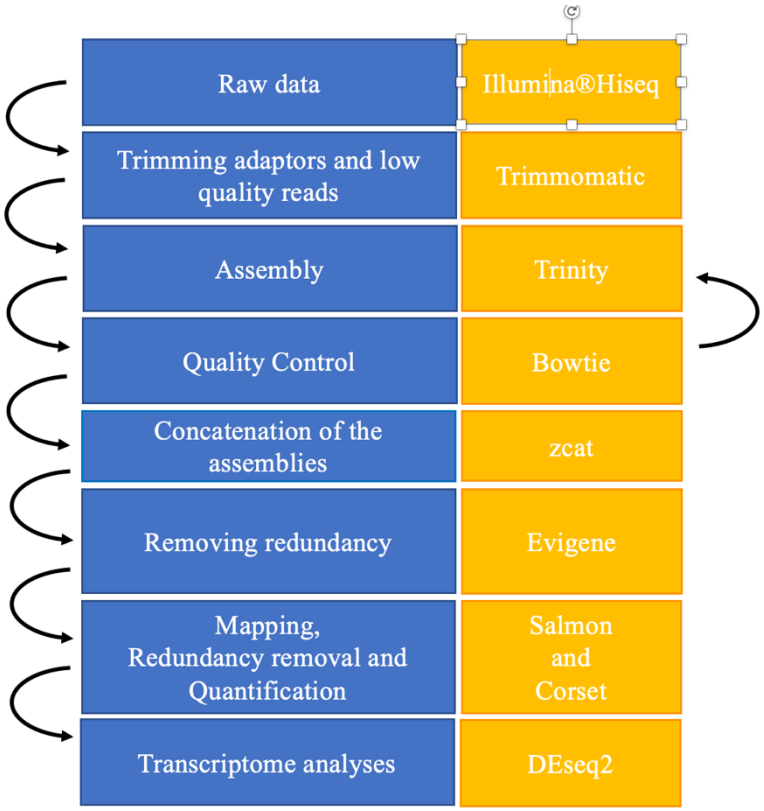

Figure 4.2: Cartoon representing the pipeline used to process RNA-sequencing data. In blue are figured the successive tasks that were performed and in yellow, the programmes or command line (in the case of 'zcat') that were used to achieve them.

4.2.3 **Transcriptome comparison**

The selection of a subset of genes was based on the assumption that the production of cuticular striations in the proximal petal region results from the up- or downregulation of genes between developmental stage 2 and 4 and/or between stages 3 and 4. The number of conditions studied here and the ambiguity surrounding the precise timing of cuticular ridges formation involved a complex comparison design to include all the potential genes involved in the development of a structurally coloured cuticle. Since striations are visible in the proximal region at stage 4, the comparison performed focalised on differential expression with stage 4 petal parts. For each comparison, genes were considered differentially expressed if their expression differed by at least 2-fold change with an adjusted p-value (padj) below 0.05 (differential expression $\geq$ 2-fold change and padj $\leq$ 0.05) and not differentially expressed if they displayed a differential expression inferior or equal to 2-fold change with a padj superior or equal to 0.05 (differential expression $\leq$ 2-fold change and padj $\geq$ 0.05). Genes were considered as evolving differently between 2 paired comparisons when the absolute value of the

difference between the 2 respective comparisons was superior to 2-fold change (Absolute Value ([DE between A and B] – [DE between C and D]) ≥ 1). Samples were compared as follow:

1) Following the assumption that genes involved in the development of striations would be differentially expressed in the proximal petal region during development, and constant in the distal petal region, I selected genes that were up- or down-regulated in the proximal petal part (striated at stage after stage 3) between stages 2 and 4 or stages 3 and 4, but not differentially expressed (constant) in the distal part (smooth) during development: Genes displaying a differential expression (DE) between the proximal region at stage 2 and stage 4, or at stage 3 and stage 4 were filtered. From this subset, genes that are not differentially expressed in the distal region between stage 2 and stage 4, or at stage 3 and stage 4, depending on the stages compared, were removed (fig. 4.3a: (DEGs in 3) – (constant in 1) + (DEGs in 4) – (constant in 2)) yielding 2804 genes.
2) Following on the previous assumption, I selected genes that were differentially expressed in proximal and distal tissues during development but in a different way (e.g. up regulated in the distal region between stages 2 and 4, and down regulated in the proximal region between stages 2 and 4). Differentially expressed genes (DEGs) between stage 2 proximal and distal regions or stage 4 proximal and distal regions, or between stage 2 and stage 4 proximal region or between stage 2 and stage 4 distal region, but necessarily differentially regulated between the distal and the proximal regions between stages 2 and 4 were filtered (fig. 4.3b: DEGs in (5 or 6 or 7 or 8) and (8 ≠ 6)) yielding 7552 genes.
3) The previous comparison strategy was repeated for stages 3 and 4 of development. DEGs between stage 3 proximal and distal regions or stage 4 proximal and distal regions, or between stage 3 and stage 4 proximal region or stage 3 and stage 4 distal region, but necessarily differentially regulated between the distal and the proximal regions between stages 3 and 4 were filtered (fig. 4.3c: DEGs in (9 or 10 or 11 or 12) and (10 ≠ 12)) yielding 14 619 genes.
4) Finally, I selected genes that were differentially expressed between proximal and distal petal parts and not during development in order to find genes that are constantly expressed during development but differentially between the proximal and distal petal parts (e.g., genes constantly up regulated in the distal petal part and down regulated in the proximal petal part). This may help us find genes that

naturally differentially expressed in the proximal petal part and take part in reaching the buckling conditions. DEGs between the proximal and distal region at stage 2 and stage 3 and stage 4 were filtered (fig. 4.3d: DEGs in 13 and 14 and 15) yielding 2202 genes.

From these 4 different filtering strategies and after removal of duplicated genes I obtained a set of 18,848 genes (≈ 16% of the total number of loci). To reduce the number of genes to analyse I applied 2 more filters to this subset of genes:

5) From the 18,848 genes, I selected the DEGs between the proximal and distal region at stage 2 following the assumption that the development of striations involves differential regulation of genes as early as stage 2, bringing down the number of genes to 5,278 genes (fig. 4.3e: 16 ≥ 2).
6) Finally, from these 5,278 genes I selected the genes for which the differential expression observed at stage 2 is equal or inferior to that observed at stage 3 between the proximal and the distal petal part, following the assumption that differentiation factors involved in the production of striations already differentially expressed at stage 2 are at least equally differentially expressed at stage 3, bringing down the number of genes to 1620 (fig. 4.3f: 16 ≤ 17).

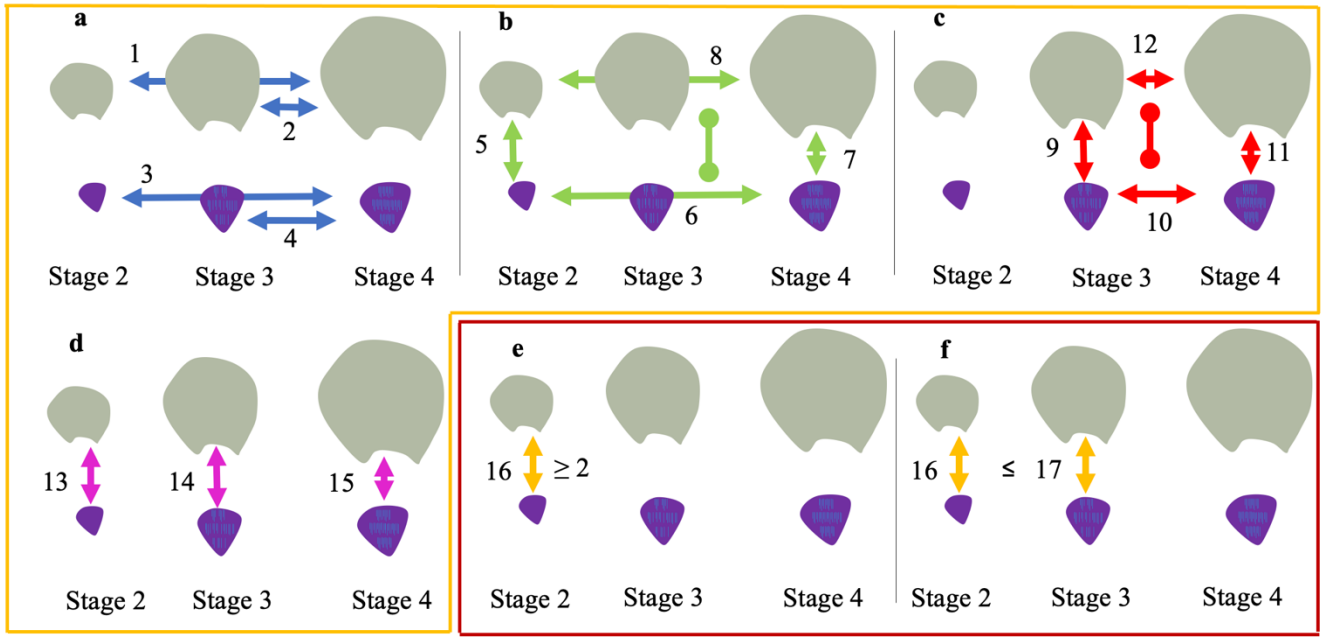

Figure 4.3: Cartoon representing the design used for transcriptomic comparisons. *Hibiscus trionum* petal at stages 2, 3 and 4 with distinction between the proximal region in purple and distal region in grey. Blue stripes figured in the proximal region at stage 3 and 4 represent the structurally coloured cuticle. **(a, b, c** and **d)** The orange frame groups together the 4 comparisons that were performed independently to narrow down the original dataset. **(e** and **f)** The red frame groups the 2 filtering strategies that were used subsequently. **(a-f)** Double headed arrows represent 1st degree comparisons between 2 transcriptomes, rounded head arrows represent 2nd degree comparison (performed between two 1st degree comparisons). A 2-foldchange threshold and a p-value of 0.05 were used for each comparison.

4.2.4 Gene annotation

Trinotate v 3.1.1 was used to annotate transcripts using the full protein database of UniprotKB accessed on June 20th, 2019 and available here https://ftp.uniprot.org/pub/databases/uniprot/previous_major_releases/release-2019_06/knowledgebase/ and complemented with the specific proteome of *Gossypium hirsutum* accessed on August 12th, 2019 following the indications provided by UniprotKB: https://www.ebi.ac.uk/training/online/courses/uniprot-exploring-protein-sequence-and-functional-info/getting-data-from-uniprot/ at the following link https://www.arabidopsis.org/download/index-auto.jsp?dir=%2Fdownload_files%2FProteins%2FTAIR10_protein_lists.

4.2.5 Gene expression

Gene expression is presented as the mean-centreed number of reads counted for a specific locus across the 5 biological replicas after correction for sequencing depth using 'regularised log' transformation and for library size using automatic features of the DEseq2 R package (Love et al., 2014).

4.2.6 Transcriptome comparison

Transcriptomes were compared with one another as described in section 4.2.3 and fig. 4.3 using the DEseq2 R package (Love et al., 2014) after correction for library size (inherent correction of the DEseq2 package) and sequencing depth using the 'regularised log' transformation, also done using the DEseq2 R package (Love et al., 2014)

4.2.7 Identification of orthologous genes of *A. thaliana* genes in *H. trionum*

Genes that were demonstrated to play a role in cuticle production or cuticle striation patterning were identified in the literature (see Chapter 1 and section 4.1.1 and 4.1.2). Orthofinder v 2.3.12 was used to find orthologous pairs between *Hibiscus trionum* transcripts and the *Arabidopsis thaliana* gene sequences published in the literature (see Chapter 1 and section 4.1.1 and 4.1.2). For maximum accuracy homologues were determined using the protein sequences data base of *Solanum lycopersicum*,

Phaseolus vulgaris, *Arabidopsis thaliana*, *Theobroma cacao* and *Gossypium raimondii* obtained from the UniprotKB database (accessed on June 23rd, 2020). Species protein data bases were downloaded as subsets of UniprotKB protein data subsets as explained for *Gossypium hirsutum* in point 4.2.3 with the following links:

- https://www.uniprot.org/uniprot/?query=lycopersicum&fil=proteome%3AUP000004994+AND+organism%3A%22Solanum+lycopersicum+%28Tomato%29+%28Lycopersicon+esculentum%29+%5B4081%5D%22&sort=score
- https://www.uniprot.org/uniprot/?query=theobroma%20cacao&fil=proteome%3AUP000026915+AND+organism%3A%22Theobroma+cacao+%28Cacao%29+%28Cocoa%29+%5B3641%5D%22&sort=score
- https://www.uniprot.org/uniprot/?query=phaseolus%20vulgaris&fil=proteome%3AUP000000226+AND+organism%3A%22Phaseolus+vulgaris+%28Kidney+bean%29+%28French+bean%29+%5B3885%5D%22&sort=score
- https://www.uniprot.org/uniprot/?query=gossypium%20raimondii&fil=proteome%3AUP000032304+AND+organism%3A%22Gossypium+raimondii+%28New+World+cotton%29+%5B29730%5D%22&sort=score
- https://www.uniprot.org/uniprot/?query=arabidopsis%20thaliana&fil=proteome%3AUP000006548+AND+organism%3A%22Arabidopsis+thaliana+%28Mouse-ear+cress%29+%5B3702%5D%22&sort=score

Protein sequences of *Hibiscus trionum* were determined using Transdecoder v 5.5.0 using a customised script (https://gitlab.com/qiwang/ngs/-/blob/master/transdecoder/transdecoder_Ht_simple.sh).

In the cases of *ABCG11*, *CER2, ABCG11* and *DEWAX* several transcripts of *Hibiscus trionum* displayed inconclusive phylogeny with their *Arabidopsis thaliana* orthologues. Recent unpublished genomic data of *Hibiscus trionum* were used to help us identify transcript variants from transcripts originating different loci. All predicted homologies were solely based on protein sequences.

In the case of *HtSHN1, HtSHN2* and *HtSHN3*, the sequences used for molecular work and expression assessment were isolated previously to the investigation of their orthology with *AtSHN* genes as presented in fig 1.5.

4.2.8 Clustering

The previously obtained subset of 1620 genes was further divided into super clusters based on their expression profiles. The 'Total within sum of square' and the 'Silhouette' methods were used to determine the optimal number of clusters. Results suggested a division into 4 super clusters.

4.2.9 Enrichment analyses

Enrichment was expressed in terms of biological processes using GO-Term analyses and calculated with topGO v 2.34.0 R package (Rahnenfuhrer & Adrian, 2018). Out of 117,961 genes 40,782 genes were annotated with at least one GO-Term (34.6%). Enrichment was then expressed as a ratio between the observed number of genes displaying a GO-Term in the fraction of the transcriptome studied and the expected number of genes displaying the same GO-term in the same fraction of the transcriptome, assuming an even distribution.

4.3 Results

4.3.1 The different sample types collected are characterised by specific gene expression profiles

The quality of the sampling was assessed by PCA, and sample to sample Pearson correlation (fig. 4.4). All the samples clustered according to their biological stage of development and their petal region of origin (fig. 4.4a). The biological replicas clustered together for each type of sample, confirming sampling quality. PC1 segregated the sample according to their developmental stage and PC2 according to their origin (proximal or distal region of the petal) and account for 91% of the variation when considered together.

Despite apparent similarities between the proximal and distal epidermal cells at stage 2 (actively dividing small cuboid cells with undifferentiated cuticle (fig. 1.2a), processes seem already at play to induce differentiation as distal and proximal samples do not group together. The distance between

proximal and distal samples increases along PC2 consistently with a progressive differentiation of these 2 regions into 2 different tissues (fig. 4.4a).

A sample-to-sample Pearson correlation assay showed a low correlation score between stage 2 distal and stage 3 proximal parts (fig. 4.4b), suggesting the occurrence of important changes in gene expression, dividing the petal epidermis into two distinct specialised epiderma. Unsurprisingly, the lowest correlation score was observed between stage 2 and stage 4 petal tissues. This result was also confirmed by Spearman and Kendall correlation assays (see supplement figure 1 in section 4.6).

I then aimed to assess whether differences in the transcriptomes of the proximal and distal regions observed in the PCA could translate into differences in expression of genes involved in the production of the cuticle.

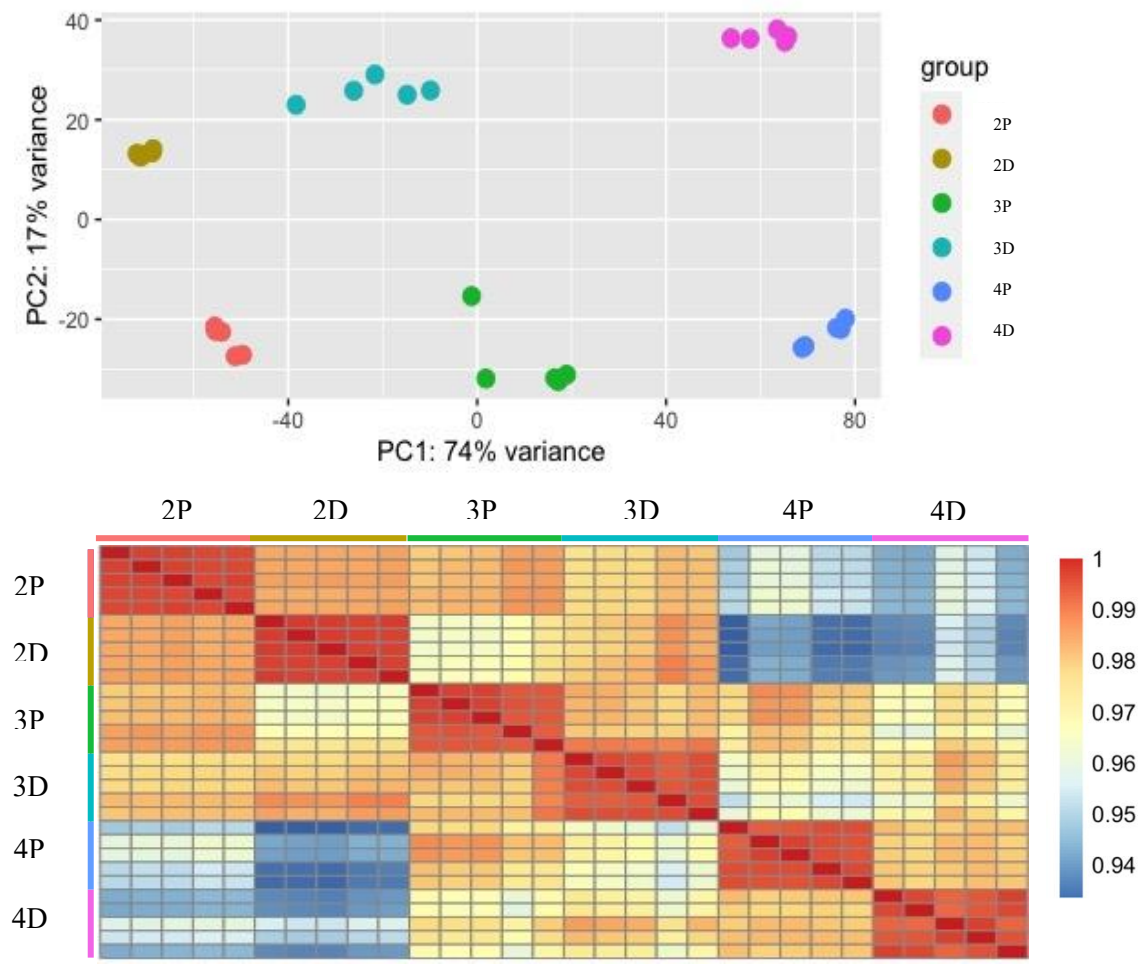

Figure 4.4: PCA and sample to sample quality control performed on the transcriptome of each sample. **(a)** Principal component analyses performed on regularised log transformed reads of the 6 different types of samples and their 5 biological replicas. **(b)** Sample to sample correlation heatmap performed on the same dataset using the Pearson correlation (1 representing the maximal score of correlation). 'P' stands for 'proximal', 'D' for distal and the digits for the developmental stage.

4.3.2 The proximal petal parts are characterised by an induction of *HtSHN3* and *HtDEWAX-like 2*

Transcriptomic data were first used to analyse the expression of a set of genes known to play a role in cuticle biosynthesis regulation and/or nano-ridge production (as described in chapter 1). Their expression profiles are represented in figure 4.5a and 4.5b. Two categories of expression profiles were identified: genes having a higher expression in proximal petal tissues (fig. 4.5a) and genes that are more expressed in distal petal tissues (fig. 4.5b).

At first *HtSHN3* is relatively weakly expressed in both the proximal and the distal parts of the petal. However, at stage 3 a strong activation of *HtSHN3* in proximal tissues and a steady increase of expression until stage 4 can be observed, while relatively little expression can be observed in distal petal tissues (fig. 4.5a).

BDG3-like2 and *CYP86A4/A7-like3* display a very similar expression profile to that of *HtSHN3* in the proximal petal part which is consistent with a *HtSHN3* mediated activation (fig. 4.5a). However, the relative higher expression of *CUS1/2-like1* in distal tissue parts may suggest the presence of a repression mechanism in proximal tissues that counteracts its *HtSHN3* mediated activation and induces *CUS1/2-like1* in the distal petal tissues in a *HtSHN3* independent manner (fig. 4.5b).

The *CYP77A6-like1* and *2*, *GPAT6-like2* and *3*, and *CYP86A4/7-like3* genes display an expression profile similar to that of *SHN3* in proximal petal epidermal tissues, suggesting its potential role in their activation. The activation of *CYP77A6-like1* and *2*, *GPAT6-like2* and *3*, and *CYP86A4/7-like3* genes is consistent with the biosynthesis of 10,16-dihydroxypalmitate, a cutin monomer (Li-Beisson et al., 2009) (fig. 4.5a). The expression profiles of *BDG3-like1* and *BDG3-like2* follow a pattern consistent with the activation of the cutin synthesis pathway with an overall increase from stage 2 to stage 4 of development in proximal epidermal tissues while remaining relatively lower in distal epidermal tissues (fig. 4.5a). *BDG3-like3* is, however, more expressed in distal tissues, yet its expression decreases over time, indicating a more moderate synthesis of cutin.

The expression profile of *DEWAX-like2* is very low at early stages of development in both proximal and distal epidermal tissues, however, its expression peaks at stage 3 in proximal tissues. This

suggests a specific activation of the *DEWAX* pathway in the proximal epidermal petal tissues, consistent with an inhibition of wax synthesis (Go et al., 2014). Despite a slight increase of the expression of *CER2-like2* at stage 3, the expression profile of *DEWAX* is consistent with a downregulation of *CER4* in proximal petal tissues at stages 3 and 4 of development.

In the distal petal part, the expression of *CYP86A4/7-like1* and *2*, as well as that of *BDG3-like3,* indicates a more moderate synthesis of cutin, with a *HtSHN3* independent activation. The progressive increase of *CYP86A4/7-like1* and *2* could indicate cuticle expansion.

The *H. trionum* homologue of *A. thaliana* GDSL esterase lipase *CUS1* and *CUS2*: *CUS1/2-like1* is overall similarly expressed in both proximal and distal tissues at stage 2, however, at stage 3, the expression of *CUS1/2-like1* is higher in the distal tissue than in the proximal region at a similar stage. At stage 4, its expression drops in both tissue types, yet remains relatively high in distal tissues. This suggests a difference in the reticulation of the cutin network in proximal and distal petal parts, which indicates a difference in the mechanical properties of the two cuticles.

Both *LACS2-like1* and *LACS3-like2* are differentially expressed at stage 2 between the two petal parts and are systematically more expressed in the distal petal tissues, suggesting a difference in the growth kinetics of the two petal regions at stage 2. These differences then disappear at later stages.

The expression of *ABCG11* is higher in distal tissues at every stage of development and increases in both tissues. This could be a response to the larger cuticular surface induced by the formation of conical cells over flat cells thus increasing the need for cuticle synthesis.

Finally, the expression of *HtSHN1* is relatively higher in distal petal tissues at stage 3 and 4. Interestingly, its expression profile appears similar to that of *BDG3-like 3* and *CUS1/2-like 1* in distal petal parts. Consistently with the potential role of *AtSHN* genes in the induction of *BDG* and GDSL esterase lipase proteins, *AtSHN1* shares similar target genes to those of *AtSHN3* (Shi et al., 2011). The relatively higher expression of *HtSHN1* in distal petal tissues could thus mediate the activation of *BDG3-like 3* and *CUS1/2-like1* in *Hibiscus trionum*. *AtSHN1* is also known to have other targets such as *CYP86a6/a7*, *LACS2* and *CER1* and *CER2* in Arabidopsis thalian (Kannangara et al., 2007b),

however, the expression profiles of *CYP86a6/a7*, *LACS2* and *CER1* and *CER2* orthologs in *Hibiscus trionum* in the distal petal region of *H.trionum* is inconsistent with a sole *HtSHN1* mediated regulation.

From this analysis, it appears that cutin production is activated in the proximal petal part of the petal, whereas the wax production is relatively repressed in the same region. In the distal part of the petal an opposite regulation pathway seems to induce the production of waxes and relatively reduces the production of cutin. Hypothetically, these expression profiles might result in cuticles with very different properties in the proximal and distal parts of the petal.

In order to identify other candidate genes and potential pathways involved in the production of striations, comparative transcriptomic analyses where then performed.

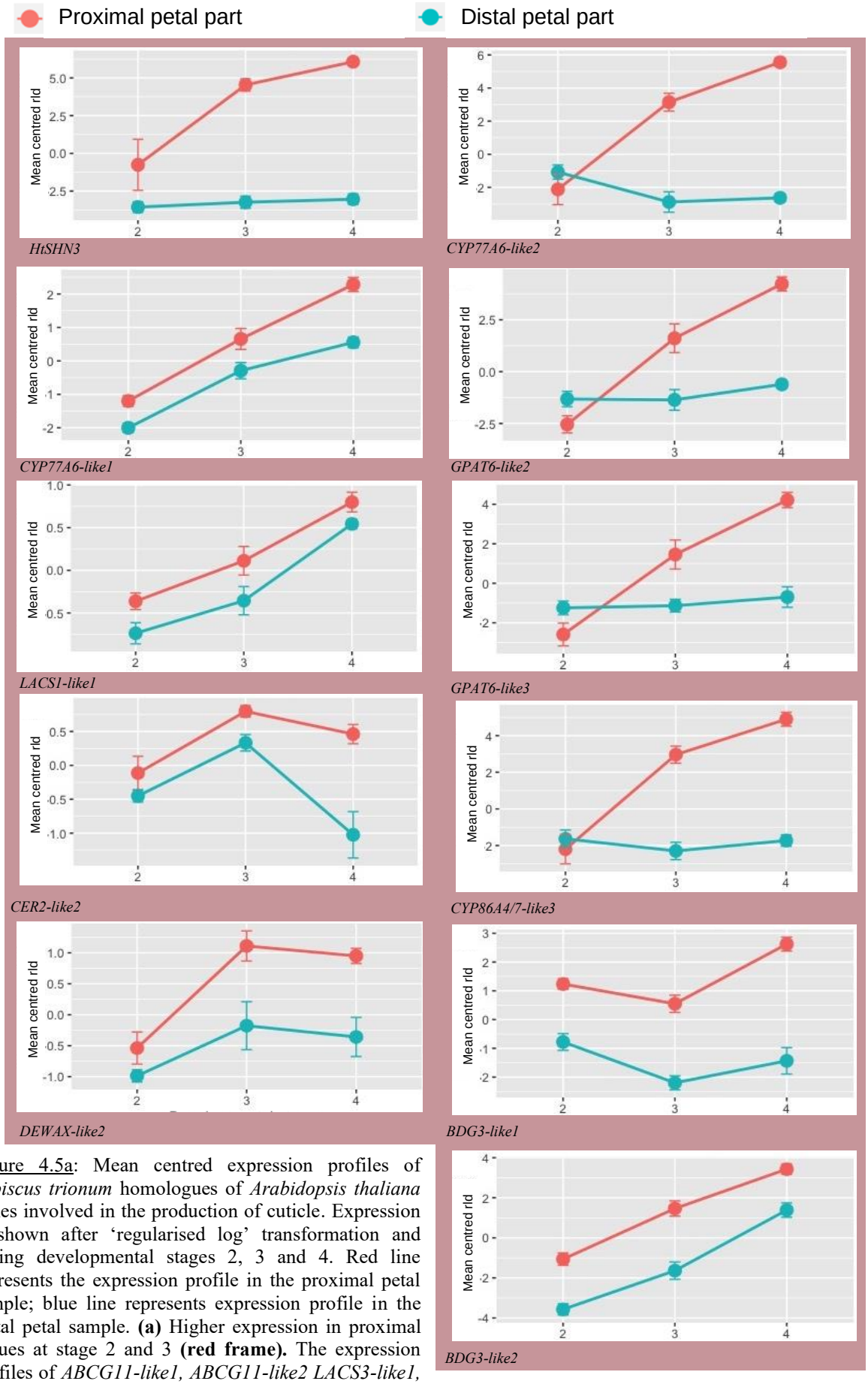

Figure 4.5a: Mean centred expression profiles of *Hibiscus trionum* homologues of *Arabidopsis thaliana* genes involved in the production of cuticle. Expression is shown after 'regularised log' transformation and during developmental stages 2, 3 and 4. Red line represents the expression profile in the proximal petal sample; blue line represents expression profile in the distal petal sample. **(a)** Higher expression in proximal tissues at stage 2 and 3 **(red frame).** The expression profiles of *ABCG11-like1, ABCG11-like2 LACS3-like1, LACS1-like1, DEWAX-like1* and *GPAT6-like1* are not shown as they do not display significant differences between proximal and distal regions.

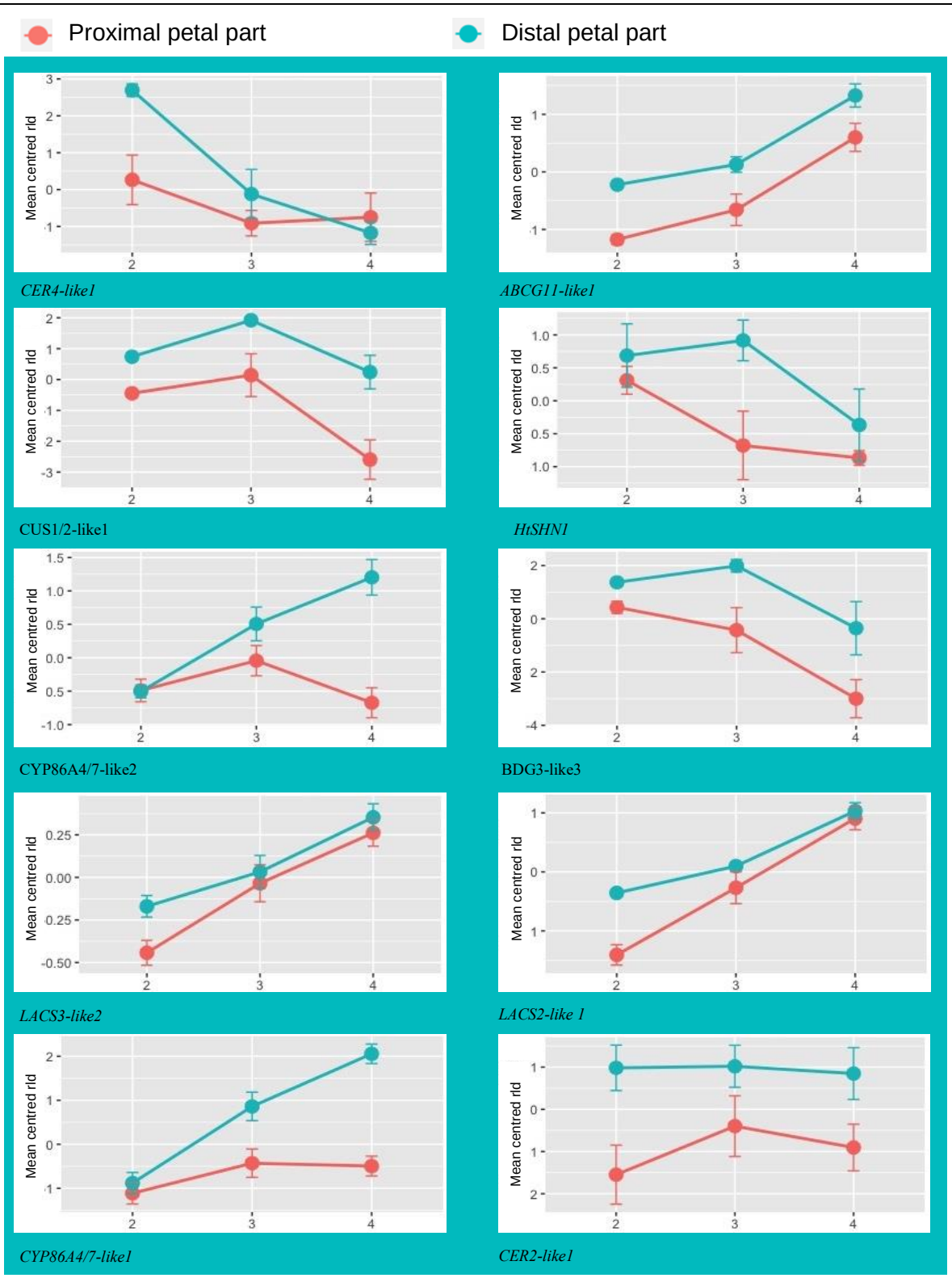

Figure 4.5b: Mean centred expression profiles of *Hibiscus trionum* homologues of *Arabidopsis thaliana* genes involved in the production of cuticle. Expression is shown after 'regularised log' transformation, during developmental stages 2, 3 and 4. Red line represents the expression profile in the proximal petal sample; blue line represents expression profile in the distal petal sample. **(b)** Higher expression in distal tissues at stage 2 and 3 **(blue frame).** The expression profiles of *ABCG11-like1, ABCG11-like2 LACS3-like1, LACS1-like1, DEWAX-like1* and *GPAT6-like1* are not shown as they do not display significant differences between proximal and distal regions.

4.3.3 Genes involved in the cell wall catabolism alkane metabolism are differentially regulated in the proximal and distal petal parts

A succession of comparisons and filters were applied to highlight genes potentially involved in the production of cuticular ridges. As detailed in the methods, the different comparisons and filters applied enabled us to identify a set of 1620 genes that are potentially involved in the development of nanoscaled-ridges. This represents about 1.4% of the total number of loci identified.

These 1620 genes were divided into two super clusters (SC) and each of them was once again divided into two subsequent super clusters. Their corresponding heatmaps as well are their average expression profiles are represented in fig. 4.6 and fig. 4.7, respectively. Gene ontology (GO) analyses were used to calculate the enrichment of different biological processes (BP) in these clusters (fig. 4.8). The enrichment score corresponds to the ratio between the number of genes found in a specific SC and the number of genes expected to be found in the same pool based on the GO-term annotation of the entire transcriptome.

Super cluster 1.1 (SC1.1) comprises 295 genes more expressed in the proximal petal region than the distal, and with an overall steady increase of their expression of about 2 $\log_2$ fold change between stage 2 and stage 4 (fig. 4.6 and 4.7). GO enrichment analyses of this super cluster revealed a high enrichment of genes involved in citrate and isocitrate metabolism and of tricarboxylic metabolism (GO:0006101 and GO:0006102, and GO:0006099 and GO:0072350, respectively), with an enrichment factor of 20.6 and 57.14 respectively. Cell wall and pectin metabolism related GO-terms were also found enriched in various proportions (GO0042545, GO0045490, GO0071555, GO0030393, GO0045488, GO0048363 and GO0048358) (fig. 4.8), which suggests that a regulation of the production of cell wall and pectin is needed for the proper buckling of the cuticle of the proximal part of petal. Differential production of cell wall and pectin compounds could influence the stiffness of the cell wall acting as a substrate to the buckling cuticle.

.

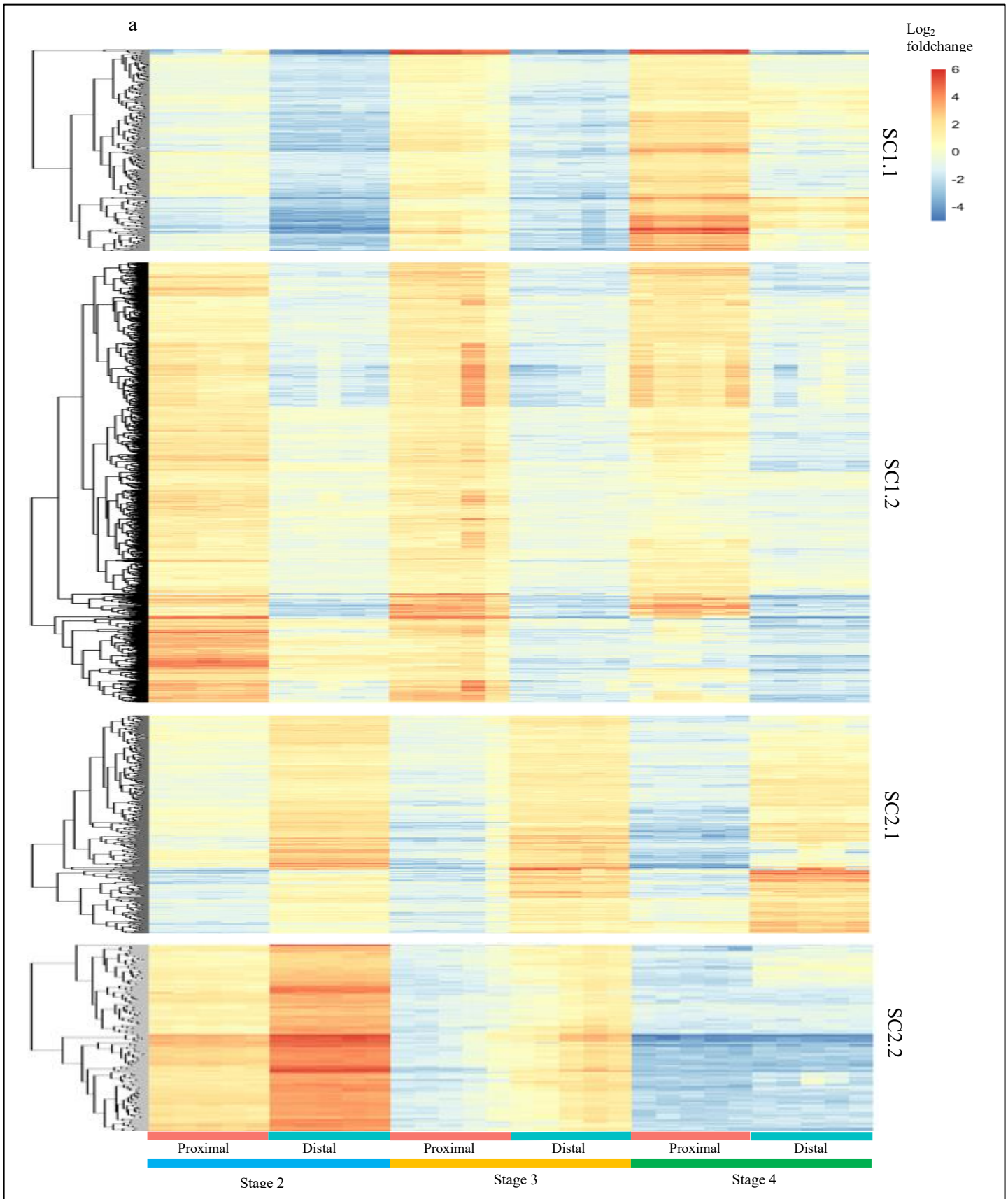

Figure 4.6: Heatmap of the four super clusters reflecting the relative expression of the 1620 genes selected. Variability between the five biological replicas and conditions are shown for each of the 1620 genes.

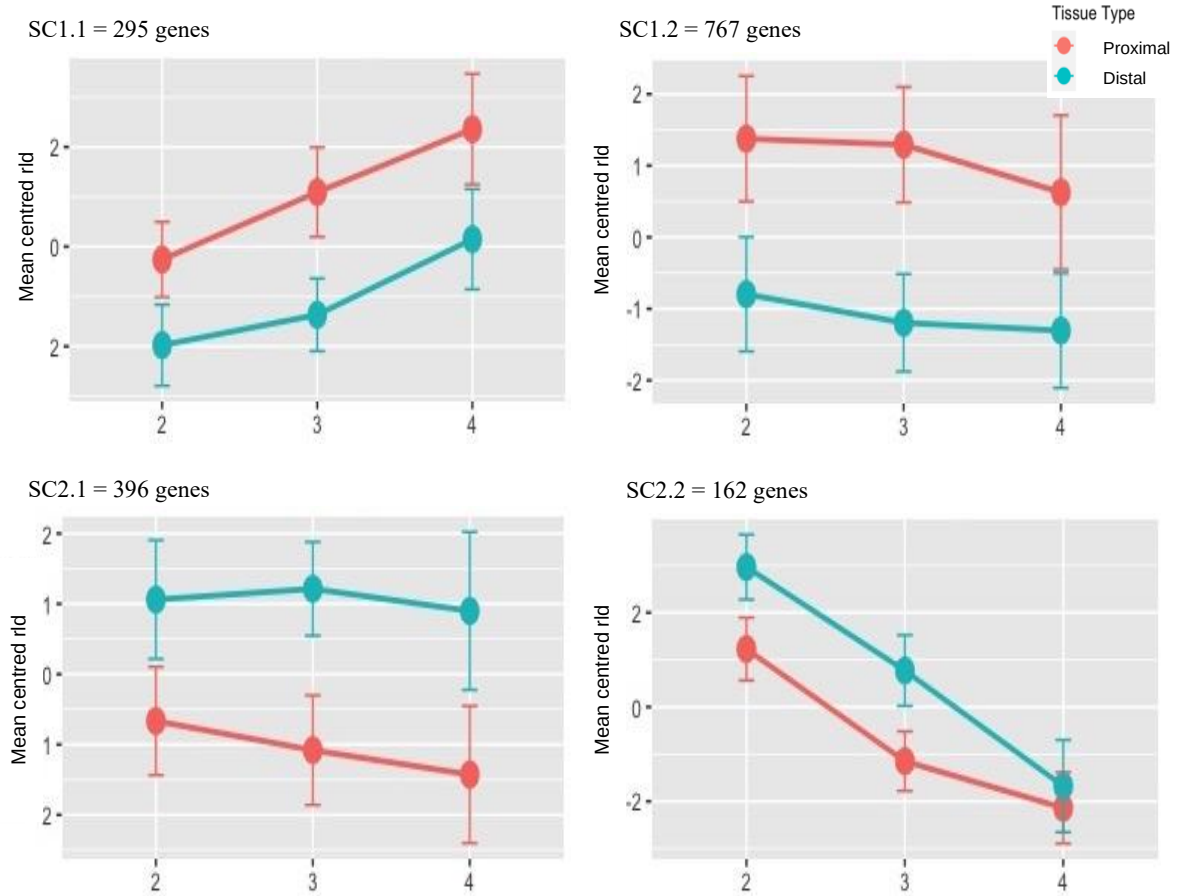

Figure 4.7: Average expression profiles of the super cluster SC1.1, SC1.2, SC2.1 and SC2.2. Expression is represented after 'regularised log' transformation during the developmental stages 2, 3 and 4 in proximal and distal petal tissues. Red line represents the expression profile in the proximal petal samples; blue line represents expression profile in the distal petal samples.

The second super cluster SC1.2 gathers 767 genes that are also more expressed in the proximal region with a slight decrease around stage 4, similarly to the distal region (fig. 4.6 and fig. 4.7). A study of the enriched genes in this super cluster showed high enrichment for petal number determining processes: (GO:0048834) 71.43 and (GO:0048832) 20.7 as well as pectin metabolism (GO:0048358, GO:0048353, GO:0045390, GO:00454880), displaying enrichment factors ranging from 4.32 to 23.9. Cell-wall metabolism (GO:0042545) was also found enriched with a factor of 5.12 (fig. 4.8).

The two last super clusters SC2.1 and SC2.2 comprise genes that are more expressed in the distal region than in the proximal region of the petal (fig. 4.6 and fig. 4.7).

SC2.1 contains 396 genes that are steadily up regulated in distal petal tissues during development and tend to be less strongly expressed in the proximal petal region. SC2.1 appears to be enriched in genes controlling epidermal cell fate (GO:0009913, GO:008544, GO:0045595, GO:0030855) with an

enrichment factor comprised between 12.9 and 16.1, and organ determinism (GO:0090700, GO:0048497 and GO:0045962) with enrichment factors reaching 34.2 and 47.37. Interestingly, an enrichment of about 30 was observed for GO-terms related to the alkane metabolic process (GO:0043447 and GO:0043446), consistently with a differential production of cuticular lipids between the distal and the proximal petal regions.

The last super cluster consists of 162 genes highly expressed at early stages of development which decrease in expression with the maturation of the bud. They are overall more expressed in the distal region and seem to be enriched in genes related to cell division and meiotic processes (GO:0055048, GO:0007053, GO:0009971:) which display an enrichment factor of 200. Other GO-Terms associated with similar processes (GO:0000280, GO:1903046, GO:0048285, GO:0051321, GO:0051301) displayed a lower enrichment ranging from 5 to 13. Another category of genes related to chromatin, chromosome and DNA organisation (GO:0030261, GO:0070192, GO:0006323, GO:0006333, GO:0071103, GO:0140013) was identified with slightly lower enrichment scores ranging from 18.33 to 43.75. Enrichment in genes related to organ development and organelle organization was also observed.

Out of the different GO-terms found enriched in the various clusters, the regulation of pectin, cell wall and alkane metabolism are consistent with the development of differentiated cuticles. I investigated further the genes behind the associated GO-terms.

I examined the genes annotated with the GO-terms GO0042545, GO0045490, GO0071555, GO0030393, GO0045488, GO0048363 and GO0048358 corresponding to pectin and cell wall metabolic processes and those annotated with the GO-terms GO:0043447 and GO:0043446 corresponding to alkane metabolism. Redundancy between the GO terms was removed and 72 and 6 genes were obtained, respectively. They were then grouped according to their annotations in table 4.9.

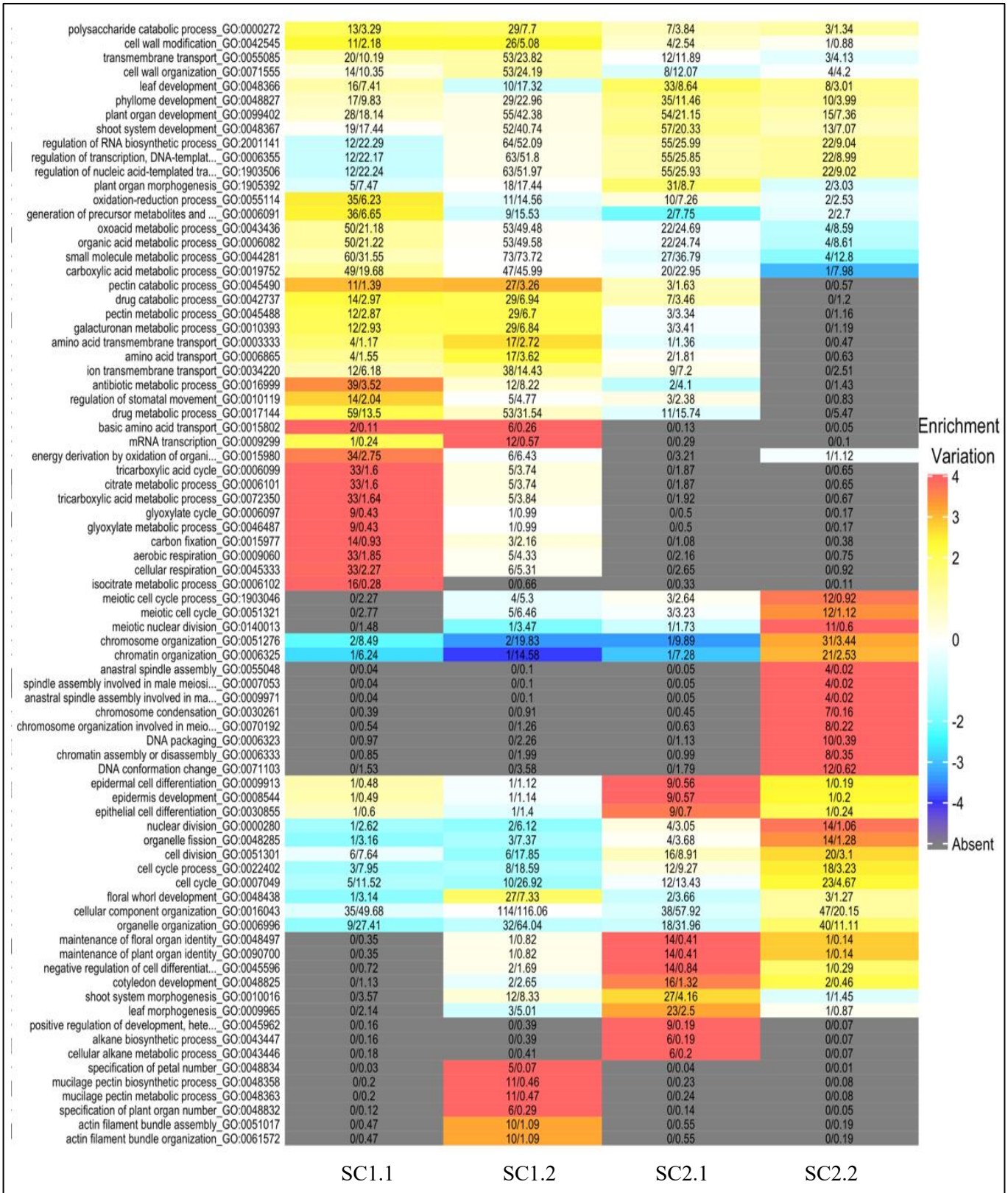

Figure 4.8: Biological process GO-Term enrichment heatmap of various biological processes of the SC1.1, 1.2, 2.1 and 2.2 super clusters. In each cell, the left side figure represents the observed occurrence of a GO-Term within the super cluster, and the right-side figure represents the predicted occurrence of the same GO-Term within the super cluster. The ratio of these two figures characterises the enrichment factor. This enrichment is reported as a log2 foldchange scale (right side). Greyed cells reflect the case were no GO-Term was found and are usually associated with a predicted occurrence < 1.

Out of the 72 genes upregulated in proximal petal tissues, 29 were annotated as pectinesterase, and two as exopolygalacturonase, suggesting a strong upregulation of pectin catabolism (table 4.9a). Other genes involved in the production and deposition of cellulose such as *COBRA* and *WAT1* were also upregulated as well as some glucan endo β(1-3) glucosidases, CYTOCHROME P450 86B1-like, CELLULOSE SYNTHASE like protein, NAC 56 transcription factor, pectinesterase inhibitor, and a CRIB domain protein containing RIC7 were also identified (table 4.9a). The upregulation of pectinase, endo β(1-3) glucosidase and exopolygalacturonase is consistent with an increase of the compliance of the extra cellular matrix and a decrease of its Young's modulus.

The six upregulated genes in distal petal tissues were annotated as *CER3*, *CER1-like* and *cytochrome b5-like transportin1-like* genes (table 4.9b). *AtCER3* was reported to play a role in the production of cuticular waxes (Rowland et al., 2007) as *AtCER1* , which was also identified in the production of waxes in cooperation with *cytochrome b5-like* and *AtCER3* (Pascal et al., 2019). The over representation of these three genes in SC2.1 and SC2.2 is consistent with an upregulation of the wax metabolic pathway in distal petal tissues.

a

Cell wall metabolism related genes over expressed in proximal petal tissue (SC1.1 and SC1.2)	
Annotation	Number of genes identified
Cellulose synthase-like protein	2
COBRA-like protein	2
CRIB domain-containing protein RIC7-like	1
Cytochrome P450 86B1-like	1
Exopolygalacturonase	2
Glucan endo-1,3-beta-glucosidase 13-like	1
Glycosyltransferase	2
Hexosyltransferase	1
Homeobox-leucine zipper protein ANTHOCYANINLESS 2-like	2
Leucine-rich repeat extensin-like protein 4	1
Major pollen allergen Ole	1
NAC transcription factor 56-like	2
Omega-hydroxypalmitate O-feruloyl transferase-like	2
Pectine acetyltransferase	1
Pectinesterase	29
pollen-specific leucine-rich repeat extensin-like	2
polygalacturonase	4
Pectinesterase/pectinesterase inhibitor	2
Uncharacterized proteins	5
WAT1-related protein	2
Xyloglucan endotransglucosylase/hydrolase	1
Pectate liase	6

b

Alkane metabolism related genes over expressed in distal petal tissues (SC2.1 and SC2.2)	
Annotation	Number of genes identified
Protein ECERIFERUM 3	4
Protein ECERIFERUM 1-like	1
Cytochrome b5-like transportin-1-like	1

Table 4.9: Annotations of the different genes associated with cell wall metabolism and alkane metabolism. (a) Genes associated with cell wall metabolism (GO-terms GO0042545, GO0045490, GO0071555, GO0030393, GO0045488, GO0048363 and GO0048358) and upregulated in proximal petal tissues. **(b)** Genes associated with alkane metabolism (GO:0043447 and GO:0043446) and up regulated in distal petal tissues. In the first column is reported the annotation based on protein sequence alignment with *Gossypium hirsutum* proteome. In the second column is reported the number of genes identified for each annotation.

4.3.4 Manual identification of potential candidate genes for molecular work

On top of GO-term analyses, the 1620 genes that were filtered were also analysed individually and several genes displayed expression profiles of potential interest theoretically consistent with a role in the development of structurally coloured cuticle. These were selected for the production of over expressing transgenic lines (fig. 4.10).

Shikimate-o-hydroxycinnamoyl transferase (HCT) is a family of enzymes involved in the production of guaiacyl and syringyl lignins (Hoffmann et al., 2004). Its absence of expression in the proximal petal region is consistent with a soft and compliant cell wall which may be crucial for the development of cuticular striations. Over expression of *HCT* may result in an abnormal stiffening of this layer and an absence of striations thus demonstrating the necessity of a soft extracellular matrix. Similarly, despite the absence of a clear characterization of the role of *PPE8B*, its potential role as a pectinesterase/pectinesterase-inhibitor may help in the modulation of the substratum of the cuticle proper. WALL ASSOCIATED KINASE (WAK) proteins have been demonstrated to be covalently bound to pectin and may play a role in cell expansion. In a wider way, they participate in the continuity of the cytosol to the extracellular matrix and participate in the coordination between extracellular matrix perturbations and cytosolic responses (Wagner et al., 2001). This suggests a potential role in the coordination of the pectin network and cell expansion. Expression of the *WAK* gene was found to be limited to proximal petal parts, which is consistent with a potential role in the development of striations. *COBRA* may also be a candidate gene for overexpression since it plays a role in cellulose production (Ben-Tov et al., 2015). Its over expression may alter the thickness of the cellulose layer and modulate its stiffness, thus preventing cuticle buckling.

OFP13 is a transcriptional repressor of the *OVATE FAMILY PROTEIN* class and is associated with the regulation of *BEL1-LIKE HOMEODOMAIN (BLH)* and *KNOTTED1-LIKE HOMEODOMAIN* genes *(KNAT).* The over expression of *OFP13* in *A. thaliana* resulted in short rosette leaves, blunted siliques, late flowering and reduced fertility. Its involvement in the production of striations remains unclear, however its implication in the regulation of *BEL1-like homeodomain* genes (*BLH*) and its relatively high expression in proximal petal tissues (fig. 4.10), suggests a potentially complex role in

the production of nano-scale ridges. BLH proteins are transcriptional repressors involved in a variety of biological processes and noticeably in the repression of *AGAMOUS* in floral meristems (Bao et al., 2004). The expression profiles of *BLH* and *OFP13* (fig. 4.10) may suggest roles in the patterning of the cuticle petal.

ABCG22 is an ATP-binding cassette transporter involved in the abscisic acid mediated stomatal water regulation in *Arabidopsis thaliana* where its inactivation was associated with abnormal water

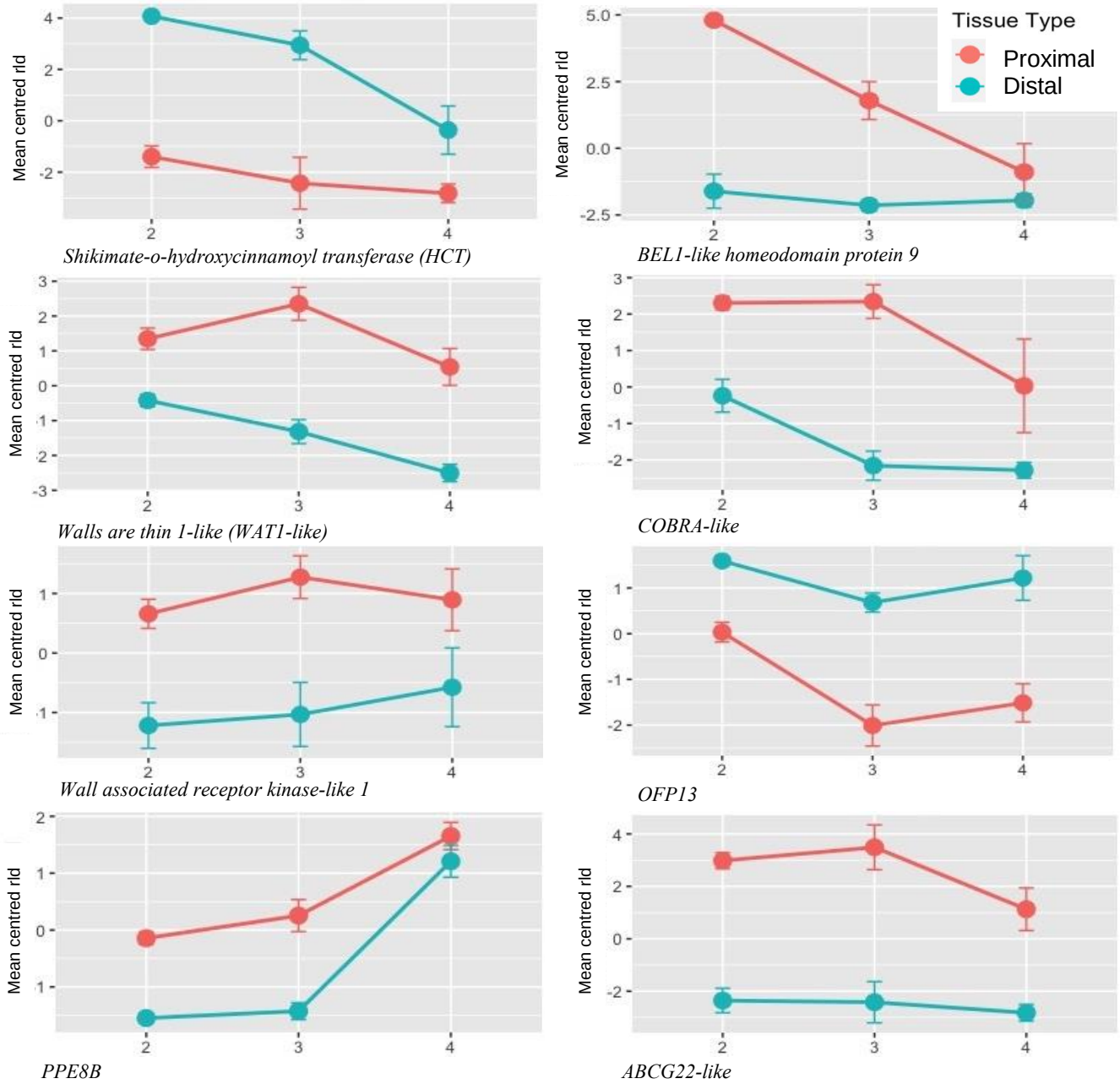

Figure 4.10: Expression of eight candidate genes potentially involved in the development of striations. These eight genes were manually picked from the 1620 genes filtered from the transcriptome comparison strategy and their expression was plotted after regularised 'log transformation' (rld) during the developmental stages 2, 3 and 4 in proximal and distal petal parts. Red line represents the expression profile in the proximal petal samples; blue line represents expression profile in the distal petal samples.

losses (Kuromori et al,, 2011). Its over expression in proximal tissues suggest a potential role in the prevention of the dehydration of proximal petal tissues, which may be important in the maintenance of the mechanical properties of the epidermis or the elongation of epidermal cells by helping in the maintenance of turgor pressure.

Finally, given the function of WALLS ARE THIN1 in the deposition of secondary cellulose fibres and metabolites as well as cell elongation (Ranocha et al., 2010), the high expression of *HtWAT1-like* expression in the proximal petal region at stage 3 might be consistent with a deposition of cellulose and compound involved in the establishment of specific properties of the epidermal cell wall, and may be involved in the induction of the elongation of epidermal cells.

A transgenic approach will be needed in the future to confirm the implication of these genes in the development of striated cuticle

4.4 Discussion

In this chapter I analysed the transcriptome of different petal samples of the non-model species *Hibiscus trionum*. The multiple assemblies and quality control that were done using Trinity and Bowtie2 give assurance that the allele variety present in the *Hibiscus trionum* individuals used for sampling has been properly represented and that most reads could be mapped to the final assembly. In parallel, the comparison of the differentiation of two tissues of common origin at three different time points, (before, during and after the development of striations) provided two axes of comparison: one during the development of the petal and and one along the spatial axis of the petal. This complex comparison design and the high number of biological replicas brings confidence that the 1620 genes that were selected display expression profiles that are specific to the proximal petal region and that some of them are directly involved in the production of striations.

Using transcriptomic analyses, I showed that the proximal petal region specifically expresses genes involved in cutin production such as *HtSHN3*, *CYP86a4a7-like1/2*, *BDG3-like1/2* and *GPAT6-like3* and demonstrates reduced expression of genes involved in wax synthesis such as *CER2* in *Hibiscus trionum*. In the distal petal part, the exact opposite pattern was observed, with the repression of genes required for cutin synthesis and the stronger expression of genes involved in wax biosynthesis (fig.

4.5a). Our analyses also show a high expression of *DEWAX* and *SHN3* in proximal tissues, suggesting a role in the up regulation of the cutin synthesis pathway and the downregulation of the wax synthesis pathway (fig. 4.5)

In parallel, GO-term enrichment analyses coupled with our gene filtering strategy (see part 4.2.3) highlighted the abundance of up-regulated genes encoding pectinesterases, polygalacturonidases, endo- and exogalacturonidases, as well as xyloglucan endotransglucanase hydrolase in the proximal petal region during development of the flower. One cellulose synthase as well as a pectinesterase inhibitor were also up regulated in this region (table 4.9).

Previous experiments studying buckling highlighted the importance of 2 parameters: the presence of a bi-layered system with a stiffer layer topping a softer substrate, and a 2-dimensional compression (Bowden et al., 1998). The model developed by Antoniou-Kourounioti et al in 2012 suggests that the thickness of the cuticular layer as well as the the 2-dimensional constraints are the main motor of buckling *in planta*. Finally, in 2017, Huang et al proposed that one of the causes for the development of cuticular micro-pattern was the anisotropic growth of epidermal cells thus explaining the development of 2-dimensional constraints mentioned in the work of Antoniou-Kourounioti.

Together these results provide a possible explanation for the development of specific mechanical properties leading to the buckling of the cuticle. Yet, this study did not allow us to highlight genes involved in the molecular pathways supporting the anisotropic growth of epidermal tissues, which is essential for the development of compressive constraints and its buckling (Bowden et al., 1998; X. Huang et al., 2017; Kourounioti et al., 2013).

The formation of striations is a necessary character for the formation of structural colours in *Hibiscus trionum*. As evoked before, star shaped striation patterns (going from the borders of the cells towards the centre of each cells) have been observed on the conical cells of the adaxial petal epidermis of *Arabidopsis thaliana* (Panikashvili et al., 2009)*,* However, no structural colours have been observed in this context suggesting that a flat epidermis is necessary for the production of relatively ordered ridges (parallel striations as opposed to star shaped) leading to structural colours. Furthermore, several plants presenting structurally coloured petal cuticle present relatively ordered striations topping flat

elongated cells (Moyroud et al., 2017). This suggests that the combination of this cuticular pattern and the flatness of the epidermis are both necessary for the production of iridescence. Other genes must thus be involved in cell differentiation and in the colocalization of flat epidermis and striated cuticle at the adaxial proximal part of the petals. A protein or group of proteins organised in a gradient from the proximal to the distal part may act as morphogens and be involved in the patterning of the whole petal.

It is also interesting to notice that cuticular striations are specific to the adaxial part of the petal, contrary to the cell shape which concerns the entire abaxial surface of the petal and the pigmentation which can also be found in the most proximal abaxial region. This suggests that a specific cellular differentiation takes place along the abaxial-adaxial axis leading to the specific expression of *SHN3* and *DEWAX* in the proximal and adaxial epidermis only.

4.5 Conclusion

In this chapter, the expression of differentially expressed genes enabled us to highlight the active molecular mechanisms at play in *Hibiscus trionum* potentially leading to the production of a cuticle structured into two mechanically distinct layers consisting of a relatively stiff cuticle proper in the proximal adaxial petal region resulting from the up regulation of the cutin synthesis pathways, topping a softer substrate resulting from the hydrolysis of the pectin network and the xyloglucans. I thus propose a model of the molecular pathways regulating the cuticle production and the development of anisotropic mechanical properties between proximal and distal adaxial petal parts (fig. 4.11a), as well as a model explaining how the epidermal polysaccharides are regulated in the proximal adaxial petal part (fig. 4.11b)

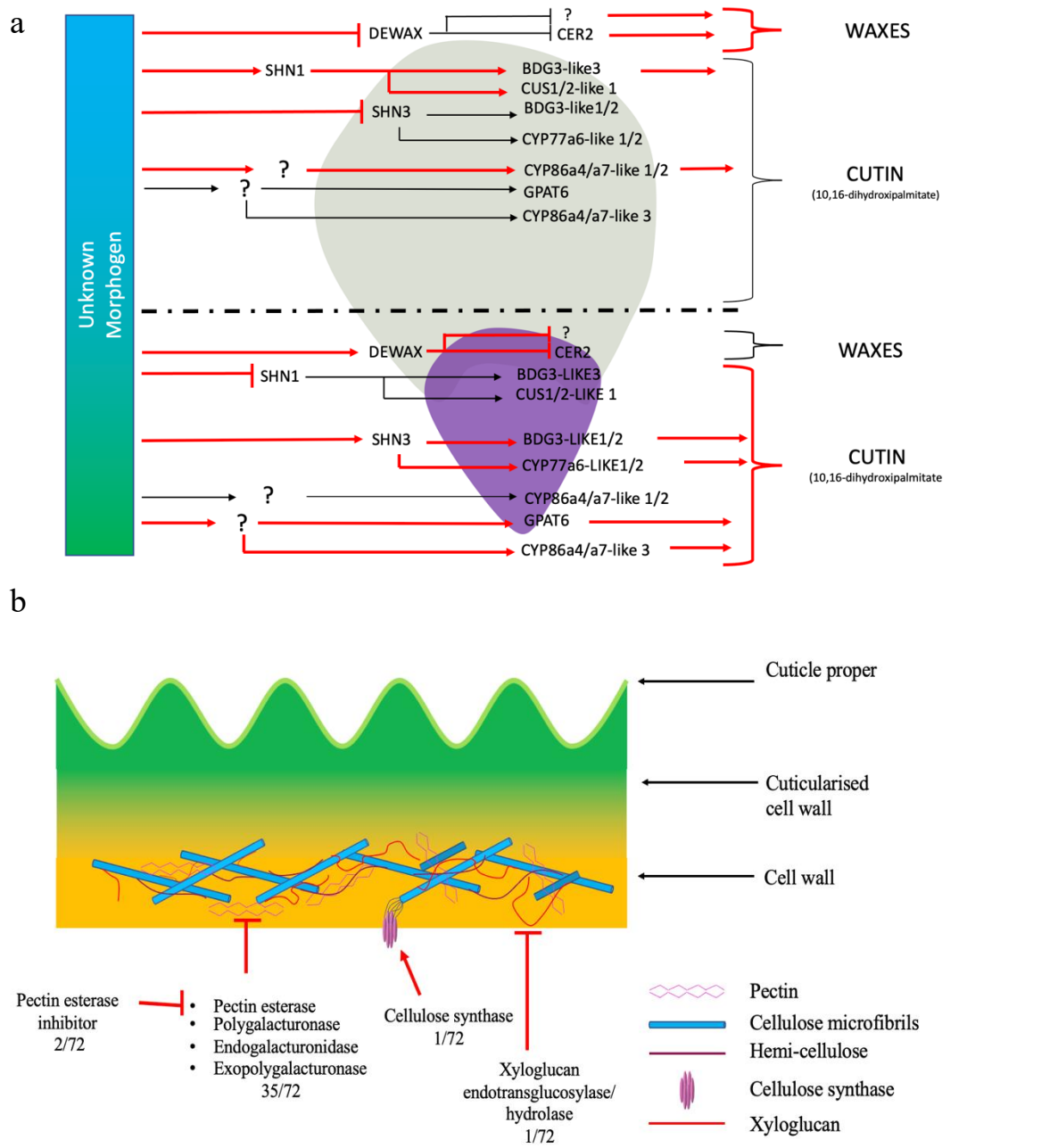

Figure 4.11: Model of the molecular regulation of the adaxial petal cuticle and cell wall composition in the proximal adaxial petal epidermis. **(a)** Partial representation of the cutin and wax synthesis pathways that are at play in the adaxial proximal and distal part of the petals of *Hibiscus trionum* as suggested by the analyses of the expression profiles of the genes mentioned in figure 4.5a and b. **(b)** Illustration of the potential mechanisms involved in the modulation of the cell wall properties in the adaxial proximal epidermis of the petal of *H. trionum,* extrapolated from the enrichment analyses (fig. 4.8 and table 4.9). The ratios presented show the number of genes found with that annotation out of the 72 genes involved in the regulation of cell wall production and properties.

4.6 Supporting data

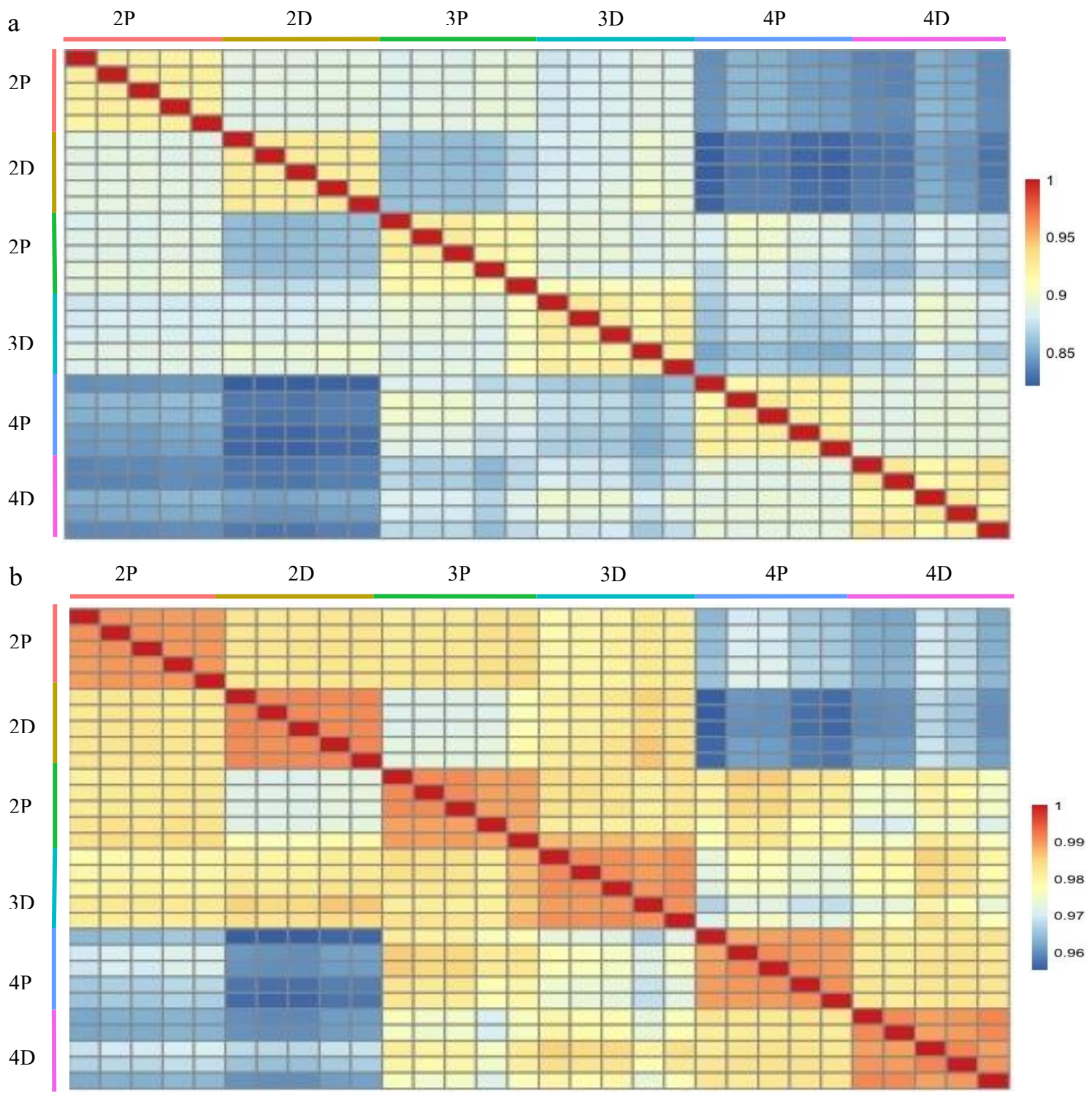

Supplement 1: Sample to sample correlation heatmaps supporting the Pearson correlation heatmap showed in figure 4.4. (**a**) Sample to sample correlation heatmap performed using the Kendall correlation method. **(b)** Sample to sample correlation heatmap performed using the Spearman correlation method. 1 representing the maximal score of correlation. 'P' stands for 'proximal', 'D' for distal and the digits for the developmental stage. Both Kendall and Spearman correlation method display the same result as the Pearson correlation method presented in fig. 4.4

Chapter 5: Over expression of *HtnsLTP-like* and *HtSHN* genes is sufficient to alter the striation pattern

Chiara Airoldi and Edwige Moyroud produced the *35S:HtSHN1* and *35S:HtSHN2* constructs, respectively.

5.1 Introduction

In this chapter, I investigated the expression of four different genes of *Hibiscus tironum*, which are believed to be involved in the regulation of the cuticle, hence, potentially in the development of striations and generated four sets of transgenic lines. The resulting transgenic phenotypes presenting altered striations were investigated in order to test and assess how gene over expression modulates the buckling parameters.

5.1.1 The bilayered structure of the cuticle

The different chemical compounds constituting the cuticle (see section 3.1.1 and chapter 1) are organised in layers and take the form of a reticulated network or simply loose elements in the cuticle. Analyses of the striated cuticle of *Hibiscus trionum* with transmission electron microscopy revealed the presence of at least three distinct layers presenting different electronic density at the surface of petal adaxial epidermal cells. The outermost layer presents the highest electronic density and corresponds to the cuticle proper (~270 nm). The innermost one displays the lowest electron density and has been hypothesised to be mostly constituted of cellulose (~160nm). In between these two layers, a large domain of medium electron density forms a layer of cuticularised cell wall (~3.25-3.9 µm) (fig. 5.1).

A previous study reported that a loss of function mutant of the *A. thaliana NON-SPECIFIC LIPID TRANSFER PROTEIN 2* (*AtLTP2*) gene resulted in an increased permeability of the cuticle without major modification of the cuticle lipid profile. Confocal microscopy and the production of recombinant proteins also revealed that the AtLTP2 protein was localised in the chloroplast and in the cell wall, consistent with a potential role in cuticular lipid transportation. Interestingly, a collapse of the epidermal cell surface and a disruption of the cuticle-cell wall ultra-structure was also reported,

suggesting that *AtLTP2* is implicated in the maintenance of cell wall-cuticle interface integrity (A. Jacq et al., 2017). The presumed homologous gene to AtLTP2 was amplified from *H. trionum* cDNA and an overexpression construct was created using a double CaMV 35S promotor. Two independent *35S:HtLTP2-like* transgenic lines were created, and their phenotype investigated in this chapter.

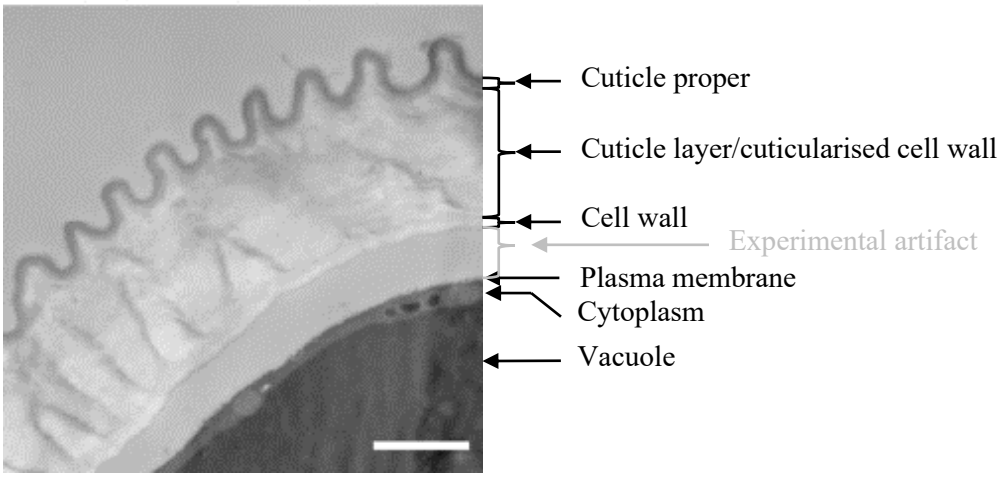

Figure 5.1: Transmission electronic microscopy of the cross of a striated epidermal cell of *Hibiscus trionum* petal. The electronic density of the layer between the cell wall and the plasma membrane is similar to the one above the cuticle proper suggesting that this layer is artifactual and results from the delamination of the cell wall from the plasma membrane during the preparation of the sample. Scale bar = 2 µm (from Whitney et al., 2009) (copyright license 5095380539584).

5.1.2 The role of *HtSHN* genes

As it has been already described in this thesis. The *SHN* genes (part of the AP2-ERF) have been consistently demonstrated as involved in the regulation of the cuticle in *Arabidopsis thaliana* and *Solanum lycopersicum* (Aharoni et al., 2004; Al-Abdallat, Al-Debei et al., 2014; Kannangara et al., 2007a; Shi et al., 2011). Furthermore, in *Hibiscus trionum*, the expression of *HtSHN3* was correlated with an alteration of striations in both *35S:HtSHN3-SRDX* and *35S:HtSHN3-VP16*. The expression profile of *HtSHN3*, as reported by the transcriptomic analyses (see chapter 4), reveals a relatively high expression in the proximal part of the petal at stages 3 and 4 of the flower development compared to the distal petal part (see fig. 4.5a), which is consistent with its potential role in the development of striations. The role of the *HtSHN1* and *HtSHN2* in the production of striations remains however unclear. In this chapter we studied the potential implication of *HtSHN1* and *2* genes in the development of structural colours by analysing their expression profile using the previously acquired transcriptomic

data (see chapter 4) and produced 2 sets of *Hibiscus trionum* transgenic lines: *35S:HtSHN1*, *35S:HtSHN2*. The role of *HtSHN3* was also once more investigated by over expressing its native protein sequence so as to try and avoid possible perturbation of its function as may have occurred in the *35S:HtSHN3-SRDX* and *35S:HtSHN3-VP16* transgenic lines. By over expressing these *HtSHN* genes, we also hope to perturb sufficiently the cuticle to induce alterations of the striation production.

5.1.3 The production of cutin and the *HtDCR* gene

As described in the chapter 3, chemical analyses of the cuticle revealed that the 10,16-DHP was preferentially found in striated cuticles. Previous work in *Arabidopsis thaliana* correlated the absence of striations with a strong depletion in 10,16-DHP and a loss of function *AtDCR* mutant (Panikashvili et al., 2009). Given the abundance of 10,16-DHP in the striated cuticle and his established correlation with the *DCR* gene, the expression of the *Hibiscus trionum* orthologue of *AtDCR* was investigated using the transcriptomic data described in chapter 4.

5.1.4 Aims

This work aims to provide more understanding of the potential genetic regulations underpinning the differences in cuticle chemical properties and structure by producing four sets of transgenic lines over expressing *HtLTP2-like*, *HtSHN1, HtSHN2* and *HtSHN*3 in *Hibiscus trionum*.

5.2 Methods

5.2.1 Production of the *HtLTP2-like* transgenic lines

The sequence of *AtLTP2* (At2g385320.1) was blasted against the *Gossypium* taxid sequence database of NCBI and the first sequence hit was selected (Gorai.006G235000.1) to be blasted against an early version of *Hibiscus trionum* transcriptome assembly (see chapter 4) using the NCBI BLAST stand-alone programme. The *HtLTP2-like* sequence was amplified from cDNA (see cDNA synthesis 2.3.4 and cDNA sequences in Annex III) by PCR using JF9 and JF10 primers (see Annex II), then cloned into pBlueSCRIPT previously blunt-end digested with EcoRV (see section 2.3.8.1). Tailed primers were then used to add a 5' BamH1 and 3' Sma1 restriction sites (JF11 and JF12 primers (see annex II)). The product was once again ligated into pBlueSCRIPT previously blunt-end digested with

EcoRV (see section 2.3.8.1). The *BamHI-HtLTP2-like-SmaI* sequence was then digested from this plasmid using BamH1 and Sma1 restriction enzymes and ligated into pEM110, thus placing *HtLTP2-like* under the control of a double CaMV 35S promotor and single CaMV 35S terminator. The pEM110 plasmid contains a plant and a bacterial Kanamycin resistance cassette as well as an e*YFPmyr* gene that were co-integrated into *H. trionum* during *Agrobacterium tumefaciens* mediated transformation, allowing for the selection of transformed calli (pEM110 and pBlueSCRIPT plasmids as well as *H. trionum* transformation are detailed in Annex V and section 2.3.8.5, respectively). Proper over-expression of *HtLTP2-like* was assessed using semi-quantitative RT-PCR on cDNA obtained from RNA extracted from leaves (fig. 5.9) (cDNA synthesis is detailed in section 2.3.4).

5.2.2 Production of *35S:HtSHN1*, *35S:HtSHN2* and *35S:HtSHN3* transgenic lines

The *35S:HtSHN3* construct was produced by Edwige Moyroud by amplification of *HtSHN3,* a type-C SHN gene, from cDNA synthethised from RNA extracted from a stage 5 flower. The *35S:HtSHN1* construct was produced in a similar way by Chiara Airoldi. The *HtSHN2* gene was amplified on similar cDNA (see section 2.3.4) using the primers JF1 and JF2 tailed with BamHI and SmaI respectively (see Annex II for primer sequences). The product of this amplification was then cloned into pBlueSCRIPT previously blunt-end opened with EcoRV (see section 2.3.8.1). The resulting plasmid was then digested with BamHI and SmaI for targeted and oriented cloning into pEM110 (see section 2.3.8.3.2) previously opened with similar restriction enzymes. The resulting plasmid was then used to transform *Agrobacterium tumefaciens* and then, *Hibiscus trionum.* (pEM110 and pBlueSCRIPT plasmids as well as *H. trionum* transformation are detailed in Annex IV and section 2.3.8.4, respectively)

5.2.3 Imaging

See section 2.2.4.

5.2.4 Gene orthology of *CYP77a4* and *At2g42990*

Orthologs of *AtCYP77a6* and *At2g42990* (a GDSL-motif protein) in *H. trionum* were identified as explained in section 4.2.7

5.2.1 Cuticle thickness measurements

Cryo-fracture coupled with cryo-SEM was used to assess cuticle thickness of the adaxial petal part (see section 2.2.4). Extra-cellular matrix (ECM) thickness was assessed in 21 WT striated cells, 7 *35S:HtLTP2-like* IL1 striated cells, 17 *35S:HtLTP2-like*IL2 striated, 10 *35S:HtLTP2-like*IL1 smooth cells and 14 *35S:HtLTP2-like*IL2 smooth cells. Thickness of the cuticle proper was measured on 20 WT striated cells, 6 *35S:HtLTP2-like*IL1 striated cells, 17 *35S:HtLTP2-like* IL2 striated, 6 *35S:HtLTP2-like*IL1 smooth cells and 14 *35S:HtLTP2-like* IL2 smooth cells. The cuticle thickness of the *35S:HtSHN1* and *2* transgenic lines was not measured as none of them presented an alteration of the striations and the cuticle of *35S:HtSHN3* could not be measured because of time constraints.

5.2.2 Protein alignment

Protein alignments were performed using the software MegAlign Pro and the default parameters of the Clustal omega algorithm. Protein sequences were extracted from the NCBI database and *Hibiscus trionum* transcriptome assembly based on the longest ORF sequence.

5.3 Results

The impact of cuticle structure on the production of striations was investigated. Firstly, the expression of *HtLTP2-like*, an orthologue of *AtLTP2*, which is involved in maintenance of cuticle integrity (A. Jacq et al., 2017), was investigated during development in striated and non-striated regions of *Hibiscus trionum* petals. Secondly, two *35S:HtLTP2-like* transgenic lines were produced and their phenotypes were investigated.

5.3.1 HtLTP2 contains the characteristic LTP family motif and the *HtLTP2* gene is differentially expressed in smooth and striated tissues

AtLTP2 (At5g38530) is involved in the maintenance of the integrity of the cuticle in *Arabidopsis thalian* (A. Jacq et al., 2017). Its function suggests a potential role in determining the

mechanical properties and structure of the petal cuticle. A potential homologue of *AtLTP2* was found in *Hibiscus trionum* by blasting the transcript of the *AtLTP2* gene against an early assembly of the transcriptome and referred to as *HtLTP2-like*. A protein sequence alignment was then performed on characterised LTP proteins from *A. thaliana, Hibiscus syriacus, Gossypium hirsutum, G. australe* and *Theobroma cacao* (HtLTP2-like, AtLTP1, AtLTP2, AtLTP3, AtLTP4, HsLTP1-like, GhLTP1, Gans-LTP1-like and TcnsLTP3) (fig. 5.2). The LTP proteins are characterized by a succession of cysteine residues (C-Xn-C-Xn- CC-Xn-CXC-Xn-C-Xn-C) necessary for the formation of disulfuric bonds and the stabilisation of the protein (Salminen et al., 2016). The protein HtLTP2-like presents the LTP characteristic motif suggesting a putative lipid transfer activity, and a relatively high percentage of

a

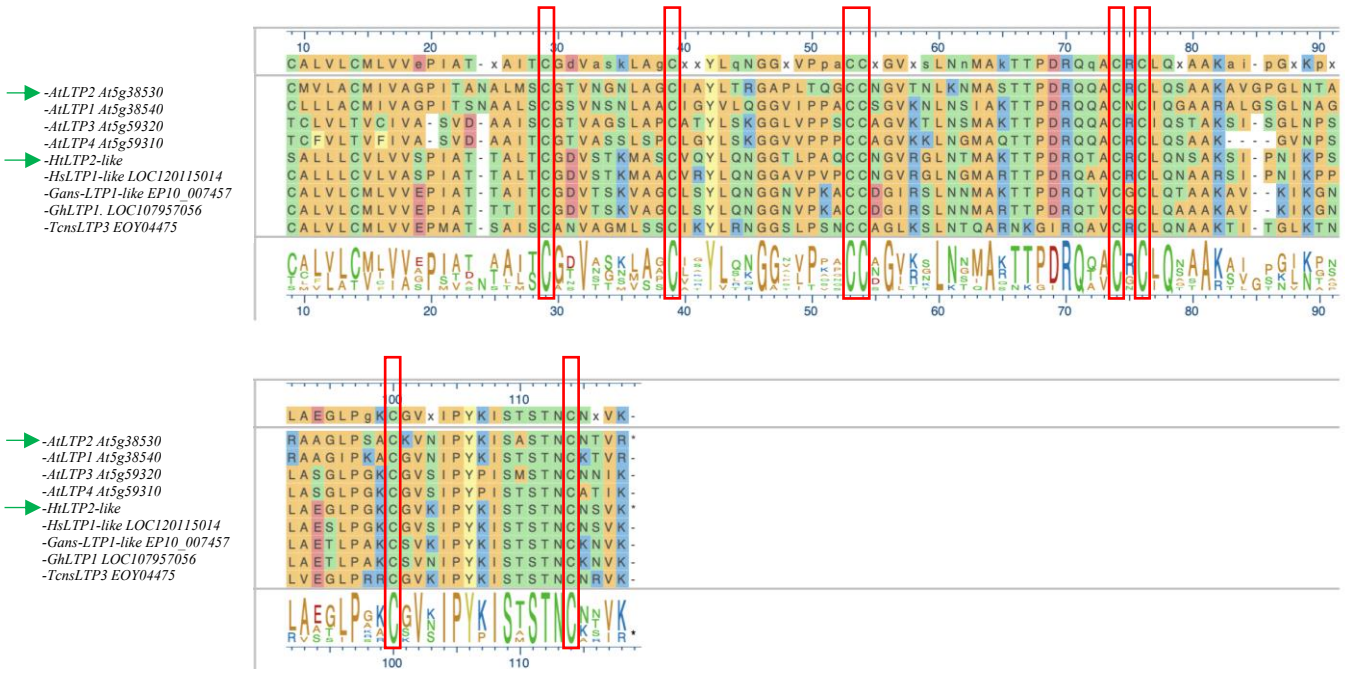

b

Protein name	AtLTP2	AtLTP1	AtLTP3	AtLTP4	HtLTP2-like1	HsLTP1-like	Gans-LTP1-li	GhLTP1	TcnsLTP3
AtLTP2	0	68,4685	49,5495	47,7477	49,5495	49,5495	46,8468	47,7477	46,8468
AtLTP1	81,0811	0	51,3514	50,4505	49,5495	52,2523	49,5495	48,6486	45,9459
AtLTP3	65,7658	70,2703	0	83,7838	54,955	52,2523	50,4505	48,6486	49,5495
AtLTP4	64,8649	72,973	89,1892	0	54,0541	54,955	52,2523	51,3514	48,6486
HtLTP2-like1	63,0631	70,2703	71,1712	71,1712	0	84,6847	71,1712	68,4685	61,2613
HsLTP1-like	63,964	71,1712	66,6667	70,2703	90,0901	0	69,3694	69,3694	58,5586
Gans-LTP1-like	63,0631	67,5676	64,8649	63,0631	82,8829	81,0811	0	96,3964	62,1622
GhLTP1	63,964	67,5676	64,8649	63,0631	81,0811	81,0811	97,2973	0	61,2613
TcnsLTP3	57,6577	65,7658	64,8649	62,1622	81,0811	77,4775	76,5766	74,7748	0

Identity (%)

Similarity (%)

Figure 5.2: Protein sequence alignment of some members of the LIPID TRANSFER PROTEIN family of *A. thaliana*, *H. trionum*, *H. syriacus*, *Gossypium australe*, *Gossypium hirsutum* and *Theobroma cacao*. (**a**) Alignment performed using AtLTP1, 2, 3 and 4 protein sequences as well HtLTP2-like, *Hibiscus syriacus* LTP1-like, *Gossypium australe* nsLTP1-like, *G. hirsutum* LTP1 and *Theobroma cacao* LTP3 protein sequences. Aligment was performed using clustal omega alignment algorithm. The Cystein residues of the LTP characteristic domain (C-Xn-C-Xn- CC-Xn-CXC-Xn-C-Xn-C) necessary for the formation of disulfure bonds are framed in red. Green arrows pointing at AtLTP2 and HtLTP2-like protein sequences. (**b**) table presenting the percentage of identity (upper right part of the table) and percentage of homology (lower left part of the table) between the proteins.

similarity with AtLTP2 (63%), which is consistent with a potentially similar function and role of the two proteins.

Using the transcriptomic data acquired in the chapter 4, the expression of *HtLTP2-like* gene was assessed during the flower development at stages 2, 3 and 4 in both the proximal and the distal petal regions. A decrease in the expression of *HtLTP2-like* during petal development in both distal and proximal tissues can be observed, with a relatively higher expression in distal petal parts at stage 2 (fig. 5.3). This result is consistent with differential regulation of cuticle production and properties in the proximal and distal petal parts. It remains however difficult to infer its potential implication in the development of striations. To perturb the production of cuticle and its structure, two *HtLTP2-like* over expressing transgenic lines were produced.

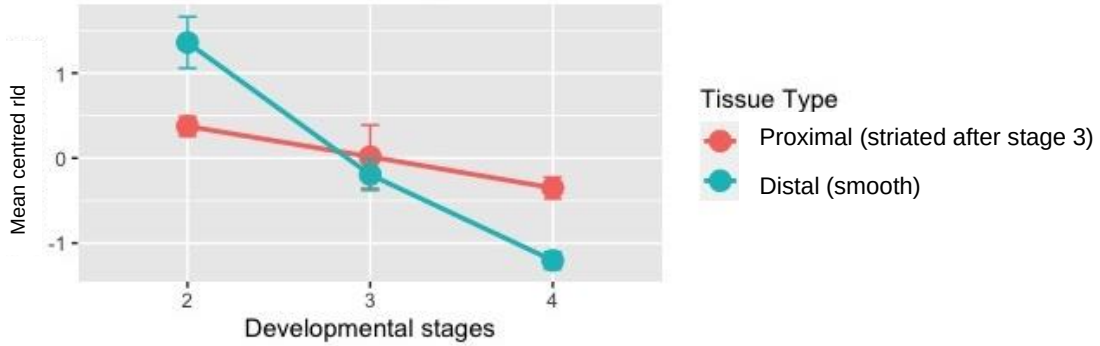

Figure 5.3: Evolution of the expression of *HtLTP2-like* in *Hibiscus trionum* during stages 2, 3 and 4 of the flower development. In the proximal petal part (striated after stage 3) (red line and dots), and the distal petal part (smooth) (blue line and dots) represented after regularised log transformation of the number of reads and centered around the mean.

5.3.2 *HtLTP2-like* was successfully over-expressed in *H. trionum*

Transformation of *H. trionum* with the *35S:HtLTP2-like* construct was assessed by semi quantitative RT-PCR performed on cDNA synthesised from RNA extracted from leaves (fig. 5.4). A clean over expression can be observed in the two independent transgenic lines produced in comparison to the wild-type in which *HtLTP2-like* is barely expressed, thus confirming the transformation of *Hibiscus trionum* with the *35S:HtLTP2-like* construct and its induced over expression.

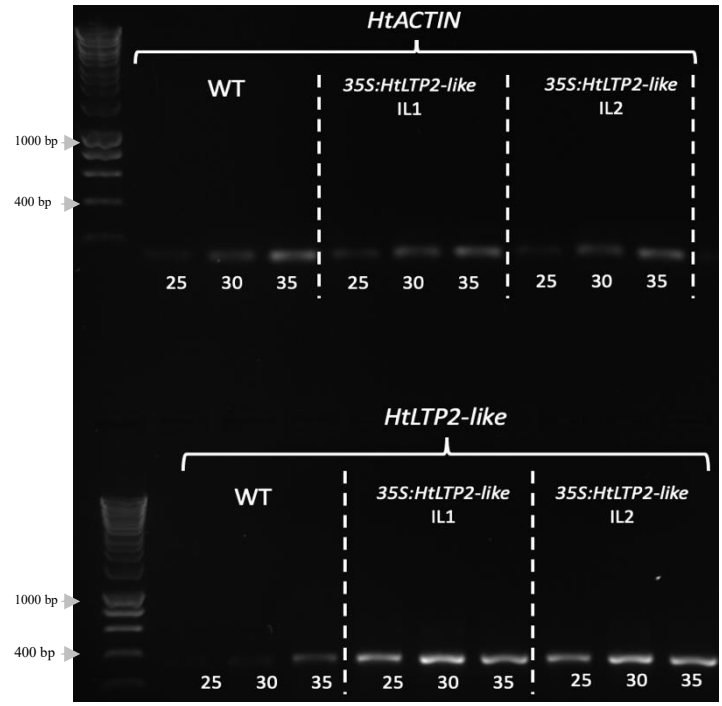

Figure 5.4: Semi quantitative RT-PCRs performed on WT *Hibiscus trionum* and *35S:HtLTP2-like* independent transgenic line 1 (IL1) and 2 (IL2). Primers for *HtACTIN* (housekeeping gene) and *HtLTP2-like* genes were used (see primer sequences in Annex II) and amplification was assessed after 25, 30 and 35 PCR cycles. The expected sizes for *HtACTIN* and *HtLTP2-like* PCR product are 118 and 346 bp, respectively.

5.3.3 *35S:HtLTP2-like* transgenic lines display organ fusion and male and female sterility

The two independent *35S:HtLTP2-like* transgenic lines, IL1 and IL2, display thin elongated stems with a very slow yet continuous growth of their vegetative organs, an abundant production of flowers with occasional abnormalities such as a high number of petals and fasciation. Anthers are not dehiscent (fig. 5.5), rendering self-fertilisation impossible. The overall size of the transgenics is also smaller than the wild type and stem fusion was observed in both lines (fig. 5.5, b and c, and g and k). These phenotypes are consistent with perturbed activity of LTP proteins in other systems (A. A. Jacq et al., 2017) and with perturbation of the cuticle more generally.

Figure 5.5: Macroscopic phenotype of the *35S:HtLTP2-like* transgenic lines IL1 and IL2. **(a, d** and **h)** Pictures of WT *Hibiscus trionum*. **(b, e, i** and **g)** Pictures of *35S:HtLTP2-like* IL1; **(c, f, j** and **k)** Pictures of *35S:HtLTP2-like* IL2. **(a, b** and **c)** Full plant picture of WT (55 day old), *35S:HtLTP2-like* IL1 (245 day-old) and *35S:HtLTP2-like* IL2 (274 day-old), respectively. scale bar = 10 cm. **(d, e, f, h** and **j)** Close up picture of the flowers and reproductive organs; scale bar = 1 cm. **(g** and **k)** Close up picture of the stems of *35S:HtLTP2-like* IL1 and IL2**.** Red arrowheads point at fused stems**.**

5.3.4 Over expression of *HtLTP-like* is sufficient to induce an alteration of the cuticle striation

Scanning electronic microscopy revealed slight differences in the striation pattern on the petal epidermis of the transgenic lines. The striation orientation was sometimes offset from the longitudinal axis of the cells in the IL 2 line (fig. 5.6e and f), some cells also present an absence of striations (fig. 5.6c) and a difference in the amount of epicuticular waxes could also be observed between the WT and the IL2 line (fig. 5.6g and i). The aspect ratio of the striations also seemed different, appeared inconsistent and was not well maintained on cuticle at cell junctions in the IL2 transgenic line (fig. 5.6i). Optical microscopy as well as SEM of cross sections of *35S:HtLTP2-like* IL2 transgenic lines also showed the presence of entirely smooth cells (fig. 5.6). Finally, some delamination of the cuticle

proper from the cuticle beneath as well as the post-buckling deposition of an unknown substance on top of the cuticle proper could be observed (fig. 5.6).

Consistently with the phenotype observed in *A. thaliana LTP2* loss of function transgenic lines (A. Jacq et al., 2017), the over expression of *HtLTP2-like* lines resulted in an alteration of the cuticle integrity which resulted in a partial loss of striations and an alteration in their regularity on the cuticle of *Hibiscus trionum* petals.

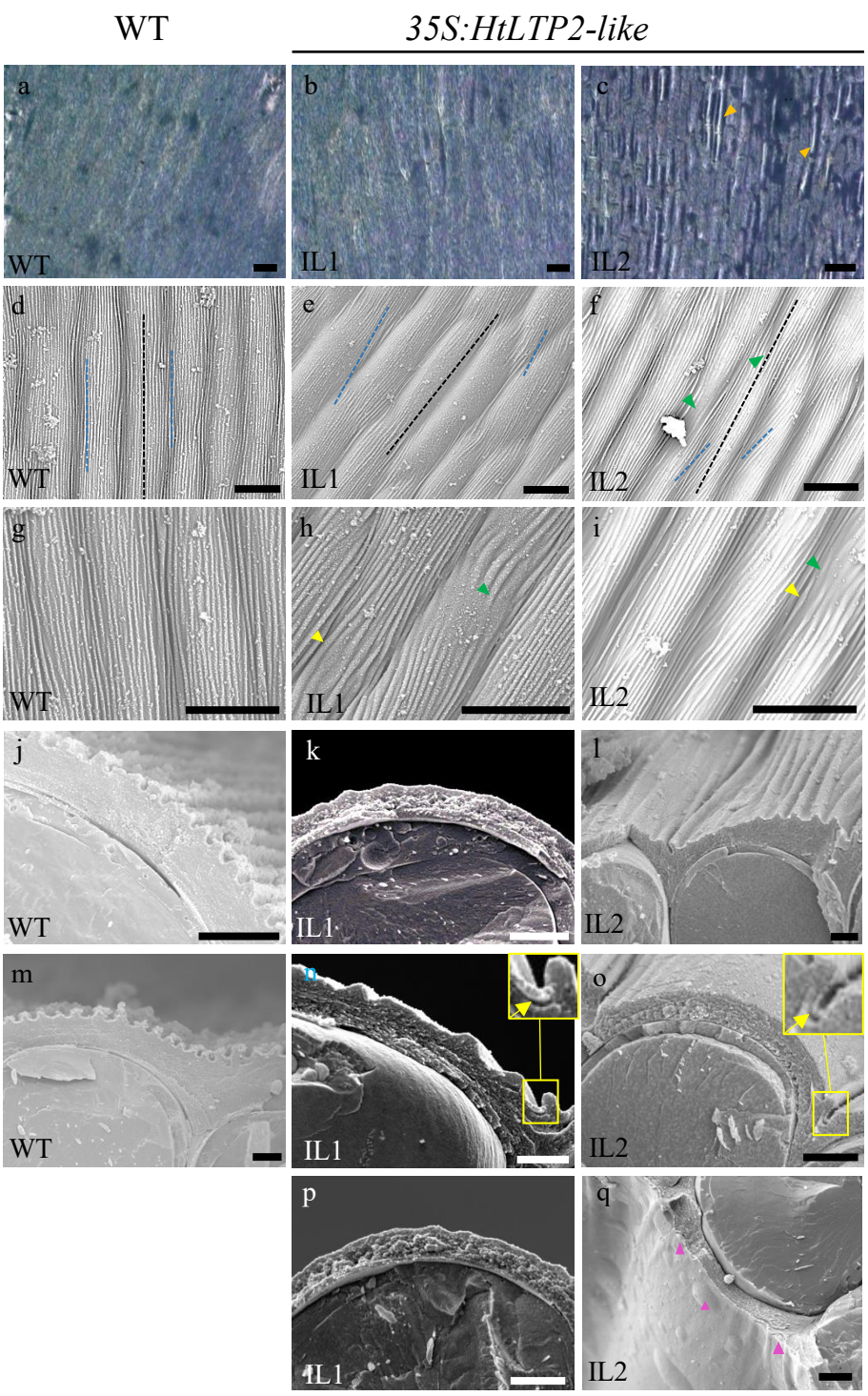

Figure 5.6: Optical and electron microscopy of the striated region of the petals of WT *H. trionum* and two independent *35S:HtLTP2-like* transgenic lines (IL1 and IL2). **(a, d, g, j and m)** WT striated region. **(b, e, h, k, n and p)** *35S:HtLTP2-like* Independent Line 1 (IL1). **(c, f, i, l, o and q)** 35S:*HtLTP2-like* Independent Line 2 (IL2). **(a, b and c)** Optical microscopy pictures (scale bar = 50 µm). **(d-i)** Cryo-scanning electron microscopy (Cryo-SEM) (scale bar = 20 µm). **(j-q)** Cross sections of striated cuticle obtained by cryo-fracture and imaged with cryo-SEM (scale bar = 2 µm). orange arrow heads pointing at isolated smooth cells, green arrowheads pointing at interrupted striations, yellow arrow heads pointing at changes in striation aspect ratio, pink arrow heads pointing at post-buckling material deposition black dashed lines indicating the axis of cell elongation, blue dashed lines indicating the axis of the striations, yellow squares showing delamination of the cuticle proper.

5.3.5 The thickness of both the cuticle proper and the ECM is smaller in both *35S:HtLTP-like* transgenic lines

Following the hypothesis of buckling as the origin of striation (Bowden et al., 1998; Huang et al., 2017; Kourounioti et al., 2012), The thickness of the cuticle proper and the extracellular matrix (ECM) (comprising the cell wall and the cuticularised cell wall) for these two transgenic lines was then investigated in order to assess whether an alteration of the structure of the cuticle could explain the irregularity of the striations. For striated cells, two different values were considered for the ECM; one called 'Bottom' goes from the bottom of the striation to the top of the plasma membrane and another one called 'Top' goes from the top of the striation to the top of the plasma membrane.

After measuring the thickness of the extracellular matrix, we observed that both smooth and striated cells in both *HtLTP2-like* transgenic lines displayed a strong reduction of the ECM thickness on the adaxial proximal petal part of the petal cuticle (fig. 5.7a), showing that the over expression of the *HtLTP2-like* gene had important consequences on the regulation of the cuticle. Interestingly, a decrease in the ECM thickness was not sufficient to prevent buckling entirely. The thickness of the extracellular matrix of smooth cells was found to be significantly different to the 'Top' measure of their respective lines only, making the thickness of the ECM in striated cells rather similar to the one of smooth cells. This suggests that the ECM thickness plays a secondary role in the buckling process.

Statistical differences in the thickness of the cuticle proper between WT striated cells and smooth and striated cells of both *HtLTP2-like* transgenic lines could be observed. However, despite a cuticle proper thinner of about 100 nm, both transgenic lines retained a capacity to buckle, suggesting that the thickness of the cuticle proper plays a less relevant role in buckling than was originally believed. Confirming this, no statistical differences in thickness could be observed between the cuticle proper of smooth and striated cuticle for both transgenic lines, respectively.

Despite obvious changes in the thickness of the extracellular matrix and the cuticle proper, the buckling capacity of the two transgenic lines was at least partially retained, indicating that the partial loss of striations is due to the perturbation of other elements.

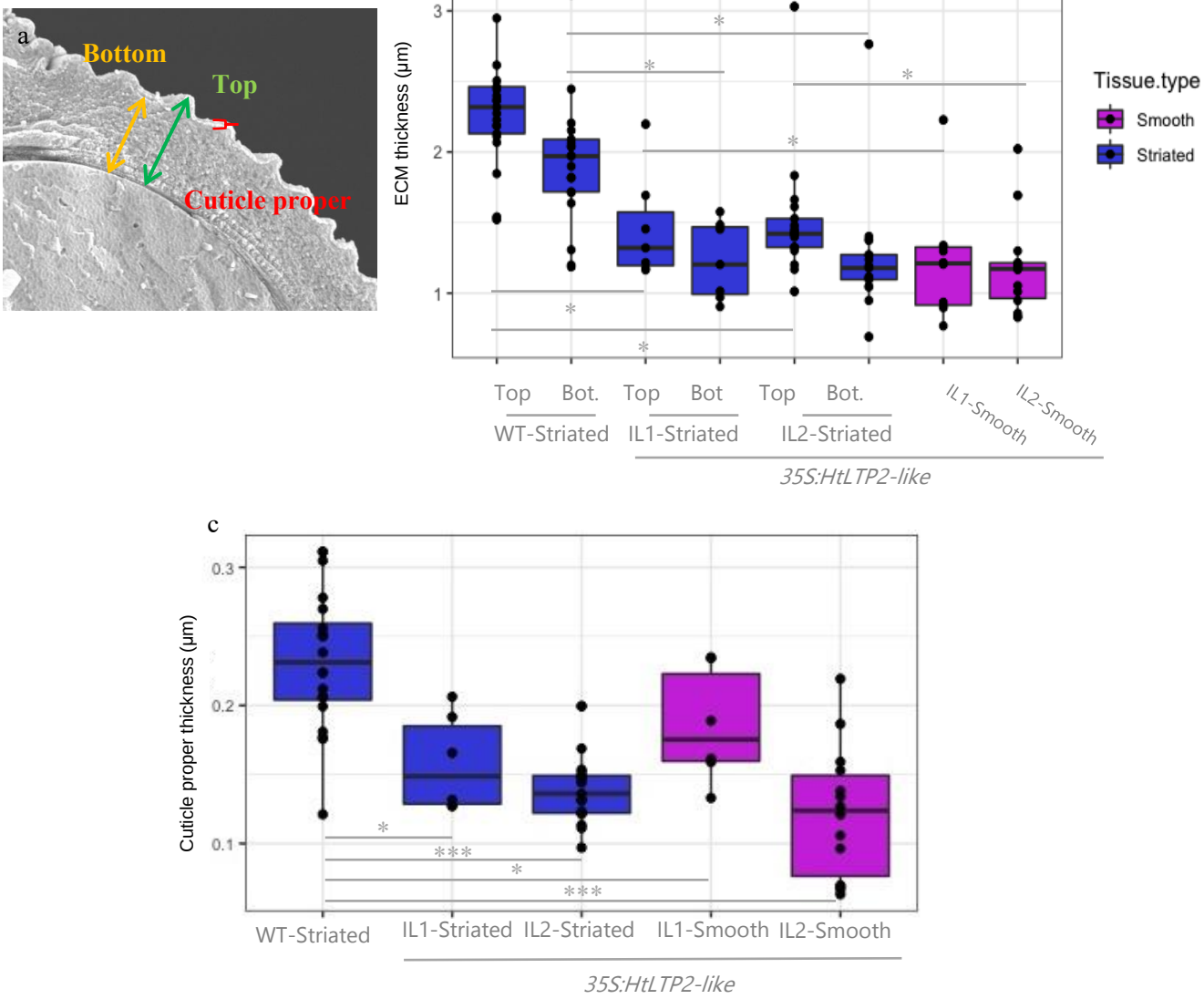

Figure 5.7: Box plots of the thickness of the extracellular matrix (ECM) and the cuticle proper of the adaxial proximal petal epidermis of WT *Hibiscus trionum* and *35S:HtLTP2-like* transgenic lines. (**a**) Cryo-SEM picture of a cross section of a striated cell. 'Top' and 'Bottom' describe the two types of measure performed on the ECM of cross sections of striated cells (see yellow element for 'Bottom', green element for 'Top' and red element for the cuticle proper). (**b**) Thickness of the ECM. The two transgenic lines were compared to the equivalent WT parts as well as the ECM thickness of the smooth cells of their respective line. (**c**) Box plot of the thickness of the cuticle proper measured on the tissues mentioned above. The thickness of the WT cuticle proper was compared to the one of smooth and striated cells of *the* two transgenic lines. The thickness of smooth and striated cuticle proper was also compared within each transgenic line. * ⇔ $0.05 > \text{p-value} \geq 1.10^{-3}$; ** ⇔ $1.10^{-3} > \text{p-value} \geq 1.10^{-4}$; *** ⇔ $1.10^{-4} > \text{p-value}$.

The roles of the *HtSHN1*, *2* and *3* genes (a type-B and two type-C *SHINE* genes, respectively) in the development of striations was investigated. Transgenic lines described in chapter 3 have shown that the upregulation of a dominant negative *HtSHN3-VP16* or the fusion of *HtSHN3* to an *SRDX* repressive domain resulted in a complete loss of striations in *Hibiscus trionum*. Other over expressing attempts were also conducted by Dr. Edwige Moyroud using a UBIQUITIN 10 promotor sequence and a native protein sequence. This resulted in the production of ectopic striations on the abaxial part of the petals (Moyroud et al. in preparation). In this section I produced a fourth *HtSHN3* transgenic line containing the endogenous *HtSHN3* cDNA sequence under the control of a double 35S promotor. Similarly, the role of *HtSHN1* and *HtSHN2* in the development of structural colours on *H. trionum* petals was investigated by the construction of *35S:HtSHN1* and *35:HtSHN2* transgenic lines.

5.3.6 *HtSHN1, HtSHN2* and *HtSHN3* are differentially expressed in the proximal and distal petal parts of the petal

From the transcriptomic data described in chapter 4, it was observed that the expression profiles of *HtSHN1*, *HtSHN2* and *HtSHN3* is different across development in both striated and smooth tissues (fig. 5.8). The *HtSHN1* gene seems to be regulated differentially in striated and smooth thissues at stages 3 and 4 of development with a consistent decrease in striated tissues and a peak at stage 3 in smooth tissues, which suggests a role in the development of smooth cuticle on conical cells in non striated tissues (fig. 5.8). However, *HtSHN2* does not appear as significantly differentially expressed in the distal and proximal petal parts which suggests that it is not determining the type of cuticle that is produced and may act as a general inducer of cuticle production. Finally, the expression of *HtSHN3* is relatively low in both distal and proximal petal parts at stage 2 and increases rapidly in the proximal petal region at stage 3 and 4 to reach more than 32 times its expression at stage 2 ($32 = 2^5$), suggesting a dominant role in the development of the proximal cuticle leading to the development of cuticular pattern.

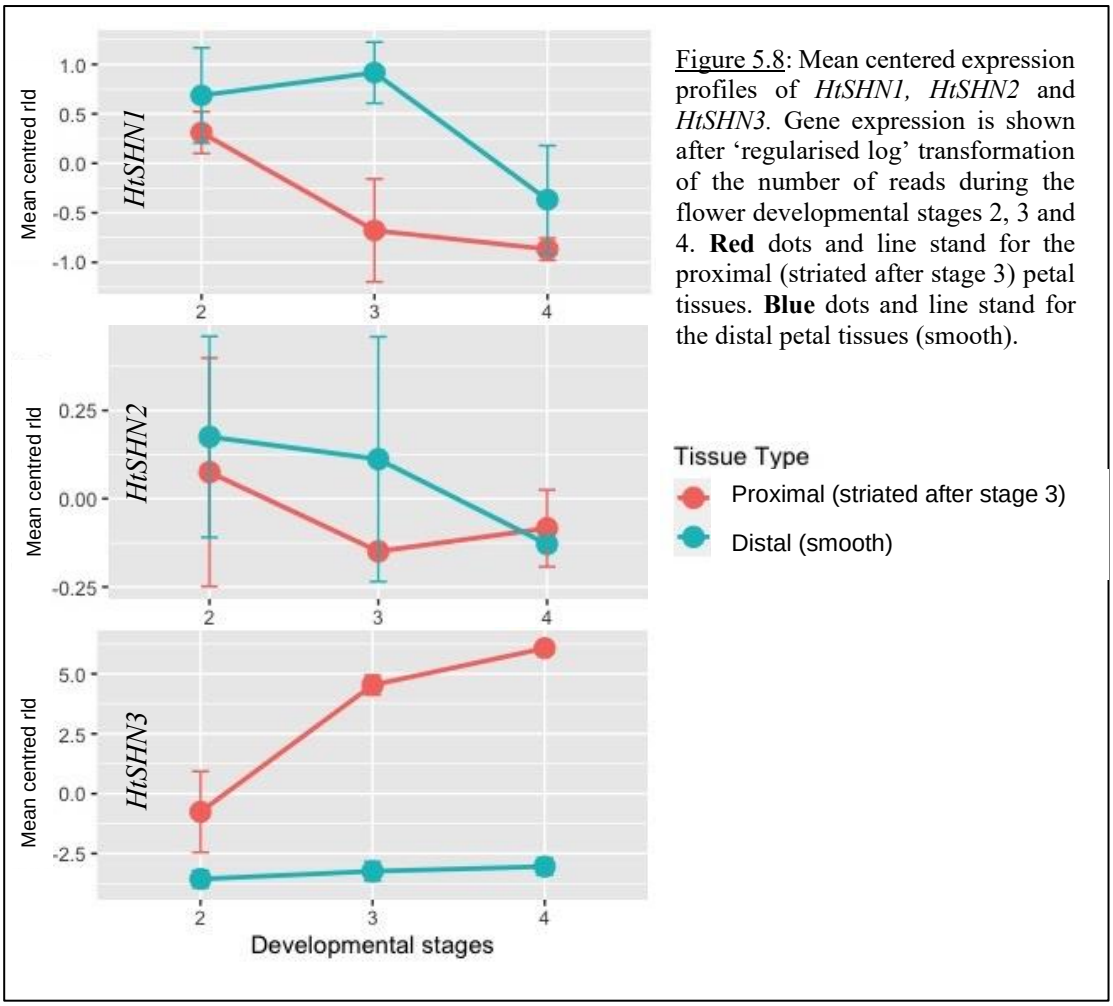

Figure 5.8: Mean centered expression profiles of *HtSHN1, HtSHN2* and *HtSHN3*. Gene expression is shown after 'regularised log' transformation of the number of reads during the flower developmental stages 2, 3 and 4. **Red** dots and line stand for the proximal (striated after stage 3) petal tissues. **Blue** dots and line stand for the distal petal tissues (smooth).

5.3.7 ***HtSHN1, HtSHN2*** **and** ***HtSHN3*** **were successfully over expressed in *H. trionum*.**

Over expressing transgenic lines of *HtSHN1*, *2* and *3* placed under a double CaMV35S promotor were produced using the same expression vector (pEM110) as for the *35S:HtLTP2-like* transgenic lines as detailed in section 5.3.1. Five over-expressing transgenic lines were produced: two *35SHtSHN1*, another two *35HtSHN2*, and one *35SHtSHN3*. Gene over expression was assessed by semi-quantitative RT-PCR (fig. 5.9). A clean over expression was detected for the five transgenic lines produced, confirming the transformation of *H. trionum*.

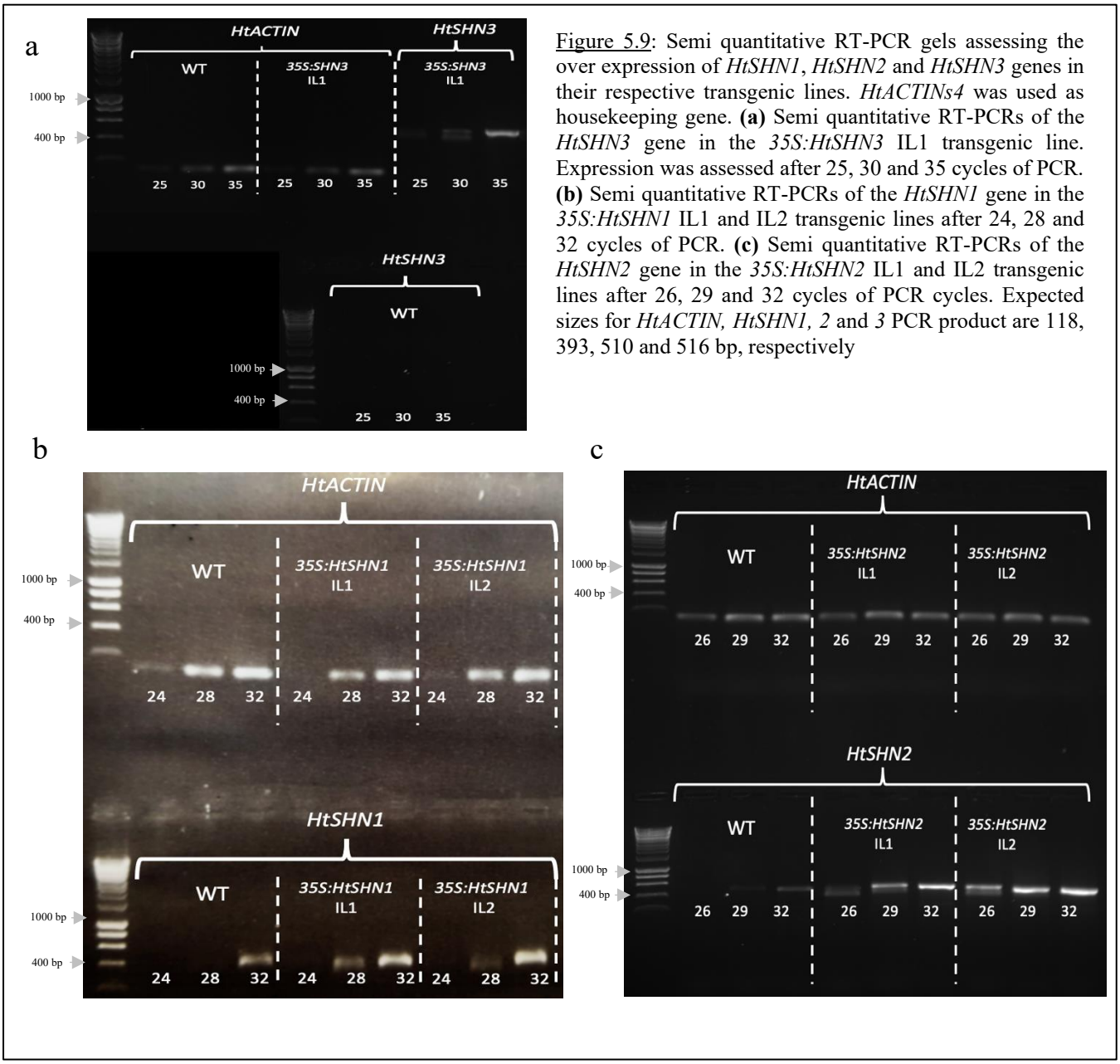

Figure 5.9: Semi quantitative RT-PCR gels assessing the over expression of *HtSHN1*, *HtSHN2* and *HtSHN3* genes in their respective transgenic lines. *HtACTINs4* was used as housekeeping gene. **(a)** Semi quantitative RT-PCRs of the *HtSHN3* gene in the *35S:HtSHN3* IL1 transgenic line. Expression was assessed after 25, 30 and 35 cycles of PCR. **(b)** Semi quantitative RT-PCRs of the *HtSHN1* gene in the *35S:HtSHN1* IL1 and IL2 transgenic lines after 24, 28 and 32 cycles of PCR. **(c)** Semi quantitative RT-PCRs of the *HtSHN2* gene in the *35S:HtSHN2* IL1 and IL2 transgenic lines after 26, 29 and 32 cycles of PCR cycles. Expected sizes for *HtACTIN, HtSHN1, 2* and *3* PCR product are 118, 393, 510 and 516 bp, respectively

5.3.8 **Only the over expression of *HtSHN3* resulted in an alteration of the cuticular striations, potentially via the silencing of *HtGDSL-like* protein**

Observation of the whole plant and flowers of the *35S:HtSHN1*, *2* and *3* transgenic lines did not reveal any alteration of the overall plant aspect, size and morphology (fig. 5.10). However, pictures of the flowers were not sufficient to assess the presence of striations on the proximal adaxial surface of the petals.

Optical microscopy pictures of the adaxial and abaxial proximal petal surface of each transgenic line were then taken in order to assess the presence of altered or ectopic striations (as described on the abaxial proximal petal surface of *UBIQUITIN10:HtSHN3* transgenic lines (Moyroud et al., in submission)). The *35S:HtSHN1* and *35S:HtSHN2* transgenic did not display altered striations on the adaxial proximal petal surface nor ectopic striations on the abaxial proximal petal surface. Surprisingly, the over expression of *HtSHN3* did not result in the production of ectopic striations and instead resulted in the complete loss of striations on the adaxial proximal petal cuticle, suggesting that other mechanisms, possibly silencing or inhibiting the effects of *HtSHN3*, are activated in this context (fig. 5.11).

In order to assess how the over expression of *HtSHN3* could alter the development of striations, the expression of 2 effectors involved in the production of cutin was investigated. The *AtCYP77a4* (*At5g04660*) gene in known to be involved in the ω-hydroxylation of the precursors of cutin monomers (see fig. 1.7) (Fich et al., 2016; Yeats & Rose, 2013). Proteins of the GDSL-esterase/lipase family were also found as involved in the polymerisation of cutin monomer (Bakan & Marion, 2017) and three GDSL esterase/lipase were identified as targets of *AtSHINE* genes in *A. thalian* (*AtRXF26* (*At1g58430*), *At2g42990* and *At5g33370*) (Shi et al., 2011). Potential orthologs of *AtCYP77a4* and *At2g42990* were identified as explained in the section 4.2.7 and their expression profile in a WT context was obtained from the transcriptomic data (see chapter 4) (primers available in annex II). The predicted orthologous gene of *AtCYP77a4* was named *HtCYP77a6-like1* due to the homology of its protein sequence with other AtCYP77a proteins. The expression of both *HtCYP77a6-like1* and *HtGDSL-like* in a WT context is higher in the proximal petal region and increases from stage 2 to stage 4, which suggests that both proteins play a role in the development of striations. Furthermore, the similarity of the expression profile of *HtGDSL-like* and *HtSHN3* in the proximal petal region is indicative of a possible regulation of *HtGDSL-like* by *HtSHN3* (fig 5.12 and fig. 5.8).

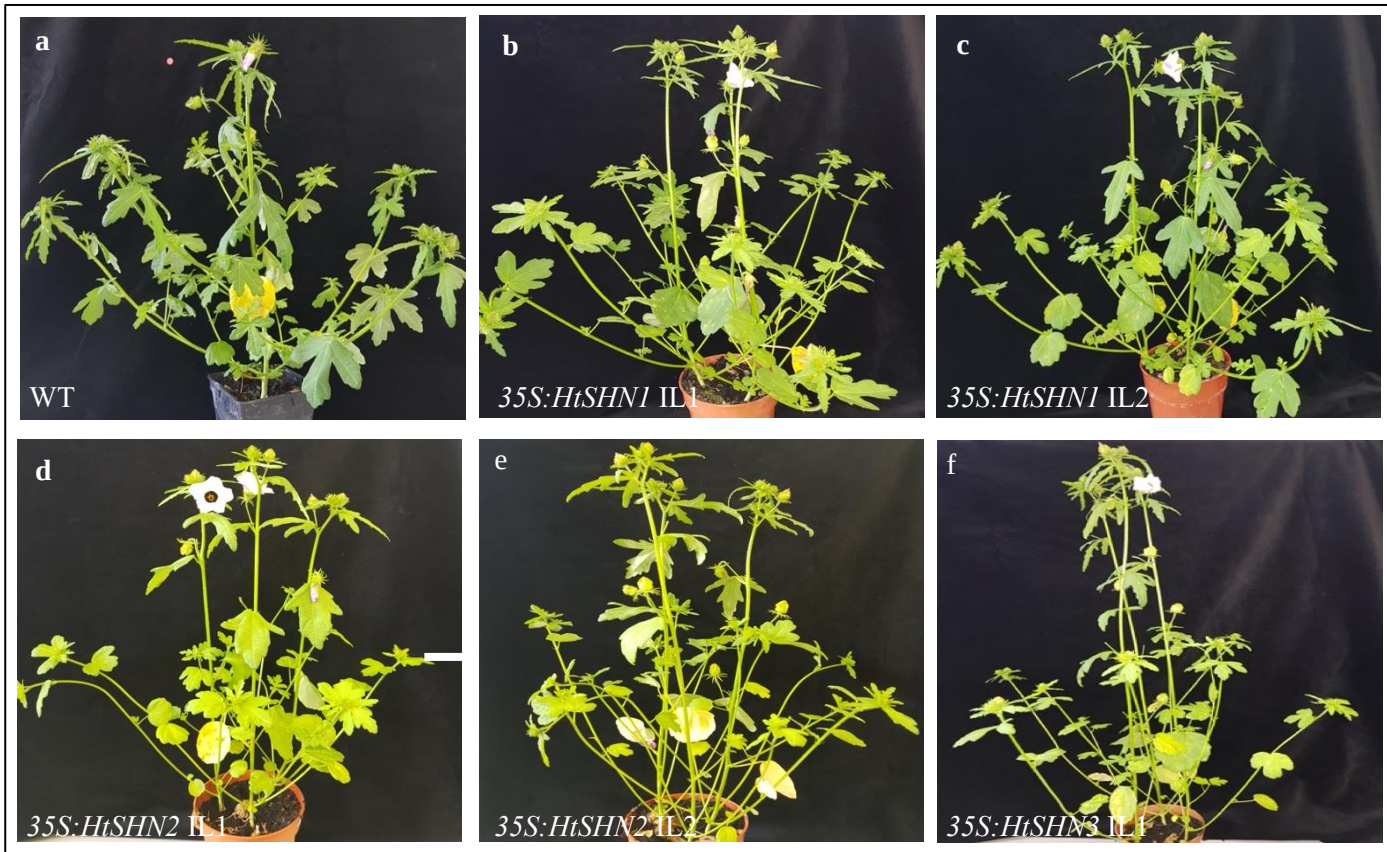

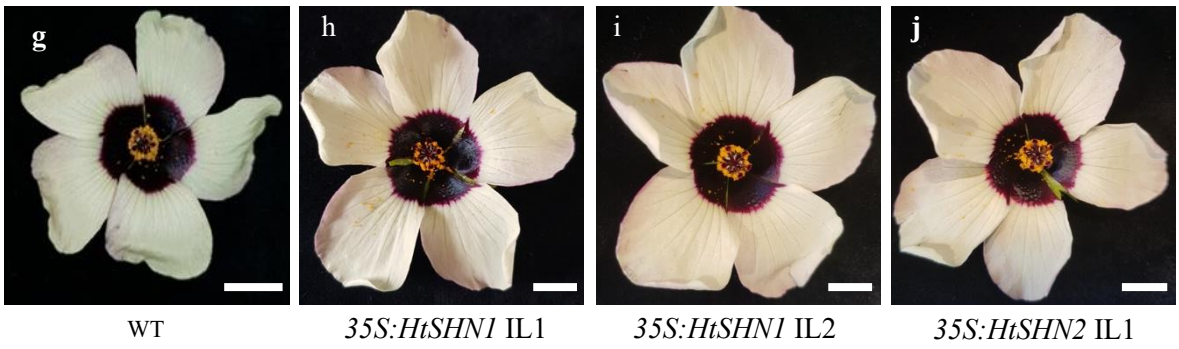

Figure 5.10: Whole-plant and flower pictures of *Hibiscus trionum 35S:HtSHN1, 2* and *3* transgenic lines. (**a** and **g**) WT *Hibiscus trionum*; (**b** and **h**) *35S:HtSHN1* IL1 transgenic line; (**c** and **i**) *35S:HtSHN1* IL2 transgenic line; (**d** and **j**) *35S:HtSHN2* IL1 transgenic line; (**e** and **k**) *35S:HtSHN2* IL2 transgenic line. (**f and l**) *35S:HtSHN3* IL1 transgenic line. (**a-f**) Whole-plant pictures. (**g-l**) Flower pictures.

Semi quantitative RT-PCR were then performed to assess the expression of *HtCYP77a6-like1* and *HtGDSL-like* in a *35S:HtSHN3* context. The expression profile of *HtCYP77a6-like1* suggests an increase in the cutin monomer production, which is consistent with an over expression of *HtSHN3*. However, the expression of *HtGDSL-like* appears lower in the *35S:HtSHN3* transgenic line than in the

WT (fig. 5.13), suggesting that the over expression of *HtSHN3* leads to the silencing of *HtGDSL-like*. GDSL proteins being important for the polymerisation of the cuticle network (Girard et al., 2012), a silencing of a such protein could impact the development of a functional cutin network in the adaxial proximal epidermal part of the petal, thus altering the mechanical properties of the cuticle, which, in turn, could result in a buckling failure. Moreover, the importance of GDSL proteins was already

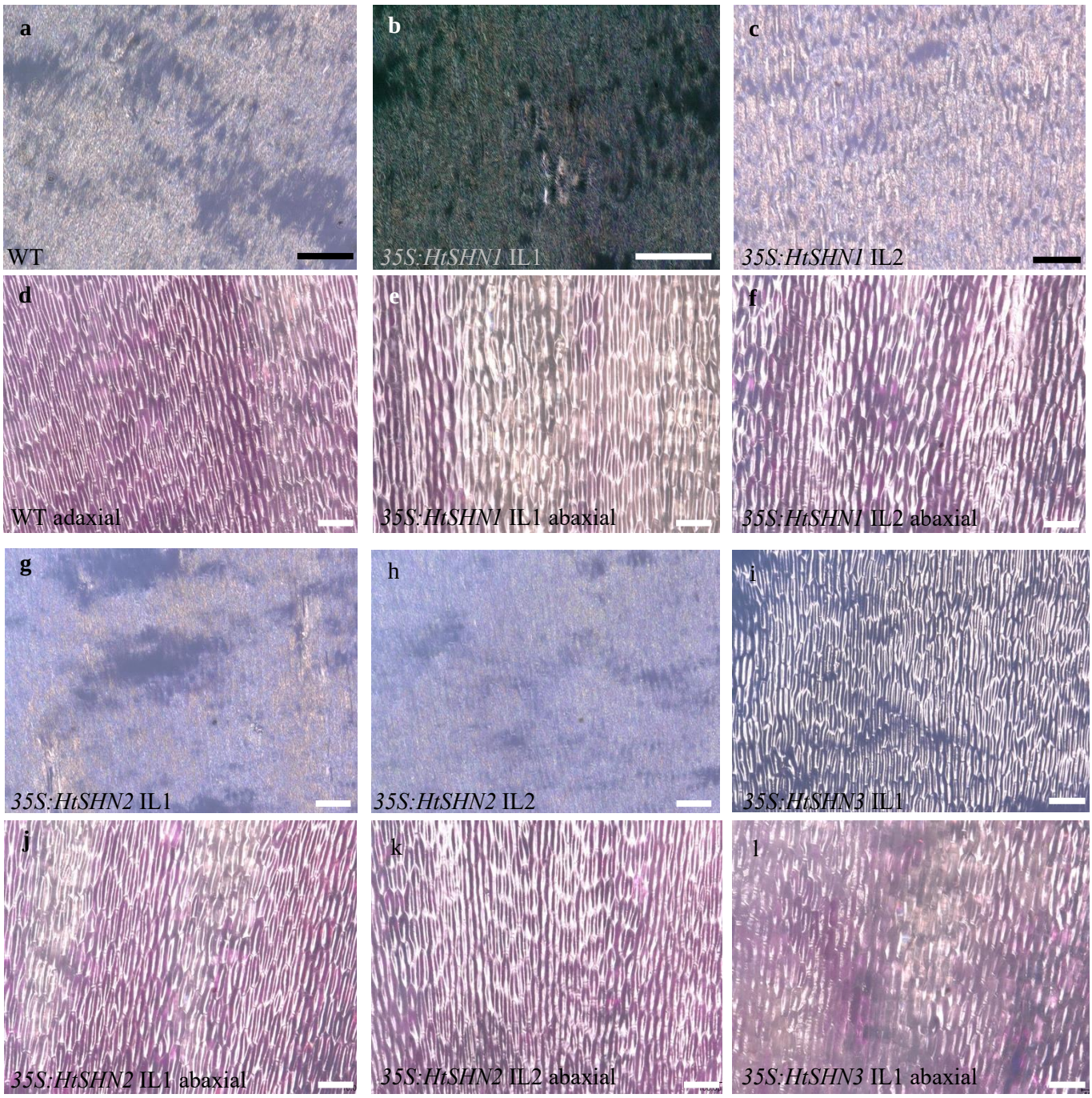

Figure 5.11: Optical microscopy of the proximal adaxial and abaxial petal epidermides of *35S:HtSHN1, 2* and *3* transgenic lines. (**a** and **d**) WT *H. trionum*. (**b** and **e**) *35S:HtSHN1* IL1. (**c** and **e**) *35S:HtSHN1* Il2. (**g** and **j**) *35S:HtSHN2* IL1. (**h** and **k**) *35S:HtSHN2* IL2. (**i** and **l**) *35S:HtSHN3*. Adaxial proximal petal epidermis (**a**, **b**, **c**, **g**, **h** and **i**). Abaxial proximal petal epidermis (**d**, **e**, **f**, **g**, **k** and **l**). Scale bar = 100 µm.

demonstrated by the production of the *35S:CD1.1* transgenic line which displayed alteration of striations (see fig. 3.3).

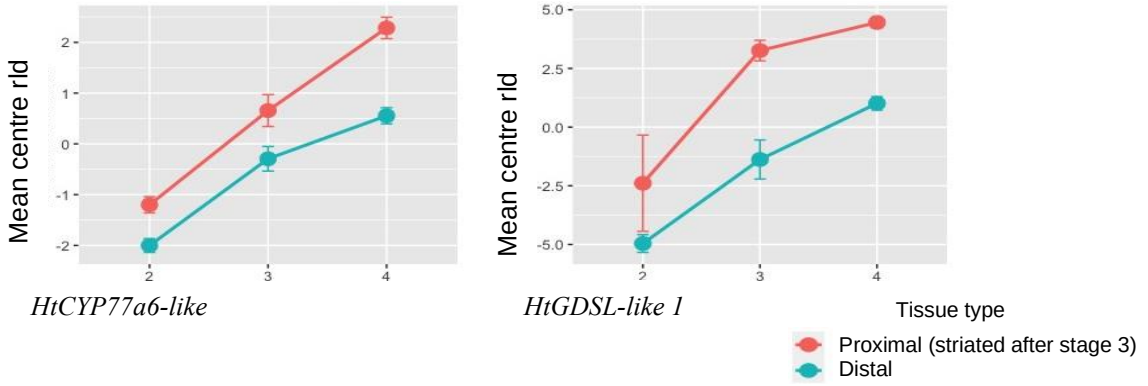

Figure 5.12: Expression profiles of *HtCYP77a6-like1* and *HtGDSL-like* genes during flower development. Expression was calculated during stages 2, 3 and 4 of development Mean centered expression profile of *HtCYP77a6-like1* and *HtGDSL* after 'regularised log' transformation of the number of reads during the flower developmental stages 2, 3 and 4. Red dots and line stand for the proximal (striated after stage 3) petal tissues. Blue dots and line stand for the distal petal tissues (smooth).

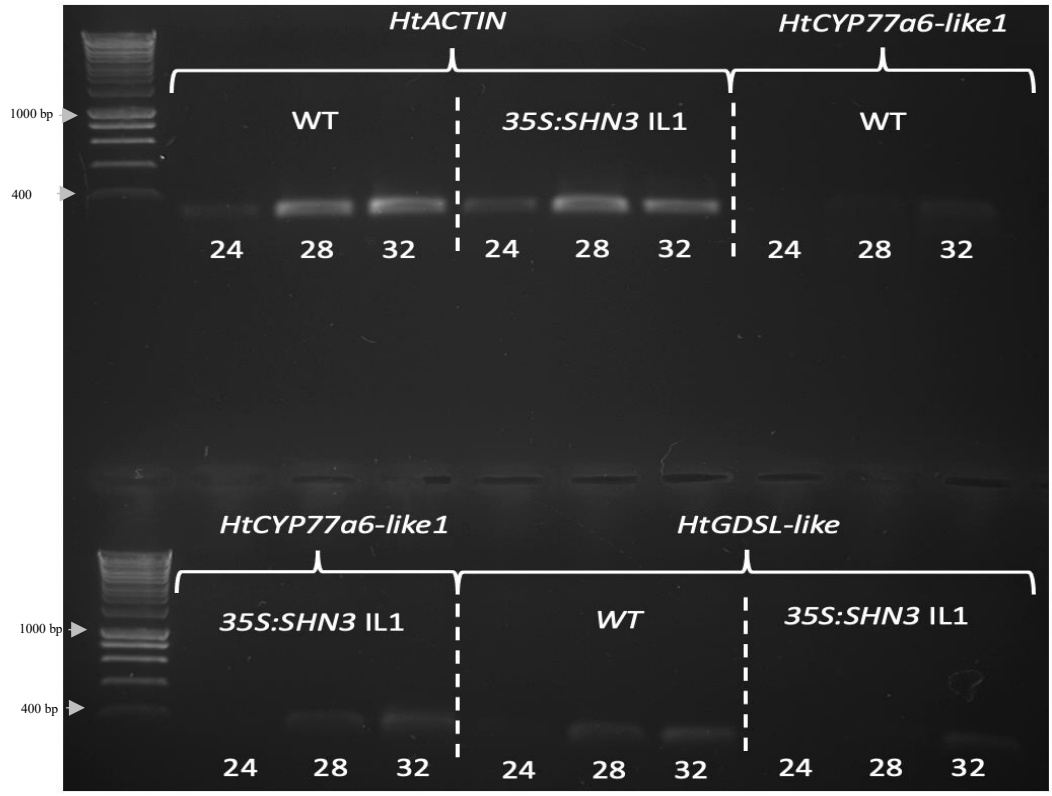

Figure 5.13: Semi-quantitative RT-PCR gels assessing the expression of *CYP77a6-like1* and *GDSL-like* genes in a WT *H. trionum* and a *35S:HtSHN3* transgenic line. *HtACTINs4* was used as housekeeping gene. Amplification was assessed after 24, 28 and 32 PCR cycles. Expected sizes of the PCR products are 117 bp (*HtCYP77a6-like1*), 87 bp (*HtGDSL*-like) and 118 bp (*HtACTINs4*).

5.3.1 The *HtDCR* gene present higher expression levels in the distal petal part

As previously described in chapter 3, a strong depletion in 10,16 dihydroxypalmitate (10,16-DHP) is correlated with a mutation of the *DCR* gene and a loss of striations in *A. thaliana* (Panikashvili et al., 2009). The expression of *H. trionum* ortholog of *AtDCR* was in striated and non-striated petal tissues across stages 2, 3 and 4 of development, to see if the correlations observed in *A. thaliana* can be inferred in *H. trionum.*

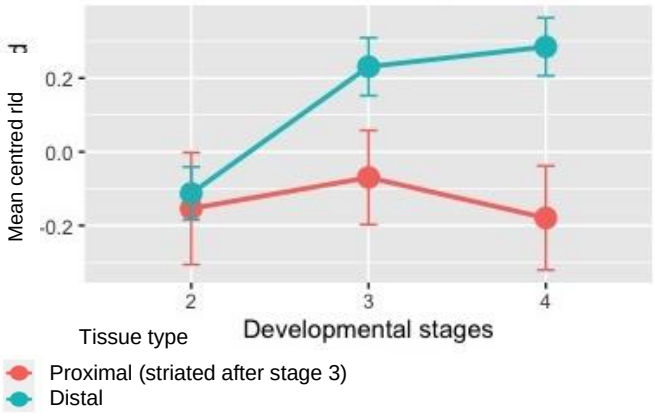

Figure 5.14: Evolution of the expression of *HtDCR* in *Hibiscus trionum* flower during developmental stages 2, 3 and 4. Red dots and line stand for the proximal (striated after stage 3) petal tissues. Blue dots and line stand for the distal petal tissues (smooth). Relative expression was calculated after regularised log transformation of the number of reads and centered around the mean.

Surprisingly, and despite an apparent increase in smooth tissues and decrease in striated tissues after stage 3, *HtDCR* is more expressed in the distal petal tissues than in the proximal ones (fig. 5.14). This shows that the difference in the amounts of 10,16-DHP measured between striated and smooth tissues (see fig. 3.6) is not explained by differences in the expression of *DCR*. This suggests that the production of 10,16-DHP in the two types of tissues does not correlate with its capacity to be detected by liquid extraction surface analysis. We hypothesise that the capacity of the LESA-MS to detect it reflects its level of polymerisation in the cutin network: the more reticulated a compound is, the less we are able to extract it for analyses or that another enzyme or molecular pathway is involved in the production of 10,16-DHP.

5.4 Discussion

The over-expression of the *HtLTP2-like* gene was also sufficient to alter the development of striations and introduced irregularity in their shape and even their complete loss in certain parts of the petal adaxial epidermis. The AtLTP2 protein was demonstrated to be involved in the maintenance of the integrity of the cuticle/cell wall interface, however, the phenotype observed in *35S:HtLTP2-like* transgenic lines suggests a delamination of the cuticle proper as well as the deposition of extra cuticular

material, suggesting that the over expression of the AtLTP2 related protein HtLTP2-like, modified the chemistry and structuration of the cuticle. Furthermore, measurement of the cuticle proper and extra cellular matrix revealed a decrease in the cuticular load at the petal adaxial epidermal surface suggesting an alteration of the cuticular synthesis and/or deposition mechanisms. Interestingly, despite an overall thinner cuticle proper and ECM in the *35S:HtLTP2-like* transgenic lines, no correlation could be seen with a loss of striations. This indicates that the thickness of both the cuticle proper and ECM is a secondary factor in the observed loss of striation and underlines the prevalence of the chemical nature of the cuticle as well as its structure.

Another attempt to modify the chemistry of the cuticle was made by over expressing *HtSHN1*, *HtSHN2* and *HtSHN3*. Protein sequences alignment showed that *HtSHN* genes could not be identified as orthologs of *AtSHN1*. As described in the chapter 1 (see figure 1.5), *HtSHN1* is the ortholog of *AtSHN2* and *AtSHN3* (all type-B *SHINE*). However, *HtSHN3* and *HtSHN2* belong to the type-C *SHINE* subgroup and show no orthology to *AtSHN* genes. This suggests that *HtSHN3* could display functions that are not shared with *A. thaliana.* The endogenous expression of *HtSHN1* and *HtSHN2* in the petal tissues does not show relevant differences between proximal and distal petal tissues, indicating that they do not a play role in the development of striations. However, the relatively higher expression of *HtSHN3* in the proximal petal parts suggests that *HtSHN3* plays an important role in the development of the cuticular pattern, as confirmed by the absence of cuticular striations observed in *35S:HtSHN3-VP16* and *35S:HtSHN3-SRDX* transgenic lines (see fig. 3.2). Furthermore, the chemical analyses performed in chapter 3 (see fig. 3.3 and 3.4) show that a modification in the expression of *HtSHN3* induces changes in the chemistry of the cuticle. Surprisingly, the production of a *35S:HtSHN3* transgenic line resulted in a loss of striations, similarly to the *35S:HtSHN3-VP16* transgenic line. Semi-quantitative RT-PCR of *GDSL-like* and *CYP77a-like1* genes revealed that the *CYP77a6-like1* gene was properly over-expressed in a *35S:HtSHN3* context, however, the *GDSL-like* gene -a potential target of *HtSHN3*- revealed a lower expression than in the WT control, indicating that a silencing mechanism takes place in a *35S:HtSHN3* context leading to the downregulation of the *GDSL-like* gene, thus potentially altering the mechanical properties of the cuticle and consequently, its capacity to buckle.

Surprisingly, analyses of the expression of *DCR* in WT *Hibiscus trionum* revealed a higher expression in distal (non-striated) tissues than in the proximal petal tissues, which is in opposition to the relatively higher levels of 10,16-DHP detected in proximal tissues. This is however consistent with a difference in the degree of polymerisation of 10,16-DHP. A *35S:HtDCR* transgenic line has been recently produced and a second generation is currently growing, however its phenotype has not been studied yet due to time constraints.

5.5 Conclusion

This study underlines the importance of *HtSHN3* in the synthesis of cuticle and in the polymerisation of the cutin network. This study also indicates that the thickness of the cuticle proper and extracellular matrix may not constitute a determining factor in the buckling of petal epidermis. The structure of the cuticle and the proper adhesion of the cuticle proper onto the substrate may however play an important role in the buckling dynamic.

Chapter 6: Discovery of the *blue* and *madeleine* mutants reveals the importance of a proper cuticle layering for the buckling

May Yeo and Edwige Moyroud took part in the EMS treatment of seeds, the sowing of plants and the screening of plants for alterations of the striations on the proximal adaxial petal cuticle.

6.1 Introduction

Molecular pathways known to regulate cell growth and cuticle synthesis were invoked in the previous chapters (see chapter 1 and chapter 4) to enable the identification of genes from the transcriptomic analyses with potential roles in the production of structural colours. This approach also allowed us to modify the cuticle and obtain perturbations of the nano scaled ridges, thus giving valuable insights into how cuticle buckling is achieved in *Hibiscus trionum* (see chapter 5). Although effective, this approach is not sufficient to provide a broad and global overview of the molecular pathways that are at play. In order to broaden our views and identify new biological processes and genes necessary for the development of such a trait, we must resort to unbiased approaches that do not presume prior understanding.

6.1.1 Mutant screens

Mutant screens usually constitute a labour-intensive task that aims to identify the potential role of unreported genes in the development of a specific trait. They consist in the induction of random mutations in a study organism followed by a screening step where the different mutants are assessed for the alteration of the trait of interest. Mutant screens have been conducted as early as the 1980s in *Arabidopsis thaliana* using ethylmethane sulfonate (EMS), ionising radiations such as X-rays, and fast neutron (FN) (Koornneef & Van Der Veen, 1980). The mutagenesis that is employed has various consequences on DNA, from a single nucleotide alteration followed by a replication error (EMS, X-rays and FN) to the deletion of larger DNA portions (FN and X-rays) (Belfield et al., 2012; Nelson et al., 1994). The probability of obtaining a mutant of interest (presenting an alteration of the phenotype of interest) is the direct consequence of the average number of mutations per gene induced by the mutagen agent, and the number of genes involved in the trait of interest (Koornneeff, Dellaert, & van

der Veen, 1982). This leads to the concept of 'saturation of the mutant screen' by which it can be established that all the genes involved in the biological process of interest have been mutated at least once (Niisslein-Volhard, Wieschaus et al., 1984). Although mutant screens do not necessarily aim to reach saturating conditions, it is important to consider that the size of the genome of the model organism will determine the number of plants that are to be screened to find relevant mutations.

The first step following the discovery of a mutant plant is to determine whether the altered phenotype results from a single point mutation. Crosses with a WT plant and the following of multiple plants across the first two generations is usually a straightforward way to assess this using Mendel's law of character segregation.

If multiple plants present a phenotype that is altered in a similar way, it is necessary to resolve the number of altered loci leading to the observed trait. The establishment of complementation groups is commonly performed by crossing the different mutants with one another: if the two mutations responsible for the phenotype observed concern the same locus, then the offspring will present a similar phenotype. If not, the WT copy of each gene will complement the mutated copy brought by the other parent.

The greatest improvement in Mutant screen experiments came from the development of next generation sequencing technologies which allowed a quick retrieval of the mutated sequence via the creation of genome databases and the ability to quickly sequence mutant genomes. This gave rise to new mapping technologies such as bulk segregant analyses (BSA) which helped localising the mutations following random mutagenesis (Huo et al., 2016).

Although, mutant screens appear as tedious, they have consistently proven their relevance in the discovery of new genes involved in specific biological process (Huo et al., 2016; Koornneef & Van Der Veen, 1980; Niisslein-Volhard et al., 1984)

6.1.2 Mutant screen in *Hibiscus trionum*

Since *Hibiscus trionum* is a new model, its number of genes and the number of mutations induced by EMS treatment cannot be predicted yet. The genome size of *H. trionum* (1.9 Gbp) is about twelve

times larger than that of *Arabidopsis thaliana* thus, potentially involves a larger number of coding genes. This suggests that a larger M1 number of plants is to be screened than in *A. thaliana* in order to alter the striation phenotype. It remains however difficult to establish the saturating conditions evoked in 6.1.1.

A mutant screen was therefore conducted in collaboration with Edwige Moyroud and May Yeo from the Sainsbury Laboratory of Cambridge University (SLCU). Ethylmethane sulfonate (EMS) was used to induce random replication mutations via guanine alkylation. Seeds were treated with EMS and a first generation of mutant plants was then obtained and allowed to self-pollinate. A second generation of plants was sown to reveal recessive mutations. Mutants presenting alteration of the striations were subsequently studied.

6.2 Material and methods

6.2.1 Random seed mutagenesis

Six hundred seeds were treated with 1.15% Ethylmethan sulfonate (EMS) in KPO4 100 mM for 16 hours to induce random mutagenesis. Seeds were then germinated by incubating them in 90°C water and let to cool down for 10 mn and then 2 days at 30°C in the dark on wet paper in petri dishes sealed with micropore® tape. M1 seedlings were then grown in soil under controlled conditions (see section 2.2.2). Plants were let to self-pollinate, and fruit were collected. Families of 15 seeds (M2 plants) per M1 plant were sown weekly in the same growth conditions as described above, in batches representing 15 M1 plants (15 families) per week. One flower per M2 mutant plant was screened with a Keyence® miscroscope for impairment of iridescence. Mutation frequency was recorded for the first 4600 M2 plants, corresponding to about 306 M1 plants. A visible mutant phenotype was recorded in 24 of these (about 8 %). Eleven more mutant phenotypes were thereafter identified during the continuation of the screening.

6.2.2 Microscopic observations

All microscopy pictures were obtained as described in section 2.2.4

6.2.3 Cell size measurement

Cell size was measured using ImageJ on transmitted light microscopy pictures obtained using a Keyence VHX microscope (see section 2.2.4). Cell length (parallel to the longitudinal axis of the petal) and cell width (perpendicular to the longitudinal axis of the petal) were measured as a proxy for cell size (fig. 6.7c). Cell length and width were measured independently for an average of 40 cells per petal and 3 petals were randomly selected per flower. A total of 220 striated cells and 240 smooth cells were measured across 2 flowers of the *blue* mutant, 281 striated cells and 360 smooth cells were measured across 3 flowers of the *mdl* mutant, and finally 360 striated cells were measured across another 3 flowers of the WT *Hibiscus trionum*.

6.2.4 Cuticle thickness measurement

Measurements were performed on petal cross sections of wild type *Hibiscus trionum* and *blue* and *madeleine* mutant lines using ImageJ. Cross sections were performed as detailed in section 2.2.4. Both the thickness of the cuticle proper and of the entire extracellular matrix (ECM) composed of cuticularised and non-cuticularized cell wall were measured. For each cell, about 8 measurements were taken along the cuticle proper. Regarding striated cells, one measure per fold was taken when possible and the measures for the top and the bottom of each fold were analysed separately. Regarding smooth cells a minimum of 5 measurements were taken along each cell. In both cell types the cell junction region was avoided and the shortest distance between the top and the bottom of the ECM was taken. Cuticle proper was assessed in 20 WT striated cells, 14 striated cells and 18 smooth cells of the *blue* mutant line and 12 striated and 2 smooth cells of the *madeleine* mutant line. ECM was assessed in 21 WT striated cells, 12 striated and 17 smooth cells of the *blue* mutant line and 11 striated and 3 smooth cells of the *madeleine* mutant line.

6.2.5 Plant crosses

Hibiscus trionum flowers are hermaphrodite and capable of self-fertilization. Flowers remain open for approximately two hours and shortly after their opening self-fertilization occurs through the curling of the style towards the anthers, resulting in close contact between the pollen and the stigma. Crosses were performed soon after the flower opening, and stigmas were inspected for endogenous

pollen. When no event of self-pollination was detected, the stigmas were manually covered with exogenous pollen thus preventing self-pollination.

Several crosses were performed using WT pollen and *mdl* (line 325) flowers. Eight resulting F1 seeds were then sown and the floral phenotype of mature F1 plants was assessed through optical microscopy using transmitted light. Plants were then allowed to self-pollinate and the F2 seeds of two F1 plants were sown for phenotype screening. Floral phenotype was assessed under the Keyence VHX microscope using transmitted light.

The detection of "madeleine" shaped cells was not possible in heterozygous individuals due to the overall dominance of the striations. The abnormal scattering of the vacuolar pigments in *madeleine* homozygous mutants was however visible in heterozygous mutants when observed with transmitted light and thus used for the identification of the heterozygous individuals.

6.2.6 Statistics

For statistical comparison of cuticle and extra cellular matrix thickness, and cell size, normal distribution and homoscedasticity were assessed using a Shapiro-Wilkinson and an F-test respectively. In case of normal distribution and variance equality a t-test was used. In any other case, a non-parametric test of Wilcoxon was preferred. For statistical comparison of phenotype frequency in the F2 generation described in section 5.3.6 a χ^2 test with 2 degrees of freedom was used. All the statistical tests were performed using R.

6.3 Results

6.3.1 EMS treatment successfully resulted in alterations of the flower development in *H. trionum*

Alteration of flower development was recorded in 35 M1 lines (table 6.1). On several occasions it was noticed that the transition between colour, cell shape and texture along the petal was not following the same order. In some mutants presenting a 'fuzzy border' phenotype the striated flat cell domain was larger than the purple domain, giving a blurry impression (fig. 6.2b). In some others, the conical cell domain overlapped with the pigmented region and translated into the presence of purple 'semi-conical' cells (fig. 6.2e). Various pigmentation intensities and hues were also observed in the proximal region

of the flower of several mutants (table 6.1 number 32, 141 and 206 and fig. 6.2g and h) and an abnormal number of petals was also encountered in one mutant line (table 6.1 number 402 and fig. 6.2i).

M1 plant line	Phenotype
15	Larger bull's eye pattern
20	Small flowers
23	Highly branched plant with a smaller white part of the petals
37	Paler bull's eye pattern
39	Discolouration at the basis of the ovary
57	Smaller bull's eye pattern
59	Blue mutant with patchy striations / pink stigma with pink stripes on the white region
80	Ectopic striations along the petal veins
82	Smaller white region
140	Abnormal white/purple ratio with small flowers
141	Red hues in the flower / Small plant with irregular petal shape / sterile plant with small flowers
146	Hybrid half sepal and half petal organs / change of hue in the bull's eye pattern
147	Change of hue in the bull's eye pattern
152	Abnormal white vs purple ratio
160	Sterile plant / pale purple region
163	Hybrid half sepal half petal organs
168	Sharp transition between conical and flat epidermal cells and small flowers
179	Abnormal white vs purple ratio
190	Serrated petal edges
191	Ectopic conical cells in the striated domain
206	Pale purple domain/ blurry boarder
219	Inconsistent petal orientation
244	Narrowing of petals near their base
247	Ectopic conical cells in the striated domain
251	Inconsistent petal orientation
267	Hybrid half sepal and half petal organs
274	Very open flowers
310	Stamen development altered
325	Ectopic conical cells in the striated domain
402	Abnormal number of petals
408	Thicker petal on the white part
426	White base of the stigma
440	Striated cells overlapping the white-purple transition
592	Might have lost blue hues in the proximal region of the flower
606	Small flowers

Table 6.1: List of 35 M1 presenting an alteration of flower development. '/' indicates that the phenotypes described were found in different M2 plants for the same M1 line

The striation pattern was significantly altered in 4 mutant lines by the presence of patches of smooth cells. Of them, 3 lines displayed a similar phenotype resulting from the abnormal presence of 'madeleine' shaped cells in the proximal region of the petals and were thus named *madeleine* (*mdl)* mutants (lines 325, 247 and 191 see table 6.1 and fig. 6.3). One line displayed an abnormally blue coloration of the proximal region and was named the *blue* mutant (table 6.1 number 59). A minimum

of thre crosses were performed for each crossing combination between the three *madeleine* mutants. The observation of the proximal adaxial epidermis of the petal did not show any complementation of the mutant phenotype (persistence of altered striations and 'madeleine' shaped cells), indicating that they belong to the same complementation group (fig. 6.3)., The [*mdl*] phenotype can thus be attributed to the mutation of the same locus in the 3 *madeleine* lines. Further characterisation of the [*mdl*] mutant phenotype was performed on the 325 mutant line (hereafter simply referred to as '*mdl* mutant'). As for the *blue* mutant, no other plant presenting a similar phenotype was identified, making of it a unique mutant in this mutant screening.

In order to unravel the phenomenon responsible for the alteration of the striation pattern in the *blue* and *madeleine* mutants, optical microscopy and scanning electron microscopy were used to assess more precisely the alteration of the striations, and multiple cross-sections enabled us to assess the state of the cuticle and the epidermis. Furthermore, according to the model developed by Kourounioti, the buckling of cuticle is the result of 2 mathematical parameters: $\lambda_{1/2}$ and β corresponding to the two-dimensional constraints and the deposition rate of cuticle during development, respectively (Kourounioti et al., 2013). In order to assess whether these parameters were altered in the *blue* and the *madeleine* mutants, I measured the size of striated and non-striated cells and their respective cuticle thickness.

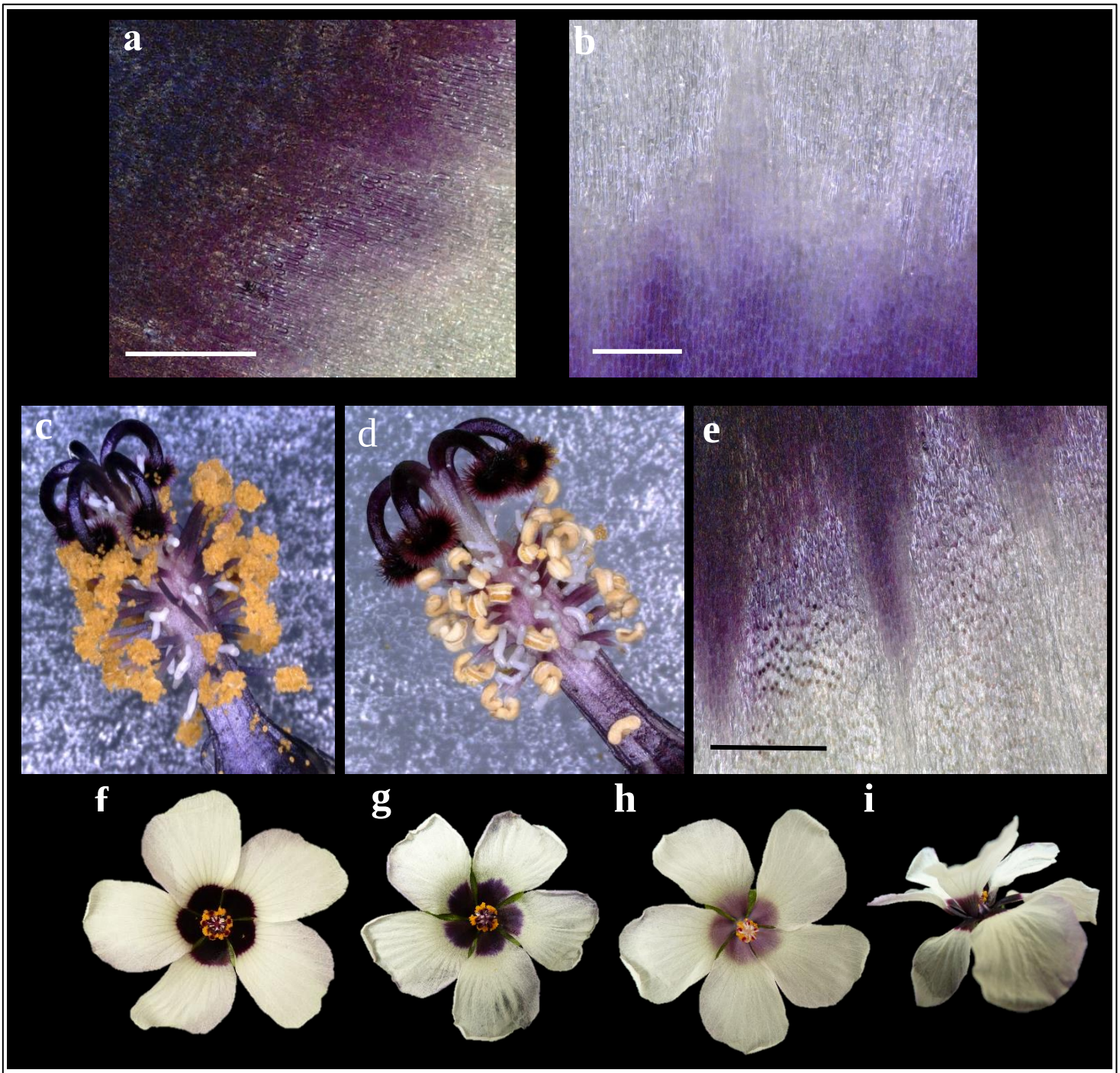

Figure 6.2: Pictures of several mutant phenotypes identified in the mutant screen. (**a**, **b** and **e)** Optical microscopy of the border region between purple and white petal parts. Scale bar = 500 µm. (**a)** Wild-type border. (**b)** Striation boundary surpasses pigmentation boundary. (**e**) Early transition from flat to conical cells and abnormal location of the anthocyanin to one side of the cell. (**c)** Wild-type anthers. (**d)** Non-dehiscent anthers. (**f-i)** WT and mutant flowers of *Hibiscus trionum*. (**f)** Wild-type flower. (**g)** Mildly decreased pigmentation in the central region. (**h)** Strongly decreased pigmentation in the central region. (**i)** Abnormal number of petals. Images by May Yeo.

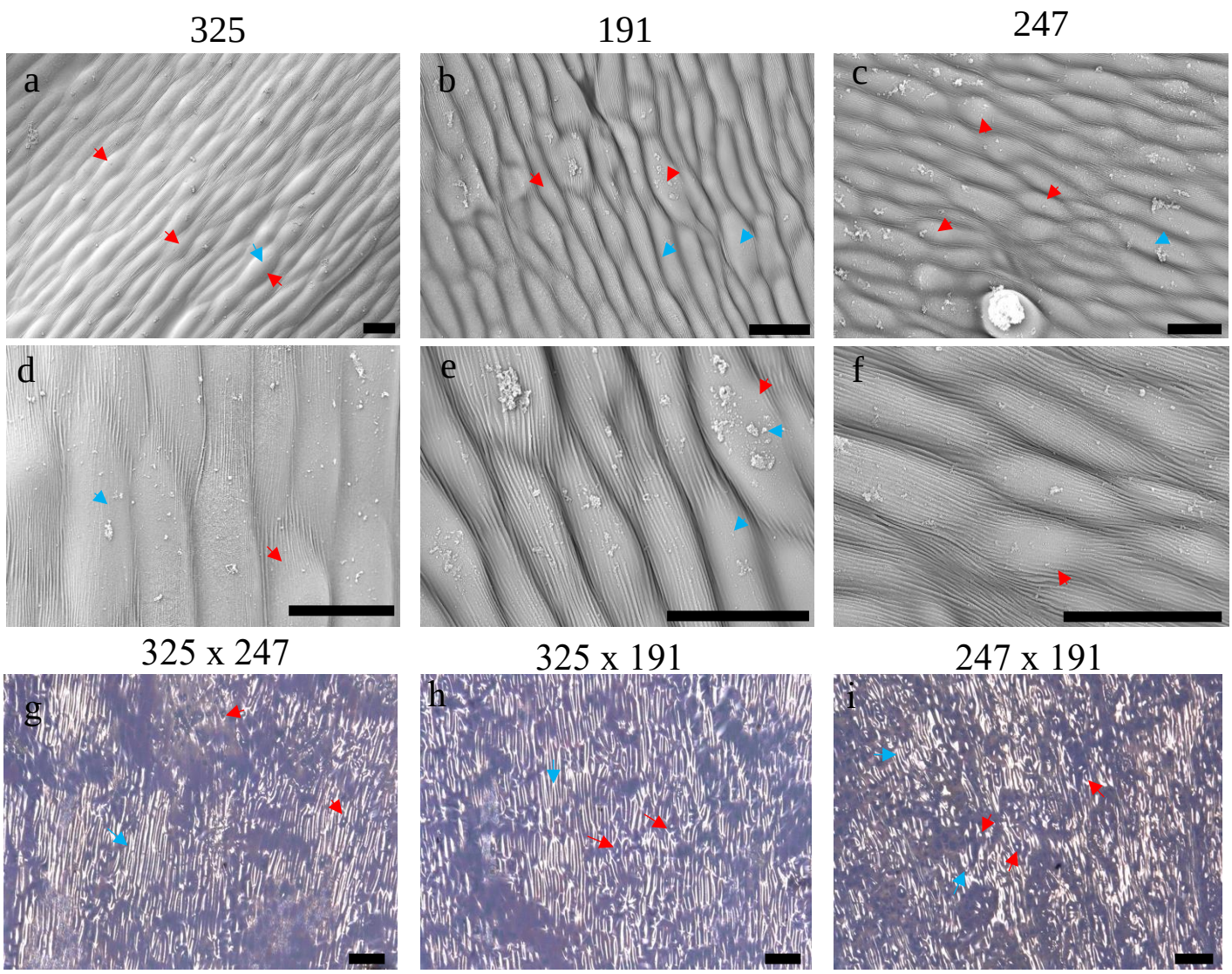

Figure 6.3: Microscopy pictures of the three *mdl* mutant lines and their crossings. (**a**-**f**) Electron microscopy of the adaxial proximal petal epidermis. (**a** and **d**) *mdl* mutant line 325. (**b** and **e**) *mdl* mutant line 191. (**c** and **f**) *mdl* mutant line 247. Scale bar = 40 µm. (**g**-**i**) Optical microscopy pictures. (**g**) 325 X 247 crossing. (**h**) 325 X 191 crossing. (**i**) 247 X 191 crossing. Scale bar = 100 µm. Red arrows pointing at canonical 'madeleine' shaped cells and blue arrows pointing at non-striated cells.

6.3.2 Both the *madeleine* and the *blue* mutants presented a complex phenotype and an altered striation pattern

The general aspect of both *madeleine* and *blue* mutant plants remained very similar to the WT plants. They could only be distinguished when focusing on the different flower organs and fruit. The *mdl* mutant displays a lighter, less vivid hue of purple on the petal and the blue mutant shows a vivid colour visibly shifted towards the blue spectrum. Both do not display any iridescence to the naked eye, in contrast to the WT (fig. 6.4 a-i). Furthermore, the anthers of *blue* mutant are not dehiscent and do not seem to be able to produce viable pollen, suggesting male sterility (fig. 6.4i). Numerous crossing attempts with WT pollen were made yet none of them resulted in the production of viable seeds (fig.

6.4l and m), suggesting both male and female sterility for the *blue* mutant. As a consequence, the *blue* mutant produced flowers abundantly across a larger period of time than the WT and the *madeleine*

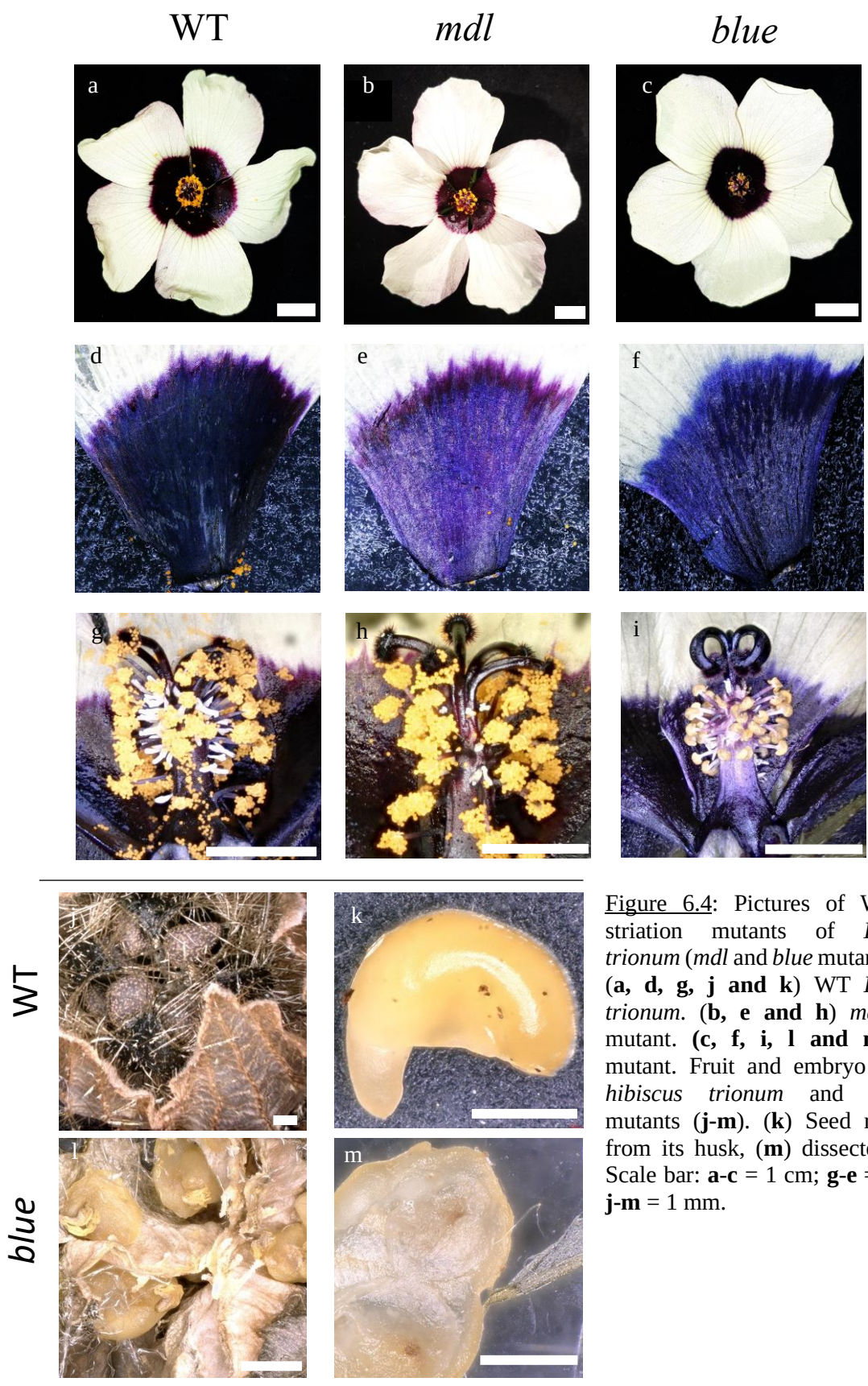

Figure 6.4: Pictures of WT and striation mutants of *Hibiscus trionum* (*mdl* and *blue* mutant lines). (**a, d, g, j and k**) WT *Hibiscus trionum*. (**b, e and h**) *madeleine* mutant. **(c, f, i, l and m)** *blue* mutant. Fruit and embryo of WT *hibiscus trionum* and striation mutants (**j-m**). (**k**) Seed removed from its husk, (**m**) dissected seed. Scale bar: **a-c** = 1 cm; **g-e** = 5 mm; **j-m** = 1 mm.

mutant and was successfully propagated by cutting.

6.3.3 Patchy striations in the *blue* and the *madeleine* mutants

Observations at higher magnification under an optical microscope revealed the presence of patches of smooth and striated cuticle in the proximal region of the petal in both the *madeleine* and the *blue* mutants (fig. 6.5b and c). The *madeleine* mutant also displayed misshaped cells that were neither entirely conical nor entirely flat, reminiscent of the shape of a madeleine cake (figure 6.5b and j). Observation with transmitted light showed anthocyanin aggregates in the vacuole of most cells of the *madeleine* mutant in the proximal region of the petal, regardless of their shape (red arrows in fig. 6.5e). In the *blue* mutant, transmitted light revealed the presence of 'collapsed' cells in which the vacuole, cytoplasm and cell wall could not be distinguished, which is characteristic of necrotic cell death (van Doorn et al., 2011). Both the occurrence of 'madeleine' shaped cells and collapsed cells could not be directly linked to the presence of smooth patches of cuticle in the respective mutant lines. These elements may however be the indirect cause for perturbation of the buckling mechanisms at a larger scale. Scanning electron microscopy also revealed a lower degree of ordering of the ridges in striated regions of the petal cuticle in both mutants, with an irregular thickness and height of the upper part of the ridges (fig. 6.5h and i). Cross sections also revealed irregularities in the thickness of the cuticle in both mutants (fig. 6.6) as well as the presence of collapsed epidermal cells in the *blue* mutant (fig. 6.6c), similar to the ones observed with transmitted light (fig. 6.5f).

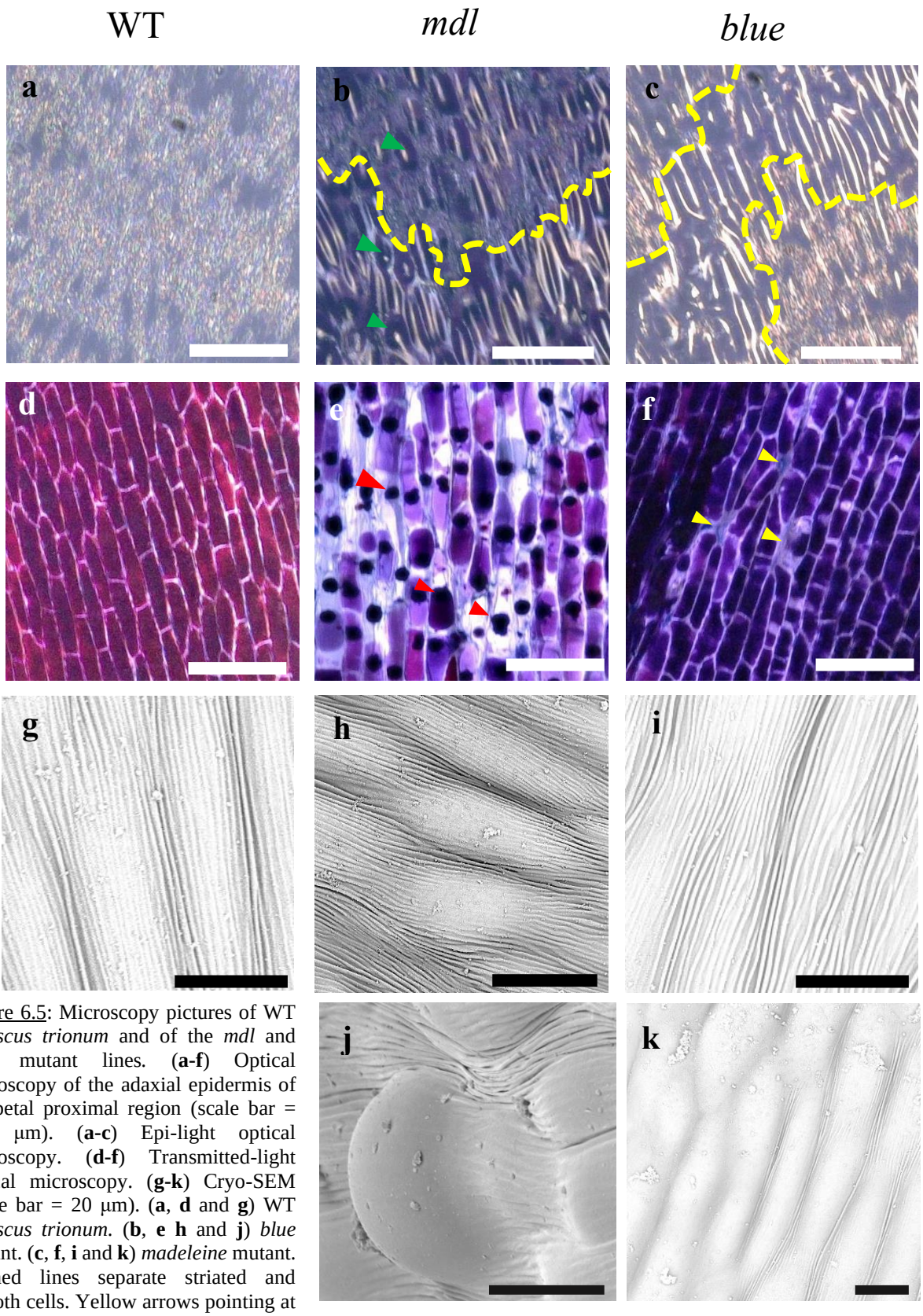

Figure 6.5: Microscopy pictures of WT *Hibiscus trionum* and of the *mdl* and *blue* mutant lines. (**a-f**) Optical microscopy of the adaxial epidermis of the petal proximal region (scale bar = 100 µm). (**a-c**) Epi-light optical microscopy. (**d-f**) Transmitted-light optical microscopy. (**g-k**) Cryo-SEM (scale bar = 20 µm). (**a**, **d** and **g**) WT *Hibiscus trionum*. (**b**, **e** **h** and **j**) *blue* mutant. (**c**, **f**, **i** and **k**) *madeleine* mutant. Dashed lines separate striated and smooth cells. Yellow arrows pointing at 'collapsed' cells. Red arrows pointing at pigment aggregates, green arrows pointing at 'madeleine' shaped cells.

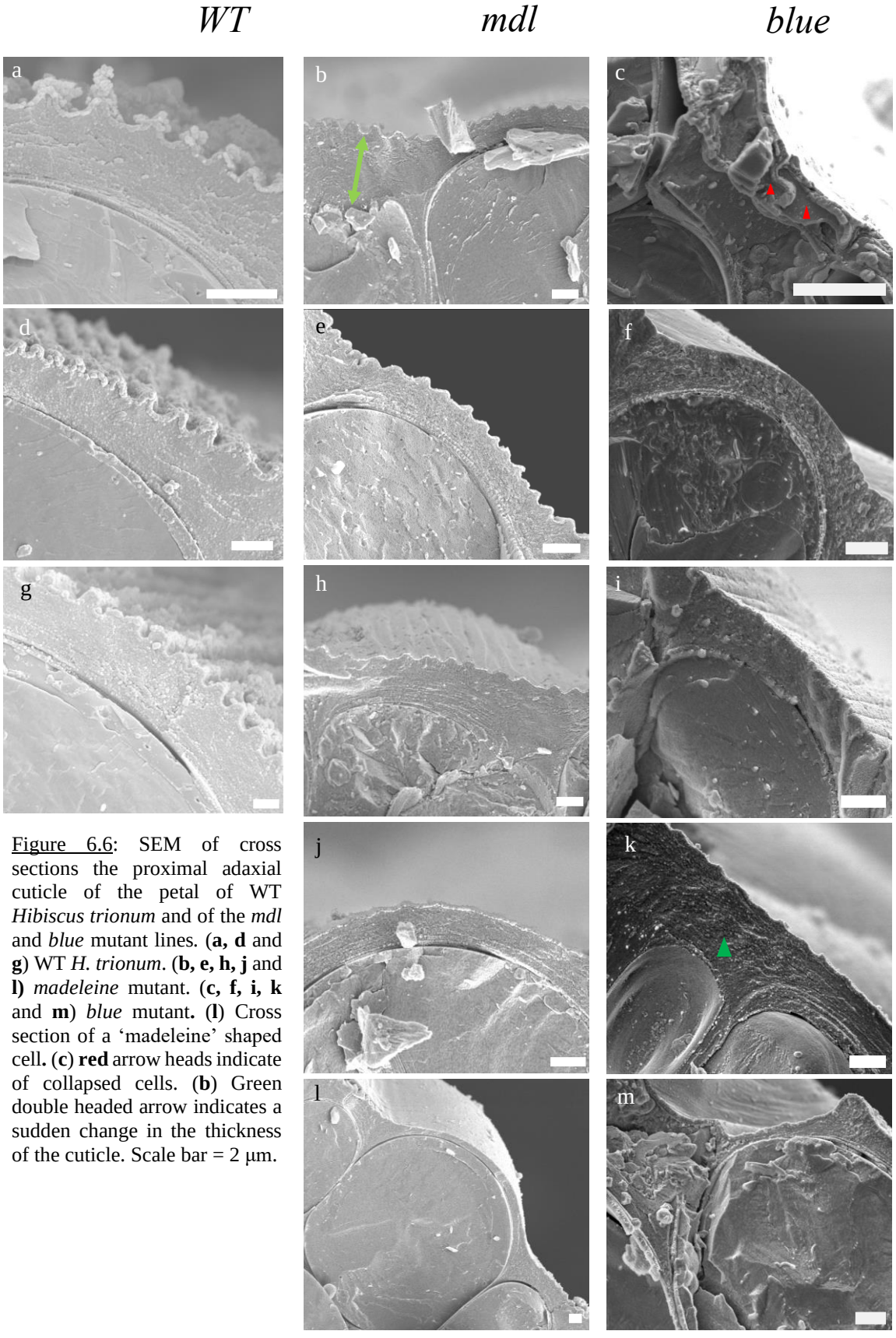

Figure 6.6: SEM of cross sections the proximal adaxial cuticle of the petal of WT *Hibiscus trionum* and of the *mdl* and *blue* mutant lines. (**a, d** and **g**) WT *H. trionum*. (**b, e, h, j** and **l)** *madeleine* mutant. (**c, f, i, k** and **m**) *blue* mutant**.** (**l**) Cross section of a 'madeleine' shaped cell**.** (**c**) **red** arrow heads indicate of collapsed cells. (**b**) Green double headed arrow indicates a sudden change in the thickness of the cuticle. Scale bar = 2 µm.

6.3.4 Cell size appeared similar in the striated and smooth cells of the *blue* and the *madeleine* mutants when compared to WT striated cells

The presence of patches of smooth cuticle might result from a perturbation of the global constraints of the tissue. According to the model predicting the formation of striations on cuticle (see fig. 1.4) (Kourounioti et al., 2013), the buckling of the cuticle depends on λ_1 and λ_2 which correspond to the stretches parallel and perpendicular to the long axis of the elongated epidermal cells, respectively. These parameters are a function of the size of the cells at developmental stage 5, therefore, I investigated whether cell size is different between smooth patches and striated patches at this stage.

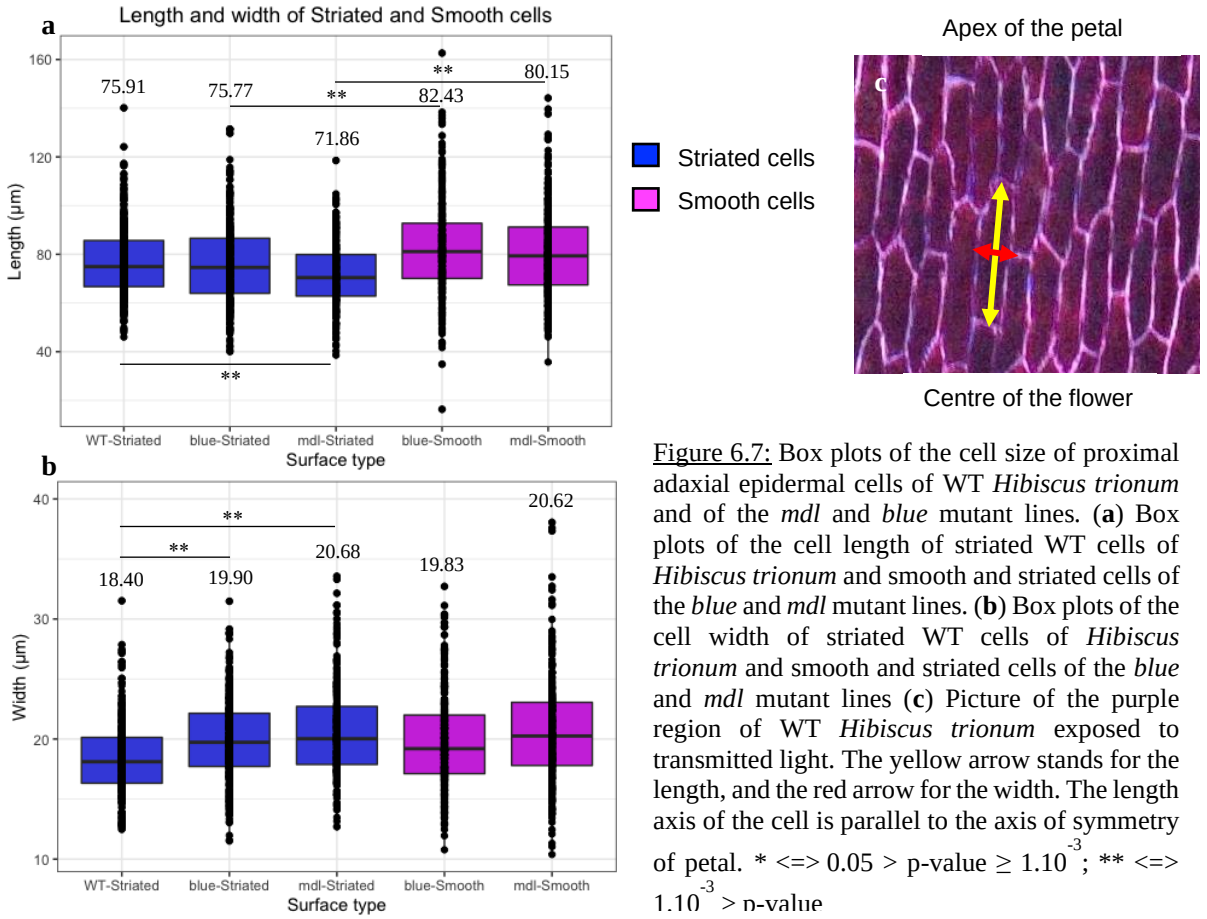

Figure 6.7: Box plots of the cell size of proximal adaxial epidermal cells of WT *Hibiscus trionum* and of the *mdl* and *blue* mutant lines. (**a**) Box plots of the cell length of striated WT cells of *Hibiscus trionum* and smooth and striated cells of the *blue* and *mdl* mutant lines. (**b**) Box plots of the cell width of striated WT cells of *Hibiscus trionum* and smooth and striated cells of the *blue* and *mdl* mutant lines (**c**) Picture of the purple region of WT *Hibiscus trionum* exposed to transmitted light. The yellow arrow stands for the length, and the red arrow for the width. The length axis of the cell is parallel to the axis of symmetry of petal. * <=> 0.05 > p-value ≥ 1.10^{-3}; ** <=> 1.10^{-3} > p-value

On average, cells are shorter in length in striated patches than in smooth patches in both the *madeleine* and the *blue* mutants by about 8% (40.15 µm against 71.86 µm) and 11% (82.43 µm against 75.77 µm) (fig. 6.7a). Thus, we can infer that the λ_1 parameter is partially altered in both mutant lines. However, with a width of 20.62 µm for *mdl* striated cells against 20.68 µm for striated *mdl* cells and 19.83 µm for *blue* smooth cells against 19.90 µm in *blue* striated cells, no statistically relevant differences were recorded between striated and smooth cells in either mutant line (fig. 6.7b).

Interestingly, the width of striated cells in both the *blue* and the *madeleine* mutants is statistically larger than that of striated cells in WT plants (18.4 μm) suggesting that the λ_2 constraint could well be altered as well in both mutant lines. Thus, smooth cells seem to display an overall larger surface than striated cells.

The model developed by Kourounioti et al (2013) (see fig. 1.4), suggests that an increase of the λ_1 parameter does not alter the buckling of the cuticle and is consistent with the maintenance of the striations. Furthermore, the observed increase in the λ_2 parameter has been predicted to induce the formation of disordered striations, which have not been observed in these 2 mutant lines. This suggests that other factors are responsible for the observed loss of striations in the *mdl* and the *blue* mutant.

6.3.5 The thickness of the cuticle proper in the smooth cells of the *blue* mutant are significantly smaller than in the striated cells of the *blue* mutant and WT lines

Once again, according to the previously established model predicting the formation of striations, another parameter that might explain the partial loss of striation is the β parameter. This translates into the cuticle deposition rate (Kourounioti et al., 2013). An approximation of this parameter is the thickness of the cuticle at stage 5. Cross sections of the petals of WT *Hibiscus trionum* as well as the *blue* and *madeleine* mutant lines were performed on the proximal region of the petals and observed under scanning electron microscopy. Various types of cuticle measurements were then performed.

The cuticle can be defined as an ensemble of several layers (see fig. 1.6 and 5.1). The outermost layer is referred to as the cuticle proper and is usually structurally and chemically different from the rest of the cuticle, making it distinguishable in cryo-SEM and with various dyes (Nadiminti et al., 2015). This layer rarely exceeds 300 nm in *Hibiscus trionum.* Below the cuticle proper two larger layers of cuticularized cell-wall and non-cuticularized cell-wall can be found. Their structure remains unclear, and the scanning electron microscopy techniques used here for measurements did not allow us to distinguish them from one another. Hence, in this work the term Extra Cellular Matrix (ECM) refers to both layers without distinction.

A difference in thickness in the cuticle proper and the ECM thickness between the smooth and striated patches found on the *blue* and the *madeleine* mutant could potentially explain a differential capacity for the cuticle to buckle.

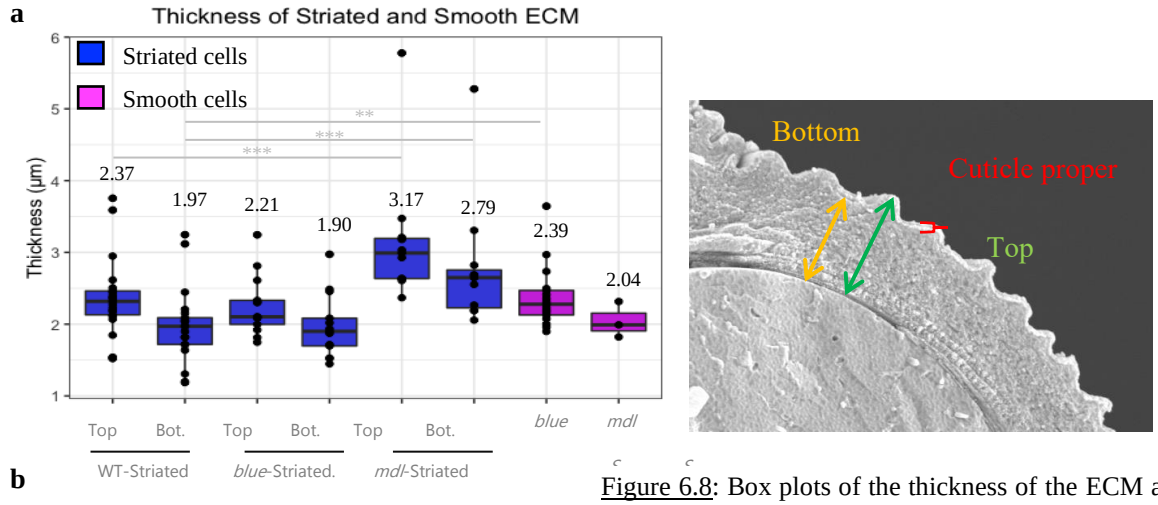

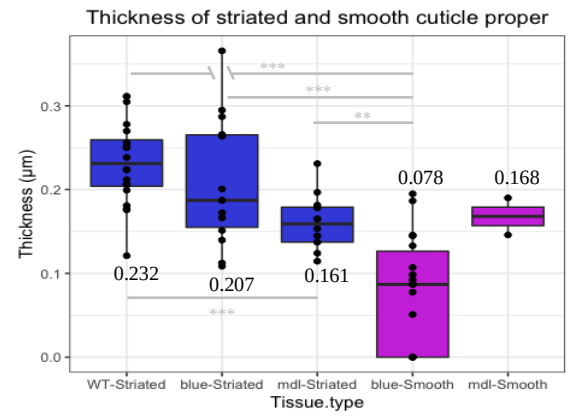

Figure 6.8: Box plots of the thickness of the ECM and cuticle proper of adaxial proximal petal cells of WT *Hibiscus trionum* and of the *mdl* and the *blue* mutant lines. (**a**) Box plot of the extra cellular matrix (ECM) thickness. 'Top' and 'Bottom' describing the type of measure performed on cross sections of striated cell (see image c). **(b)** Box plot of the thickness of the cuticle proper. **(c)** Scanning electron microscopy picture of a WT striated cells illustrating the different measures performed: orange double arrow represents a 'Bottom' measure of the ECM, green double arrow a 'Top' measure and the red element frames the cuticle proper. * ⇔ $0.05 \geq$ p-value $> 1.10^{-3}$; ** ⇔ $1.10^{-3} \geq$ p-value $> 1.10^{-4}$; *** ⇔ $1.10^{-4} >$ p-value

Remarkably, striated cells (from both mutants and WT *H. trionum*) display a variety of ECM thickness spanning from about 0.5 up to 6 µm in extreme cases, suggesting that the thickness of this layer plays little role in the development of striations. Furthermore, smooth cells in both the *madeleine* and the *blue* mutant lines display ECM thickness between 1.75 and 3.75 µm which is within the array of values observed in striated cells (fig. 6.8a). This suggests that the absence of striations observed in the two mutant lines is not caused by an alteration of the extracellular matrix thickness.

Measurements of the cuticle proper revealed significant differences between smooth and striated cuticles. Indeed, in the striated cells of WT *H. trionum* as well as the *mdl* and the *blue* mutant lines, the cuticle proper is consistently more than 100 nm thick, whereas in smooth cells of the 2 mutant lines, cuticles thinner than 100 nm were measured in more than 50% of the cells, and no cuticle could be observed in one third of the cells (fig. 6.8b). This suggests a potential correlation between thin or absent

cuticle and the lack of cuticular striations. However, the sample size for the smooth cells of the *mdl* mutant did not allow for statistical comparison, hence, more measurements would be needed for a proper characterisation of the thickness of its cuticle proper.

In order to assess the genetic basis underlying the [*mdl*] phenotype, I proceeded to several crosses and investigated whether the frequencies of phenotype observed in the offspring were consistent with Mendel's laws of genetics.

6.3.6 The *madeleine* phenotype is the result of a single locus mutation

Since the *blue* mutant displayed both male and female sterility, I was not able to assess character segregation across generations, hence, it could not be determined whether the *blue* phenotype results from the alteration of a single locus.

However, the *madeleine* mutant displays a normal capacity to self and cross pollinate. Four independent crosses were made with WT pollen, producing an F1 generation. Eight F1 plants were grown, and their phenotype was assessed. Optical microscopic observation using epi-light revealed an apparent dominance of the WT phenotype: the buckling capacity appeared restored (fig. 6.9a, b and c) and fewer 'madeleine' shaped cells were detected. Although the presence of a few conical cells can be inferred (red arrowheads in fig. 6.9b) this trait is not reliable for the identification of potential heterozygotes. Microscopic observations using transmitted light revealed patches of cells with an abnormal pigmentation, typical of the *mdl* mutants (fig. 6.5e). The presence of these two traits in F1 plants (fig. 6.9e and f) is consistent with a partial restoration of the mutated phenotype by a single WT copy of the mutated gene.

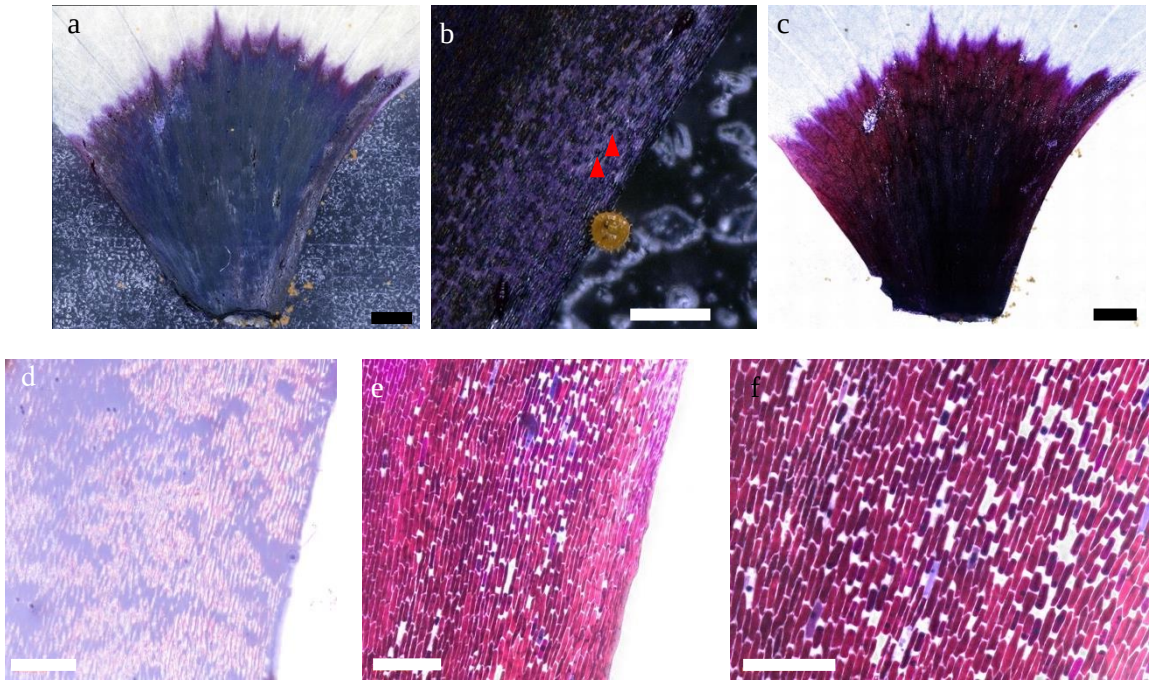

g

Observed phenotype proportions		
[WT]	[*mdl*]	[Heterozygote]
34/121 (28%)	38/121 (31%)	49/121 (41%)

h

Theoretical genotype frequencies in a case of single locus governed trait		
Male gamete\ Female gamete	mdl^{mdl}	mdl^{WT}
mdl^{mdl}	mdl^{mdl} / mdl^{mdl} (25%)	mdl^{mdl} / mdl^{WT} (25%)
mdl^{WT}	mdl^{mdl} / mdl^{WT} (25%)	mdl^{WT} / mdl^{WT} (25%)
Theoretical phenotype frequencies		
[WT]	[*mdl*]	[Heterozygote]
25% (30.25/121)	25% (30.25/121)	50 % (60.5/121)
$\chi^2_{df=2}$=4.63		

Figure 6.8: Optical microscopy pictures of an *mdl* mutant crossed with a WT *Hibiscus trionum* (F1) and phenotype frequencies of an F2 generation. **(a-f)** Flower from a cross between an *mdl* mutant and a WT *H. trionum*. **(a, b** and **d)** Microscopy picture exposed to epi-light. **(c, e** and **f)** Microscopy pictures exposed to transmitted light. (**a** and **c**) Scale bar = 1 mm. (**b**, **d**, **e** and **f**) Scale Bar = 200 µm. Red arrowheads pointing at conical cells. (**g**)Table showing the phenotype frequencies of the various phenotypes observed in the F2 plants resulting from the self-pollination of F1 plants. This comprises WT phenotype: [WT], *madeleine* phenotype: [*mdl*], and the intermediate phenotype: [Heterozygote]. (**h**)Table showing the theoretical frequency of the various genotypes that are observed in the case of a single locus governed character. mdl^{mdl} stands for the mutated copy of the *mdl* gene; mdl^{WT} stands for the WT version of the *mdl* gene. A Chi-square test (χ^2) was performed to test the segregation hypothesis of the [mdl] phenotype: $\chi^2_{df=2} = 4.63$ ⇔ probability of observation > 5%: the H_0 hypothesis cannot be rejected, hence, the observed distribution of the [*mdl*] phenotype is consistent with a single locus governed trait.

An F2 generation was obtained after self-fertilization of two F1 individuals, and the frequency of homozygote and heterozygote phenotypes was assessed across 121 F2 plants (fig. 6.9g). Out of the 121 plants that were screened under a microscope using transmitted light, 38 yielded an [*mdl*] phenotype, 34 a [WT] phenotype and 49 a [Heterozygote] phenotype thus representing a phenotype frequency of 31, 28 and 41 per cent, respectively. In order to assess whether the frequencies observed were conforming with Mendel's law of character inheritance (in this case: ¼ [*mdl*], ¼ [WT] and ½ [heterozygote]), a $\chi^2_{df=2}$ score was calculated using the following theoretical frequencies: ¼ [*mdl*] ⇔ 30.25/121, ¼ [WT] ⇔ 30.25/121 and ½ [heterozygote] ⇔ 60.5/121. A $\chi^2_{df=2}$ score of 4.63 was found, which corresponds to a p-value superior to 0.05 and inferior to 0.1 ($\chi^2_{df=2} = 4.63$ ⇔ p-value > 0.05). Therefore, the frequencies observed for each phenotype are statistically close enough to the theoretical frequencies predicted by Mendel's law to infer that the [*mdl*] phenotype is governed by a single locus.

6.4 Discussion

With this study I have shown proof of a successful random mutagenesis induced by EMS treatment resulting in the production of numerous mutant lines presenting abnormalities of their flower organs in the non-model species *Hibiscus trionum.* Four mutant lines presented an alteration of the striation pattern, categorised into 2 complementation groups: the *mdl* mutants and the *blue* mutant. Although both mutants displayed an alteration of the production of structurally coloured cuticle at the proximal adaxial region of their petals, they also showed specific traits of their own. The *blue* mutant line is also characterised by an anthocyanin coloration shifted towards blue hues, the presence of collapsed cells in the proximal region of the petals and a complete sterility (both male and female gametes being affected), whereas the *madeleine* mutant displays a normal coloration of the proximal region and capacity to cross and self-pollinate as well as the presence of ectopic madeleine shaped cells on the proximal adaxial part of the petals. In order to investigate the partial loss of striations further microscopy observations and measurements were performed. A strong alteration of the production of cuticle or the 2 dimensional constraints necessary for the buckling of the cuticle might explain a partial loss of striations on the cuticle (Kourounioti et al., 2013b). The cell size measurements performed on striated and smooth cells of the *madeleine* and the *blue* mutants show that the cells are slightly longer in smooth patches which is consistent with an increase of the longitudinal constraint, (λ_1), yet, according

to Kourounioti et al (2013), an augmentation of the constraints is consistent with the maintenance of the striations. Hence this difference cannot explain the alteration of the striation pattern we observed.

A closer look at the cuticle reveals that smooth and striated cells display similar thicknesses of the extra cellular matrix in both mutant lines, showing that the thickness of this layer, which acts as a substrate to the cuticle proper, does not influence the buckling capacity of the cuticle. Measurements of the cuticle proper, however, revealed that this layer is overall thinner in smooth epidermides. Even if this does not constitute an absolute criterion (some smooth cells displaying a cuticle thickness within normal range), this might explain a loss of striations in some cases.

Furthermore, in both mutants, no strict co-localisation was observed between the presence of 'madeleine' shaped cells or 'collapsed' cells, and the presence of patches of smooth cells, suggesting that the presence of these two types of abnormal cells could interfere with the global dynamics of buckling at the scale of the petal. Indeed, in the *madeleine* mutant the presence of 'madeleine' shaped cells might allow for the accommodation of the cuticle load by increasing the overall epidermal surface. This would be consistent with a decrease of the β parameter evoked in the work of Kourounioti et al. (2013) and an alteration of the buckling capacity. Furthermore, in *mdl* heterozygote plants, a restoration of the striations is consistent with the presence of fewer 'madeleine' shaped cells. In the *blue* mutant, the regular presence of 'collapsed' cells might also alter the ratio of cuticle and epidermal surface thus diminishing the buckling capacity of the cuticle.

The structure of the cuticle is also an important factor for buckling: A bilayer system composed of a thin rigid layer topping a softer and larger layer is required in some models to buckle (Bowden et al., 1998). Hence, a change in the structure of the substrate could alter its mechanical properties, including its stiffness. Despite numerous electron microscopy observations of cryo-fractured petals, we failed to observe any difference in the structure of the extracellular matrix (substrate layer) between smooth and striated patches.

This could be investigated further using transmission electron microscopy coupled with immuno-chemical staining (Fernández et al., 2016) such as enzyme-gold (Guzmán et al., 2014) and immuno-gold labelling (Kwiatkowska et al., 2014) which can help differentiate the cutin network from the

polysaccharide network. The stiffness of both the cuticle proper and the extracellular matrix could be assessed directly using atomic force microscopy. The use of liquid extraction surface analyses coupled with mass spectrometry may also provide valuable information regarding the chemical composition of abnormally smooth cuticle.

The mutation responsible for the *madeleine* phenotype caused an alteration of the buckling properties of the petal cuticle; however, it remains hazardous to conclude that this is directly due to alteration in the regulation of the cuticle production. The presence of ectopic pseudo-conical cells in the proximal region of the petal suggests a defect in the over-all petal patterning that translates into a shift of the border separating conical cells from flat cells. This, suggests that the *madeleine* mutation concerns a morphogen.

Furthermore, the crossing results obtained suggest that a single gene is involved in the *madeleine* phenotype and the intermediate phenotype observed in the heterozygote individuals is consistent with a dose dependant phenotype; A single functional copy of the *mdl* gene appears as insufficient to fully restore the [WT] phenotype. However, the loss of striations is most likely a consequence of the production of misshaped cells, thus the *madeleine* gene would not be involved in the control of striation productions directly. Identification of the mutated locus may be achieved in the future via bulk segregant analysis by the team of Dr Edwige Moyroud at SLCU.

In the *blue* mutant, on top of a loss of striations, three apparently unrelated traits are altered: a change of anthocyanin coloration for bluer hues, the presence of ‘collapsed’ cells and the male and female sterility. The first one suggests a defect in the anthocyanin biosynthesis pathway, however, the abnormal presence of necrotic cells in the petal epidermis suggests a different type of locus has been altered. Finally, male and female sterility is characteristic of an alteration of the regulation of meiosis. At this stage it is difficult to pinpoint the kind of mutation that might affect such a diverse range of biological processes. Unfortunately, the sterility of the *blue* mutant prevents us from determining whether one or more mutated genes are involved.

6.5 Conclusion

Despite the lack of information regarding the mutations involved in the two phenotypes observed, this work suggests potential mechanisms by which the cuticle buckling may be regulated. Thus, cell shape appears important for the buckling in *Hibiscus trionum* petals, suggesting that a rather large surface of flat cells is necessary to generate consistent striation. This work also showed that the thickness of the cuticle proper is a determining parameter in the capacity of the cuticle to buckle.

Chapter 7: Structurally coloured cuticle shows a decrease in the gripping capacity of *Leptinotarsa decemlineata*

7.1 Introduction

7.1.1 Plant epidermis architecture

Plant epidermises serve a primary role in water insulation and in protection from external biotic and abiotic stresses. The cuticle usually provides a naturally hydrophobic surface thanks to the abundance of aliphatic acids and epicuticular waxes (which display a low molecular polarity) and the presence of insoluble compounds such as the cutin network (Yeats & Rose, 2013). Furthermore, it has been demonstrated that micro-patterns can increase the contact angle of a water droplet by inducing a Cassie-Baxter state, where the liquid is only in contact with the top part of the asperity and does not wet its bottom part, thus trapping air within the asperities of the surface and minimising contact surface with water (Rohrs, Azimi, & He, 2019). Anisotropic wettability was also observed in the presence of nano-scaled cuticular ridges in *Bellis perenis*, *Gazania rigens, Calendula officinalis* and *Chrysanthemum maximum* ray florets (Koch et al., 2013).

Furthermore, the cuticle usually tops epidermal cells displaying remarkable cell shapes such as conical cells or papillose cells which may take part in the modulation of the wetting properties of the epidermis. For example, conical cells were shown to modulate the wettability of petals independently from the nature of the cuticle in *Antirrhinum majus* (Whitney et al., 2011).

Thus, the physical properties of plant epidermal surfaces usually result from the chemical nature of the cuticle and hierarchical patterning of the epidermis (e.g. trichomes, cuticular grooves and cell shape) holding different properties and contributing together to the emergence of a new physical property (Darmanin & Guittard, 2015; Feng et al., 2002) as observed on the leaves of the sacred lotus, *Nelumbo nucifera* (also known as the lotus effect) which shows high hydrophobicity and self-cleaning properties thanks to the abundance of epicuticular wax crystalloids and papillose shaped cells (Barthlott et al., 2005; Barthlott & Neinhuis, 1997) and the petals of red roses which present conical cells topped

with nano-scaled cuticular ridges which displayed improved hydrophobic properties compared to conical cells only (Bhushan & Nosonovsky, 2010; Darmanin & Guittard, 2015).

Epidermal patterns relying on nano-scaled structures can also exhibit optical properties, as demonstrated in the flowers of *Hibiscus trionum* and *Paeonia mascula* (*Po. mascula*), which can increase the foraging efficiency of their pollinators (Moyroud et al., 2017; Vignolini et al., 2015). Larger structures such as conical cells on the adaxial petal surface of *Antirrhinum majus* were also shown to interact with light, enabling the production of more vivid hues of red (Gorton & Vogelmann, 1996).

Figure 7.1: Optical microscopy pictures of the feet of a female bumblebee (*Bombus terrestris*). **(a)** Rear leg. **(b)** Middle leg. (**c**) Front leg. Scale bar = 200 µm.

7.1.2 Insect adhesive features

Petal surfaces are usually a significant point of interaction between the plant and landing pollinators, leading to the development of specific structures. In addition to their optical properties, conical cells were also shown to provide extra grip to landing pollinators (Whitney et al., 2009). Pollinators such as *Bombus terrestris* display specific foot features such as claws (see fig. 7.1) which enable them to grip onto petal surfaces by the interlocking of their claws in-between the asperities of the surface, such as conical cells. It has been shown that claw-gripping can be achieved with asperities of a dimeter equal or larger to the tip of the claw, however, for smaller asperities, the claw is likely to slip. Claws can then provide certain gripping capacity depending on the scale of the asperity (Pattrick et al., 2018). The traction exerted on the claws as a result of the insect mass is also an important factor contributing to its gripping capacity: the heavier the insect, the stronger the interlocking forces need to be to provide a secured adhesion (Pattrick et al., 2018).

Thus, the gripping mediated by claws relies on the diameter of the claw-tip, the diameter of the asperity and the mass of the insect.

A large variety of insect feet exist and other foot features than claws have also been reported. Beetles such as *Leptinotarsa decemlineata* rely on the presence of adhesive pads on their three most terminal tarsi composed of setae or bristle-like chitinous hairs. These pads are also the point of secretion of a viscous liquid (Abou et al., 2010). The relative flexibility and resistance of the setae can help provide stronger contact interactions and increase friction forces resulting in an improved adhesion to the substrate. The secretion of fluids from theses pads may also help generate capillary forces resulting in a suction effect onto the substrate. Moreover, beetle secretions are often composed of n-alkanes, methyl-branched alkanes of about 25 to 33 carbon residues thus mimicking the non-polar nature of the cuticle surface and generating van der Waals adhesion forces (Gilet et al., 2018).

7.1.3 **Aims**

In this chapter I investigate the adhesive properties of nano-scaled ridges involved in the production of structural colours and their wettability.

Although a decrease in the gripping capacity of *L. decemlineata* was shown on striated PDMS replicas of *Hevea brasiliensis* (rubber tree) leaves when compared to glass or non-striated *H. brasiliensis* leaf replicas (Surapaneni et al., 2020), No gripping test has been done on structurally coloured cuticle. The size of the structurally coloured region of the *Hibiscus trionum* petal did not allow us to produce epoxy replicas of sufficient quality for our experiment. Therefore, I relied on *Paeonia mascula* which presents petal striations having an aspect ratio (ridge height/ridge spacing) of about 0.97 (against 0.283 for *H. brasiliensis* mature leaves (Surapaneni et al., 2020)), a ridge spacing of about 0.5 to 3.7 μm, a higher level of ridge ordering and displaying optical properties (Moyroud et al., 2017). As a control, I used *Papaver orientalis* (*Pr. orientalis*) petals, which present flat elongated cells, similarly to *Po. mascula*, but topped with a smooth cuticle (fig. 7.2a-f).

In order to isolate the structural properties of the cuticle I produced colourless epoxy replicas of smooth and striated petal surfaces, thus removing the potential effect of the cuticle chemistry. The gripping performance of *Leptinotarsa decemlineata* was tested on the two surface types. Its feet are

composed of three tarsal segments topped with liquid secreting setose pads and a terminal segment ending with two parallel claws facing downwards (fig. 7.2g and h) with a tip diameter of about 6 µm. Thus, the adhesion capacity of potato beetles relies on two different anatomical features: claws that provide interlocking gripping with the asperities of the substrate, resulting in focal adhesion, and hairy pads, providing multiple smaller points of adhesion, adapting to surface roughness (Federle, 2006).

To go further, the wetting properties of structurally coloured cuticle was also investigated by measuring the contact angle of water droplets on striated epoxy replicas of *Po. mascula* and smooth epoxy replicas of *Pr. orientalis*.

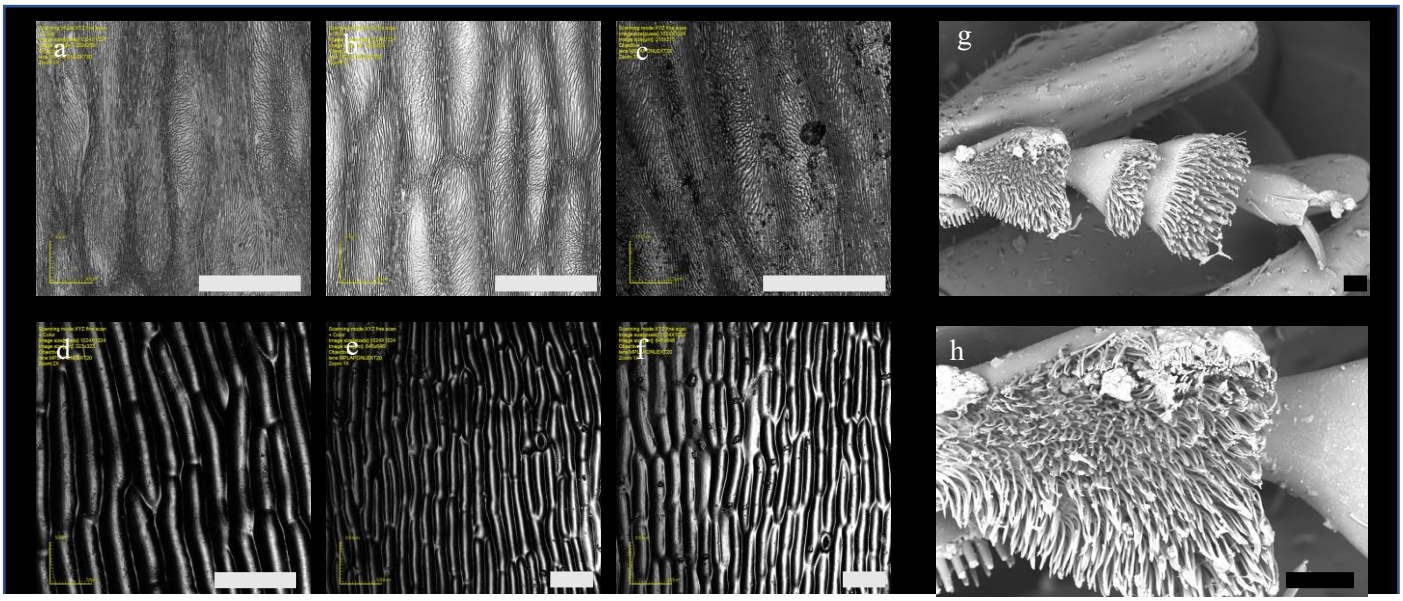

Figure 7.2: Scanning laser microscopy of *Po. mascula* and *Pr. orientalis* adaxial surfaces and their replicas and Cryo-SEM of *L. decemlineata* anterior foot. **(a-f)** Scanning laser microscopy of adaxial petal surfaces and replicas. (**a-c**) *Po. Mascula.* (**d-f**) *Pr. orientalis*. (**a** and **d**) Petal surface. (**c** and **e**) PVS negative molds of adaxial petal surfaces. (**c** and **f**) epoxy positive replicas of petal surfaces. (**g** and **h**) Cryo-SEM pictures of the anterior foot of *L. decemlineata.* Scale bar = 100 µm.

7.2 Material and methods

7.2.1 **Production of petal replicas**

Smooth and structurally coloured (striated) petal replicas were produced by replication of *Papaver orientalis* and *Paeonia mascula* petals respectively, following the protocol described by (Kumar et al., 2019). Fresh petals were collected from the botanic garden of the University of Freiburg (Botanischer Garten der Albert-Ludwigs-Universität Freiburg), and then stuck flat on petri dishes using double sided tape. Negative replicas were produced by pouring on polyvinyl siloxane (PVS, President

Light Body®, Coltene Whaledent, Altstätten, Switzerland), also known as dental wax, which was left for curation for 24 hours. Positive casts were produced using epoxy resin (Epoxydharz HT2, R&G Faserverbundwerkstoffe GmbH, Wandelbuch, Germany). The mixing ratio (by weight) of resin and hardener was 100:48. After vigorous mixing of the 2 compounds, bubbles were removed using vacuum before the epoxy hardened. Bubble free epoxy was then poured onto the PVS negative replicas and left for curation at room temperature for 24 hours. The quality of the positive replicas was assessed using a LEXT® scanning laser microscope from the Albert-Ludwigs Universität, Freiburg, Germany.

7.2.2 Beetles

Beetles were harvested from an organic potato field in the Kirchzarten area near Freiburg, Germany. Females were exclusively used for this experiment as providing a larger size specimen, thus easing manipulation and because of sexual dimorphism in attachment features characterised by the absence of discoidal setae in female *L. decemlineata* (Voigt et al., 2008).

7.2.3 Centrifugation experiment

A customed device made by the Albert-Ludwigs University (Freiburg, Germany) was used to measure gripping. This device is composed of an electric rotating motor placed at the centre of a compact disc thus providing a high-speed rotation surface on which our two surface replicas were placed as well as a counting system to assess the number of rotations per minute. Beetles were placed on either a striated or smooth petal replica before starting the motor. Beetles then started to grip onto the surface by reflex. Rotation speed was given by the device and video recordings were made using a Logitech webcam. The distance between the centre of the centrifuge and the centre of the beetle as well as the rotation speed were recorded on the very last picture preceding ejection of the beetle from the centrifuge to determine the force required to eject the beetle. Beetles were also weighed after the experiment. The gripping capacity of 10 female Colorado potato beetles (*L. decemlineata*) was tested multiple times on smooth replicas (about 3.4 tests per beetle) and 8 of them were also tested on striated replicas (about 4 tests per beetle), adding up to a total number of 32 measurements on striated replicas and 34 on smooth replicas.

7.2.4 Calculation of the Ejection Force

The centrifuge effect or ejection force required (EFR) to compensate for the beetle grip was calculated as follows:

- $EFR = m.\omega^2.r = m.(0.104*rpm)^2.r$ (mN ($g.m.s^{-2}$)).
- r: radius: distance from the position of the beetle to the centre of the centrifuge (m).
- rpm: rotation per minute (rpm).
- m: mass of the beetle (g).
- ω : angular velocity $\omega=0.105*rpm$ (rad/s).

7.2.5 Statistical analyses

The sub-datasets ‘smooth’ and ‘striated’ surfaces were considered as unpaired data even though the same population was used to test the 2 different surface types as a different number of measures was acquired for these 2 conditions.

Normal distribution of the EFR parameter according to the surface type was assessed using a Shapiro-Wilkinson test. With a p-value of 0.1764 for ‘striated’ surface and 0.025 for ‘smooth’ surface I concluded that the distribution of EFR on a ‘Smooth’ surface did not follow a normal distribution. Equality of variances between the ‘smooth’ and ‘striated’ datasets was also assessed using a Bartlett test. With a p-value of 0.00185 I concluded that variances could not be considered equal. Hence, I used the non-parametric test of Wilcoxon to compare means of EFR in the ‘smooth’ surface and ‘striated’ surface conditions. P-value = 0.006095. Statistical tests were performed using R.

7.2.6 Contact angle measurement

Contact angles were measured parallel to the longitudinal axis of the petal (0°) and perpendicular to the longitudinal axis (90°) to account for the relative orientation of the striations along the petal. Four measurements were performed on striated and smooth petal replicas at 90°, 4 were performed on striated replicas at 0°, and 3 on smooth replicas at 0°. Two microliters of water were deposited on the surface replicas using an FTA1000 Drop shape Instrument B Frame system and measured using the FTA32 software.

7.3 Results

7.3.1 Striated surfaces provide less grip for *L. decemlineata*

In order to assess the capacity of beetles to grip onto different surfaces, I placed them on one of the two epoxy replicas before the disc started to rotate. The rapid and steady increase in the rotation speed usually induces a gripping reflex in the beetle. The disc keeps on turning with increasing speed until the beetle is finally ejected from the platform. Knowing the diameter of the disc, the weight of the beetle and the speed of the disc at the moment of ejection, I calculated the force of ejection applied onto the beetle at the moment of ejection and considered it as the ejection force required (EFR) to compensate for the grip of the beetle onto the substrate. A significantly lower EFR was necessary to eject beetles from striated surfaces than smooth surfaces (fig. 7.3b), suggesting that beetles struggle to grip onto striated surfaces.

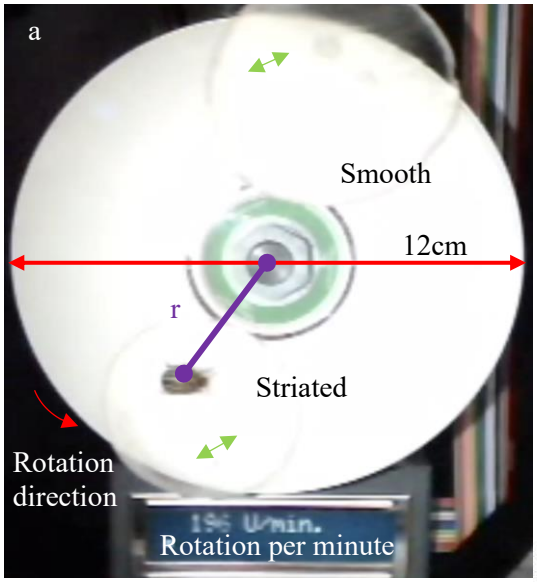

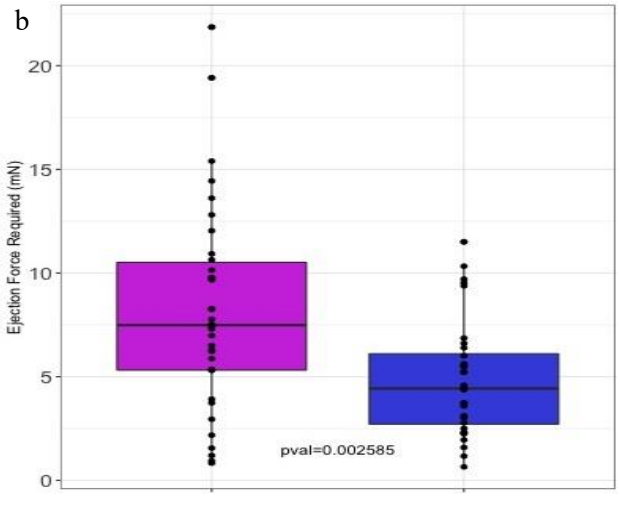

Figure 7.3: Box plot of the ejection force required (EFR) to compensate the gripping of *L. decemlineata* onto smooth and striated replicas. **(a)** Example of a picture analysed representing the experimental set up. Green double arrows representing the axis of elongation of the epidermal cells and the main orientation of the cuticular striations when present. Purple line indicating the radius (r) used for calculations **(b)** Box plot representing the EFR to detach a gripping beetle from striated and smooth petal replicas**.** Dots represent all the data points.

7.3.2 Striations result in anisotropic wetting properties

Leptinotarsa decemlineata can secrete liquid substances at the end of their bristles leading to an increased adhesion capacity (Eisner & Aneshansley, 2000; Geiselhardt et al., 2010).

The presence of micro scaled ridges on the surface of *Strelitzia* was shown to modulate the wetting properties of the leaves (Mele et al., 2012). In order to investigate the wetting properties of nano-scale ridges, I measured the contact angles formed by a drop of water on *Papaver orientalis* and *Paeonia mascula* epoxy replicas. These contact angles were measured along the main axis of the striations or cell elongation when absent (0° see fig. 7.4), and perpendicular to the main axis of the striations or cell elongation when absent (90° see fig. 7.4). No statistical difference was observed between the contact angles measured between the two different surface types at 0° and 90°. The number of measurements remains however too low (only 3 to 4 data points per condition) to draw conclusions from these results. However, the contact angles measured were consistently lower on striated replicas: about 20° lower in the 0° configuration and about 15° lower in the 90° configuration (fig. 7.4). Lower

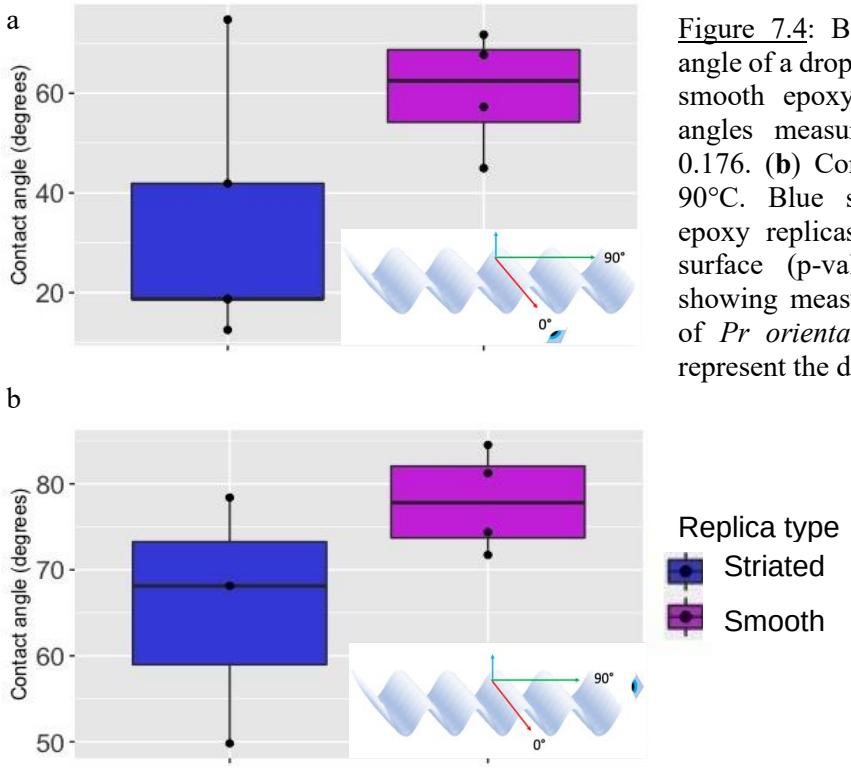

Figure 7.4: Box plot of the contact angle of a drop of water on striated and smooth epoxy replicas. (**a**) Contact angles measured at 0° (p-value = 0.176. (**b**) Contact angle measued at 90°C. Blue showing measures for epoxy replicas of *Po mascula* petal surface (p-value = 0.216). Purple showing measures for epoxy replicas of *Pr orientalis* petal surface. Dots represent the data points.

contact angles being characteristic of a higher wettability, suggesting that nano-scaled striations induce an increase in the wettability of the petal surface.

7.4 Discussion

I have shown that the presence of nano-scaled ridges responsible for the production of structural colours can also influence other physical properties of the petal. The adhesion test using beetles showed that the presence of striations can alter the gripping capacity of insects and potentially their interactions

with plants. The preliminary wettability experiment suggests that the presence of nano-scaled ridges can alter the wetting properties of plant epidermides. Together, this provides evidence that nano-scaled striations modulate the properties of the plant surface.

Furthermore, during the experiment, it was observed that beetles were not at 'ease' on striated replicas and frequently tried to leave them, which was not observed on smooth replicas. This suggests that the beetles may 'prefer' smooth epidermis when given the choice. The large anatomical variety of feet amongst insects does not allow us to extrapolate these results to pollinators such as *Bombus terrestris* (*Hymenoptera*) which presents a pair of claws (fig. 7.1) and an arolium at the end of the tarsus but no setose pads (Pouvreau, 1991) (fig. 7.1).

Measures performed on electron microscopy pictures and laser scanning microscopy pictures revealed that the diameter of the tip of the claw is of about 10 µm and the spacing between the ridges of *Po. mascula* is smaller than 3.7 µm. The difference in dimensions of the claw tip and the ridge spacing of *Po. mascula* suggest that *L. decemlineata* claws are unlikely to provide interlocking grip within the groves of the striations, indicating that the differences observed in gripping capacity of the Colorado potato beetle are most likely not involving the claws.

The lower contact angles of water droplets measured on striated replicas suggest a higher wettability of the substrate induced by the striations. This may interfere with the setose pad secretions of *L. decemlineata* by increasing the diffusion of fluids onto the cuticle surface, however this phenomenon is most likely not the main cause of adhesion loss in this context. The setae present a tip diameter of about 6 µm, given that the spacing between ridges of *Po. mascula* is comprised between 0.5 and 3.7 µm, it is likely that the loss of adhesion is the result of a smaller contact surface between the setae and the cuticle when compared to smooth cuticle.

These results constitute a preliminary study on the non-optical properties of nano scaled petal striations. In order to go further with it, it would be interesting to study beetle adhesion on a larger variety of flower surfaces presenting optical properties such as *Adonis aestivalis*, *Leucocoryne purpurea*, the tulip 'Queen of the night', *Mentzenia lidlenyii* and *Oenothera stricta* (Moyroud et al., 2017). Pollinators should be preferred to Colorado potato beetles as the latter do not specifically interact

with flowers and present different anatomical features (see *Bombus terrestris* feet fig. 7.1). However, the usual reluctance of potato beetles and ladybugs (*Coccinella septempunctata*) to fly, and their easy maintenance, make them good models to study adhesion.

Studying the tactile preference of pollinators towards striated or smooth surfaces remains difficult given the fact that the physical experience cannot be dissociated from the optical stimulus. However, this study shows that striations associated with structural colours can alter the gripping capacity of insects. In *Hibiscus trionum*, given the size of the region presenting cuticular striations, the effect on the grip of pollinators is likely to be limited. The optical properties thus remain the main relevant characteristic of nano-scaled striations in this species. On the tulip 'Queen of the night', however, where the structurally coloured cuticle covers the entire abaxial surface, this grip effect plays a larger role in the interaction with pollinators.

Plant surfaces constitute an important feature that leads to indirect interactions via their optical properties and direct interactions via contact.

7.5 Conclusion

This study demonstrated that nano-scaled ridges responsible for the production of structural colours can interfere with the adhesive capacity of beetles. The scale of these ridges is unlikely to alter claw-mediated gripping and may alter the adhesive properties of other gripping features such as setose pads, possibly via modulation of the wetting properties of the substrate. In *Hibiscus trionum*, the smallness of the structurally coloured region most likely deflects any relevant ecological implication when it comes to direct interactions with insects. Furthermore, not all potential pollinators of the *Hymenoptera* order that are sensitive to *Hibiscus trionum* structural colours present setose pads (Beutel & Gorb, 2001), suggesting that the adhesive properties of nano-scaled ridges has influence on a limited number of pollinators. Moreover, the majority of the petal adaxial surface is covered with conical cells, which has been demonstrated to provide grip to pollinators in other plant species (Beutel & Gorb, 2001).

results of this study suggest that larger structurally coloured petal surfaces may present other ecological properties.

Chapter 8: General discussion and future work

The main objective of this Ph.D. was to gain understanding of the molecular pathways supporting the development of a structurally coloured cuticle.

The chemical analyses that were performed allowed us to highlight the role of the chemistry in the development of structurally coloured cuticle. The dominance of the cutin monomer 10,16-DHP in striated cuticle suggests that the cutin network plays an important role in the development of striations. On the distal part, compounds with a high number of carbon residues, of most likely waxy nature, appeared as dominant. A duality between striated and smooth cuticle chemistry thus translated into an enrichment in either waxy compounds or cutin monomers.

Transcriptomic analyses also showed the up-regulation of pectin catabolism-related genes, which suggests that the regulation of cell wall reticulation plays an important role in the development of nano-scaled ridges in *Hibiscus trionum*. This observation is also consistent with the need for a compliant substrate during *in vitro* experiments on thin film buckling (Bowden et al., 1998)

The overall thickness of the extra cellular matrix (composed of cell wall and cuticularised cell wall) did not seem to influence the development of petal cuticular patterns, as observed on the *35S:HtLTP2-like* transgenic lines and in the *madeleine* and *blue* mutants. This suggests that the β parameter evoked in the work of Kourounioti et al (2013) reflecting the cuticle production rate (cuticle proper and cuticularised cell wall), may not reflect accurately the role of the cuticle in the development of striations. The results of this study suggest that only the thickness of the cuticle proper may alter the development of such structures.

The production of *HtLTP2-like* over expressing transgenic line resulted in an alteration of the adhesion of the cuticle proper onto its substrate which may have led to the development of non-striated cells. This indicates that the proper structure of the cuticle is important to induce the efficient production of striations.

All these elements are coherent with the generation of cuticular striations by the physical phenomenon of buckling, and potential molecular mechanisms supporting cuticular buckling have been partially elucidated in *Hibiscus trionum.* The transcriptomic analyses revealed a tight regulation of the cuticle production involving two AP2/ERF transcription factors: *HtDEWAX* and *HtSHN3.* Following the *in vitro* study of buckling (Bowden et al., 1998) showing the necessity of having a stiff top layer over a compliant bottom layer, It can be hypothesised that the decrease in the abundance of waxy compounds and the increase in cutin monomers induces a stiffening of the cuticle whilst the co-occurring catabolism of pectin suggested by the gene ontology analyses results in a softening of the cuticularised cell wall and cell wall, thus potentially creating the bilayer system evoked by Bowden et al (1998). It remains however essential to test this hypothesis with stiffness measurements to conclude on the mechanical consequences of this differential regulation of the cuticle metabolism.

However, no correlation has yet been made between the chemistry of the cuticle and its stiffness. In order to prove that the observed differences in gene regulation and in chemical composition may result in an alteration of the cuticle stiffness, further experiments need to be conducted. The use of Atomic Force Microscopy (AFM) has proven reliable in the measurement of the Young's modulus of cell wall (Milani et al., 2011; Radotić et al., 2012) and is currently being optimized for the measurement of the stiffness of the different cuticle layers of *Hibiscus trionum.* To assess how chemistry can influence the cuticle stiffness, a 35S:*HtDCR* transgenic line is currently being produced. This should result in an increase of the 10,16-DHP content of the cuticle (Panikashvili et al., 2009; Rani et al., 2010) and thus a potential stiffening of the cuticle which may be sufficient to induce ectopic cuticle buckling. The cell wall has not yet been targeted for molecular work as little is known about its potential implications in the buckling, yet the transcriptomic analyses that were performed suggest that a softening of the cuticularised cell wall occurs specifically in buckling petal regions. The role of the cell wall in the production of striations is currently being investigated by the production of *35S:HtHCT* transgenic line. The involvement of *HCT* in the lignin synthesis pathway and its low expression in the proximal petal part suggest that the compliance of the cell wall is important to develop a structurally coloured cuticle. Hence, the production of an *HtHCT* over expressing transgenic line should result in stiffening of the cell wall which may in turn lead to the failure of buckling on *H trionum* petals. AFM

mediated stiffness measurements of the cuticle and cell wall of these two sets of transgenic lines should bring more knowledge on the molecular mechanisms regulating the production of cuticle and cell walls of variable Young's moduli.

The presence of 2-dimensional constraints was also demonstrated as crucial to the development of striations both *in vitro* and *in vivo* (Bowden et al., 1998; X. Huang et al., 2017). The mild differences of cell size observed in the *mdl* and *blue* mutants were however not sufficient to explain the presence of smooth cells, suggesting a certain robustness of the buckling against alteration of the cell size or 2-dimensional constraints. Furthermore, the *mdl* phenotype was shown to be the result of a single locus mutation and the presence of ectopic conical cells suggest that the expression of a morphogen was altered. Together with the partial retention of the buckling capacity of the cuticle, this suggests that the *mdl* gene is exclusively implicated in the localization of conical cells, thus excluding potential alteration of the cuticle and cell wall properties in non-madeleine shaped cells. Therefore, it appears that the loss of striations in large sections composed of both flat and smooth cells is most likely the consequence of more subtle perturbations acting at a different scale. We suppose that the presence of conical cells scattered on the proximal region of the petal enables the accommodation of the supplementary cuticle material generated, thus occasionally altering the thickness of the cuticle proper on the entire adaxial petal epidermis. Surprisingly, the gene ontology analyses did not reveal the presence of genes involved in anisotropic growth, thus, the molecular pathways underpinning the development of elongated flat cells on the proximal petal epidermis are yet to be elucidated in *Hibiscus trionum*.

In a final chapter I examined the wetting and adhesion properties of structurally coloured cuticle. Experiments showed that structurally coloured cuticular ridges could alter the gripping ability of Colorado potato beetles. Given the size of the claw tips and the aspect ratio of the striations, I concluded that the nano-scaled ridges did not interfere with claw mediated gripping. However, due to the scale of the striations and setae, it is likely that the setae fail to reach the bottom part of the striations, resulting in an overall reduction of the contact surface, leading to a loss of adhesion. In this context, the possible anisotropic wetting properties of the striations and the apparent increased wetting properties they induce is most likely playing a negligeable role in the alteration of the setose pads' adhesive properties.

In *Paeonia mascula*, the structurally coloured region overlaps with the entire adaxial petal surface, it can thus be assumed that landing pollinators will have to cope with a relatively slippery surface, thus potentially acting as a deterrent to some species, leading to potential pollinator isolation. In *Hibiscus trionum*, the largest region of the petal is covered with conical cells which have been shown to provide grip to pollinators such as bumblebees (*Bombus terrestris*) (Whitney et al., 2009). Consequently, this greatly limits the potential impact of the structurally coloured cuticle on the grip of landing pollinators. Furthermore, each flower only remains open for a couple of hours thus limiting their interaction time with pollinators. Together, this suggests that the main ecological features of nano-scaled striations in *Hibiscus trionum* concern the production of structural colours as a visual cue to potential pollinators.

However, the presence of arolium and tarsal adhesive thorns in some species of *Hymenoptera* such as *Apis mellifera* (Beutel & Gorb, 2001) may induce gripping sensitivity to nano-scaled striations. In order to test this hypothesis, further adhesion experiment may be conducted with other insects presenting different adhesive structures. Nonetheless, for flowers visited by both *Hymenoptera* and *Coleoptera* pollinators, the presence of nano-scaled striations may induce a selection pressure towards insects that do not present setose pads. Nonetheless, this phenomenon is most likely not restricted to setose pads and may also affect other adhesive structures.

In summary, the main findings of this Ph.D. are: (1) that structurally coloured and non-structurally coloured cuticle have a different chemical composition, (2) the potential role of *HtSHN3, HtDEWAX,* and pectinesterases in the generation of a structurally coloured cuticle, (3) the importance of the thickness of the cuticle proper in the development of nano-scaled striations and (4) the decreased adhesion of *L. decemlineata* on structurally coloured cuticle. A key point for future experiment will be the investigation of the Young's modulus of cuticle and the cell wall. Another aspect to develop concerns the mechanical properties of such patterns and their ecological impacts on landing pollinators by acquiring larger data sets involving diverse pollinating insects and structurally coloured flowers.

This study of the development of nano-scaled striations leading to the production of structural colours may in turn inspire us on how to artificially generate iridescent surfaces or insect selecting surfaces.

Reference

Abou, B., Gay, C., Laurent, B., Cardoso, O., Voigt, D., Peisker, H., & Gorb, S. (2010). Extensive collection of femtolitre pad secretion droplets in the beetle *Leptinotarsa decemlineata* allows nanolitre microrheology. *Journal of The Royal Society Interface*, *7*(53), 1745–1752. https://doi.org/10.1098/rsif.2010.0075

Adato, A., Mandel, T., Mintz-Oron, S., Venger, I., Levy, D., Yativ, M., … Aharoni, A. (2009). Fruit-surface flavonoid accumulation in tomato is controlled by a SlMYB12-regulated transcriptional network. *PLoS Genetics*, *5*(12), e1000777. https://doi.org/10.1371/journal.pgen.1000777

Aharoni, A., Dixit, S., Jetter, R., Thoenes, E., van Arkel, G., & Pereira, A. (2004). The SHINE clade of AP2 domain transcription factors activates wax biosynthesis, alters cuticle properties, and confers drought tolerance when overexpressed in Arabidopsis. *The Plant Cell*, *16*(9), 2463–2480. https://doi.org/10.1105/tpc.104.022897

Airoldi, C.A., Ferria, J., & Glover, B. J. (2019). The cellular and genetic basis of structural colour in plants. *Current Opinion in Plant Biology*, *47,* 81-87. https://doi.org/10.1016/j.pbi.2018.10.002

Airoldi, Chiara A., Lugo, C. A., Wightman, R., Glover, B. J., & Robinson, S. (2021). Mechanical buckling can pattern the light-diffracting cuticle of Hibiscus trionum. *Cell Reports*, *36*(11), 109715. https://doi.org/10.1016/J.CELREP.2021.109715

Al-Abdallat, A. M., Al-Debei, H. S., Ayad, J. Y., & Hasan, S. (2014). Over-expression of SLSHN1 gene improves drought tolerance by increasing cuticular wax accumulation in tomato. *International Journal of Molecular Sciences*, *15*(11), 19499-19515. https://doi.org/10.3390/ijms151119499

Ambavaram, M. M. R., Krishnan, A., Trijatmiko, K. R., & Pereira, A. (2011). Coordinated activation of cellulose and repression of lignin biosynthesis pathways in rice. *Plant Physiology*, *155*(2), 916–931. https://doi.org/10.1104/pp.110.168641

and, R. F., Barthlott, W., Neinhuis, C., & Walzel, P. (2005). *Wetting and Self-Cleaning Properties of Artificial Superhydrophobic Surfaces*. *Langmuir* 21, 956-961. https://doi.org/10.1021/LA0401011

Bakan, B., & Marion, D. (2017). Assembly of the cutin polyester: From cells to extracellular cell walls. *Plants*, Vol. 6(4), 57. https://doi.org/10.3390/plants6040057

Baker, E. A., & Holloway, P. J. (1970). The constituent acids of angiosperm cutins. *Phytochemistry*, *9*(7), 1557–1562. https://doi.org/10.1016/S0031-9422(00)85275-9

Bao, X., Franks, R. G., Levin, J. Z., & Liu, Z. (2004). Repression of AGAMOUS by BELLRINGER in floral and inflorescence meristems. *The Plant Cell*, *16*(6), 1478–1489. https://doi.org/10.1105/tpc.021147

Barthlott, W., & Neinhuis, C. (1997). Purity of the sacred lotus, or escape from contamination in biological surfaces. *Planta*, *202*(1), 1–8. https://doi.org/10.1007/s004250050096

Bashline, L., Li, S., & Gu, Y. (2014). The trafficking of the cellulose synthase complex in higher plants. *Annals of Botany*, *114*(6), 1059–1067. https://doi.org/10.1093/aob/mcu040

Belfield, E. J., Gan, X., Mithani, A., Brown, C., Jiang, C., Franklin, K., … Harberd, N. P. (2012). Genome-wide analysis of mutations in mutant lineages selected following fast-neutron irradiation mutagenesis of Arabidopsis thaliana. *Genome Research*, *22*(7), 1306–1315. https://doi.org/10.1101/gr.131474.111

Ben-Tov, D., Abraham, Y., Stav, S., Thompson, K., Loraine, A., Elbaum, R., … Harpaz-Saad, S. (2015). COBRA-LIKE2, a Member of the Glycosylphosphatidylinositol-Anchored COBRA-LIKE Family, Plays a Role in Cellulose Deposition in Arabidopsis Seed Coat Mucilage Secretory Cells,. *Plant Physiology*, *167*(3), 711–724. https://doi.org/10.1104/PP.114.240671

Bernard, A., & Joubès, J. (2013). Arabidopsis cuticular waxes: Advances in synthesis, export and regulation. *Progress in Lipid Research*, *52*(1), 110–129. https://doi.org/10.1016/j.plipres.2012.10.002

Beutel, R. G., & Gorb, S. N. (2001). Ultrastructure of attachment specializations of hexapods (Arthropoda): evolutionary patterns inferred from a revised ordinal phylogeny. *Journal of Zoological Systematics and Evolutionary Research*, *39*(4), 177–207. https://doi.org/10.1046/j.1439-0469.2001.00155.x

Bhushan, B., & Nosonovsky, M. (2010). The rose petal effect and the modes of superhydrophobicity. *Philosophical Transactions of the Royal Society A: Mathematical, Physical and Engineering Sciences*, *368*(1929), 4713–4728. https://doi.org/10.1098/rsta.2010.0203

Bird, D., Beisson, F., Brigham, A., Shin, J., Greer, S., Jetter, R., … Samuels, L. (2007). Characterization of Arabidopsis ABCG11/WBC11, an ATP binding cassette (ABC) transporter that is required for cuticular lipid secretion†. *The Plant Journal*, *52*(3), 485–498. https://doi.org/10.1111/j.1365-313X.2007.03252.x

Bolger, A. M., Lohse, M., & Usadel, B. (2014). Trimmomatic: a flexible trimmer for Illumina sequence data. *Bioinformatics (Oxford, England)*, *30*(15), 2114–2120. https://doi.org/10.1093/bioinformatics/btu170

Borisjuk, N., Hrmova, M., & Lopato, S. (2014). Transcriptional regulation of cuticle biosynthesis. *Biotechnology Advances*, *32*(2), 526–540. https://doi.org/10.1016/J.BIOTECHADV.2014.01.005

Borisjuk, N., Peterson, A. A., Lv, J., Qu, G., Luo, Q., Shi, L., … Shi, J. (2018). Structural and Biochemical Properties of Duckweed Surface Cuticle. *Frontiers in Chemistry*, *6*, 317. https://doi.org/10.3389/fchem.2018.00317

Bowden, N., Brittain, S., Evans, A. G., Hutchinson, J. W., & Whitesides, G. M. (1998). Spontaneous formation of ordered structures in thin films of metals supported on an elastomeric polymer. *Nature*, *393*(6681), 146–149.

Broun, P., Poindexter, P., Osborne, E., Jiang, C.-Z., & Riechmann, J. L. (2004). WIN1, a transcriptional activator of epidermal wax accumulation in Arabidopsis. *Proceedings of the National Academy of Sciences of the United States of America*, *101*(13), 4706–4711. https://doi.org/10.1073/pnas.0305574101

Brummell, D. A., Harpster, M. H., Civello, P. M., Palys, J. M., Bennett, A. B., & Dunsmuir, P. (1999). Modification of expansin protein abundance in tomato fruit alters softening and cell wall polymer metabolism during ripening. *The Plant Cell*, *11*(11), 2203–2216. https://doi.org/10.1105/tpc.11.11.2203

Buschhaus, C., & Jetter, R. (2011). Composition differences between epicuticular and intracuticular wax substructures: How do plants seal their epidermal surfaces? *Journal of Experimental Botany*, *62*(3), 841–853. https://doi.org/10.1093/jxb/erq366

Cernac, A., & Benning, C. (2004). WRINKLED1 encodes an AP2/EREB domain protein involved in the control of storage compound biosynthesis in Arabidopsis. *The Plant Journal*, *40*(4), 575–585. https://doi.org/10.1111/j.1365-313X.2004.02235.x

Chan, J. (2012). Microtubule and cellulose microfibril orientation during plant cell and organ growth. *Journal of Microscopy*, *247*(1), 23–32. https://doi.org/10.1111/j.1365-2818.2011.03585.x

Chandler, C. J., Wilts, B. D., Vignolini, S., Brodie, J., Steiner, U., Rudall, P. J., … Walker, R. H. (2015). Structural colour in Chondrus crispus. *Scientific Reports*, *5*(1), 11645. https://doi.org/10.1038/srep11645

Chen, D., Yoon, J., Chandra, D., Crosby, A. J., & Hayward, R. C. (2014). Stimuli-responsive buckling mechanics of polymer films. *Journal of Polymer Science Part B: Polymer Physics*, *52*(22), 1441–1461. https://doi.org/10.1002/polb.23590

Choi, D., Lee, Y., Cho, H.-T., & Kende, H. (2003). Regulation of expansin gene expression affects growth and development in transgenic rice plants. *The Plant Cell*, *15*(6), 1386–1398. https://doi.org/10.1105/tpc.011965

Christenhusz, M. J. M., & BYNG, J. W. (2016). The number of known plants species in the world and its annual increase. *Phytotaxa*, *261*(3), 201. https://doi.org/10.11646/phytotaxa.261.3.1

Cominelli, E., Sala, T., Calvi, D., Gusmaroli, G., & Tonelli, C. (2008). Over-expression of the Arabidopsis AtMYB41 gene alters cell expansion and leaf surface permeability. *The Plant Journal*, *53*(1), 53–64. https://doi.org/10.1111/j.1365-313X.2007.03310.x

Cyr, R. (1994). Microtubules in Plant Morphogenesis: Role of the Cortical Array. *Annual Review of Cell and Developmental Biology*, *10*(1), 153–180. https://doi.org/10.1146/annurev.cellbio.10.1.153

Darmanin, T., & Guittard, F. (2015). Superhydrophobic and superoleophobic properties in nature. *Materials Today*, *18*(5), 273–285. https://doi.org/10.1016/J.MATTOD.2015.01.001

de Premorel, G., Giurfa, M., Andraud, C., & Gomez, D. (2017). Higher iridescent-to-pigment optical effect in flowers facilitates learning, memory and generalization in foraging bumblebees. *Proceedings of the Royal Society B: Biological Sciences*, *284*(1865), 20171097. https://doi.org/10.1098/rspb.2017.1097

Deshmukh, A. P., Simpson, A. J., Hadad, C. M., & Hatcher, P. G. (2005). Insights into the structure of cutin and cutan from Agave americana leaf cuticle using HRMAS NMR spectroscopy. *Organic Geochemistry*, *36*(7), 1072–1085. https://doi.org/10.1016/J.ORGGEOCHEM.2005.02.005

Domínguez, E., España B, D, L., López-Casado B, G., Cuartero, J., & Heredia, A. (2009). *Biomechanics of isolated tomato (Solanum lycopersicum) fruit cuticles during ripening: the role of flavonoids*. *Functional Plant Biology, 36,* 613-120. https://doi.org/10.1071/FP09039

Domínguez, E., Heredia-Guerrero, J. A., & Heredia, A. (2015). Plant cutin genesis: unanswered questions. *Trends in Plant Science*, *20*(9), 551–558. https://doi.org/10.1016/J.TPLANTS.2015.05.009

Dongowski, G. (2001). Enzymatic degradation studies of pectin and cellulose from red beets. *Nahrung/Food*, *45*(5), 324-331. https://doi.org/10.1002/1521-3803(20011001)45:5<324::AID-FOOD324>3.0.CO;2-C

Doucet, S. M., & Meadows, M. G. (2009). Iridescence: a functional perspective. *Journal of the Royal Society, Interface*, *6 Suppl 2*(Suppl 2), S115-32. https://doi.org/10.1098/rsif.2008.0395.focus

Dray, S., & Dufour, A.-B. (2007). The ade4 Package: Implementing the Duality Diagram for Ecologists. *Journal of Statistical Software*, *22*(4). https://doi.org/10.18637/jss.v022.i04

Eisner, T., & Aneshansley, D. J. (2000). Defense by foot adhesion in a beetle (Hemisphaerota cyanea). *Proceedings of the National Academy of Sciences of the United States of America*, *97*(12), 6568–6573. https://doi.org/10.1073/pnas.97.12.6568

Elhiti, M., & Stasolla, C. (2009). Structure and function of homodomain-leucine zipper (HD-Zip) proteins. *Plant Signaling & Behavior*, *4*(2), 86–88. https://doi.org/10.4161/psb.4.2.7692

Federle, W. (2006). Why are so many adhesive pads hairy? *The Journal of Experimental Biology*, *209*, 2611–2621. https://doi.org/10.1242/jeb.02323

Federle, W., Maschwitz, U., Fiala, B., Riederer, M., & Hölldobler, B. (1997). Slippery ant-plants and skilful climbers: selection and protection of specific ant partners by epicuticular wax blooms in Macaranga (Euphorbiaceae). *Oecologia*, *112*(2), 217–224. https://doi.org/10.1007/s004420050303

Feng, L., Li, S., Li, Y., Li, H., Zhang, L., Zhai, J., … Zhu, D. (2002). Super-Hydrophobic Surfaces: From Natural to Artificial. *Advanced Materials*, *14*(24), 1857–1860. https://doi.org/10.1002/adma.200290020

Fernández, V., Guzmán-Delgado, P., Graça, J., Santos, S., & Gil, L. (2016). Cuticle Structure in Relation to Chemical Composition: Re-assessing the Prevailing Model. *Frontiers in Plant Science*, *7(427)*. https://doi.org/10.3389/fpls.2016.00427

Fich, E. A., Segerson, N. A., & Rose, J. K. C. (2016). The Plant Polyester Cutin: Biosynthesis, Structure, and Biological Roles. *Annual Review of Plant Biology*, *67*(1), 207–233. https://doi.org/10.1146/annurev-arplant-043015-111929

Fiebig, A., Mayfield, J. A., Miley, N. L., Chau, S., Fischer, R. L., & Preuss, D. (2000). Alterations in CER6, a gene identical to CUT1, differentially affect long-chain lipid content on the surface of pollen and stems. *The Plant Cell*, *12*(10), 2001–2008. https://doi.org/10.1105/TPC.12.10.2001

Furutani, I., Watanabe, Y., Prieto, R., Masukawa, M., Suzuki, K., Naoi, K., … Hashimoto, T. (2000). The SPIRAL genes are required for directional control of cell elongation in Aarabidopsis thaliana. Development, 127(20) 4443-4453. https://doi.org/10.1242/dev.127.20.4443

Geiselhardt, S. F., Federle, W., Prüm, B., Geiselhardt, S., Lamm, S., & Peschke, K. (2010). Impact of chemical manipulation of tarsal liquids on attachment in the Colorado potato beetle, Leptinotarsa decemlineata. *Journal of Insect Physiology*, *56*(4), 398–404. https://doi.org/10.1016/J.JINSPHYS.2009.11.016

Geitmann, A., & Ortega, J. K. E. (2009). Mechanics and modeling of plant cell growth. *Trends in Plant Science*, *14*(9), 467–478. https://doi.org/10.1016/J.TPLANTS.2009.07.006

Gilbert, D., Gilbert, & Don. (2016). Gene-omes built from mRNA seq not genome DNA. *F1000Research*, *5*. https://doi.org/10.7490/F1000RESEARCH.1112594.1

Gilet, T., Heepe, L., Lambert, P., Compère, P., & Gorb, S. N. (2018). Liquid secretion and setal compliance: the beetle's winning combination for a robust and reversible adhesion. *Current Opinion in Insect Science*, *30*, 19–25. https://doi.org/10.1016/J.COIS.2018.08.002

Giménez, E., Dominguez, E., Pineda, B., Heredia, A., Moreno, V., Lozano, R., & Angosto, T. (2015). Transcriptional Activity of the MADS Box ARLEQUIN/TOMATO AGAMOUS-LIKE1 Gene Is Required for Cuticle Development of Tomato Fruit. *Plant Physiology*, *168*(3), 1036–1048. https://doi.org/10.1104/pp.15.00469

Giorio, C., Moyroud, E., Glover, B. J., Skelton, P. C., & Kalberer, M. (2015). Direct Surface Analysis Coupled to High-Resolution Mass Spectrometry Reveals Heterogeneous Composition of the Cuticle of Hibiscus trionum Petals. *Analytical Chemistry*, *87*(19), 9900–9907. https://doi.org/10.1021/acs.analchem.5b02498

Girard, A.-L., Mounet, F., Lemaire-Chamley, M., Gaillard, C., Elmorjani, K., Vivancos, J., … Bakan, B. (2012). Tomato GDSL1 Is Required for Cutin Deposition in the Fruit Cuticle. *The Plant Cell*, *24*(7), 3119–3134. https://doi.org/10.1105/tpc.112.101055

Glover, B. J., Perez-Rodriguez, M., & Martin, C. (1998). Development of several epidermal cell types can be specified by the same MYB-related plant transcription factor. Development, 125(17), 3497-3508. https://doi.org/10.1242/dev.125.17.3497

Go, Y. S., Kim, H., Kim, H. J., & Suh, M. C. (2014). Arabidopsis Cuticular Wax Biosynthesis Is Negatively Regulated by the DEWAX Gene Encoding an AP2/ERF-Type Transcription Factor. *The Plant Cell*, *26*(4), 1666-1681. https://doi.org/10.1105/tpc.114.123307

Go, Young Sam, Kim, H., Kim, H. J., & Suh, M. C. (2014). Arabidopsis Cuticular Wax Biosynthesis Is Negatively Regulated by the DEWAX Gene Encoding an AP2/ERF-Type Transcription Factor. *The Plant Cell*, *26*(4), 1666–1680. https://doi.org/10.1105/tpc.114.123307

Gonzalez, A., Zhao, M., Leavitt, J. M., & Lloyd, A. M. (2008). Regulation of the anthocyanin biosynthetic pathway by the TTG1/bHLH/Myb transcriptional complex in Arabidopsis seedlings. *The Plant Journal*, *53*(5), 814–827. https://doi.org/10.1111/j.1365-313X.2007.03373.x

González, E., & Joly, S. (2013). Impact of RNA-seq attributes on false positive rates in differential expression analysis of de novo assembled transcriptomes. *BMC Research Notes*, *6*, 503-511. https://doi.org/10.1186/1756-0500-6-503

Gorton, H. L., & Vogelmann, T. C. (1996). Effects of Epidermal Cell Shape and Pigmentation on Optical Properties of Antirrhinum Petals at Visible and Ultraviolet Wavelengths. *Plant Physiology*, *112*(3), 879–888. https://doi.org/10.1104/pp.112.3.879

Gou, J.-Y., Miller, L. M., Hou, G., Yu, X.-H., Chen, X.-Y., & Liu, C.-J. (2012). Acetylesterase-mediated deacetylation of pectin impairs cell elongation, pollen germination, and plant reproduction. *The Plant Cell*, *24*(1), 50–65. https://doi.org/10.1105/tpc.111.092411

Graça, J., Schreiber, L., Rodrigues, J., & Pereira, H. (2002). Glycerol and glyceryl esters of ω-hydroxyacids in cutins. *Phytochemistry*, *61*(2), 205–215. https://doi.org/10.1016/S0031-9422(02)00212-1

Guzmán, P., Fernández, V., García, M. L., Khayet, M., Fernández, A., & Gil, L. (2014). Localization of polysaccharides in isolated and intact cuticles of eucalypt, poplar and pear leaves by enzyme-gold labelling. *Plant Physiology and Biochemistry*, *76*, 1–6. https://doi.org/10.1016/J.PLAPHY.2013.12.023

Haas, B. J., Papanicolaou, A., Yassour, M., Grabherr, M., Blood, P. D., Bowden, J., … Regev, A. (2013). De novo transcript sequence reconstruction from RNA-seq using the Trinity platform for reference generation and analysis. *Nature Protocols*, *8*(8), 1494–1512. https://doi.org/10.1038/nprot.2013.084

Halkier, B. A. (1996). Catalytic reactivities and structure/function relationships of cytochrome P450 enzymes. *Phytochemistry*, *43*(1), 1–21. https://doi.org/10.1016/0031-9422(96)00263-4

Haslam, T. M., Mañas-Fernández, A., Zhao, L., & Kunst, L. (2012). Arabidopsis ECERIFERUM2 is a component of the fatty acid elongation machinery required for fatty acid extension to exceptional lengths. *Plant Physiology*, *160*(3), 1164–1174. https://doi.org/10.1104/pp.112.201640

Hayashi, T., & Kaida, R. (2011). Functions of Xyloglucan in Plant Cells. *Molecular Plant*, *4*(1), 17–24. https://doi.org/10.1093/MP/SSQ063

Hebant, C., & Lee, D. W. (1984). Ultrastructural Basis and Developmental Control of Blue Iridescence in Selaginella Leaves. *American Journal of Botany*, *71*(2), 216-219. https://doi.org/10.2307/2443748

Hellens, R. P., Edwards, E. A., Leyland, N. R., Bean, S., & Mullineaux, P. M. (2000). pGreen: a versatile and flexible binary Ti vector for Agrobacterium-mediated plant transformation. *Plant Molecular Biology*, *42*(6), 819–832. https://doi.org/10.1023/A:1006496308160

Heredia-Guerrero, J. A., BenÃ-tez, J. J., DomÃ-nguez, E., Bayer, I. S., Cingolani, R., Athanassiou, A., & Heredia, A. (2014). Infrared and Raman spectroscopic features of plant cuticles: a review. *Frontiers in Plant Science*, *5*, 305. https://doi.org/10.3389/fpls.2014.00305

Hirsch, C. D., Springer, N. M., & Hirsch, C. N. (2015). Genomic limitations to RNA sequencing expression profiling. *The Plant Journal : For Cell and Molecular Biology*, *84*(3), 491–503. https://doi.org/10.1111/tpj.13014

Hoffmann, L., Besseau, S., Geoffroy, P., Ritzenthaler, C., Meyer, D., Lapierre, C., … Legrand, M. (2004). Silencing of hydroxycinnamoyl-coenzyme A shikimate/quinate hydroxycinnamoyltransferase affects phenylpropanoid biosynthesis. *The Plant Cell*, *16*(6), 1446–1465. https://doi.org/10.1105/tpc.020297

Hong, L., Brown, J., Segerson, N. A., Rose, J. K. C., & Roeder, A. H. K. (2017). CUTIN SYNTHASE

2 Maintains Progressively Developing Cuticular Ridges in Arabidopsis Sepals. *Molecular Plant*, *10*(4), 560–574. https://doi.org/10.1016/j.molp.2017.01.002

Huang, G., Han, M., Jian, L., Chen, Y., Sun, S., Wang, X., & Wang, Y. (2020). An ETHYLENE INSENSITIVE3-LIKE1 Protein Directly Targets the GEG Promoter and Mediates Ethylene-Induced Ray Petal Elongation in Gerbera hybrida. *Frontiers in Plant Science*, *10*, 1737. https://doi.org/10.3389/fpls.2019.01737

Huang, X., Hai, Y., & Xie, W.-H. (2017). Anisotropic cell growth-regulated surface micropatterns in flower petals. *Theoretical and Applied Mechanics Letters*, *7*(3), 169–174. https://doi.org/10.1016/J.TAML.2017.03.004

Huo, H., Henry, I. M., Coppoolse, E. R., Verhoef-Post, M., Schut, J. W., de Rooij, H., … Bradford, K. J. (2016). Rapid identification of lettuce seed germination mutants by bulked segregant analysis and whole genome sequencing. *The Plant Journal*, *88*(3), 345–360. https://doi.org/10.1111/tpj.13267

Isaacson, T., Kosma, D. K., Matas, A. J., Buda, G. J., He, Y., Yu, B., … Rose, J. K. C. (2009). Cutin deficiency in the tomato fruit cuticle consistently affects resistance to microbial infection and biomechanical properties, but not transpirational water loss. *The Plant Journal*, *60*(2), 363–377. https://doi.org/10.1111/j.1365-313X.2009.03969.x

Jacobs, M., Lopez-Garcia, M., Phrathep, O.-P., Lawson, T., Oulton, R., & Whitney, H. M. (2016). Photonic multilayer structure of Begonia chloroplasts enhances photosynthetic efficiency. *Nature Plants*, *2*(11), 16162. https://doi.org/10.1038/nplants.2016.162

Jacq, A., Pernot, C., Martinez, Y., Domergue, F., Payre, B., Jamet, E., … Pacquit, V. B. (2017). The Arabidopsis Lipid Transfer Protein 2 (AtLTP2) Is Involved in Cuticle-Cell Wall Interface Integrity and in Etiolated Hypocotyl Permeability. *Frontiers in Plant Science*, *8*, 263. https://doi.org/10.3389/fpls.2017.00263

Jaffe, F. W., Tattersall, A., & Glover, B. J. (2007). A truncated MYB transcription factor from Antirrhinum majus regulates epidermal cell outgrowth. *Journal of Experimental Botany*, *58*(6), 1515–1524. https://doi.org/10.1093/jxb/erm020

Jakobson, L., Lindgren, L. O., Verdier, G., Laanemets, K., Brosché, M., Beisson, F., & Kollist, H. (2016). BODYGUARD is required for the biosynthesis of cutin in Arabidopsis. *New Phytologist*, *211*(2), 614–626. https://doi.org/10.1111/nph.13924

Javelle, M., Vernoud, V., Depège-Fargeix, N., Arnould, C., Oursel, D., Domergue, F., … Rogowsky, P. M. (2010). Overexpression of the epidermis-specific homeodomain-leucine zipper IV transcription factor Outer Cell Layer1 in maize identifies target genes involved in lipid metabolism and cuticle biosynthesis. *Plant Physiology*, *154*(1), 273–286. https://doi.org/10.1104/pp.109.150540

Kannangara, R., Branigan, C., Liu, Y., Penfield, T., Rao, V., Mouille, G., … Broun, P. (2007a). The transcription factor WIN1/SHN1 regulates Cutin biosynthesis in Arabidopsis thaliana. *The Plant Cell*, *19*(4), 1278–1294. https://doi.org/10.1105/tpc.106.047076

Kannangara, R., Branigan, C., Liu, Y., Penfield, T., Rao, V., Mouille, G., … Broun, P. (2007b). The Transcription Factor WIN1/SHN1 Regulates Cutin Biosynthesis in Arabidopsis thaliana. *The Plant Cell Online*, *19*(4), 1278–1294. https://doi.org/10.1105/tpc.106.047076

Khaled, A.-S., Vernoud, V., Ingram, G. C., Perez, P., Sarda, X., & Rogowsky, P. M. (2005). Engrailed-ZmOCL1 fusions cause a transient reduction of kernel size in maize. *Plant Molecular Biology*, *58*(1), 123–139. https://doi.org/10.1007/s11103-005-5219-y

Kim, G. T., Tsukaya, H., Saito, Y., & Uchimiya, H. (1999). Changes in the shapes of leaves and flowers upon overexpression of cytochrome P450 in Arabidopsis. *Proceedings of the National Academy of Sciences of the United States of America*, *96*(16), 9433–9437. https://doi.org/10.1073/pnas.96.16.9433

Kimbara, J., Yoshida, M., Ito, H., Kitagawa, M., Takada, W., Hayashi, K., … Ezura, H. (2013). Inhibition of CUTIN DEFICIENT 2 Causes Defects in Cuticle Function and Structure and Metabolite Changes in Tomato Fruit. *Plant and Cell Physiology*, *54*(9), 1535–1548. https://doi.org/10.1093/pcp/pct100

Koch, K., Bennemann, M., Bohn, H. F., Albach, D. C., & Barthlott, W. (2013). Surface microstructures of daisy florets (Asteraceae) and characterization of their anisotropic wetting. *Bioinspiration & Biomimetics*, *8*(3), 036005. https://doi.org/10.1088/1748-3182/8/3/036005

Koch, K., Bhushan, B., & Barthlott, W. (2008). Diversity of structure, morphology and wetting of plant surfaces. *Soft Matter*, *4*(10), 1943–1963. https://doi.org/10.1039/B804854A

Koch, K., & Ensikat, H.-J. (2008). The hydrophobic coatings of plant surfaces: Epicuticular wax crystals and their morphologies, crystallinity and molecular self-assembly. *Micron*, *39*(7), 759–772. https://doi.org/10.1016/J.MICRON.2007.11.010

Kolde, R. (2019). *pheatmap: pretty heatmaps. R package version*. Retrieved from https://cran.r-project.org/package=pheatmap

Koornneef, M., & Van Der Veen, J. H. (1980). Induction and Analysis of GibbereUin Sensitive Mutants in Arabidopsis thaliana (L.) Heynh. In Theor. Appl. genet (Vol. 58), 257-263. https://doi: 10.1007/BF00265176

Koornneeff, M., Dellaert, L. W. M., & van der Veen, J. H. (1982). EMS- and relation-induced mutation frequencies at individual loci in Arabidopsis thaliana (L.) Heynh. *Mutation Research/Fundamental and Molecular Mechanisms of Mutagenesis*, *93*(1), 109–123. https://doi.org/10.1016/0027-5107(82)90129-4

Kourounioti, R. L. A., Band, L. R., Fozard, J. A., Hampstead, A., Lovrics, A., Moyroud, E., … Glover, B. J. (2013b). Buckling as an origin of ordered cuticular patterns in flower petals. *Journal of The Royal Society Interface*, *10*(80). https://doi.org/10.1098/rsif.2012.0847

Kumar, C., Palacios, A., Surapaneni, V. A., Bold, G., Thielen, M., Licht, E., … Le Houérou, V. (2019). Replicating the complexity of natural surfaces: technique validation and applications for biomimetics, ecology and evolution. *Philosophical Transactions of the Royal Society A: Mathematical, Physical and Engineering Sciences*, *377*(2138),. https://doi.org/10.1098/rsta.2018.0265

Kunst, L., & Samuels, A. L. (2003). Biosynthesis and secretion of plant cuticular wax. *Progress in Lipid Research*, *42*(1), 51–80. https://doi.org/10.1016/S0163-7827(02)00045-0

Kurdyukov, S., Faust, A., Nawrath, C., Bär, S., Voisin, D., Efremova, N., … Yephremov, A. (2006). The epidermis-specific extracellular BODYGUARD controls cuticle development and morphogenesis in Arabidopsis. *The Plant Cell*, *18*(2), 321–339. https://doi.org/10.1105/tpc.105.036079

Kuromori, T., Sugimoto, E., & Shinozaki, K. (2011). Arabidopsis mutants of AtABCG22, an ABC transporter gene, increase water transpiration and drought susceptibility. *The Plant Journal*, *67*(5), 885–894. https://doi.org/10.1111/j.1365-313X.2011.04641.x

Kwiatkowska, M., Wojtczak, A., Popłońska, K., Polit, J. T., Stępiński, D., Domínguez, E., & Heredia, A. (2014). Cutinsomes and lipotubuloids appear to participate in cuticle formation in Ornithogalum umbellatum ovary epidermis: EM–immunogold research. *Protoplasma 2014 251:5*, *251*(5), 1151–1161. https://doi.org/10.1007/S00709-014-0623-2

Lai, P.-H., Huang, L.-M., Pan, Z.-J., Jane, W.-N., Chung, M.-C., Chen, W.-H., & Chen, H.-H. (2020). PeERF1, a SHINE-Like Transcription Factor, Is Involved in Nanoridge Development on Lip Epidermis of Phalaenopsis Flowers. *Frontiers in Plant Science*, *10*, 1709. https://doi.org/10.3389/fpls.2019.01709

Langmead, B., & Salzberg, S. L. (2012). Fast gapped-read alignment with Bowtie 2. *Nature Methods*,

9(4), 357–359. https://doi.org/10.1038/nmeth.1923

Lau, S.-E., Schwarzacher, T., Othman, R. Y., & Harikrishna, J. A. (2015). dsRNA silencing of an R2R3-MYB transcription factor affects flower cell shape in a Dendrobium hybrid. *BMC Plant Biology*, *15*(1), 194. https://doi.org/10.1186/s12870-015-0577-3

Lee, H. G., Park, M.-E., Park, B. Y., Kim, H. U., & Seo, P. J. (2019). The Arabidopsis MYB96 Transcription Factor Mediates ABA-Dependent Triacylglycerol Accumulation in Vegetative Tissues under Drought Stress Conditions. *Plants*, *8*(9), 296. https://doi.org/10.3390/plants8090296

Lee, H. G., & Seo, P. J. (2019). MYB96 recruits the HDA15 protein to suppress negative regulators of ABA signaling in Arabidopsis. *Nature Communications*, *10*(1), 1713. https://doi.org/10.1038/s41467-019-09417-1

Lee, S. B., Kim, H. U., & Suh, M. C. (2016). MYB94 and MYB96 Additively Activate Cuticular Wax Biosynthesis in Arabidopsis. *Plant and Cell Physiology*, *57*(11), 2300–2311. https://doi.org/10.1093/pcp/pcw147

Lee, Y. K., Kim, G.-T., Kim, I.-J., Park, J., Kwak, S.-S., Choi, G., & Chung, W.-I. (2006). LONGIFOLIA1 and LONGIFOLIA2, two homologous genes, regulate longitudinal cell elongation in Arabidopsis. *Development (Cambridge, England)*, *133*(21), 4305–4314. https://doi.org/10.1242/dev.02604

Li-Beisson, Y., Pollard, M., Sauveplane, V., Pinot, F., Ohlrogge, J., & Beisson, F. (2009). Nanoridges that characterize the surface morphology of flowers require the synthesis of cutin polyester. *Proceedings of the National Academy of Sciences*, *106*(51), 22008–22013. https://doi.org/10.1073/pnas.0909090106

Li-Beisson, Yonghua, Pollard, M., Sauveplane, V., Pinot, F., Ohlrogge, J., & Beisson, F. (2009). Nanoridges that characterize the surface morphology of flowers require the synthesis of cutin polyester. *Proceedings of the National Academy of Sciences of the United States of America*, *106*(51), 22008–22013. https://doi.org/10.1073/pnas.0909090106

Li, S., Wang, X., He, S., Li, J., Huang, Q., Imaizumi, T., … Gu, H. (2016). CFLAP1 and CFLAP2 Are Two bHLH Transcription Factors Participating in Synergistic Regulation of AtCFL1-Mediated Cuticle Development in Arabidopsis. *PLoS Genetics*, *12*(1), e1005744. https://doi.org/10.1371/journal.pgen.1005744

Li, Z., Peng, R., Tian, Y., Han, H., Xu, J., & Yao, Q. (2016). Genome-Wide Identification and Analysis of the MYB Transcription Factor Superfamily in Solanum lycopersicum. *Plant and Cell Physiology*, 1665–1677. https://doi.org/10.1093/pcp/pcw091

Lin, Q., Ohashi, Y., Kato, M., Tsuge, T., Gu, H., Qu, L.-J., & Aoyama, T. (2015). GLABRA2 Directly Suppresses Basic Helix-Loop-Helix Transcription Factor Genes with Diverse Functions in Root Hair Development. *The Plant Cell*, *27*(10), 2894–2906. https://doi.org/10.1105/tpc.15.00607

Ling, H.-Q., Bauer, P., Bereczky, Z., Keller, B., & Ganal, M. (2002). The tomato fer gene encoding a bHLH protein controls iron-uptake responses in roots. *Proceedings of the National Academy of Sciences of the United States of America*, *99*(21), 13938–13943. https://doi.org/10.1073/pnas.212448699

Ling, K.-H. J., & Hanzlik, R. P. (1989). Deuterium isotope effects on toluene metabolism. Product release as a rate-limiting step in cytochrome P-450 catalysis. *Biochemical and Biophysical Research Communications*, *160*(2), 844–849. https://doi.org/10.1016/0006-291X(89)92511-4

Love, M. I., Huber, W., & Anders, S. (2014). Moderated estimation of fold change and dispersion for RNA-seq data with DESeq2. *Genome Biology*, *15*(12), 550. https://doi.org/10.1186/s13059-014-0550-8

Lu, X., Kim, H., Zhong, S., Chen, H., Hu, Z., & Zhou, B. (2014). De novo transcriptome assembly for rudimentary leaves in Litchi chinesis Sonn. and identification of differentially expressed genes in

response to reactive oxygen species. *BMC Genomics*, *15*(1), 805. https://doi.org/10.1186/1471-2164-15-805

Martin, L. B. B., Sherwood, R. W., Nicklay, J. J., Yang, Y., Muratore-Schroeder, T. L., Anderson, E. T., … Zhang, S. (2016). Application of wide selected-ion monitoring data-independent acquisition to identify tomato fruit proteins regulated by the CUTIN DEFICIENT2 transcription factor. *PROTEOMICS*, *16*(15–16), 2081–2094. https://doi.org/10.1002/pmic.201500450

Mazurek, S., Garroum, I., Daraspe, J., De Bellis, D., Olsson, V., Mucciolo, A., … Nawrath, C. (2017). Connecting the Molecular Structure of Cutin to Ultrastructure and Physical Properties of the Cuticle in Petals of Arabidopsis. *Plant Physiology*, *173*(2), 1146–1163. https://doi.org/10.1104/pp.16.01637

McGettigan, P. A. (2013). Transcriptomics in the RNA-seq era. *Current Opinion in Chemical Biology*, *17*(1), 4–11. https://doi.org/10.1016/J.CBPA.2012.12.008

Mckinney, D. E., Bortiatynski, J. M., Carson, D. M., Clifford, D. J., De Leeuw, J. W., & Hatcher, P. G. (1996). Tetramethylammonium hydroxide (TMAH) thermochemolysis of the aliphatic biopolymer cutan: insights into the chemical structure. *Organic Geochemistry*, *24*(6–7), 641–650. https://doi.org/10.1016/0146-6380(96)00055-1

Mele, E., Girardo, S., & Pisignano, D. (2012). Strelitzia reginae Leaf as a Natural Template for Anisotropic Wetting and Superhydrophobicity. *Langmuir*, *28*(11), 5312–5317. https://doi.org/10.1021/la300243x

Middleton, R., Sinnott-Armstrong, M., Ogawa, Y., Jacucci, G., Moyroud, E., Rudall, P. J., … Vignolini, S. (2020). Viburnum tinus Fruits Use Lipids to Produce Metallic Blue Structural Color. *Current Biology*, *30*(19), 3804-3810.e2. https://doi.org/10.1016/J.CUB.2020.07.005

Milani, P., Gholamirad, M., Traas, J., Arnéodo, A., Boudaoud, A., Argoul, F., & Hamant, O. (2011). In vivo analysis of local wall stiffness at the shoot apical meristem in Arabidopsis using atomic force microscopy. *The Plant Journal*, *67*(6), 1116–1123. https://doi.org/10.1111/j.1365-313X.2011.04649.x

Młodzińska, E. (2009). Survey of Plant Pigments: Molecular and Environmental Determinants of Plant Colors. *ACTA BIOLOGICA CRACOVIENSIA Series Botanica*, (51), 7–16. Retrieved from http://abcbot.pl/pdf/51_1/07_16_mlodzinska.pdf

Molina, I., & Kosma, D. (2015). Role of HXXXD-motif/BAHD acyltransferases in the biosynthesis of extracellular lipids. *Plant Cell Reports*, *34*(4), 587–601. https://doi.org/10.1007/s00299-014-1721-5

Moyroud, E., Monniaux, M., Thévenon, E., Dumas, R., Scutt, C. P., Frohlich, M. W., & Parcy, F. (2017). A link between LEAFY and B-gene homologues in Welwitschia mirabilis sheds light on ancestral mechanisms prefiguring floral development. *The New Phytologist*, *216*(2), 469–481. https://doi.org/10.1111/nph.14483

Moyroud, E., Wenzel, T., Middleton, R., Rudall, P. J., Banks, H., Reed, A., … Glover, B. J. (2017). Disorder in convergent floral nanostructures enhances signalling to bees. *Nature*, *550*(7677), 469–474. https://doi.org/10.1038/nature24285

Murray, B. G., Craven, L. A., & De Lange, P. J. (2008). *New observations on chromosome number variation in Hibiscus trionum s.l. (Malvaceae) and their implications for systematics and conservation*, *New zeland Journal of Botany*, 46, 315-319 https://doi.org/10.1080/00288250809509769

Nadiminti, P. P., Rookes, J. E., Boyd, B. J., & Cahill, D. M. (2015). Confocal laser scanning microscopy elucidation of the micromorphology of the leaf cuticle and analysis of its chemical composition. *Protoplasma*, *252*(6), 1475–1486. https://doi.org/10.1007/s00709-015-0777-6

Nakamura, M., Katsumata, H., Abe, M., Yabe, N., Komeda, Y., Yamamoto, K. T., & Takahashi, T. (2006). Characterization of the class IV homeodomain-Leucine Zipper gene family in

Arabidopsis. *Plant Physiology*, *141*(4), 1363–1375. https://doi.org/10.1104/pp.106.077388

Navarro, M., Ayax, C., Martinez, Y., Laur, J., El Kayal, W., Marque, C., & Teulières, C. (2011). Two EguCBF1 genes overexpressed in Eucalyptus display a different impact on stress tolerance and plant development. *Plant Biotechnology Journal*, *9*(1), 50–63. https://doi.org/10.1111/j.1467-7652.2010.00530.x

Negruk, V., Yang, P., Subramanian, M., McNevin, J. P., & Lemieux, B. (1996). Molecular cloning and characterization of the CER2 gene of Arabidopsis thaliana. *The Plant Journal*, *9*(2), 137–145. https://doi.org/10.1046/j.1365-313X.1996.09020137.x

Nelson, S. L., Giver, C. R., & Grosovsky, A. J. (1994). *Spectrum of X-ray-induced mutations in the human hprt gene. Carcinogenesis* (Vol. 15 n°3), 495-502 Retrieved from https://academic.oup.com/carcin/article/15/3/495/259635

Niisslein-Volhard, C., Wieschaus, E., & Kluding, H. (1984). Mutations affecting the pattern of the larval cuticle in Drosophila melanogaster I. Zygotic loci on the second chromosome. Roux's Archives of Developmental Biology (Vol. 193), 267-282. https:// 10.1007/BF00848156

Oh, E., Kim, J., Park, E., Kim, J.-I., Kang, C., & Choi, G. (2004). PIL5, a phytochrome-interacting basic helix-loop-helix protein, is a key negative regulator of seed germination in Arabidopsis thaliana. *The Plant Cell*, *16*(11), 3045–3058. https://doi.org/10.1105/tpc.104.025163

Oshima, Y., & Mitsuda, N. (2013). The MIXTA-like Transcription factor MYB16 is a major regulator of cuticle formation in vegetative organs. *Plant Signaling & Behavior*, *8*(11), e26826. https://doi.org/10.4161/psb.26826

Oshima, Y., Shikata, M., Koyama, T., Ohtsubo, N., Mitsuda, N., & Ohme-Takagi, M. (2013). MIXTA-like transcription factors and WAX INDUCER1/SHINE1 coordinately regulate cuticle development in Arabidopsis and Torenia fournieri. *The Plant Cell*, *25*(5), 1609–1624. https://doi.org/10.1105/tpc.113.110783

Panikashvili, D., Shi, J. X., Schreiber, L., & Aharoni, A. (2009). The Arabidopsis DCR encoding a soluble BAHD acyltransferase is required for cutin polyester formation and seed hydration properties. *Plant Physiology*, *151*(4), 1773–1789. https://doi.org/10.1104/pp.109.143388

Panikashvili, D., Shi, J. X., Schreiber, L., & Aharoni, A. (2011). The Arabidopsis ABCG13 transporter is required for flower cuticle secretion and patterning of the petal epidermis. *New Phytologist*, *190*(1), 113–124. https://doi.org/10.1111/j.1469-8137.2010.03608.x

Pascal, S., Bernard, A., Deslous, P., Gronnier, J., Fournier-Goss, A., Domergue, F., … Joubès, J. (2019). Arabidopsis CER1-LIKE1 Functions in a Cuticular Very-Long-Chain Alkane-Forming Complex. *Plant Physiology*, *179*(2), 415–432. https://doi.org/10.1104/pp.18.01075

Patro, R., Duggal, G., Love, M. I., Irizarry, R. A., & Kingsford, C. (2017). Salmon provides fast and bias-aware quantification of transcript expression. *Nature Methods*, *14*(4), 417–419. https://doi.org/10.1038/nmeth.4197

Pattrick, J. G., Labonte, D., & Federle, W. (2018). Scaling of claw sharpness: mechanical constraints reduce attachment performance in larger insects. *Journal of Experimental Biology*, *221*(24). https://doi.org/10.1242/jeb.188391

Perez-Rodriguez, M., Jaffe, F. W., Butelli, E., Glover, B. J., Martin, C., & Schwarz-Sommer, Z. (2005). Development of three different cell types is associated with the activity of a specific MYB transcription factor in the ventral petal of Antirrhinum majus flowers. *Development (Cambridge, England)*, *132*(2), 359–370. https://doi.org/10.1242/dev.01584

Petit, J., Bres, C., Mauxion, J. P., Tai, F. W. J., Martin, L. B. B., Fich, E. A., … Rothan, C. (2016). The glycerol-3-phosphate acyltransferase GPAT6 from tomato plays a central role in fruit cutin biosynthesis. *Plant Physiology*, *171*(2), 894-913. https://doi.org/10.1104/pp.16.00409

Pighin, J. A., Zheng, H., Balakshin, L. J., Goodman, I. P., Western, T. L., Jetter, R., … Samuels, A. L. (2004). Plant Cuticular Lipid Export Requires an ABC Transporter. *Science*, *306*(5696), 702–704. https://doi.org/10.1126/science.1102331

Pouvreau, A. (1991). Morphology and histology of tarsal glands in bumble bees of the genera Bombus , Pyrobombus , and Megabombus. *Canadian Journal of Zoology*, *69*(4), 866–872. https://doi.org/10.1139/z91-130

Quave, C. L., Estévez-Carmona, M., Compadre, C. M., Hobby, G., Hendrickson, H., Beenken, K. E., & Smeltzer, M. S. (2012). Ellagic acid derivatives from Rubus ulmifolius inhibit Staphylococcus aureus biofilm formation and improve response to antibiotics. *PloS One*, *7*(1), e28737. https://doi.org/10.1371/journal.pone.0028737

Radotić, K., Roduit, C., Simonović, J., Hornitschek, P., Fankhauser, C., Mutavdžić, D., … Kasas, S. (2012). Atomic Force Microscopy Stiffness Tomography on Living Arabidopsis thaliana Cells Reveals the Mechanical Properties of Surface and Deep Cell-Wall Layers during Growth. *Biophysical Journal*, *103*(3), 386–394. https://doi.org/10.1016/J.BPJ.2012.06.046

Rahnenfuhrer, J., & Adrian, A. (2018). *topGO: Enrichment Analysis for Gene Ontology*.

Rani, S. H., Krishna, T. H. A., Saha, S., Negi, A. S., & Rajasekharan, R. (2010). Defective in cuticular ridges (DCR) of Arabidopsis thaliana, a gene associated with surface cutin formation, encodes a soluble diacylglycerol acyltransferase. *The Journal of Biological Chemistry*, *285*(49), 38337–38347. https://doi.org/10.1074/jbc.M110.133116

Ranocha, P., Denancé, N., Vanholme, R., Freydier, A., Martinez, Y., Hoffmann, L., … Goffner, D. (2010). Walls are thin 1 (WAT1), an Arabidopsis homolog of Medicago truncatula NODULIN21, is a tonoplast-localized protein required for secondary wall formation in fibers. *The Plant Journal*, *63*(3), 469–483. https://doi.org/10.1111/j.1365-313X.2010.04256.x

Ren, H., Dang, X., Yang, Y., Huang, D., Liu, M., Gao, X., & Lin, D. (2016). SPIKE1 Activates ROP GTPase to Modulate Petal Growth and Shape. *Plant Physiology*, *172*(1), 358–371. https://doi.org/10.1104/pp.16.00788

Riechmann, J. L., & Ratcliffe, O. J. (2000). A genomic perspective on plant transcription factors. *Current Opinion in Plant Biology*, *3*(5), 423–434. https://doi.org/10.1016/S1369-5266(00)00107-2

Riederer, M., & Muller, C. (2006). *Biology of the plant cuticle,* Chapter 4: Composition of the plant cuticle*. Annual Plant reviews Vol 23,* 145-207. Blackwell Publishing Ltd. Retrieved from https://books.google.co.uk/books?hl=fr&lr=&id=qaJVSVYZhVQC&oi=fnd&pg=PA145&dq=Composition+of+plant+cuticular+waxes.+Jetter+2007&ots=UU_qc4u-PV&sig=_nJ8lIIWgOOjrDF-thB3DisGdPY#v=onepage&q&f=false

Rohrs, C., Azimi, A., & He, P. (2019). *Wetting on Micropatterned Surfaces: Partial Penetration in the Cassie State and Wenzel Deviation Theoretically Explained*. Langmuir, 35, 15421-15430 https://doi.org/10.1021/acs.langmuir.9b03002

Rowland, O., Lee, R., Franke, R., Schreiber, L., & Kunst, L. (2007). The CER3 wax biosynthetic gene from Arabidopsis thaliana is allelic to WAX2/YRE/FLP1. *FEBS Letters*, *581*(18), 3538–3544. https://doi.org/10.1016/J.FEBSLET.2007.06.065

Rowland, O., Zheng, H., Hepworth, S. R., Lam, P., Jetter, R., & Kunst, L. (2006). CER4 encodes an alcohol-forming fatty acyl-coenzyme A reductase involved in cuticular wax production in Arabidopsis. *Plant Physiology*, *142*(3), 866–877. https://doi.org/10.1104/pp.106.086785

Saleh, A., & Pagés, M. (2003). Plant AP2/ERF transcription factors. *Genetika*, *35*(1), 37–50. https://doi.org/10.2298/GENSR0301037S

Salminen, T. A., Blomqvist, K., & Edqvist, J. (2016). Lipid transfer proteins: classification, nomenclature, structure, and function. *Planta*, *244*(5), 971–997. https://doi.org/10.1007/s00425-016-2585-4

Samuels, L., Kunst, L., & Jetter, R. (2008). Sealing Plant Surfaces: Cuticular Wax Formation by Epidermal Cells. *Annual Review of Plant Biology*, *59*(1), 683–707. https://doi.org/10.1146/annurev.arplant.59.103006.093219

San Segundo, I. M., Scavée, G. M. L., Pedersen, S. B. R., Segerson, N., Rose, J. K. C., & Clausen, M. H. (2019). Synthesis and Oligomerization of 10,16-Dihydroxyhexadecanoyl Esters with Different Head-Groups for the Study of CUS1 Selectivity. *European Journal of Organic Chemistry*, *2019*(33), 5704–5708. https://doi.org/10.1002/ejoc.201900863

Sharma, V., Crne, M., Park, J. O., & Srinivasarao, M. (2014). Bouligand Structures Underlie Circularly Polarized Iridescence of Scarab Beetles: A Closer View. *Materials Today: Proceedings*, *1*, 161–171. https://doi.org/10.1016/J.MATPR.2014.09.019

Shi, J. X., Adato, A., Alkan, N., He, Y., Lashbrooke, J., Matas, A. J., … Aharoni, A. (2013). The tomato SlSHINE3 transcription factor regulates fruit cuticle formation and epidermal patterning. *New Phytologist*, *197*(2), 468–480. https://doi.org/10.1111/nph.12032

Shi, J. X., Malitsky, S., De Oliveira, S., Branigan, C., Franke, R. B., Schreiber, L., & Aharoni, A. (2011). SHINE Transcription Factors Act Redundantly to Pattern the Archetypal Surface of Arabidopsis Flower Organs. *PLoS Genetics*, *7*(5), e1001388. https://doi.org/10.1371/journal.pgen.1001388

Specht, C. D., & Bartlett, M. E. (2009). *Flower Evolution: The Origin and Subsequent Diversification of the Angiosperm Flower*. *Annu. Rev. Ecol. Evol. Syst*, 40, 217-243 https://doi.org/10.1146/annurev.ecolsys.110308.120203

Staehelin, L. A. (1997). The plant ER: a dynamic organelle composed of a large number of discrete functional domains. *The Plant Journal*, *11*(6), 1151–1165. https://doi.org/10.1046/j.1365-313X.1997.11061151.x

Stafford, C. M., Harrison, C., Beers, K. L., Karim, A., Amis, E. J., VanLandingham, M. R., … Simonyi, E. E. (2004). A buckling-based metrology for measuring the elastic moduli of polymeric thin films. *Nature Materials*, *3*(8), 545–550. https://doi.org/10.1038/nmat1175

Stępiński, D., Kwiatkowska, M., Wojtczak, A., Polit, J. T., Domínguez, E., Heredia, A., & Popłońska, K. (2020). The Role of Cutinsomes in Plant Cuticle Formation. *Cells*, *9*(8), 1778. https://doi.org/10.3390/cells9081778

Stracke, R., Werber, M., & Weisshaar, B. (2001). The R2R3-MYB gene family in Arabidopsis thaliana. *Current Opinion in Plant Biology*, *4*(5), 447–456. https://doi.org/10.1016/S1369-5266(00)00199-0

Stuart-Fox, D., Ospina-Rozo, L., Ng, L., & Franklin, A. M. (2021). The Paradox of Iridescent Signals. *Trends in Ecology & Evolution*, *36*(3), 187–195. https://doi.org/10.1016/J.TREE.2020.10.009

Sudheeran, P. K., Ovadia, R., Galsarker, O., Maoz, I., Sela, N., Maurer, D., … Alkan, N. (2020). Glycosylated flavonoids: fruit's concealed antifungal arsenal. *New Phytologist*, *225*(4), 1788–1798. https://doi.org/10.1111/nph.16251

Sun, G., Ji, Q., Dilcher, D. L., Zheng, S., Nixon, K. C., & Wang, X. (2002). Archaefructaceae, a new basal angiosperm family. *Science (New York, N.Y.)*, *296*(5569), 899–904. https://doi.org/10.1126/science.1069439

Sun, W., Li, Y., Zhao, Y., & Zhang, H. (2015). The TsnsLTP4, a Nonspecific Lipid Transfer Protein Involved in Wax Deposition and Stress Tolerance. *Plant Molecular Biology Reporter*, *33*(4), 962–974. https://doi.org/10.1007/s11105-014-0798-x

Surapaneni, V. A., Bold, G., Speck, T., & Thielen, M. (2020). Spatio-temporal development of cuticular ridges on leaf surfaces of *Hevea brasiliensis* alters insect attachment. *Royal Society Open Science*, *7*(11), 201319. https://doi.org/10.1098/rsos.201319

Szécsi, J., Joly, C., Bordji, K., Varaud, E., Cock, J. M., Dumas, C., & Bendahmane, M. (2006).

BIGPETALp, a bHLH transcription factor is involved in the control of Arabidopsis petal size. *The EMBO Journal*, *25*(16), 3912–3920. https://doi.org/10.1038/sj.emboj.7601270

Takahashi, K., Shimada, T., Kondo, M., Tamai, A., Mori, M., Nishimura, M., & Hara-Nishimura, I. (2010). Ectopic Expression of an Esterase, Which is a Candidate for the Unidentified Plant Cutinase, Causes Cuticular Defects in Arabidopsis thaliana. *Plant and Cell Physiology*, *51*(1), 123–131. https://doi.org/10.1093/pcp/pcp173

Taylor, D. W., Li, H., Dahl, J., Fago, F. J., Zinniker, D., & Moldowan, J. M. (2006). Biogeochemical Evidence for the Presence of the Angiosperm Molecular Fossil Oleanane in Paleozoic and Mesozoic Non-Angiospermous Fossils. *Paleobiology*, Vol. 32, pp. 179–190. https://doi.org/10.2307/4096994

Thomas, K. R., Kolle, M., Whitney, H. M., Glover, B. J., & Steiner, U. (2010). Function of blue iridescence in tropical understorey plants. *Journal of the Royal Society, Interface*, *7*(53), 1699–1707. https://doi.org/10.1098/rsif.2010.0201

To, A., Joubès, J., Barthole, G., Lécureuil, A., Scagnelli, A., Jasinski, S., … Baud, S. (2012). WRINKLED transcription factors orchestrate tissue-specific regulation of fatty acid biosynthesis in Arabidopsis. *The Plant Cell*, *24*(12), 5007–5023. https://doi.org/10.1105/tpc.112.106120

Tsuge, T., Tsukaya, H., & Uchimiya, H. (1996). Two independent and polarized processes of cell elongation regulate leaf blade expansion in Arabidopsis thaliana (L) Heynh. *Development*, *122*(5), 1589–1600. Retrieved from http://www.ncbi.nlm.nih.gov/pubmed/8625845

Urbano, F. (2017). *corset: Arbitrary Bounding of Series and Time Series Objects*.

USDA, Agricultural Research Service, N. P. G. S. N. G. R. (2020). The Hibiscus genus. Retrieved December 2, 2020, from https://npgsweb.ars-grin.gov/gringlobal/taxonomygenus?id=5665

van Doorn, W. G., Beers, E. P., Dangl, J. L., Franklin-Tong, V. E., Gallois, P., Hara-Nishimura, I., … Bozhkov, P. V. (2011). Morphological classification of plant cell deaths. *Cell Death & Differentiation*, *18*(8), 1241–1246. https://doi.org/10.1038/cdd.2011.36

van Es, S. W., Silveira, S. R., Rocha, D. I., Bimbo, A., Martinelli, A. P., Dornelas, M. C., … Immink, R. G. H. (2018). Novel functions of the Arabidopsis transcription factor TCP5 in petal development and ethylene biosynthesis. *The Plant Journal*, *94*(5), 867–879. https://doi.org/10.1111/tpj.13904

VATTEM, D. A., & SHETTY, K. (2005). BIOLOGICAL FUNCTIONALITY OF ELLAGIC ACID: A REVIEW. *Journal of Food Biochemistry*, *29*(3), 234–266. https://doi.org/10.1111/j.1745-4514.2005.00031.x

Vignolini, S., Moyroud, E., Hingant, T., Banks, H., Rudall, P. J., Steiner, U., & Glover, B. J. (2015). The flower of Hibiscus trionum is both visibly and measurably iridescent. *New Phytologist*, *205*(1), 97–101. https://doi.org/10.1111/nph.12958

Vignolini, S., Rudall, P. J., Rowland, A. V, Reed, A., Moyroud, E., Faden, R. B., … Steiner, U. (2012). Pointillist structural color in Pollia fruit. *Proceedings of the National Academy of Sciences of the United States of America*, *109*(39), 15712–15715. https://doi.org/10.1073/pnas.1210105109

Voigt, D., Schuppert, J. M., Dattinger, S., & Gorb, S. N. (2008). Sexual dimorphism in the attachment ability of the Colorado potato beetle Leptinotarsa decemlineata (Coleoptera: Chrysomelidae) to rough substrates. *Journal of Insect Physiology*, *54*(5), 765–776. https://doi.org/10.1016/J.JINSPHYS.2008.02.006

Wagner, T. A., & Kohorn, B. D. (2001). Wall-associated kinases are expressed throughout plant development and are required for cell expansion. *The Plant Cell*, *13*(2), 303–318. https://doi.org/10.1105/tpc.13.2.303

Wang, J., Wang, H., Ding, L., Song, A., Shen, F., Jiang, J., … Chen, · Fadi. (2017a). Transcriptomic and hormone analyses reveal mechanisms underlying petal elongation in Chrysanthemum

morifolium “Jinba.” *Plant Molecular Biology*, *93*, 593–606. https://doi.org/10.1007/s11103-017-0584-x

Wang, J., Wang, H., Ding, L., Song, A., Shen, F., Jiang, J., … Chen, F. (2017b). Transcriptomic and hormone analyses reveal mechanisms underlying petal elongation in Chrysanthemum morifolium ‘Jinba.’ *Plant Molecular Biology*, *93*(6), 593–606. https://doi.org/10.1007/s11103-017-0584-x

Weng, H., Molina, I., Shockey, J., & Browse, J. (2010). Organ fusion and defective cuticle function in a lacs1 lacs2 double mutant of Arabidopsis. *Planta*, *231*(5), 1089–1100. https://doi.org/10.1007/s00425-010-1110-4

Whitney, H. M., Chittka, L., Bruce, T. J. A., & Glover, B. J. (2009). Conical Epidermal Cells Allow Bees to Grip Flowers and Increase Foraging Efficiency. *Current Biology*, *19*(11), 948–953. https://doi.org/10.1016/J.CUB.2009.04.051

Whitney, H. M., Kolle, M., Andrew, P., Chittka, L., Steiner, U., & Glover, B. J. (2009). Floral Iridescence, Produced by Diffractive Optics, Acts As a Cue for Animal Pollinators. *Science*, *323*(5910), 130–133. https://doi.org/10.1126/science.1166256

Whitney, H. M., Poetes, R., Steiner, U., Chittka, L., & Glover, B. J. (2011). Determining the Contribution of Epidermal Cell Shape to Petal Wettability Using Isogenic Antirrhinum Lines. *PLoS ONE*, *6*(3), e17576. https://doi.org/10.1371/journal.pone.0017576

Whitney, H. M., Reed, A., Rands, S. A., Chittka, L., & Glover, B. J. (2016). Flower Iridescence Increases Object Detection in the Insect Visual System without Compromising Object Identity. *Current Biology*, *26*(6), 802–808. https://doi.org/10.1016/j.cub.2016.01.026

Wickham, H. (2016). Ggplot2 : elegant graphics for data analysis. In *Sprinter-Verlag*. Retrieved from https://cran.r-project.org/web/packages/ggplot2/citation.html

Xia, Y., Nikolau, B. J., & Schnable, P. S. (1997). Developmental and hormonal regulation of the arabidopsis CER2 gene that codes for a nuclear-localized protein required for the normal accumulation of cuticular waxes. *Plant Physiology*, *115*(3), 925–937. https://doi.org/10.1104/pp.115.3.925

Yang, W., Pollard, M., Li-Beisson, Y., & Ohlrogge, J. (2016). Quantitative analysis of glycerol in dicarboxylic acid-rich cutins provides insights into Arabidopsis cutin structure. *Phytochemistry*, *130*, 159–169. https://doi.org/10.1016/J.PHYTOCHEM.2016.03.017

Yang, Y., Pan, Y., & Guo, P. (2017). Structural coloration of metallic surfaces with micro/nano-structures induced by elliptical vibration texturing. *Applied Surface Science*, *402*, 400–409. https://doi.org/10.1016/j.apsusc.2017.01.026

Yanhui, C., Xiaoyuan, Y., Kun, H., Meihua, L., Jigang, L., Zhaofeng, G., … Li-Jia, Q. (2006). The MYB Transcription Factor Superfamily of Arabidopsis: Expression Analysis and Phylogenetic Comparison with the Rice MYB Family. *Plant Molecular Biology*, *60*(1), 107–124. https://doi.org/10.1007/s11103-005-2910-y

Yeats, T. H., Huang, W., Chatterjee, S., Viart, H. M.-F. H. M.-F., Clausen, M. H., Stark, R. E., & Rose, J. K. C. (2014). Tomato Cutin Deficient 1 (CD1) and putative orthologs comprise an ancient family of cutin synthase-like (CUS) proteins that are conserved among land plants. *Plant Journal*, *77*(5), 667–675. https://doi.org/10.1111/tpj.12422

Yeats, T. H., Martin, L. B. B., Viart, H. M.-F., Isaacson, T., He, Y., Zhao, L., … Rose, J. K. C. (2012). The identification of cutin synthase: formation of the plant polyester cutin. *Nature Chemical Biology*, *8*(7), 609–611. https://doi.org/10.1038/nchembio.960

Yeats, T. H., & Rose, J. K. C. (2013). The Formation and Function of Plant Cuticles. *Plant Physiology*, *163*(1), 5–20. https://doi.org/10.1104/pp.113.222737

Yephremov, A., Wisman, E., Huijser, P., Huijser, C., Wellesen, K., & Saedler, H. (1999). Characterization of the FIDDLEHEAD Gene of Arabidopsis Reveals a Link between Adhesion

Response and Cell Differentiation in the Epidermis. *THE PLANT CELL ONLINE*, *11*(11), 2187–2202. https://doi.org/10.1105/tpc.11.11.2187

Zenoni, S., Reale, L., Tornielli, G. B., Lanfaloni, L., Porceddu, A., Ferrarini, A., … Pezzotti, M. (2004). Downregulation of the Petunia hybrida alpha-expansin gene PhEXP1 reduces the amount of crystalline cellulose in cell walls and leads to phenotypic changes in petal limbs. *The Plant Cell*, *16*(2), 295–308. https://doi.org/10.1105/tpc.018705

Zhang, J.-Y., Broeckling, C. D., Blancaflor, E. B., Sledge, M. K., Sumner, L. W., & Wang, Z.-Y. (2005). Overexpression of WXP1, a putative Medicago truncatula AP2 domain-containing transcription factor gene, increases cuticular wax accumulation and enhances drought tolerance in transgenic alfalfa (Medicago sativa). *The Plant Journal*, *42*(5), 689–707. https://doi.org/10.1111/j.1365-313X.2005.02405.x

Zhang, J.-Y., Broeckling, C. D., Sumner, L. W., & Wang, Z.-Y. (2007). Heterologous expression of two Medicago truncatula putative ERF transcription factor genes, WXP1 and WXP2, in Arabidopsis led to increased leaf wax accumulation and improved drought tolerance, but differential response in freezing tolerance. *Plant Molecular Biology*, *64*(3), 265–278. https://doi.org/10.1007/s11103-007-9150-2

Zhao, L., Haslam, T. M., Sonntag, A., Molina, I., & Kunst, L. (2019). Functional overlap of long-chain acyl-CoA synthetases in Arabidopsis. *Plant and Cell Physiology*, *60*(5). https://doi.org/10.1093/pcp/pcz019

Zhu, Y.-Q., Xu, K.-X., Luo, B., Wang, J.-W., & Chen, X.-Y. (2003). An ATP-Binding Cassette Transporter GhWBC1 from Elongating Cotton Fibers. *Plant Physiology*, *133*(2), 580–588. https://doi.org/10.1104/pp.103.027052

Zhu, Z., Chen, G., Guo, X., Yin, W., Yu, X., Hu, J., & Hu, Z. (2017). Overexpression of SlPRE2, an atypical bHLH transcription factor, affects plant morphology and fruit pigment accumulation in tomato. *Scientific Reports*, *7*(1), 5786. https://doi.org/10.1038/s41598-017-04092-y

Zimmermann, E. A., Gludovatz, B., Schaible, E., Dave, N. K. N., Yang, W., Meyers, M. A., & Ritchie, R. O. (2013). Mechanical adaptability of the Bouligand-type structure in natural dermal armour. *Nature Communications*, *4*(1), 2634. https://doi.org/10.1038/ncomms3634

Annexes

Medium	Composition
LB	• Tryptone (10g/L) • NaCl (10g/L) • yeast extract (5g/L)
LBAgar	• Tryptone (10g/L) • NaCl (10g/L) • yeast extract (5g/L) • Agar (15g/L)
MS Hib	• Murashige and Skoog medium (4.4g/L) • sucrose (35g/L), L-cystein (40mg/L) • Ascorbic acid (15mg/L) • Plant Agar (8g/L) • pH was balanced to 5.7 with KOH
MS/2 Hib	• Murashige and Skoog medium (2,2g/L) • Sucrose (25g/L) • Plant Agar (6g/L) • pH was balanced to 5.7 with KOH
MS 3% sucrose	• 1.1g Murashige and Skoog • 15g sucrose • Up to 500mL ddH20 • pH was balanced to 5.7 with KOH

Annex I: Recipes of media for bacterial culture and *Hibiscus trionum* transformation and tissue culture

Primer name (F for Forward; R for Reverse)	Sequence (5'→ 3')	Locus	Purpose
JF9 F	CGACACCCAGCAGTTTTCAA	*HtLTP*	Gene cloning
JF10 R	AACAAAACATAAACGTTCATTCATAAAACAC	*HtLTP*	Gene cloning
JF44 F	GGCTTGTCTTAAGCTTGTTTCTG	*HtLTP*	semiQ RT-PCR
JF45 R	TCACTTCACACTGTTGCAGTTAG	*HtLTP*	semiQ RT-PCR
JF11 F	GGGGGGATCCCGACACCCAGCAGTTTTCAA	*HtLTP*	5' tailing
JF12 R	GGGCCCGGGAACAAAACATAAACGTTCATTCATAAAACAC	*HtLTP*	3' tailing
JF1 F	GGGGATCCATGGTGCAGTCGAAGAAGT	*HtSHN2*	5' tailing
JF2 R	**GGGCCCGGGCTAAAGAAACAAGTTACTCTCCC**	*HtSHN2*	3' tailing
JF 48 F	TACTAAAGAGAAGGGTGTGGC	*HtSHN2*	semiQ RT-PCR
JF 49 R	CCCCTTCAGCAAACGAAG	*HtSHN2*	semiQ RT-PCR
JF46 F	GGTACAGTCCAAGAAGTTCAGAG	*HtSHN3*	semiQ RT-PCR
JF47 R	ATCATCTGCAATGCCGCCTTCT	*HtSHN3*	semiQ RT-PCR
JF50F	TATGGCTCGGGACATTCGAG	*HtSHN1*	semiQ RT-PCR
JF51R	TAGTCGAAGACGAAGACCCC	*HtSHN1*	semiQ RT-PCR
JF40 F	GGG-GCTCTTC-GTCTC-A-AAGCTT-ATGATTTTCATTGCGGTTGC	*HtHAT*	5' tailed primer for TypeII S assembly
JF41 R	GGG-GCTCTTC-GTCTC-A-CCCGGG-CGACGATTTTCATCCAACAA	*HtHAT*	3' tailed primer for TypeII S assembly
JF 38 F	GGG-GCTCTTC-GTCTC-A-CCCGGG-ATCAAGGACATGGCAGCCGAA	*HtDCR*	5' tailed primer for TypeII S assembly
JF39 R	GGG-GCTCTTC-GTCTC-A-GAATTC-GCAGAGGAGGAGGAACTAGACTTCC	*HtDCR*	3' tailed primer for typeII S assembly
JF 35S F	CCCAGCTATCTGTCACTTCATCGA	*35S promotor (pEM110)*	Genotyping
JF 35S R	TTATCGGGAAACTACTCACACA	*35 S terminator (pEM110)*	Genotyping
M13 F	TGTAAAACGACGGCCAGT	*pBlueSCRIPT*	Genotyping
M13 R	CAGGAAACAGCTATGACCATG	*pBlueSCRIPT*	Genotyping
ActS4 F	CCCAGATCATGTTTGAGACCTT	*ActinS4*	Housekeeping gene for semi quantitative PCR
ActS4 R	ACCGGAATCCAGCACAATAC	*ActinS4*	Housekeeping gene for semi quantitative PCR
AC284	TCACGGAGAAGTTGTACGAACTCG	HtGDSL-like	semiQ RT-PCR
AC292	CGGTTCTCTCCAATGGCATACAC	HtGDSL-like	semiQ RT-PCR
AC309	TCAGCGACGCCAAGCTCTG	HtCYP77a6-like1	semiQ RT-PCR
AC310	CATTGACGGTGAACTTGTTGCAG	HtCYP77a6-like1	semiQ RT-PCR

Annex II: Sequences of primers used for the molecular work in this thesis.

HtSHN1 cDNA sequence:

ATGGTACAATCAAACAAGTCCAGAGGTGTCCGGCAGCGTCAGTGGGGCTCTTGGGTGTCTGAAATTCGCCACCCTTTGCTGAAGAGGAG
GGTATGGCTCGGGACATTCGAGACGGCGGAGGCGGCCGCGAGAGCGTACGACCAAGCTGCTATCTTGATGAGTGGGGCAAATGCGAAG
ACTAATTTCCCAAGGGTTCATACAAATGCATGTGATGGTATTGATGAGGAGTCTCCATTGCCTCCTAAGGCACTTTCTGAGCTTCTGAATG
CGAAGCTCAGAAAGTGTTGCAAAGACCAATCTCCTTCCTTGACTTGCCTTAGGCTTGATACCGATAATGCTCATATCGGGGTGTGGCAAA
AACGTGCCGGGACTCGGTCGAGTTCGAATTGGGTCATGAGGGTCGAGCTCGGGAATACTAATAACAAGAAGAATGTTAATACGGTGGCA
TCGGAAGATGGGATGTCGGGGTCTTCGTCTTCGACTACGGCGGACGAGATCGGAGGTGGAAGCCTAATGGGAGAGGAAGATAGGATTGC
ATTGCAGATGATAGAAGAATTACTCAACTGGAATTCTCCAAGTGGAGTTTAA

HtSHN2 cDNA sequence:

ATGGTGCAGTCGAAGAAGTTCAGAGGTGTCAGGCAGCGACACTGGGGCTCCTGGGTTTCTGAAATTCGCCACCCTTTACTAAAGAGAAG
GGTGTGGCTTGGTACATTTGAAACAGCTGAAGAGGCAGCCCGAGCGTATGATCAAGCTGCAATCTTAATGAGTGGGAGGAATGCGAAAA
CGAACTTCCCCATATCACAAACACCAAGCGGAGATCAGCAGCAAGGCACTGAAAGTTCTTCCCATTCGTCACCTCCGAATGAGCTGTCTG
AACTTCTCCATGCAAAGCTTAGAAAATGCAGCAAGGCACCATCTCCTTCCGTGACTTGTCTAAGGCTGGACACAGAGAATTCGCACATCG
GCGTGTGGCAAAAGCGGGCAGGGAAGACCTCGGACTCACATTGGGTGATGACCGTCCAGCTTGGGAAACAGAATAATGCTCAAGTCTCT
GCCAATACGTTGCCTTCCAAAACACAAGGGTCGACGGAAACTACCCAACTGAGAGGAGAGATTGATGAAGAAGAGAGAATTGCACTGC
AAATGATAGAAGAGCTGCTGCATAGGAACTGTTCTTCGTTTGCTGAAGGGGAGAGTAACTTGTTTCTTTAG

HtSHN3 cDNA sequence:

ATGGTACAGTCCAAGAAGTTCAGAGGCGTTCGGCAGCGACAGTGGGGCTCTTGGGTCTCGGAGATTCGCCACCCTTTGCTGAAACGAAG
GGTATGGCTTGGAACATTTGAAACGGCCGAAGAGGCGGCTCGAGCATACGATGAAGCAGCGGTTTTGATGAGCGGACGTAACGCCAAGA
CCAACTTCCCGGTGCCGGACAGAAACCCTACAGGAAACGAGAACACCACGACTTGCAACGCCCTGTCTTCGATCCTCAGCGAAAAGCTT
CGGAAATGTTGCAAAGCCCCATCTCCTTCCCTGACTTGTTTGAGGCTCGACACCGAAAATTCTCACATCGGGGTGTGGCAAAAGAGAGCA
GGGAGTCGATCGGATTCGTGCTGGGTGATGACAATTGAGCTAGGGAACGAAAATGGGGAAGTGACTCGGGCCAATAAAATGCCGGTTTC
CGATGAACCCGTCGTCGACGAAGTCGGCAACAATGGGTTGGACGAGGAACAGAAGGCGGCATTGCAGATGATAGAAGAGCTTCTCAAT
AGGAAT

HtLTP2-like cDNA sequence:

CGACACCCAGCAGTTTTCAAACGACACAAGTAAAACCATTTTCTCCTGTCTTCAAAACTCATCTCCTTTGTTTCTTTTTCAACAAAAACCC
CATGGCTTGTCTTAAGCTTGTTTCTGCTCTATTGTTGTGCGTGTTGGTGGTTTCGCCTATTGCCACAACTGCACTAACGTGTGGAGATGTGT
CGACAAAGATGGCCTCTTGCGTTCAATACTTGCAGAACGGAGGGACGTTGCCGGCACAATGCTGCAATGGGGTTCGAGGCCTGAACACC
ATGGCTAAAACCACCCCGGACCGACAAACCGCCTGCCGGTGCTTGCAGAATTCGGCTAAATCCATCCCCAACATCAAACCTTCCTTGGCC
GAGGGCCTTCCGGGGAAATGCGGTGTCAAAATTCCTTACAAGATCAGCACCTCCACTAACTGCAACAGTGTGAAGTGAGATGGATGAAG
GCAAGGGGTTTTAAGCAGCATGCAGGAAATAAATATATACTACCAGATAGAAGTTGTGTATGAATAAAGATTTTGGGATGCTTCCAGAA
TCTAAAACCAGTCTCCACTTTGGTTTAGCGAGGCTTGTCTGATTTGTTTTTGTCTTGTTTTAAATGTTGGTTTTTCCTGCATGTTGGCTCTTA
TTATGTGGTTCATGTATCGGCTTCGGCTGTGTTGGTGTTTTATGAATGAACGTTTATGTTTTGTTAAAAAAAAAAAAA

>*HtCYP77-like* cDNA sequence

ATGAAGAATTAAGAACTACAAATAAAGTAGAGTGAAACTAGAGCTTCTAAGACATGAATATAATATTAAATTACGGCTTAAACGCAACA
TAAGAATTGTTTTATATATAAGGAATTTTAAAGTGAATTAAAATCATAGTTATATTGGAGTGAATGGAAATGGAAAAGAGTAAATATTGT
CTTAAACCCTTGGCTTGATGGTTGCTTTCAAGGTGTTCTTCAACACAACGGTAAACTCCAATTTCCCTCCAAAATCCACTTTAGCGTTGAT
CGGATAAGCTCTCCATTCAAATTCCTGAACCATTTTGGCCAACATCAGGTGAACATGCACCATCGCCATCCCCAAACCAGGGCAAATCCT
TCTCCCGACACCGAATGGCATCATTCTGATCTCCCCTTTCACCCCCGTTATATCGGCTACCTCCCTCCCTAAGTAGAATCTATCCGGGTCG
AACTTCTCCGGGTCGCTCCATATCCTCGGATCGCTGCTGATCCCCGGCAGGAATATCTCCAGGTTCGCATCCGTTGGTATGTCGTATCCCC
CCAGCGTCGCCGCTTCCTCAACGGCTGCGTGCGTCAGTGACAAGTACGTCGGCGGGTGTTTCCGTAGCAGTTCTTTGACCACCGCTTGTA
AGTACGGGAGTCTTTCGATATCGGATTCGTCCACTTTTCGATCCCCGACGGTGGATTTAATTTCGTCCAACAGTTTGGACTGGATTTCTGG
GTTTTCGATCAGCTGTGCGATTCCCCATTCGATTGCGGTTGCAGTGGTGTCGGTTCCGCCGTTGAGGAACTCGGAGCAAAGCGTGACGAG
CTCTGAGTTGGACGGTGCTGATTTTCTTCCTTCAACTTTGAGATCGAAGAGGGTGTCGAGGTACGAAAACGACATGGCGGAGGATCGATC
CGGAGCTGGTTTTAAAAGAGCTTCACGGCGGTTCTCGATGAACGGGACGATGTAATCAATTTGCTCTTTACGAACTTGCAGCGCTCGCCG
GCGTTGCTTGTAGAAAAACGGGGTTAAAACGGGAAGATAATCGTCGATTCTTGGAGTAACTGTGATCAGAACAGTTTTCATTACTTCATC
CATTTTCTCAACAGTTTCTTCATCCATTTCGACCCCGAAACACATGGCTAAAAGTATACAAAACACCGCGAAACGAGCGTTTTTCAGCAC
CGAGACGACGCCGTCGTTTGCGTCGGCCTCGGCTCTGAGACGGTCGATGAGTTTATCCATTGCATGCTCTCTAACGCTACGAAACTCTTTG
AGTTTACTCGAGCTCAGCATGTTCTGGACCATGTTCCGTCTCAGGGACCGCCACACGGGGCCGTAAACGGCGGCATTGACGGTGAACTTG
TGCAGCTAAAGATGTTCCGAGTTGGGTTTTCCCGTGGCCGGCTGGCGAAGAGTGCACTCTTCTCAATAAACGCTTCGTGGCAGAGCTTGG
CGTCGCTGAGTACAATCAGGGTCCGAGTCCCCATTCTGAGAGTGAAAATCGGCCCGTACTGCCGACGAAGATCTTCGAGGAATTCAAAG
AATTGTTTCCCGGAGCGATAAGCCTGAAAAAGATTGCCAACAACAGGCCAACCGGGGGGACCCGGAGGCAGGTTGAGGCGGCGTTTGGC
TCTTGATTTGCAAGAAAAAAACAAAACCAGACATGAAACGACGAATGCAAGAAGATGGTAAAACGAAGTAGCCATTTTTGTGAAGAATT
GTGGGTGGAAAAC

>*HtGDSL-like* cDNA sequence

TTACAGCATCACTGTTCTTATCCTCGACACTTTCCTTATCAGCAACAGCATCGCTGTAGCTCTCGACACACTCGCTTCCTCCCATAAAATTC
CCGGTTCTCTCCAATGGCATACACCCCATCGGAGGCAGCCCTCCTAACGATATTTTCCGCGCTCCGAGTTCGTACAACTTCTCCGTGAAAC
TTCCCGCGATACCGACCAGGAAGTTCTCGTATTCTTCGACGCTGTATTCCGATGAACGGCCCGGGATCGCGTAGTAGTTTTCGAGGAAAT
CGTTTGTTCCCATGCTGATCATGTATAAAGCATGGCTGATTATGTCCTTGGCTTTCCCATCTCCGAGATAGGCTCTCAGTTTCTTTTGATAG
TTTTTGTAGTATTCTAGTTGTTTCCACAGGGGTATCACAGAAAGAACATCGGAAGTGGCATTGTCGTATCCGGTTGCGGCAGAAGCGAAG
GTGACTCCGGTAGCGAAATCCGATATATGGTAGGAGGGATCGAGGTAGGCTGGAATAGTATGTTTGAGCCCGAATGCCTCGGAGATGAA
GTCGGTTGTGATTTTGCCATTGGAGAACCTTCCCGTTGGGCGGCCACCATTAAAGTCACGACCATAGGGCTGAAAATTGCTTCTGGCAAC
GGTGGAGATGTAGTTGTTGTTGCCGGCGTCAACCGATGAGTCCCCGAACACTATGATGGCTGGAATTTTGGCCCCATTAATCTTTACAAC
CAACACCAACAACTGAATTGGAACAAGGCATAAGATGTTTAACAATGGAGCCATTTTCTTCAAATGCGT

Annex III: Sequences of cDNA used for the molecular work in this thesis

SRDX/EAR tail sequence:

GGCCTAGATTTGGATTTGGAACTCCGTTTGGGTTTCGCTTAA

VP16 tail sequence:

CACCACCGACCGATGTCAGCCTGGGGGACGAGCTCCACTTAGACGGCGAGGACGTGGCGATGGCGC
ATGCCGACGCGCTAGACGATTTCGATCTGGACATGTTGGGGGACGGGGATTCCCCGGGGCCGGGATT
TACCCCCCACGACTCCGCCCCCTACGGCGCTCTGGATACGGCCGACTTCGAGTTTGAGCAGATGTTTA
CCGATGCCCTTGGAATTGACGAGTACGGTGGGTGA

Double CaMV double 35S promotor referred to as 35S:

CCTACTCCAAAAATGTCAAAGATACAGTCTCAGAAGACCAAAGGGCTATTGAGACTTTTCAACAAAG
GGTAATTTCGGGAAACCTCCTCGGATTCCATTGCCCAGCTATCTGTCACTTCATCGAAAGGACAGTAG
AAAAGGAAGGTGGCTCCTACAAATGCCATCATTGCGATAAAGGAAAGGCTATCATTCAAGATGCCTC
TGCCGACAGTGGTCCCAAAGATGGACCCCCACCCACGAGGAGCATCGTGGAAAAAGAAGACGTTCC
AACCACGTCTTCAAAGCAAGTGGATTGATGTGACATCTCCACTGACGTAAGGGATGACGCACAATCC
CACCCCTACTCCAAAAATGTCAAAGATACAGTCTCAGAAGACCAAAGGGCTATTGAGACTTTTCAAC
AAAGGGTAATTTCGGGAAACCTCCTCGGATTCCATTGCCCAGCTATCTGTCACTTCATCGAAAGGAC
AGTAGAAAAGGAAGGTGGCTCCTACAAATGCCATCATTGCGATAAAGGAAAGGCTATCATTCAAGA
TGCCTCTGCCGACAGTGGTCCCAAAGATGGACCCCCACCCACGAGGAGCATCGTGGAAAA

Annex IV: VP16, SRDX and CaMV double 35S sequences used for the production of recombinant proteins and over-expressing promotors.

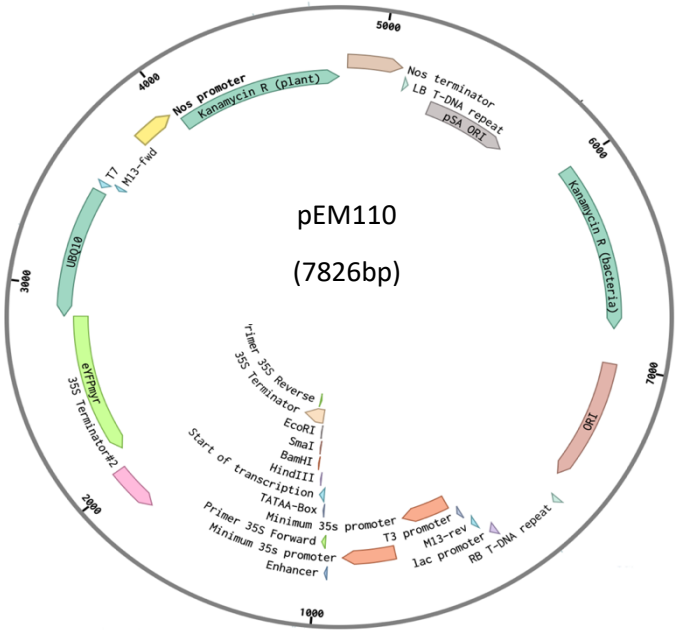

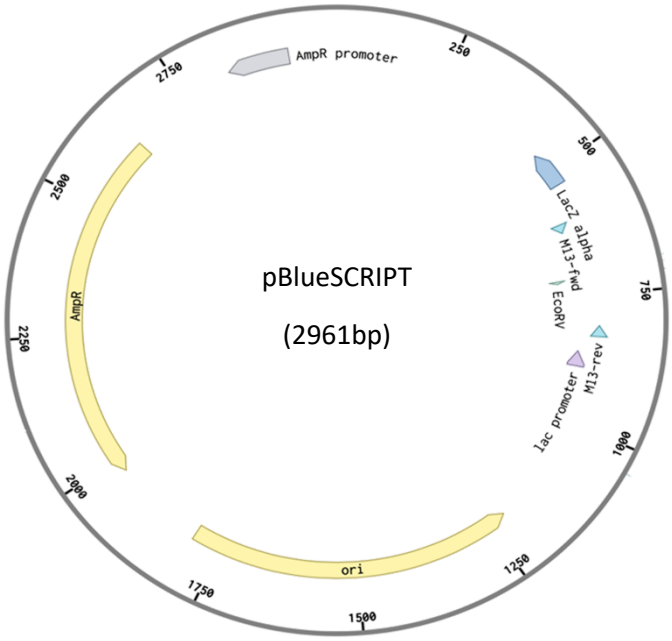

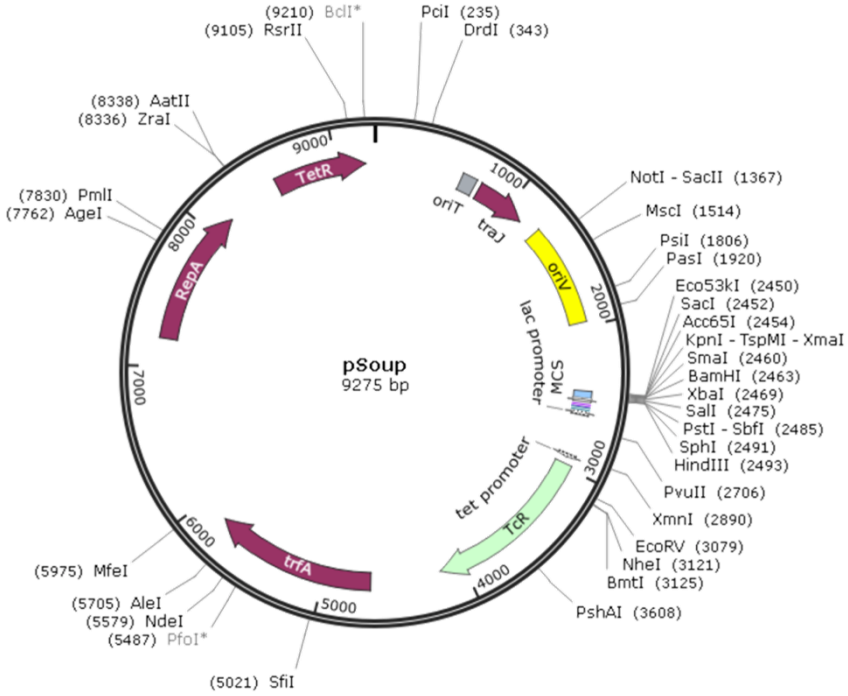

Annex V: Plasmid maps of pEM110, pBlueSCRIPT and pSoup